# Novel Pathways Involved in Nephrotoxicity Induced Damage and Recovery

Yihe Li, BSc.

Thesis submitted to The University of Nottingham for the degree of Doctor of Philosophy, November 2019

Division of Food, Nutrition and Dietetics,

School of Biosciences

University of Nottingham

Sutton Bonington Campus

Loughborough

LE12 5RD

**ABSTRACT**

Acute kidney injury (AKI) has become a rising global concern affecting over 13 million people every year and one of the main causes is nephrotoxic drugs-induced AKI. Understanding the mechanisms of which and the genetic pathway involved during damage and recovery enable further investigation on targeted treatments. Therefore, the overall aim of this study was to investigate the key genes or pathways involved in nephrotoxic drug-induced damage and recovery, thus help understanding further the paths of damage and potential recovery in nephrotoxic injury.

Firstly, AKI was induced by injecting aristolochic acid (AA) to ICR mice. We found that 5mg/kg bodyweight dose of AA did not cause significant damage to mice kidneys; HK2 cells responded to AA and folic acid (FA) treatments in time-dependent and dose-dependent manner and were able to recover after acute damage. Compare to AA treated cells, FA treated cells tended to detach from the plates after injury, making it easier to observe the recovery process after damage, thus FA at concentration of 18mM was selected for the remainder of the project. During 24-hour FA treatment, the level of both high mobility group box 1 (HMGB1) and light chain 3 B (LC3B) protein increased significantly ($p<0.05$) and reduced to a normal level during recovery. The inhibition of LC3B protein did not aggravate the injury nor slowed down the recovery process. In addition, the level of GRP78 protein showed a significant increase during FA treatment, indicated an elevation of unfolded or misfolded protein accumulated in ER. Moreover, reactive oxygen species (ROS) level was observed a

significant elevation after 4-hour FA treatment, peaked at 24-hour treatment and gradually decreased during recovery period.

Next, RNA-seq was used to investigate the mRNA change during FA treatment and recovery. HMGB1 targeted on translation during FA induced injury and recovery, and potentially induced the expression of pro-inflammatory cytokines through the C-X-C motif chemokine 12 (CXCL12) or toll-like receptor 2 (TLR2) signalling pathways. The mRNA expression of Pax2 was elevated after FA treatment, which indicated Pax2 might have a protective role over FA induced acute injury. Matrix metalloproteinase7 (MMP7) might not have a protective role in this study as its mRNA expression significantly decreased during FA treatment ($p<0.05$).

In conclusion, FA-induced damage in HK2 cells may be mediated by ROS damage and results in HMGB1 protein induction within a few hours of exposure. Whilst the cells in which this translocation is observed survive, they also induce the expression of pro-inflammatory cytokines potentially through the CXCL12 or TLR2 signalling pathways. The autophagy response is activated after FA injury which may be induced independently or through an HMGB1 mediated process, but it is not solely responsible for enabling the survival seen in FA exposed HK2 cells. The processes identified in this thesis may be helpful in understanding further the paths of damage and potential recovery in nephrotoxic injury.

**ACKNOWLEDGEMENTS**

First of all, I would like to say a huge thank you to my supervisors, Dr Simon Welham and Prof David Gardner, who have given me this precious opportunity to conduct my PhD under their supervision. I am very grateful to both of my supervisors for their expert advice, guidance and patience; I very appreciate their priceless support and encouragement when I needed the most. They are my supervisors during this project, but they are more like my families that I could trust in this foreign country.

My next thank you goes to all of the amazing technicians in the Nutritional Sciences, your expertise and patience are the key to the completion of my project. A special thank you goes to Kirsty and Zoe, whose knowledge and humour created such enjoyable working environment for all of the post-graduates. I would also like to thank technician Alan in the Vet School who gave me countless guidance and help in histology work. A warm thank you goes to all my friends in post-graduate office, the laughter we had, the sweet and sour we shared were unforgettable. Alex, Maddy and Crystal, thank you for all of your advice and encouragement; Jessica, Elaine, Fitriana and Negahan, thank you for always being with me throughout the study. I hope you all know how much I appreciate your friendship and I hope you all have an amazing bright life ahead of you.

Finally, I would like to thank my amazing parents and my grandma, who generously supported my study and encouraged me greatly while I am in the UK. I would also like to thank my boyfriend Jack who has been amazingly understandable and supportive throughout all these years.

## TABLE OF CONTENTS

**LIST OF FIGURES**

## LIST OF TABLES

## LIST OF ABBREVIATIONS

| | |
|---|---|
| 10f | 10formyl |
| MTT | 3-(4, 5- dimethylthiazol-2-yl)-2, 5-diphenyltetrazolium bromide |
| MTHFD | 5,10-methylenetetrahydrofolate dehydrogenase |
| MTHFR | 5,10-methylenetetrahydrofolate reductase |
| 5Me | 5-methyl |
| 5-MTHF | 5-methyltetrahydrofolate |
| AAN | AA-induced nephrotoxicity |
| ADQI | Acute dialysis quality initiative |
| AKI | Acute kidney injury |
| APC | Adenomatosis polyposis coli |
| Ang II | Angiotensin II |
| AT2R | Angiotensin II type 2 receptor |
| ADH | Antidiuretic hormone |
| AA | Aristolochic acid |
| Atg7 | Autophagy-related genes 7 |
| BA1 | Bafilomycin A1 |
| Bcl2 | B-cell lymphoma 2 |
| BNIP3 | Bcl2 interacting protein 3 |
| BUN | Blood urea nitrogen |
| BSA | Bovine serum albumin |
| BrdU | Bromodeoxyuridine |
| CPB | Cardiopulmonary bypass |
| CK1α | Casein kinase 1 α |
| CAT | Catalase |
| CCL2 | C-C motif chemokine ligand 2 |

| | |
|---|---|
| CCL5 | C-C motif chemokine ligand 5 |
| CHOP | CCAAT-enhancer-binding protein homologous protein |
| CDC42 | Cell division cycle 42 |
| CQ | Chloroquine |
| CRM1 | Chromosome region maintenance1 |
| CKD | Chronic kidney disease |
| JNK | C-JUN n-terminal kinases |
| CD24 | Cluster of differentiation 24 |
| cDNA | Complimentary DNA |
| CTGF | Connective tissue growth factor |
| CXCL12 | C-X-C motif chemokine 12 |
| CXCL11 | C-X-C motif chemokine ligand 11 |
| CXCL2 | C-X-C motif chemokine ligand 2 |
| CXCR4 | C-X-C receptor 4 |
| DAMP | Danger associated molecular pattern |
| SkQR1 | Decylrhodamine 19 |
| dTMP | Deoxythymidine monophosphate |
| dUMP | Deoxyuridine monophosphate |
| DHF | Dihydrofolate |
| DHFR | Dihydrofolate reductase |
| DMSO | Dimethyl sulfoxide |
| DNA-PK | DNA-dependent protein kinase |
| SDS | Dodecyl sulfate |
| DSH | Drosophila dishevelled |
| DMEM | Dulbecco’s modified eagle’s medium |
| ETF-QOR | Electron transfer flavoprotein-ubiquinone oxidoreductase |
| ER | Endoplasmic reticulum |
| EGF | Epidermal growth factor |
| EP | Ethyl pyruvate |
| ERK | Extracellular signal regulated kinase |
| FasL | Fas ligand |
| FAK | Focal adhesion kinase |
| FA | Folic acid |
| GO | Gene ontology |
| GDNF | Glial-derived neurotrophic factor |
| GFRD38D1C5:D132 | Glomerular filtration rate |
| GSH | Glutathione |
| GSH-Px | Glutathione peroxidase |
| GSK3 | Glycogen synthase kinase 3 |
| GRB7 | Growth factor receptor bound protein 7 |
| H&E | Haematoxylin eosin |
| HSPB1 | Heat shock protein β 1 |

| | |
|---|---|
| HGF | Hepatocyte growth factor |
| HMGB1 | High mobility group box 1 |
| Hcy | Homocysteine |
| $H_2O_2$ | Hydrogen peroxide |
| HIF | Hypoxia-inducible factors |
| HIF1- α | Hypoxia-inducible factors 1 α |
| IRPTC | Immortalized renal proximal tubular cells |
| ILK | Integrin-linked kinase |
| IL18 | Interleukin 18 |
| JGA | Juxtaglomerular apparatus |
| KIM-1 | Kidney injury molecule 1 |
| LC3B | Light chain 3 B |
| LPO | Lipid peroxidation |
| L-FABP | Liver-type fatty acid-binding protein |
| MD | Macula densa |
| mTORC | Mammalian target of rapamycin complex |
| MnSOD | Manganese superoxide dismutase |
| MMP7 | Matrix metalloproteinase 7 |
| MS | Methionine synthase |
| TFAM | Mitochondrial transcription factor A |
| MAPK | Mitogen activated protein kinase |
| MAPK | Mitogen-activated protein kinase |
| MKK3 | Mitogen-activated protein kinase kinase 3 |
| MDRD | Modification of Diet in Renal Disease |
| MAO | Monoamine oxidase |
| MCP1 | Monocyte chemoattractant protein 1 |
| Nox4 | NADPH oxidase 4 |
| NK | Natural killer |
| NTDs | Neutral tube defects |
| NGAL | Neutrophil gelatinase-associated lipocalin |
| NGAL | Neutrophil gelatinase-associated lipocalin |
| Nrf2 | NF-E2-related factor 2 |
| NO | Nitric oxide |
| NF-kB | Nuclear factor kappa-light-chain-enhancer of activated B cells |
| Pax2 | Paired box gene 2 |
| PFA | Paraformaldehyde |
| PGC1α | Peroxisome proliferator gamma coactivator 1α |
| PI3K | Phosphoinositide 3-kinase |
| PDK2 | Phosphoinositide-dependent kinase 2 |
| PSMB9 | Proteasome subunit beta 9 |
| PANTHER | Protein analysis through Evolutionary Relationships |
| PINK1 | PTEN-induced kinase 1 |

| | |
|---|---|
| RNS | Reactive nitrogen species |
| ROS | Reactive oxygen species |
| ROC | Receiver operating characteristic |
| RAGE | Receptor for advanced glycation end products |
| RIFLE | Risk, injury, failure, loss of kidney function, end-stage kidney disease |
| SAH | S-adenosylhomocysteine |
| SAM | S-adenosylmethionine |
| SFRP2 | Secreted frizzled related protein |
| SCr | Serum creatinine |
| SHH | Sonic hedgehog |
| SEM | Standard error of the mean |
| SACN | Standing Advisory Committee on Nutrition |
| SOD | Superoxide dismutase |
| SOD1 | Superoxide dismutase 1 |
| THF | Tetrahydrofolate |
| AUC | The area under the ROC curve |
| TS | Thymidylate synthase |
| TLR2 | Toll-like receptor 2 |
| TGF-β1 | Transforming growth factor beta 1 |
| TGM4 | Transglutaminase 4 |
| TREM1 | Triggering receptor expressed on myeloid cells 1 |
| TNF | Tumor necrosis factor |
| TNFα | Tumour necrosis factor α |
| UV | Ultraviolet |
| UCP2 | Uncoupling protein 2 |
| UO | Urine output |
| VEGF | Vascular endothelial growth factor |
| XDH | Xanthine dehydrogenase |
| XO | Xanthine oxidase |
| XOR | Xanthine oxidoreductase |

# CHAPTER 1: INTRODUCTION

## 1.1 RENAL STRUCTURE AND FUNCTIONS

### 1.1.1 Kidney structure

The kidneys are two bean-shaped organs that lie on the posterior wall of the abdomen on both sides of the vertebral column. In a healthy adult, each kidney weighs between 115g-170g (Bruce *et al*., 2013). The outer layer of the kidney is named the cortex, it contains all of the glomeruli, some of the proximal tubules and distal tubules (Figure 1.1). The next layer is named the medulla, it contains most of the loops of Henle and the collecting ducts. The medulla consists of seven to nine pyramids, which are connected with pelvis. One of the main functions of the medulla is to concentrate urine, due to this function, the extracellular fluid in medulla has higher concentration of solutes than it is in plasma, so as the osmolarity level (Briggs *et al*., 2014).

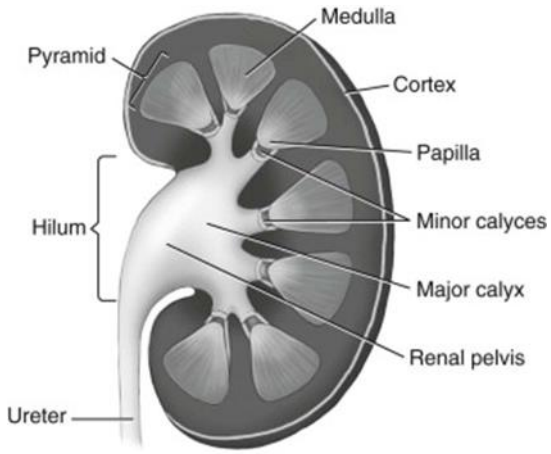


**Figure 1. 1 Structure of a human kidney.**

A cross-section image of a human kidney. Figure is taken from Paz J.C. (2014) Genitourinary System. Acute Care Handbook for Physical Therapists (Fourth Edition). 9: 225-241.

The functional unit of the kidney is the nephron. In human, each healthy kidney may contain 1.2 million nephrons (Briggs *et al*., 2014). There are two types of nephrons (Figure 1.2): juxtamedullary nephrons and superficial nephrons. Juxtamedullary nephrons have long loops of Henle which deeply dip into the inner medulla, and they have slightly larger glomeruli which are located around the corticomedullary border. Cortical nephrons, on the other hand, have shorter loops of Henle in comparison to juxtamedullary nephrons, the glomeruli of which locate in the outer medulla. Each nephron consists of a glomerulus, Bowman's capsule, proximal tubule, loop of Henle, distal tubule and collecting duct. Each part of the nephron is made up with specific type of cells that suit specific functions. For example, proximal tubules have unique brush borders on the urine side of the cell. The cells on the blood side of proximal tubules contain abundant number of mitochondria, whereas the cells in thin ascending and descending limbs of loop of Henle only have few mitochondria (Briggs *et al*., 2014).

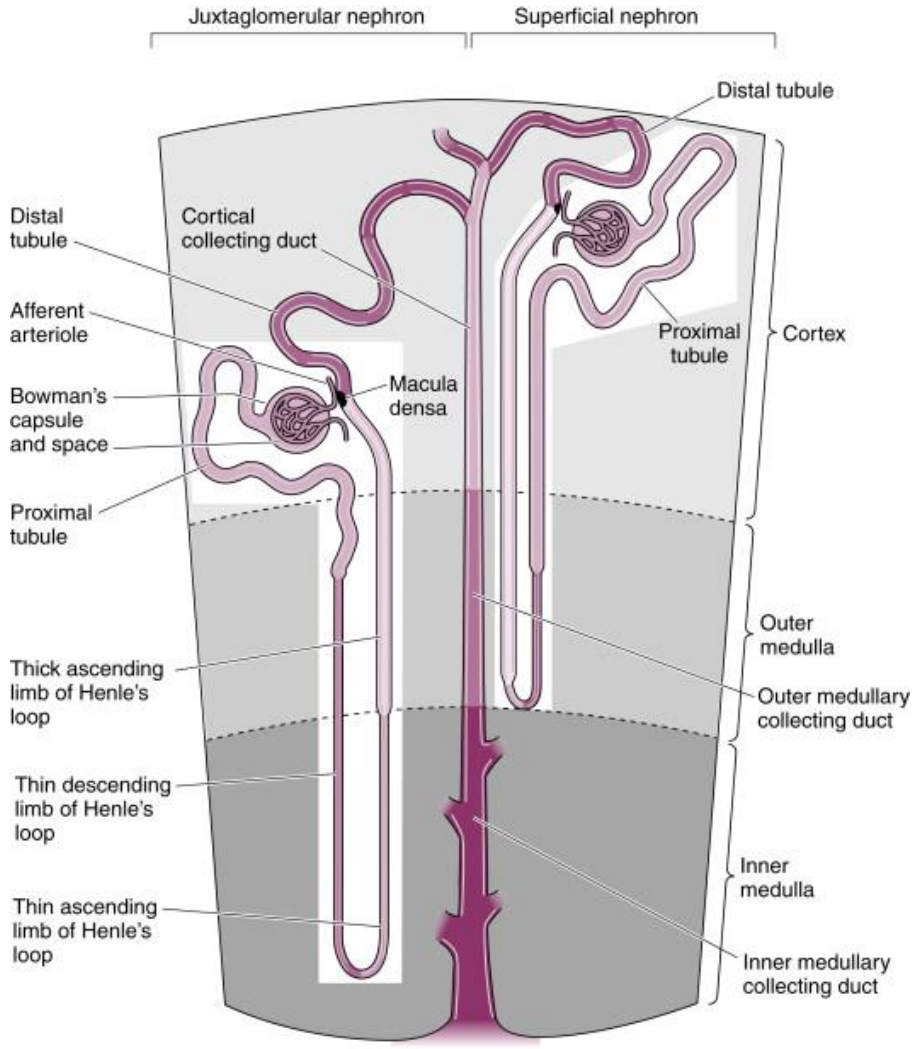


**Figure 1. 2 Structure of the nephron.**

The structure of two types of nephrons: Juxtaglomerular nephron (left) and superficial nephron (right). Figure is taken from Bruce M., Koeppen M.D. (2013) Structure and Function of the Kidneys. Renal Physiology (Fifth Edition). 2: 15-26.

### 1.1.2 Glomerular filtration

The glomerulus is a ball-shaped collection of capillaries (Figure 1.3), in association with mesangial cells the principal role of which is to encase the glomerular capillaries, together with capillary endothelium and basement membrane create a filtration barrier. This filtration barrier is freely permeable to water and other small solutes such as $Na^+$ and glucose, but not permeable to the majority of proteins, red and white blood cells and any molecules bigger than 60-70kDa (D'Amico *et al*., 2003).

The glomerular filtration rate (GFR) is a calculation that determines how well the kidneys work. It is one way to measure renal function and determine the stage of chronic kidney disease. GFR cannot be measured directly, it can be estimated via a formula: $GFR = L_p \times Area \times P_{net}$, $P_{net}$ represents the net ultrafiltration pressure, $L_p$ represents hydraulic permeability, and area represents the filtration area (Briggs *et al*., 2014). Average GFR value for an adult man is 120ml/min and 100ml/min for an adult woman, however other factors such as age and body size should also be considered when GFR is estimated (Bruce *et al*., 2013).

Juxtaglomerular apparatus (JGA) is a crucial part of the tubuloglomerular feedback mechanism that regulates renal blood flow and GFR. Macula densa (MD) locates at the end of thick ascending limb, before transition to the distal convoluted tubule, this is a primary location where the salt concentration is highly variable: when the tubular flow rate is low, the NaCl concentration remains low; when tubular flow rate is increased, the NaCl concentration

increases accordingly. This is because the flow rate change in loop of Henle regulate luminal salt concentration, which then regulate afferent arteriolar resistance. The change of afferent arteriolar resistance induces opposite changes in glomerular blood flow and filtration rate (Briggs *et al*., 2014).

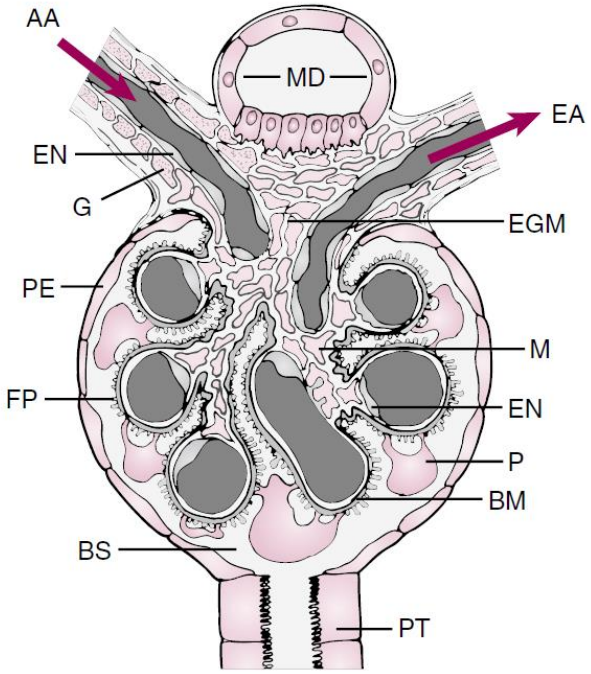


**Figure 1. 3 Structure of the glomerulus and juxtaglomerular apparatus.**

**MD**: macula densa. **EGM**: extraglomerular mesangial cells. **G**: renin- and angiotensin II–producing granular cells. **AA**: afferent arterioles; **BM**: Basement membrane; **BS**: Bowman's space; **EA**: efferent arteriole; **EN**: endothelial cell; **FP**: foot processes of podocyte; **M**: mesangial cells between capillaries; **P**: podocyte cell body (visceral cell layer); **PE**: parietal epithelium; **PT**: proximal tubule cell. Figure is taken from Bruce M., Koeppen M.D. (2013) Structure and Function of the Kidneys. Renal Physiology (Fifth Edition). 2: 15-26.

### 1.1.3 Tubular reabsorption and secretion

After filtration, the glomerular filtrate undergoes a process of reabsorption and secretion of solutes and fluid before being excreted as urine (Briggs *et al*., 2014). Reabsorption is a process that recycles the useful solutes from tubular lumen back to blood, this includes sodium, chloride, water, bicarbonate, glucose, amino acids, protein, phosphates, calcium, Magnesium ion, urea and uric acid. Secretion is the movement of solutes from blood or surrounding interstitial fluid back to tubular lumen to be excreted in urine, these solutes include hydron, potassium ion, ammonium ion etc. (Meltzer J., 2013). During reabsorption, some solutes are transported by enzymes, some of solutes are transported by diffusion. Tubular sodium absorption, for instance, is an active process driven by $Na^+$/ $K^+$-ATPase. $Na^+$/ $K^+$-ATPase acts as a pump that translocates $Na^+$ out of the cells while pumping $K^+$ into the cells, therefore reducing intracellular $Na^+$ level whilst increasing $K^+$ level. This is further supported by a number of the luminal transporters located at different segment of nephrons: $Na^+$ dependent cotransporter and $Na^+/H^+$ exchanger (NHE3) at early proximal tubules, $Na^+/H^+$ exchanger and $Cl^-$ anion exchanger in late proximal tubules and NKCC2 cotransporter in thick ascending limb (Briggs *et al*., 2014; Blaine *et al*., 2015).

The majority of the glomerular solute is reabsorbed by the proximal tubules. It is estimated that more than half of the sodium, chloride, calcium and water, and over 90% $HCO_3^-$ are absorbed in the proximal tubule. In addition, almost all of the glucose and amino acids are absorbed in the proximal tubule, as well as some phosphate. $H_2O$ is reabsorbed as solutes pass through the descending

limb leading to concentrated tubular fluid; however, the thick ascending limb is water-impermeable, therefore it is only relatively permeable to NaCl which results in a relatively diluted tubular fluid as water remains in the tubule (Weiner *et al*., 2015). The adjustment of urine composition and volume is made in the distal nephron, which includes distal tubule, connecting tubule and medullary collecting duct. Under the influence of aldosterone, the activity of sodium channel ENaC is greatly increased, therefore $Na^+$ and $Cl^-$ are absorbed, followed by $K^+$ and $H^+$ secretion (Sands *et al*., 2009). The final adjustment takes place in the collecting duct before the fluid leaves as urine: around 5% of NaCl and some urea are reabsorbed in addition to $H_2O$, which the latter is regulated by antidiuretic hormone (ADH). ADH is a hormone that helps to regulate the water content in the body: when the body is dehydrated, ADH acts in restoration of water in the collecting duct back in the body (Briggs *et al*., 2014).

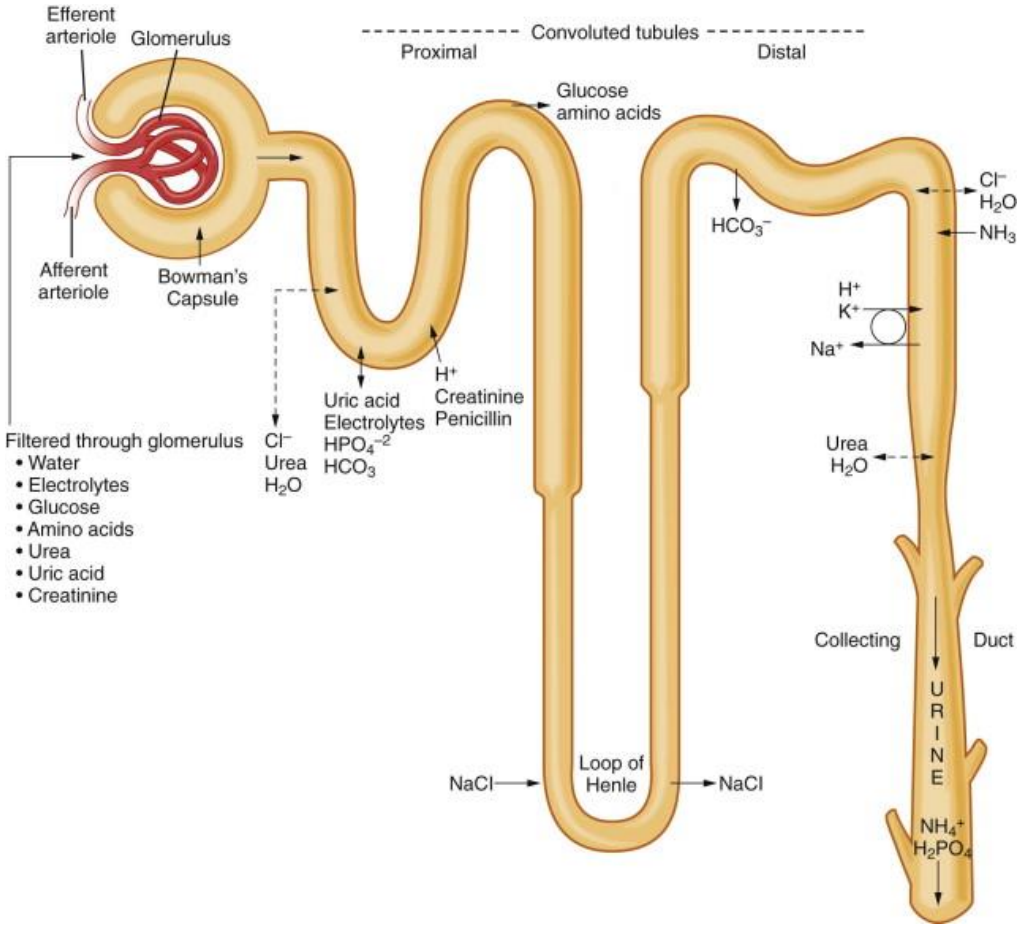


**Figure 1. 4 Nephron reabsorption and secretion.**

This diagram shows the movement of some glomerular filtrates been reabsorbed by tubules and movement of some other solutes from blood or surrounding interstitial fluid back to tubular lumen. Figure is taken from Joseph Meltzer (2013) Pharmacology and Physiology for Anesthesia. 32: 561-573.

## 1.2 ACUTE KIDNEY INJURY

### 1.2.1 Definition of AKI

AKI is defined as acute deterioration of glomerular functions over a period of hours, it could be reflected by the aggregation of products such as creatinine and plasma urea (Bellomo *et al.*, 2012). Most studies agreed with the definition of AKI as serum creatinine of 2 mg/dL to 3 mg/dL (200–250 μmol/L), an escalation of >0.5 mg/dL (45 μmol/L) over a baseline creatinine below 2 mg/dL, or baseline creatinine level is elevated by two times (Kellum *et al.*, 2011). Other clinical indices include the potential reduction of urine output, accumulation of metabolic acid and increased potassium and phosphate concentrations (Bellomo *et al.*, 2012). Each year, AKI affects more than 13 million patients and associates high morbidity rate especially in hospitalized patients (Mehta *et al.*, 2015), however, the survivors often suffer from long-term disease and are particularly susceptible to development of chronic kidney disease (Coca *et al*., 2009), therefore leading to poor quality life and long-term expense (Zuk *et al*., 2016).

### 1.2.2 Classification of AKI

When considering the impact of AKI, many studies have concentrated on the ways to identify patients that are at risk of developing AKI or identify those with subclinical AKI. With the development of tubular damage biomarkers, the diagnosis accuracy has been greatly enhanced (Husain-Syed *et al.*, 2018).

There are three major ways of classifying the severity of AKI: RIFLE classification, AKIN classification and KDIGO classification.

The RIFLE criteria (risk, injury, failure, loss of kidney function, end-stage kidney disease) were first published in 2004 after the Acute Dialysis Quality Initiative (ADQI) group conference, which aimed to decide a universal AKI definition (Bellomo *et al.*, 2004). This system classifies AKI based on the change of serum creatinine (SCr) or GFR together with urine output (UO), it defines the clinical consequences as 'loss of kidney function' and 'end-stage kidney disease'. RIFLE system relies on the baseline SCr, however, when the baseline SCr is unknown, the Modification of Diet in Renal Disease (MDRD) equation is needed to estimate the baseline SCr (Manjunath *et al.*, 2001). It defines the AKI as an increase in SCr by 1.5 times or a reduction of GFR more than 25%. The RIFLE classification has been used clinically to determine the occurrence of AKI, identifying the severity based on multiple data, and was the first system to establish the connection between AKI severity and mortality (Chertow *et al.*, 2005; Silvester *et al.*, 2001).

The AKIN system, or 'acute kidney injury network' system, was established in 2007 by the AKIN working group (Mehta *et al.*, 2007). Studies found that there was growing evidence indicating that even a small elevation of SCr was linked with severe consequences, therefore revising the RIFLE classification appeared to be more crucial (Uchino *et al.*, 2006; Hoste *et al.*, 2006). The AKIN system is more straightforward than the RIFLE system as it only depends on SCr level change within 48 hours. AKIN defines AKI as an increase in SCr equal to or more than 0.3mg/dL, or by a reduction in UO less than 0.5ml/kg/h for over

6 hours. However, the conclusion could only be considered when an adequate hydration status was achieved. The proposal of AKIN system has increased the sensitivity and the specificity of the diagnosis compared to the RIFLE system.

In 2012, the KDIGO work group proposed another classification named KDIGO, short for ‘kidney disease improving global outcomes’. This is a combination of the RIFLE and the AKIN systems which provides a simplified system to be used clinically (Khwaja *et al.*, 2012). As shown in Figure 1.5, KDIGO defines AKI in the same definition as the AKIN system does for stage 1 and 2 AKI; for stage 3 AKI, KDIGO provides a simpler definition by an increase in SCr more than 3 times or no less than 4mg/dL, or a reduction in UO less than 0.3ml/kg/h within 24 hours for adult.

Multiple studies have compared the incidence of AKI between the three classifications. Nisula *et al*. reported that the similar incidence of AKI was found using AKIN and KDIGO in a cohort study of over 2900 patients. The three classification were also reported to have a similar incidence in a retrospective study of 1881 cardiac surgery patients (Bastin *et al.*, 2013). In addition, a similar incidence was also demonstrated by another retrospective cohort study of 31970 patients defined their AKI severity by RIFLE, AKIN and KDIGI (Zeng *et al.*, 2014). However, there is also evidence showing that KDIGO classification performed better than RIFLE or AKIN. Rodrigues and colleagues reported that KDIGO classification was more accurate than RIFLE in defining AKI over 1050 patients with acute myocardial infarction, 36.6% patients were diagnosed to have AKI using KDIGO classification whereas only 14.8% of patients were diagnosed to have AKI using RIFLE classification (Rodrigues *et al*., 2013). Luo

and colleagues also demonstrated that KDIGO classification showed a higher incidence (51%) over 3107 patients, whereas RIFLE and AKIN only showed 46.9% and 38.4% respectively.

Although RIFLE, AKIN and KDIGO are all conducted from clinical research, they all have different advantages and limitations. Even though the KDIGO classification offers higher accuracy than RIFLE and AKIN, more studies with more larger patients population are still needed to examine its sensitivity and performance.

| Class/Stage | SCr/GFR | | | UO | | |
|---|---|---|---|---|---|---|
| | RIFLE | AKIN | KDIGO | RIFLE | AKIN | KDIGO |
| Risk/1 * | ↑ SCr X 1.5 or ↓ GFR > 25% | ↑ SCr ≥ 26.5 µmol/L (≥0.3 mg/dL or ↑ SCr ≥ 150 to 200% (1.5 to 2X) | ↑ SCr ≥ 26.5 µmol/L (≥0.3 mg/dL) or ↑ SCr ≥ 150 to 200% (1.5 to 2X) | <0.5 mL/kg/h (>6 h) | <0.5 mL/kg/h (>6 h) | <0.5 mL/kg/h (>6 h) |
| Injury/2 * | ↑ SCr X 2 or ↓ GFR > 50% | ↑ SCr > 200 to 300% (>2 to 3X) | ↑ SCr > 200 to 300% (>2 to 3X) | <0.5 mL/kg/h (>12 h) | <0.5 mL/kg/h (>12 h) | <0.5 mL/kg/h (>12 h) |
| Failure/3* | ↑ SCr X 3 or ↓ GFR >75% or if baseline SCr ≥ 353.6 µmol/L (≥4 mg/dL) ↑ SCr > 44.2 µmol/L (>0.5 mg/dL) | ↑ SCr >300% (>3X) or if baseline SCr ≥ 353.6 µmol/L (≥4 mg/dL) ↑ SCr ≥ 44.2 µmol/L (≥0.5 mg/dL) or initiation of renal replacement therapy | ↑ SCr > 300% (>3X) or ↑ SCr to ≥353.6 µmol/L (≥4 mg/dL) or initiation of renal replacement therapy | <0.3 mL/kg/h (>24 h) or anuria (>12 h) | <0.3 mL /kg/h (24 h) or anuria (12 h) | <0.3 mL/kg/h (24 h) or anuria (12 h) or GFR < 35 mL/min/1.73 $m^2$ in patients younger than 18 years |

SCr: serum creatinine; GFR: glomerular filtration rate; UO: urine output; RIFLE: Risk, Injury, Failure, Loss of kidney function (dialysis dependence for at least 4 weeks), End-stage kidney disease (dialysis dependence for at least 3 months); AKIN: Acute Kidney Injury Network; KDIGO: Kidney Disease Improving Global Outcomes. * Risk class (RIFLE) corresponds to stage 1 (AKIN and KDIGO), Injury class (RIFLE) corresponds to stage 2 (AKIN and KDIGO), and Failure class (RIFLE) corresponds to stage 3 (AKIN and KDIGO), ↑ increase, ↓ decrease.

**Figure 1. 5 Classifications of AKI according to SCr and UO.**

Comparison of RIFLE, AKIN and KDIGO classifications. The table ia taken from Khwaja, A. (2012) KDIGO clinical practice guideline for acute kidney injury. Nephron Clin. Pract. 120, 179-184.

### 1.2.3 The main causes of AKI

The incidence of developing AKI gradually raised between 1988 – 2003, after which, due to the spread of awareness of AKI and effective means of early diagnosis, the incidence of AKI slowly decreased (Ali *et al.*, 2007; Waikar *et al*., 2006; Amin *et al*., 2012). On the other hand, it has been identified that several risk factors including patient's age, organ dysfunction, cardiac surgery etc., as well as other factors such as clinical settings, could affect the severity of AKI (Case *et al*., 2013; Farooqi *et al*., 2016). The two primary causes of AKI are ischemia reperfusion injury (I/R) and nephrotoxicity (Basile *et al*., 2014).

#### 1.2.3.1 Renal ischemia/reperfusion (I/R) injury

I/R injury is a major cause of AKI, it often occurs after infarction, sepsis, renal surgery and organ transplantation etc. (Jonker *et al*., 2016; Jang *et al.*, 2009). It is characterized as a temporary disruption of blood flow to kidneys, leading to restriction of oxygen and nutrients for a period of time, followed by restoration of blood flow (Malek *et al*., 2015). During ischemia, the restriction of blood flow reduces oxygen and nutrient delivery to tissue, which interrupts ATP generation (Figure 1.6). The reduction of ATP restricts ion pump function in cell membranes, leading to accumulation of calcium ($Ca^{2+}$) and sodium ($Na^{+}$) in cells; it also forces cells to generate energy through anaerobic glycolysis which leads to cellular acidification, hence leading to apoptosis and necrosis. Upon reperfusion, the injured tissue is re-introduced with blood flow and oxygen; however, a burst of ROS is produced due to xanthine oxidase, NADPH oxidase

and electron transport chain (ETC) dysfunction as a result of the previous hypoxic environment. ROS-dependent expression of inflammatory mediators and adhesion molecules by tissue cells and leukocytes accelerate the infiltration process, the presence of superoxide further contribute to the oxidative stress which directly damage cells and lead to cell apoptosis and necrosis. In addition, ROS directly injure cells through lipid peroxidation in membrane and organelles, damage DNA, open mitochondrial permeability transition pores, which all results in cell swelling and lysis and therefore cell death. ROS also occurs at low level in recovery stage where it takes part as signalling molecules, promoting the activation of transcription factors and growth factors that contribute to cell proliferation, differentiation and migration (Figure 1.6).

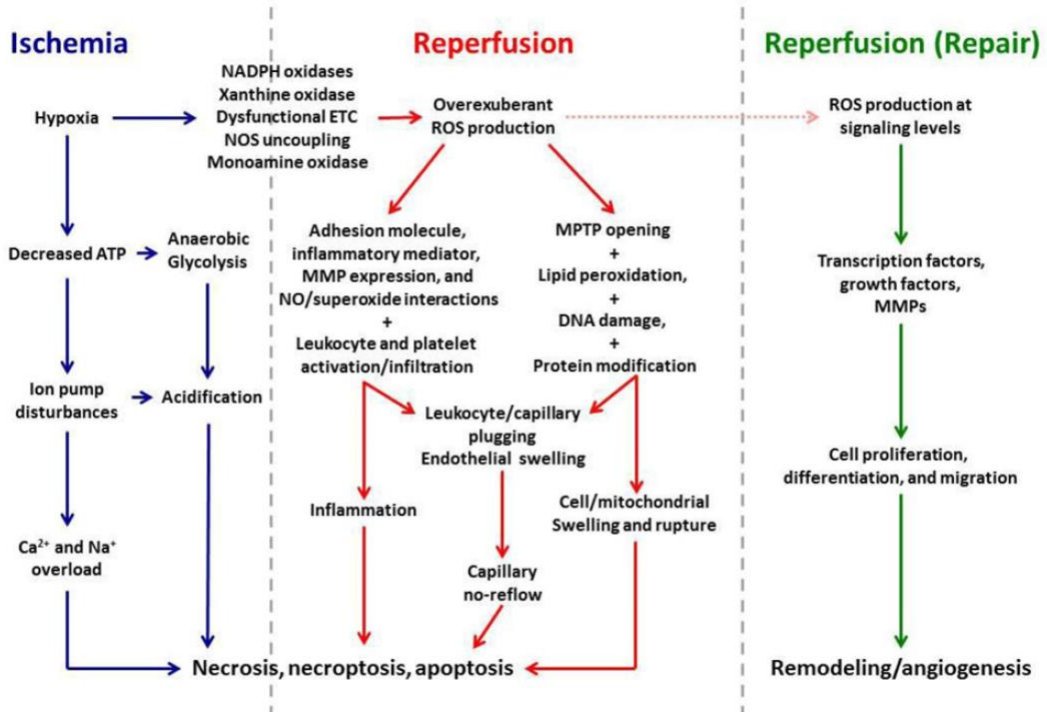


**Figure 1. 6 Potential mechanisms contributing to tissue damage when exposed to I/R.**

The restriction to blood flow leads to a reduction of ATP production, disruption to ion pump and overload of $Ca^{2+}$ and $Na^{+}$. The reduction of ATP further promotes anaerobic glycolysis which contributes to cell apoptosis and necrosis. Upon reperfusion, the restoration of blood flow results in a burst of ROS production which leads to the consequence of inflammation, cell and mitochondrial dysfunction and cell apoptosis and necrosis. The ROS production also occurs when damaged tissue under recovery at a lower level, serving as signalling molecules promoting cell proliferation, differentiation and migration. Figure was taken from Kalogeris T., Bao Y.M., Korthuis R.J. (2014) Mitochondrial reactive oxygen species: A double edged sword in ischemia / reperfusion vs preconditioning. Redox Biology. 2: 702–714.

In the kidneys, I/R injury contributes to renal malfunction by initiating an inflammatory cascade, resulting in the release of ROS and cytokines and activation of leukocytes, which further exacerbate tissue damage and lead to a high mortality rate (Hoste *et al.,* 2006). Two factors that are considered as the main contributors causing damage in AKI: 1) Vascular factors, such as reduced blood flow in vessels, tissue damage due to the limitation of oxygen and cell necrosis. 2) Tubular factors, including disruption of normal kidney functions like reabsorption, as well as interstitial inflammation (Lameire *et al*., 2005). Although I/R injury has been intensively researched in the past years, the pathophysiology underlying I/R injury is not fully discovered yet. However, it has been evidenced that ROS and downstream activated cytokines may have significant contribution in I/R injury (Gillani *et al.,* 2012).

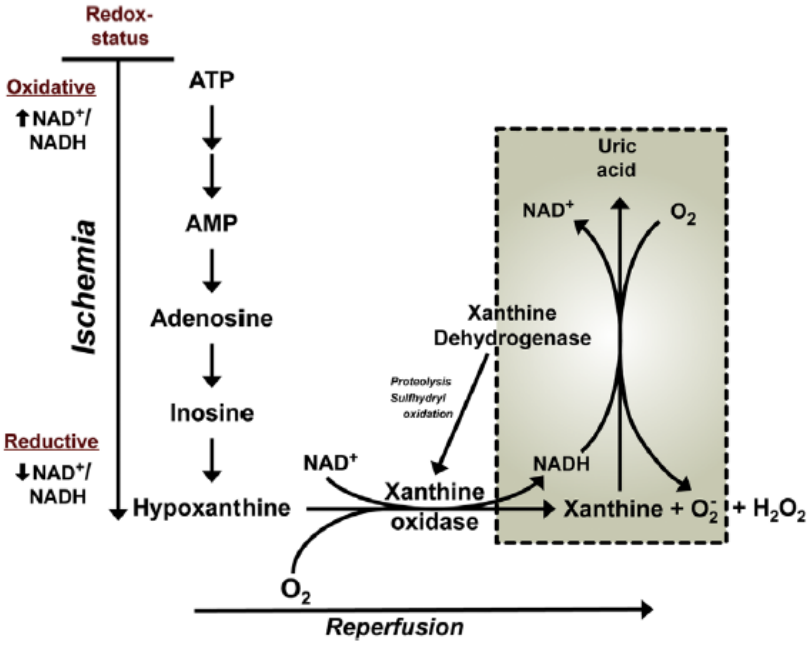


**Figure 1. 7 Potential mechanism of XOR may contribute to ROS generation in tissue during ischemia and reperfusion.**

When tissue is exposed to ischemia, ATP is catabolized to hypoxanthine, xanthine dehydrogenase (XDH) is converted to xanthine oxidase (XO) via proteolysis and sulfhydryl oxidation. Upon reperfusion, oxygen is restored and reacts with hypoxanthine and generate xanthine, superoxide ($O_2^-$) and hydrogen peroxide ($H_2O_2$). Figure is taken from Granger N.D., Kvietys P.R. (2015) Reperfusion injury and reactive oxygen species: The evolution of a concept. Redox Biology. 6: 524–551.

During I/R injury, the injured tissue, especially the S3 segment of the proximal tubule and medullary thick ascending limb, produce large amounts of ROS including hydrogen peroxide which leads to oxidative stress (Sharfuddin *et al.,* 2008). The induction of oxidative stress leads to the alteration of mitochondrial oxidative phosphorylation, depletion of ATP, increased cellular calcium level and activation of membrane phospholipid proteases, which contributes to the cell injury and necrosis (Granger *et al*., 2015; Bonventre, 1993). When the blood flow is restored during the reperfusion phase, the oxygen free radicals are produced and may cause renal injury via lipid peroxidation. The production of free radicals causes oxidative degradation of lipids (lipid peroxidation) which damage the cell membrane, DNA and protein, contributing to cell apoptosis and death (Granger *et al*., 2015). The oxidative stress during and after I/R injury has been reported to be associated to multiple sources of ROS, this includes haemoglobin and myoglobin acting as potential inducer of oxidative stress, as well as some enzymes that are able to generate hydrogen peroxide during reperfusion stage, such as xanthine oxidoreductase (XOR) (Mcleod *et al*., 1999; Xu *et al*., 1993). XOR is an enzyme that controls the hydroxylation of xanthine to uric acid. One of its isoforms xanthine oxidase (XO) has been intensively investigated in the past decade as the major resource of ROS when tissues are exposed to I/R injury, as XO uses oxygen as the terminal electron acceptor (Granger *et al*., 2015). The original hypothesis proposed (Figure 1.7) that when tissue was exposed to ischemia, ATP was catabolized to hypoxanthine, xanthine dehydrogenase (XDH) was converted to xanthine oxidase (XO) via limited proteolysis and sulfhydryl oxidation. When the blood flow was restored

at reperfusion stage, the interactions between oxygen ($O_2$) and hypoxanthine were significantly increased and xanthine, superoxide ($O_2^-$ ) and hydrogen peroxide ($H_2O_2$) were largely generated, therefore it was concluded that this potential XO-derived mechanism might be the key source of ROS during I/R injury (Granger *et al*., 1981). There are a few XO inhibitors such as allopurinol and oxypurinol claimed to reduce the oxidant activity and therefore limit ROS damage to tissue after I/R injury. It was reported that allopurinol significantly reduced oxidative stress after I/R injury in rat model (Rhoden *et al.,* 2000); however, Zager and colleague found that pre-treatment with oxypurinol prior ischemia in rat model failed to show protection against tissue damage, some other studies have also failed to show protection in post-ischemic tissues following XO inhibition (Downey *et al*., 1987; Kennedy *et al*., 1989).

Although XO may contribute to ROS production during I/R injury, mitochondria are commonly reckoned as the main source of cellular ROS (Lee *et al*., 2012). Mitochondria contain a few enzymes in the mitochondrial electron transport chain, also known as respiratory chain, that convert oxygen to $O_2^-$ and $H_2O_2$ (Figure 1.8). In healthy cells, there are up to 95% of ROS produced in the complexes in the respiratory chain; however, the ROS production could be significantly elevated during ischemia and reperfusion (Turrens *et al*., 1997; Kalogeris *et al*., 2014). Complex I and complex III both localized in the inner mitochondrial membrane (Figure 1.8), produce superoxide, which then forms hydrogen peroxide with the help of manganese superoxide dismutase (MnSOD). $H_2O_2$ could further interact with transition metals and form reactive hydroxyl radical ($OH^{\bullet}$) or react with nitric oxide (NO) and form peroxynitrite

($ONOO^-$). Other enzymes such as Nox4 and MAO localized in the outer mitochondrial membrane are also sources of $H_2O_2$ in mitochondria, as ETF-QOR (electron transfer flavoprotein-ubiquinone oxidoreductase) generate $H_2O_2$ through beta-oxidation of fatty acids. On the other hand, it has been demonstrated that the mitochondrial ROS production could be significantly reduced by hypoxic pre-conditioning in animal models. Plotnikov and colleague reported that there was a 48% increase in mitochondrial membrane potential in hypoxic preconditioning group compared with I/R group, and the production of ROS after I/R injury in hypoxic pre-conditioning group was 66% lower than I/R injury group in rat model (Plotnikov *et al*., 2007).

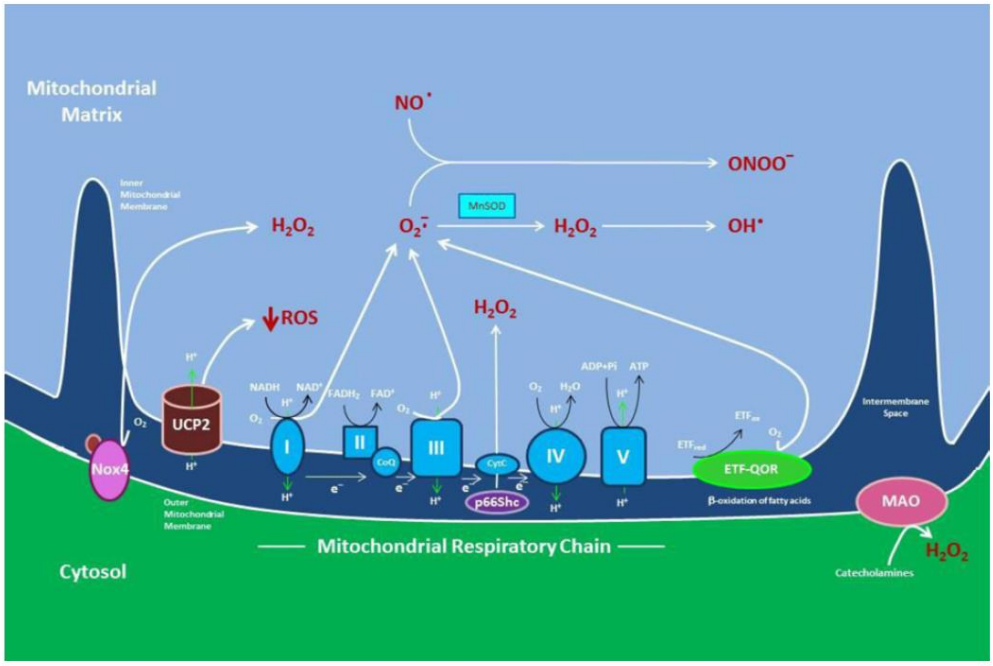


**Figure 1. 8 Mechanism of ROS production in mitochondria.**

Mitochondrial respiratory chain produces a small amount of ROS in healthy cells under normal condition, but when cells are under ischemia or reperfusion condition, the production of ROS could be significantly increased and therefore become the main resource od ROS during I/R injury. **Complex I**: NADH dehydrogenase; **Complex III**: coenzyme Q and cytochrome C oxidoreductase); **MnSOD**: manganese superoxide dismutase; **ETF-QOR**: electron transferring flavoprotein ubiquinone oxidoreductase; **MAO**: Monoamine oxidase; **Nox4**: NADPH oxidase-4; **UCP2**: uncoupling protein-2. Figure is taken from Kalogeris T., Bao Y.M., Korthuis R.J. (2014) Mitochondrial reactive oxygen species: A double edged sword in ischemia / reperfusion vs preconditioning. Redox Biology. 2: 702–714.

### 1.2.3.2 Nephrotoxicity

#### 1.2.3.2.1 Aristolochic acid nephrotoxicity

Aristolochic acid (AA) is a generic name for nitrophenanthrene carboxylic acids that are primarily found in herbs belonging to the Aristolochiaceae family of plants. Aristolochic acid first appeared in Chinese medicine in the fifth century AD. During ancient times, it was used to treat urinary problems, snakebites, was used as a contraceptive drug. However, in recent years, AA was suspected to be the main reason of nephrotoxicity associated with interstitial fibrosis and carcinoma (Debelle *et al.,* 2002; Stiborova *et al.,* 2001). Nephropathy caused by AA was initially reported in Belgium in 1993, when a group of people who regularly consumed slimming pills were diagnosed with rapidly progressive tubulointerstitial injuries (Vanherweghem *et al*., 1993). Evidence pointed out that one of the main components of the slimming pills belongs to *Aristolochia* species, which then resulted in a rapidly developing renal interstitial fibrosis in the patients and more than 70% of them were diagnosed with end-stage renal disease (Bunel *et al.*, 2016; Vanherweghem J.L., 1998). In the past two decades, the cases of patients developing renal injury after consuming AA have been reported all over the world, such as China (Yang *et al*., 2007), Japan (Tanaka *et al*., 2000), France (Stengel *et al*., 1998), UK (Lord *et al*., 1999), Bangladesh (Michk *et al*., 2013 ), Korea (Lee *et al.*, 2004), Germany (Krumme *et al*., 2001), USA (Meyer *et al*., 2000) and Australia (Chau *et al*., 2011). The fact that those medicine that contain AA can be easily bought online without a prescription, lack of understanding of the mechanism of injury and weak

awareness of the potential consequences, AA-induced nephrotoxicity (AAN) remains a global health issue even to date (Jadot *et al*., 2017).

Aristolochic acid is chemically composed of AAI and AAII, they both share a similar molecular structure (Figure 1.9), and both are cytotoxic (Nitzsche *et al*., 2013); however only AAI is responsible for AAN. Shibutani and colleagues found that significant renal tubular damage and interstitial fibrosis were observed in mice treated with AAI whereas AAII treated mice did not show significant renal injury (Shibutani *et al*., 2007). It has been shown that AAN is strongly associated with mitochondrial damage and DNA adduct formation in tissue, leading to impaired regeneration and proximal tubular apoptosis and necrosis (Nitzsche *et al*., 2013).

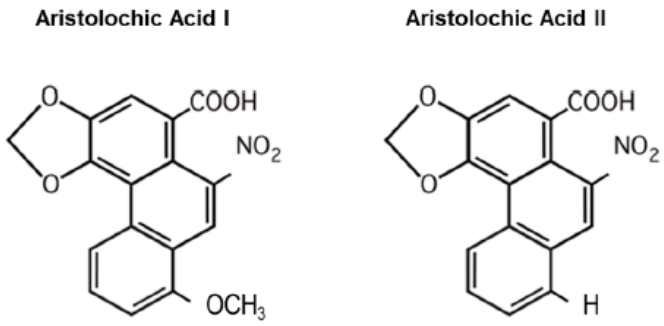


**Figure 1. 9 Molecular structure of AAI and AAII.**

Figure is taken from Jadot I., Decleves A.E., Nortier J., Caron N. (2017) An Integrated View of Aristolochic Acid Nephropathy: Update of the Literature. Int. J. Mol. Sci. 18: 297-321.

Multiple studies have indicated that activated AAI is associated with DNA adduct formation (Schmeiser *et al*. 1988; Bieler *et al*. 1997; Arlt *et al*. 2001; Xiao *et al*. 2008). The main types of DNA adduct formed from AAI in animal models and human patients includes 7-(deoxyadenosine-$N^6$-yl) aristolactam I (dA-AAI), 7-(deoxyadenosine-$N^2$-yl) aristolactam I (dG-AAI) and 7-(deoxyadenosine-$N^6$-yl) aristolactam II (dA-AAII), in rodent tumours, dA-AAI was reported to induce mutagenic effects and led to AT→TA transversions especially in the kidneys and bladder (Yun *et al*., 2012; Grollman *et al*., 2007; Jelakovie *et al*., 2012; Rosenquist *et al*., 2016). This mutation was initially found in 1994 when a significant overexpression of p53 protein was observed in AAN patients, suggesting that the mutation might be in p53 gene (Cosyns *et al*., 1994). Later on, the mutation was described as an AAG to TAG transversion in codon 139 of exon 5 in the p53 gene, this mutation could lead to carcinogenetic transformation in some cases (Lord *et al.*, 2004).

AAN is also connected with the ROS production in tissues. A number of studies showed that there was a significant increase in ROS and reactive nitrogen species (RNS) in cells after they were exposed to AA (Yu *et al*., 2011; Romanov *et al*., 2015; Wu *et al*., 2015; Bunel *et al*., 2016). Romanov and colleague reported that the longer HK2 cells were exposed to AA, the higher the ROS level in the cells (Romanov *et al*., 2015). The increased ROS was suggested to be responsible for the depletion of intracellular glutathione (GSH) as well as cell cycle arrest in G2/M phase, however when cells were treated with antioxidants such as glutathione, a reduced ROS production was observed, as well as AA-induced DNA adducts and cell apoptosis, which suggested that AA may induce

DNA adduct formation through oxidative stress (Yu *et al*., 2011; Wu *et al*., 2015; Romanov *et al*., 2015). Similar results were found in animal studies. Pozdzik and colleagues found out that in a rat model of AAN, the normal activation of antioxidative enzymes and mitochondria function were interfered (Pozdzik *et al*., 2008); in addition, a decrease of renal antioxidant capacity was observed in mice model of AAN, suggesting that an excessive amount of ROS was produced during AAN (Li *et al*., 2012).

#### 1.2.3.2.2 Folic acid nephrotoxicity

Folic acid, or pteroylmonoglutamic acid, can be found in dark green leafy vegetables and most fruits like asparagus, avocados, spinach and lettuce. Human cannot synthesize folic acid *de novo,* therefore, it must be supplied through the diet or supplements to meet their daily requirements. A healthy adult needs approximately 400μg folic acid per day, pregnant women need more (1000μg). In a recent report from the UK Standing Advisory Committee on Nutrition (SACN) suggested that adding folic acid in the flour may reduce the number of infants born with neutral tube defects (NTDs). It has been estimated that between 77-162 NTD infants might be saved from developing NTD by fortification at a level of 300μg folic acid per 100g flour (Smith *et al*., 2008). Evidence also suggested that folic acid supplementation taken before and during pregnancy might reduce the risk of heart defects as well as reduce the risk for children to develop metabolic syndrome (Bazzano LA., 2011).

Vitamin B9 is critical for numerous processes like DNA synthesis and repairing RNA. The active form of which is folate, also known as 5-methyltetrahydrofolate (5-MTHF). When dietary folate enters the digestive system, it is transformed to 5-MTHF and then transported in the blood stream (Patanwala *et al*., 2014). Folic acid, conversely, is a synthetic form of vitamin B9, it needs to be modified to dihydrofolate, then tetrahydrofolate and then to folate in the liver before entering the folate cycle (Figure 1.10) (Wright *et al*., 2007; Patanwala *et al*., 2014). The dietary folate enters the folate cycle, during which one-carbon units are generated and contribute to DNA and RNA synthesis; the methyl groups are also generated in order to regenerate methionine from homocysteine (Kennedy D.O., 2016).

Although folic acid (FA) is essential for biological methylation and DNA, RNA synthesis, it has been demonstrated that overdosing folic acid might lead to folic acid-induced acute kidney injury. Studies found that intraperitoneal administration of FA in rats and mice at around 250mg/kg significantly increased blood urea nitrogen (BUN) and serum creatinine (Scr). Animals also showed signs of acute tubular apoptosis and necrosis followed with interstitial fibrosis (Long *et al*., 2001; Byrnes *et al*., 1972; Doi *et al*., 2006). Along with the appearance of acute injury in the tubules, FA crystals were also found in renal tubules after administration, which indicated that FA could induce physical damage. Fink and colleagues observed that by co-administrating FA with $NaHCO_3$, the amount of FA crystals significantly decreased, however the proximal tubular damage still occurred, which suggested that FA did not only

induce proximal tubular injury through the formation of FA crystals, but also had direct nephrotoxic effect independent of FA crystals (Fink *et al*., 1987).

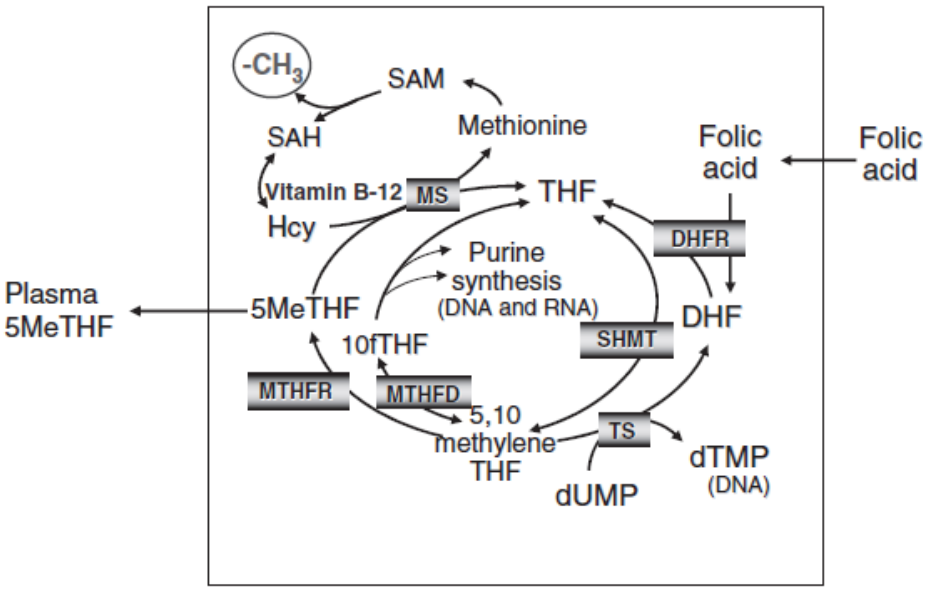


**Figure 1. 10 The simplified folate cycle.**

A simplified version of the folate cycle and the methionine cycle. **Hcy**: homocysteine; **SAM**: S-adenosylmethionine; **DHFR**: dihydrofolate reductase; **MS**: methionine synthase; **MTHFD**: 5,10-methylenetetrahydrofolate dehydrogenase; **MTHFR**: 5,10-methylenetetrahydrofolate reductase; **TS**: thymidylate synthase; **DHF**: dihydrofolate; **THF**: tetrahydrofolate; **5Me**: 5-methyl; **10f**: 10formyl-; **SAH**: S-adenosylhomocysteine; **dUMP**: deoxyuridine monophosphate; **dTMP**: deoxythymidine monophosphate. Figure is taken from Smith A.D., Kim Y.I., Refsum H. (2008) Is folic acid good for everyone? Am. J. Clin. Nutr. 87: 517-533.

Although the precise mechanism behind FA nephrotoxicity is still unclear, the fact that folic acid-induced AKI shares similar features as human AKI, such as proximal tubular apoptosis and necrosis, cell proliferation and inflammation as well as fibrosis, it is considered as an experimental model that mimics human AKI (Gupta *et al.,* 2010). A recent mice study focused on FA induced AKI reported that the renal function was interrupted by increased pro-oxidant state after administration of 250mg/kg FA (Gupta *et al*., 2010). It was observed that serum BUN and SCr level significantly increased after the administration, followed by a significant 29.51% elevation of lipid peroxidation (LPO) level. On top of that, there was a significant drop of superoxide dismutase (SOD) activity by 32.25% accompanied by reduced activities of catalase (CAT) and glutathione peroxidase (GSH-Px) by 15.99% and 23.87% respectively, which indicated that FA might induce AKI by inhibiting antioxidant activities. Stallons and colleagues suggested FA could induce damage to kidneys by suppressing mitochondrial functions (Stallons *et al*., 2014). After intraperitoneal administration of 250mg/kg FA in mice, serum BUN level increased about 8-fold compared to control and SCr increased around 3-fold. In contrast, mitochondrial biogenesis regulators such as peroxisome proliferator gamma coactivator 1α (PGC-1α) and mitochondrial transcription factor A (TFAM) decreased 80% the day after administration of FA, and the expression remained at a low level even after day 14. Nuclear factor kappa-light-chain-enhancer of activated B cells (NF-kB) represent the family of transcription factors which regulate DNA transcription, inflammation and cell growth etc. It was demonstrated that along with significant elevation of serum BUN and SCr

level, the expression of relA, NF-kB2 and p53 increased by 4-fold, 8-fold and 9-fold respectively 12-hour after administration of FA in mice (250mg/kg). Treatment of NF-kB inhibitor reduced the expression of relA, NF-kB2 and p53, as well as SCr level, suggesting that NF-kB might play a vital role in regulating renal function after FA induced AKI (Kumar *et al*., 2015).

### 1.2.4 Biomarkers for AKI

Although RIFLE, AKIN and KDIGO classifications have remarkably contributed in diagnosing patients with AKI or the severities of AKI, the fact that all classifications are heavily dependent on the values of SCr and UO has been the biggest limitation, as both SCr and UO are not sensitive enough and are not AKI specific markers (Thomas *et al.*, 2015). Patient's age, gender, diet etc. are some factors that affect the value of SCr, and any previous kidney dysfunction would potentially affect SCr removal. On top of that, the baseline SCr is often unknown, although it could be estimated using the MDRD equation, the results are often not as accurate (Thongprayoon *et al.*, 2015; Thongprayoon *et al.*,2016). In addition, UO is challenging to measure without a urinary catheter, and its value could be changed by hypovolemic status and diuretics (Macedo *et al.*, 2011). With difficulty in accurately measuring two major factors of the classification system in defining the severity of AKI, the more sensitive and accurate novel biomarkers appear to improve the classification of AKI and identify the potential outcomes. Biomarkers are defined as a biochemical, physiological or genetic change which can suggest the initiation or the severity of a disease. Cellular damage is one of the prime consequences when the

kidneys are exposed to AKI, which leads to biological and molecular changes that enable biomarkers to be released and detected early (Beker *et al.*, 2018). The most researched novel biomarkers include neutrophil gelatinase-associated lipocalin (NGAL), interleukin-18 (IL-18) and kidney injury molecule-1 (KIM-1) etc.

The ability of a biomarker to predict AKI is shown using a receiver operating characteristic (ROC) curve, as shown in Figure 1.11. The ROC curve provides a full description of the sensitivity and specificity of a biomarker, it is a curve with sensitivity on the vertical axis and specificity on the horizontal axis. The closer the ROC curve to the top left corner, the better classification performance the biomarker has (Parikh *et al*., 2011). The area under the ROC curve (AUC) provides a measure of the clinical efficiency, the closer the value reaches 1, the better the performance is. For instance, an AUC of 1 indicates a perfect test as the sensitivity is 1 while specificity is 1, while an AUC of 0 is perfectly inaccurate.

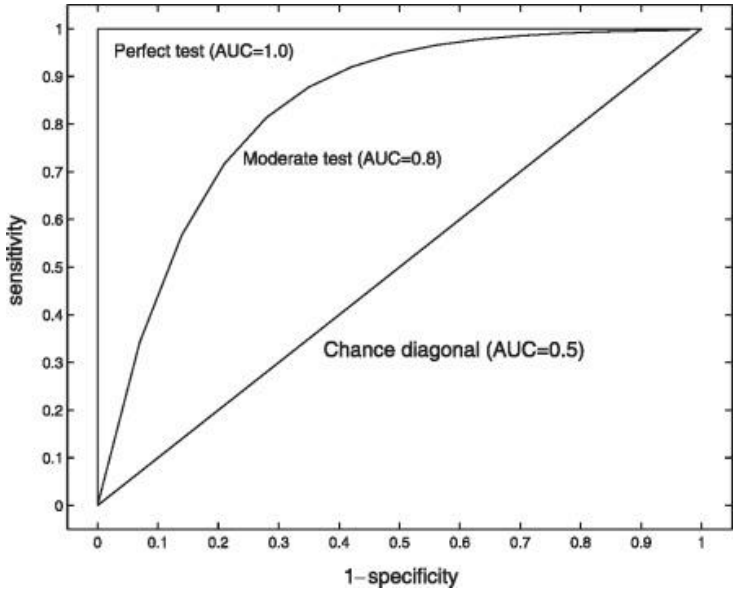


**Figure 1. 11 Example of a receiver operating characteristic (ROC) curve.**

The ROC curve shows a full description over the sensitivity and specificity of a biomarker. The area under the ROC curve (AUC) indicate the efficiency of the tested biomarker. Image taken from Devos A.K., Huffel S.V., Simonetti A. W., Graaf M.V.D., Heerschap A. and Buydens L.M.C (2007) Classification of brain tumours by pattern recognition of magnetic resonance imaging and spectroscopic data 11: 285-318.

### 1.2.4.1 Neutrophil gelatinase-associated lipocalin (NGAL)

NGAL is a 25kDa protein that belongs to the lipocalin superfamily. NGAL mainly functions in innate immunity, ion binding and oxidative stress response (Chakraborty *et al.*, 2012). NGAL is predominantly produced in the liver and white cells (Hvidberg *et al.*, 2005), minimum levels of which could be found in kidneys, lungs, and colon (Mishra *et al.*, 2003). Plasma NGAL is filtered in glomerulus and reabsorbed by proximal tubules, therefore once proximal tubule damage occurs, the reabsorption of NGAL would be interrupted, thus being released excessively in the urine.

With the support of further clinical and research evidence, NGAL is identified as one of the most upregulated genes in animal models soon after AKI especially ischemia-reperfusion injury (I/R) or nephrotoxic injury (Supavekin *et al.,* 2003; Mishra *et al.*, 2003; Mishra *et al.*, 2004). In a study focusing on children that were undergoing cardiopulmonary bypass (CPB) pointed out that the urine and plasma concentration of NGAL significantly increased after 2-6 hours after surgery among the children who developed AKI at the end (AUC>0.9), whereas AKI was defined as to have a 50% rise of serum creatinine within 24-72 hours after surgery (Mishra *et al.*, 2005). In comparison, the change of NGAL concentration was clearly more sensitive in response to the damage as well as in predicting potential AKI in children. Similar conclusion was indicated in another study targeting 374 children undergoing CPB, it was found that the concentration of plasma and urine NGAL were significantly elevated as soon as 2 hours after CPB (AUC ranged from 0.88-0.97) and both concentrations remained high for more than 48 hours (Krawczeski *et al.*, 2010).

A study focused on adults undergoing cardiac surgery pointed out that the concentration of the urinary and plasma NGAL significantly increased within 1-3 hours after the surgery in these who suffered from post-operative AKI, however, the AUCs for NGAL predicting AKI ranged from 0.61-0.96. The factors that potentially impacted the AUC values were the age groups, chronic disease, diabetes and previous kidney injuries (Perry *et al.*, 2010).

NGAL is also reported to be a biomarker for predicting nephrotoxic injury like contrast-induced nephropathy. In a study of children receiving elective cardiac catheterization, both plasma and urine NGAL increased significantly 2 hours after contrast administration, which predicted contrast-induced nephropathy with an AUC of 0.91-0.92 (Hirsch *et al.*, 2007). Similar conclusion was suggested from an adult study in which NGAL predicted contrast-induced nephropathy with an average AUC of 0.894 within 6 hours of administration (Haase *et al.*, 2009).

These studies suggested that NGAL could be a helpful biomarker that predicts the occurrence of AKI, however, the reported concentrations of urinary and plasma NGAL from clinical reports are highly variable and makes it difficult to generate a standard value to define AKI. Both concentrations could be affected by other coexisting conditions. For example, plasma NGAL concentration could be altered by chronic kidney disease (CKD) and other inflammatory conditions coexisting in patients (Devarajan *et al.*, 2010; Misnefes *et al.*, 2007). Overall, NGAL showed a promising sensitivity and result for early detection of AKI in clinical practice, however the concentration of which is highly variable and

dependent on the underlying coexisting conditions, therefore the concentration to define AKI might not be generalized.

#### 1.2.4.2 Interleukin-18 (IL-18)

IL-18 is a proinflammatory cytokine from the IL-1 family of cytokines. It is typically synthesised as an inactive 23kDa precursor by proximal tubular epithelial cells, macrophages etc., when it is activated, it turns into an 18.3kDa cytokine by caspase-1 (Dinarello C.A., 2007) and is a sensitive biomarker of ischemic injury in heart, kidneys and brain. IL-18 is expressed in the distal tubules, the collecting duct and the connecting tubules of the kidneys (Beker *et al.*, 2018) and could be easily detected in the urine when the kidney is undergoing I/R injury in animal studies (Melnikov *et al.*, 2001).

Studies found that among all patients who suffered from respiratory distress syndrome and developed AKI later on, the urinary IL-18 level significantly increased even 24 hours prior to the upregulation of serum creatinine level, with an AUC of 0.73 (Parikh *et al.*, 2005). In another study on children undergoing CPB who developed AKI, the level of urinary IL-18 started to increase 6 hours after CPB and reached the highest level at around 12 hours after CPB with an AUC of 0.75 (Parikh *et al.*, 2006). Also, a study on adults who developed AKI reported that in that study, the urinary level of IL-18 had an AUC of 0.62 in diagnosis of AKI, and the level of urine IL-18 in patients who had pre-renal AKI was significantly higher than those who did not have pre-AKI (Kokkoris *et al.*, 2013). All evidence suggested that the increase of urinary IL-18 is associated

with AKI, and the fact that it could be found as early as 4-6 hours after I/R injury and could remain for up to 48 hours makes it a sensitive biomarker in diagnosing AKI (Slocum *et al.*, 2012). However, urinary IL-18 level does not only increase in response to I/R injuries, it also responds to sepsis, inflammatory arthritis etc. Such characteristics limit its sensitivity and specificity in predicting AKI (Haase *et al.*, 2015 and Beker *et al.*, 2018), the standardised clinical values of urinary IL-18 in diagnosing AKI remain to be developed.

#### 1.2.4.3 Kidney injury molecule-1 (KIM-1)

KIM-1, or T-cell immunoglobulin and mucin-domain-containing molecule-1 (TIM-1), was reported to show a significant increase in expression in the proximal tubules when the rats were undergoing I/R injury (Ichimura *et al*., 1998). It is a type 1 transmembrane glycoprotein whose expression is not detectable in the normal conditions, however when the kidney is under ischemic injury or nephrotoxic injury, the expression level of KIM-1 could be highly detected in the proximal tubule cells and urine (Obermuller *et al*., 2014).

In children who developed AKI post CPB surgery, the urinary KIM-1 level was elevated significantly within 12 hours and the AUC value of predicting AKI was 0.83 (Han *et al.*, 2008). Another supporting study claimed that among 86 children who suffered AKI after circulatory collapse, KIM-1 was the best biomarker compared with NGAL and IL-18 and had the highest AUC of 0.81 (Assadi *et al.*, 2019). However other studies suggested that KIM-1 alone was not sensitive enough to be used in predicting AKI. Urinary KIM-1 was measured immediately in 90 adults after cardiac surgery to predict the appearance of AKI,

the AUC of which was only 0.68 (Han *et al.*, 2009). This was further supported by a study on adults after cardiac surgery, the AUC of urinary KIM-1 in predicting AKI was only 0.55 (Ghatanatti *et al.*, 2014). Although evidence has shown urinary KIM-1 levels increase in response to AKI, it has been documented that the level of urinary KIM-1 also increases when patients develop renal cell carcinoma (Vanmassenhove *et al.*, 2013), which might decrease its specificity in predicting AKI.

#### 1.2.4.4 Combination of biomarkers

Although NGAL, IL-18 and KIM-1 are able to predict AKI respectively, however, the fact that the level of these biomarkers is not only elevated by the presence of AKI reduces their specificity and sensitivity. Recently, it has been suggested that a combination of a few biomarkers might increase the AUC in predicting AKI. In the same study which urinary KIM-1 was measured immediately on 90 adults after cardiac surgery to predict the appearance of AKI, the AUC for KIM-1 in predicting AKI was 0.68, while other biomarkers like NAG and NGAL were also measured and the AUC of which were 0.61 and 0.59 respectively. When the combination of the three biomarkers was evaluated together, the combination AUC was higher than any of the biomarkers individually and reached 0.75 (Han *et al.*, 2009). Another study tracked the performance of nine biomarkers in predicting AKI, it was concluded that the combination of KIM-1, NGAL, hepatocyte growth factor (HGF) and total protein had the best performance with a better AUC of 0.94 compared to other biomarkers individually (Ghatanatti *et al.*, 2014). Other combinations like NGAL and

Liver-type fatty acid-binding protein (L-FABP) increased the prediction AUC to 0.93 compared to other individual biomarkers performed in the same study (Wasung *et al.*, 2015). All evidence suggested that evaluating the combination of a few biomarkers provided a higher sensitivity and specificity in early detection of AKI.

Even though there are sufficient evidence to support that the expression of specific biomarkers could be elevated, and by evaluating one or a combination of a few biomarkers may predict the appearance of AKI, it is worth mentioning that the novel biomarkers are still not the primary choice in clinical practice yet as there are still few concerns over their specificity in predicting AKI. First, each biomarker might respond to a few different clinical settings such as sepsis, inflammatory arthritis etc. therefore by simply evaluating the level of certain biomarkers may not provide the most accurate results. Secondly, it was reported that the performance of biomarkers might differ from different age group, for example, NGAL generally works better in children than adults in predicting AKI. Biomarkers in the specific population like the elderly might not have the same sensitivity compared to adults and children. In addition, in each study, the performance of biomarkers was reported to be specific to the type of clinical setting such as CPB or cardiac surgery, however, those data could not be applied to other clinical settings such as AKI induced by nephrotoxic drugs. Such characteristics limit the performance and accuracy of the novel biomarkers, therefore unless further studies could demonstrate the usefulness of the biomarkers and generate a standard value that could cover all age

groups, otherwise classic AKI marker like serum creatinine could not be replaced (Pozzoli *et al.*, 2017).

### 1.2.5 Treatments for AKI

#### 1.2.5.1 Antioxidants

Oxidative stress commonly occurs when kidneys were under acute damage, it is one of the most crucial factors that is relative to multiple pathologies during AKI. Oxidative stress is induced when the creating and eliminating rate of oxidant is not balanced, which is a common cause of certain disease such as ischemia and ageing (Sorg, 2004; Salmon *et al.*, 2010). Reactive oxygen species, which are oxidative stress-mediated molecules, are extremely reactive molecules that could be toxic to lipids and DNA and therefore result in interruption of normal cellular functions (Palipoch, 2013).

vitamin C (ascorbate) has received a rising interest acting as an antioxidant against ROS damage developed by renal I/R injury, nephrotoxic drug-induced injury in both animal models and human studies (Dennis *et al.*, 2017). Ascorbate acts as a cofactor for cytoplasmic prolyl hydroxylases, which contributes to the activation of hypoxia-inducible factors (HIF) as well as increasing the expression level of pro-survival glycolytic and angiogenic genes (Du *et al.*, 2012). A large number of studies have illustrated that ascorbate could inhibit biomolecule oxidation in humans as it could interact with a wide range of ROS (Carr *et al*., 1999; Buettner 1993). In multiple animal studies focusing on renal ischemia-reperfusion injury in rats, when animals were pre-treated with

sufficient amount of vitamin C (100mg/kg or 250mg/kg were used in different studies), there was a significant reduction in tissue lipid oxidation and an increase in tissue GSH and nitrate/nitrite, the damage induced by AKI such as serum urea level, creatinine level and tubular injury were significantly reduced (Korkmaz *et al*., 2009; Koul *et al*., 2015; Zhu *et al*., 2016). Similar conclusions were demonstrated (Groebler *et al*. 2012; El-Shafei *et al*., 2016) that when rats under nephrotoxic drugs induced AKI were supplied with vitamin C at dosage of 100mg/kg intraperitoneally immediately, the tissue oxidation level was significantly decreased, as was the inflammation level as well as the expression level of monocyte chemoattractant protein 1 (MCP- 1) and mitogen-activated protein kinase (MAPK). A significant reduction of urea and creatinine levels was also observed, as well as significant normalisation of epithelial brush border. The reno-protective functions of vitamin C might derive from its well-known antioxidant activity and maintaining GSH activity through its biochemical activity or physiological role (Dennis *et al.*, 2017).

Mitochondrial damage has been shown by multiple studies to contribute to tubular cell death in AKI. Mitochondria do not only provide ATP to maintain normal cell activities but also regulate several cellular functions such as cell proliferation (Ishimoto *et al.,* 2016). When tubular cells are exposed to low oxygen level, cellular injury occurs because of ATP depletion (Thadhani *et al*., 1996), the sudden decrease of ATP changes the cytoskeletal structure of epithelial cells, which then leads to the loss of brush border and cell apoptosis (Shafuddin *et al.,* 2011). The interruption of mitochondrial function enhances the generation of ROS which makes mitochondria one of the main contributors

to other diseases (Jankauskas *et al*., 2012; Ishimoto *et al*., 2016). It has been reported that under the condition of nephrotoxic injury, the presence of mitochondrial fragmentation exacerbates the injury (Brooks *et al.*, 2009). Recently, several mitochondria-targeted antioxidants have been demonstrated to have reno-protective effects on cells in AKI. They were shown to significantly inhibit the development of oxidative stress as well as promote mitochondrial biogenesis. Decylrhodamine 19 (SkQR1), a mitochondria-targeted compound of the SKQ group, was shown to have reno-protective functions in AKI under conditions relative to an elevation of ROS level in tubular cells such as ischemia and glycerol-induced AKI (Plotnikov *et al*., 2011). Jankauskas and colleagues showed that pre-treating EaHy926 cells with SKQR1 at 25nM for 1 hour could increase the viability by 18% when cells were exposed to I/R injury. Their *in vivo* experiment showed that by treating rats with SKQR1 (100nmol/kg) 3 hours before, 18, 30 and 42 hours after I/R injury, the level of SCr and BUN were significantly decreased compared with I/R group and reduced the effect on endothelial function (Jankauskas *et al*., 2016). d-Arg-2′, 6′-dimethyltyrosine-Lys-Phe-NH2, also known as SS-31, is a mitochondria-targeted, water-soluble compound that was demonstrated to diminish oxidative stress induced by I/R injury both *in vivo* and *in vitro* (Whiteman *et al.,* 2008; Calkins *et al*., 2011; Reddy *et al.,* 2011; Szeto *et al*., 2011; Cao *et al.,* 2012). It was reported that pre-treating human kidney tubular cells (NRK52E) with SS-31 4 hours before inducing hypoxic injury could significantly increase cell viability as well as reduce ROS generation (Zhao *et al*., 2013). In a rat model of I/R injury, Szeto et al demonstrated that treatment with SS-31 could protect mitochondrial

structure, promote ATP recovery as well as decrease cellular apoptosis and necrosis (Szeto *et al*., 2011). Although the exact mechanism of SS-31 reduces oxidative stress is not fully understood yet, studies have indicated the reno-protective function of SS-31 in prevention and treatment of AKI.

#### 1.2.5.2 Dietary nutrients

Yoon and colleagues (2008) suggested that sulforaphane, which is a compound commonly found in cruciferous vegetables such as cauliflowers and cabbages, would induce NF-E2-related factor-2 (Nrf2) antioxidative system to fight against I/R injury. Similar antioxidative activities was also reported by Hsu in 2010 and 2011 to protect against contrast-induced AKI. It has also been shown that two extracts from soybean have reno-protective functions over AKI. Demirbilek and colleagues found that the extract polyenylphosphatidycholine protected against AKI by decreasing the level of aspartate aminotransferase in the serum as well as the expression of NF-kB and blood urea nitrogen (Demirbilek *et al.*, 2006). Another extract named isoflavone was shown to protect against I/R injury by inducing oxygenase (Watanabe *et al.*, 2007).

Resveratrol, a type of polyphenol which could be found in the skin of grapes and blueberries, is known for its benefits in preventing cancer, extending lifespan etc. (Howitz *et al.*, 2003; Baur *et al.*, 2006). It was reported that resveratrol improved renal microcirculation and had a protective role over tubular epithelium when animals were induced AKI via I/R injury and sepsis. Evidence suggested that resveratrol contributed in clearing out reactive

oxygen/nitrogen species, releasing nitric oxide and blocked apoptosis by inhibiting p53 (Holthoff *et al.*, 2012; Sener *et al.,* 2006; Chander *et al.*, 2006).

## 1.3 CELLULAR REPAIR PROCESS

After AKI, the surviving tubular cells can undergo a repair process. The proximal tubular cells lose their polarity and brush border which may lead to cell apoptosis if injury persists. The survivors then migrate and de-differentiate to tubular cells. Under normal repair process, the new de-differentiated cells then proliferate and differentiate to normal functional proximal tubule cells; however, in some cases, AKI may lead to abnormal repair process which may cause G2/M cell cycle arrest, release of connective tissue growth factor (CTGF) and TGF-β1, fibroblast proliferation and collagens I, III and fibronectin deposition (Figure 1.12).

For decades, patients who had AKI were commonly believed to be able to fully recover if they survived the acute injury (Canaud *et al*., 2015); however recent studies have shown that it is unlikely that kidneys, especially proximal tubules, are able to fully recover, and some studies also linked AKI to renal fibrosis and the development of chronic kidney disease (CKD) (Yang *et al*., 2010; Hsu C.Y., 2012). Endo and colleagues demonstrated that in their I/R mice model, the recovered proximal tubules in I/R treated group seemed to be shorter compared to control group, which indicated that the proximal tubule might not fully recover after AKI. It was also mentioned that after AKI, the proximal tubule complexity in I/R group was around 40% less than the control group, which resulted in

dysfunctional tubules and fibrosis. This may partially explain the later progression to CKD after patients survived AKI (Endo *et al*., 2015).

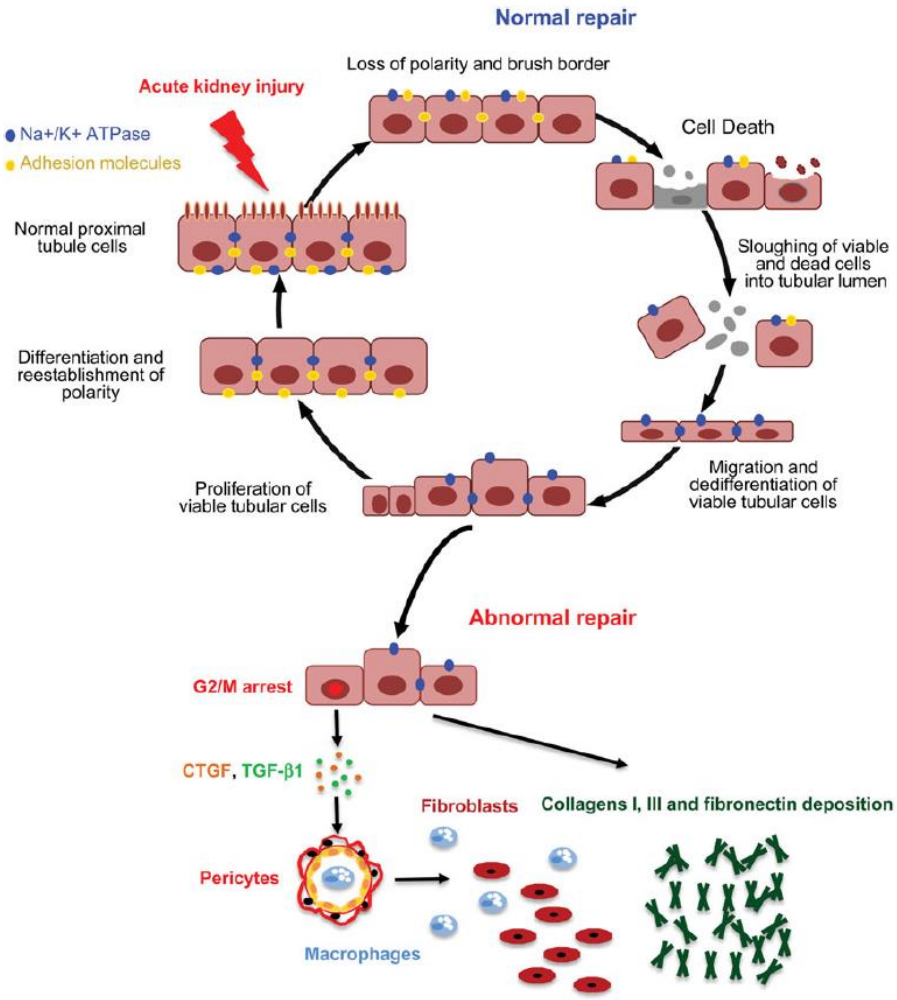


**Figure 1. 12 Normal repair process and abnormal repair process after AKI.**

Under most conditions, proximal tubular cells go through normal recovery process. When AKI occurs, the main target proximal tubular cells lose polarity and brush border, and cells undergo apoptosis and necrosis if injury persists. The surviving cells migrate and undergo dedifferentiation, proliferation and then differentiation to restore functional tubules. In some cases, abnormal recovery process may occur, which may cause G2/M cell cycle arrest, release of CTGF and TGF-β1, fibroblast proliferation and collagens I, III and fibronectin deposition. **CTGF**: connective tissue growth factor. **TGF-β1**: transforming growth factor beta-1. Figure is taken from Canaud G., Bonventre J.V. (2015) Cell cycle arrest and the evolution of chronic kidney disease from acute kidney injury. Nephrol Dial Transplant. 30: 575–583.

## 1.4 AIM AND OBJECTIVES

### 1.4.1 Aim of the project

The overall aim of this project is to identify the novel pathways involved in nephrotoxicity induced AKI and recovery.

### 1.4.2 Objectives

1. Develop a functional experimental model (*in vivo* and/or *in vitro*) which responds to nephrotoxic drug damage and be able to recover after the damage.
2. Develop a nephrotoxic drug at working concentration to be able to induce acute damage to *in vitro* model but not enough to damage the whole population. We aim to damage around 50% of the cell population (Figure 1.13), and analyse the gene expression and pathways involved during damage and recovery.

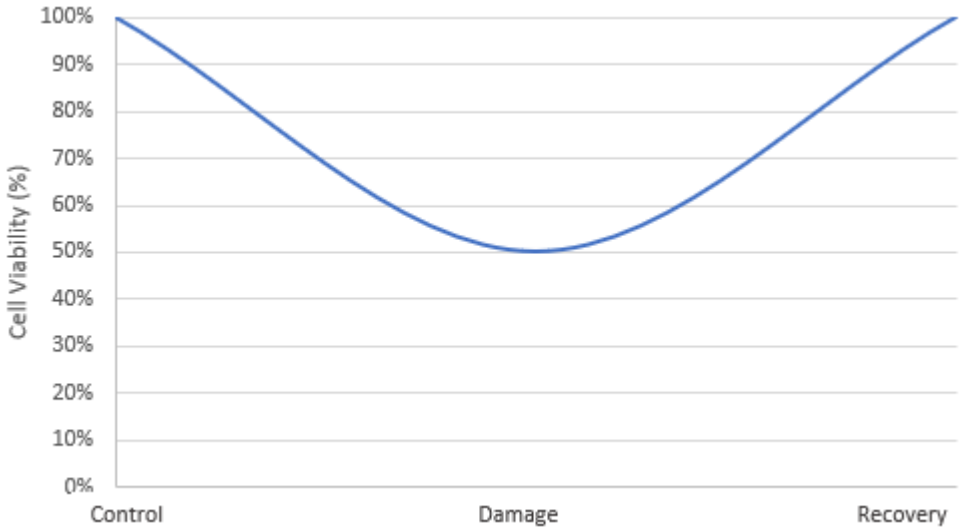


**Figure 1. 13 Experimental objectives in damage and recovery.**

# CHAPTER 2: GENERAL METHODS AND MATERIALS

## 2.1 CELL CULTURE

All cell culture work was carried out using sterile techniques inside an Escogobal Class II biological safety cabinet (Model AC2-4S1, Esco Micro Pte) and both cell types were cultured in a humidified incubator (Galaxy S+, RS Biotech) at 37°C with 5% $CO_2$ at all time.

### 2.1.1 Cell lines

#### 2.1.1.1 Human kidney 2 cells (HK2 cells)

Human kidney 2 is an immortalized human proximal kidney cell line that is derived from human normal kidney. HK2 cells are made from primary proximal tubular cells collected from adult human kidney cortex, then incubated with recombinant retrovirus that contain human papilloma virus (HPV 16) E6/E7 genes (Ryan *et al.*, 1994). HPV 16 E6/E7 genes have been proved to immortalize epithelial cells without changing their functions significantly. HK2 cells still retain some functions of normal proximal tubular epithelium, such as sodium dependent/phlorizin sensitive sugar transport and recovery after injury (Vousden, K., 1990; Hawley-Nelson *et al.*, 1989; Halbert *et al.*, 1991), therefore they are commonly used as an experimental model for renal damage and recovery.

HK2 cells were thawed from storage in liquid nitrogen at 37°C in water bath (Sub Aqua 26 Plus, Grant), and transferred to a T75 cell culture flask containing 12ml warm media. HK2 cells were incubated in a 37°C humidified incubator with 5% $CO_2$. The cells were maintained in Dulbecco's Modified Eagle's

Medium (DMEM) – 4500mg/L glucose, 110mg/L sodium pyruvate and 3700mg/L sodium bicarbonate, without L-glutamine (D6546, Sigma-Aldrich) supplemented with 100µg/ml penicillin-streptomycin (Pen Strep, 11548876, Gibco, Life Technologies Ltd.), 10% fetal bovine serum (FBS, 10500-064, Gibco, Life Technologies), and 1% L-glutamine (25030-024, Gibco, Life Technologies). The supplements were pipetted into DMEM and the mixed solution was sterile filtered through 500ml Filtration Systems (431097, Corning) prior to cell culture work. The media was changed every 48 hours and HK2 cells were sub-cultured every 5 days or when HK2 cells reached 80% confluence.

#### 2.1.1.2 Human embryonic kidney cells (HEK293 cells)

Human embryonic kidney cells (HEK293) were firstly obtained from a healthy legally aborted human foetus and were transfected by exposing them with sheared adenovirus type 5 DNA (Graham *et al.*, 1977). HEK293 cells are easy to be cultured and often used for cell transfection experiments and analysis for gene expression.

HEK293 cells were cultured under the same conditions and used the same media as HK2 cells (see 2.1.1.1 Human kidney 2 cells).

### 2.1.2 Splitting cells

Five Phosphate buffer saline tablets (PBS, P4417, Sigma-Aldrich) were added to 1L Elix water, mixed and autoclaved at 121°C for 15 minutes (MP24 Control System, Rodwell Scientific Instruments). To split HK2 cells, cells were washed

with warm sterile PBS solution, then add 2ml trypsin-EDTA solution (0.25% trypsin-EDTA, Gibco, Life Technologies) for 60 seconds in 5% $CO_2$ humidified incubator. 8ml media with 10% FBS was added in order to terminate the trypsin activity. The mixed solution was collected in a 20ml universal and spun at 1,000 rpm for 5 minutes in the centrifuge (5702R, Eppendorf UK, Ltd.). After discarding the supernatant, the cell pellet was resuspended in media and was diluted at 1 in 10 in T75 flask with 12ml fresh media.

### 2.1.3 Freezing and thawing cells

In this project, only cells between passage 10-30 were used to avoid alteration in gene expression. To maintain the stock of low passage cells, cells at low passage would be split and stored in liquid nitrogen for future use. Low passage cells were cultured until around 80% confluence in a T75 flask, after spinning cells down in a centrifuge (see 2.1.2 Splitting cells), cell pellet was resuspended with mixed solution which contained FBS and dimethyl sulfoxide (DMSO; D/4120/PB08, Fisher Chemicals) at 9:1 ratio. An 80% confluence T75 flask was plit into four CryoPure tubes (72.379, 1ml/cryovial, Sarstedt). The tubes were then placed in a Mr FrostyTM Freezing Container (5100-0001, Thermo Scientific TM) contained 100% isopropanol (P/7500, Fisher Scientific), then stored the container in the -80°C freezer to allow the cells slowly freeze overnight. CryoPure tubes were then transferred to liquid nitrogen in the cell culture for long-term storage.

To thaw frozen cells, CryoPure tubes were warmed up in the water bath at 37°C, as soon as the cells were thawed, they were transferred to a T75 flask

with 14ml DMEM media and then incubated overnight. DMEM would be refreshed the next morning.

### 2.1.4 Cell counting and seeding

In this project, cells were counted prior to experiments before seeding in order to maintain a constant number per well. Cells were counted using a Hawksley haemocytometer (BS748-AC1000). After the cells were resuspended in DMEM (see 2.1.2 Splitting cells), 10µl cell well-mixed suspension was added per chamber of the haemocytometer and an average of the three main chamber squares were calculated according to the following formula:

*Total cell number = Average cell number x $10^4$ x Total volume of cell suspension (µl)*

A set number of cells were seeded in different size of wells. The following formula was used to determine how much cell suspension needed for the specific cell number:

*Volume required= (Cell number required/Total cell number) x Total volume of cell suspension (µl)*

Different types of plates, amount of media in each well and seed cell number per well were listed in the following table (Table 2.1).

| Plates | Corning Product Number | Growth media(ml) | Cell number per well |
|---|---|---|---|
| **6-well plates** | 3516 | 2ml | $0.6 \times 10^6$ |
| **12-well plates** | 3513 | 1ml | $0.2 \times 10^6$ |
| **24-well plates** | 3526 | 1ml | $0.1 \times 10^6$ |
| **96-plates** | 3596 | 200µl | $0.05 \times 10^6$ |

**Table 2. 1 Different types of plates used in cell culture, volume of media needed in each well and seed cell number per well.**

### 2.1.5 Cell culture treatments

All treatments were prepared in the sterile cabinet and were sterilized before added into the cells. Folic acid (FA, F7876, Sigma-Aldrich), aristolochic acid (AA, A5512, Sigma-Aldrich) and hydrogen peroxide ($H_2O_2$, H1009, Sigma-Aldrich) were used as nephrotoxic treatment. AA and FA were made into stock solution according to manufacturer's manual and were stored at 4°C. To generate treatment solutions, stock solutions were diluted with serum free DMEM media prior to cell culture work. Control group was given FBS-free DMEM when AA or FA treatment was applied. The PH of the treatment solution including the control group was measured and adjusted to 7.5 after the solution was warmed up in the water bath at 37°C. All treatment solutions were freshly made prior to every experiment.

## 2.2 WOUND HEALING

HK2 cells were seeded into DMEM at a density of 0.6 x $10^6$ into a 6-well plate as described in section 2.1.4 cell counting and seeding. When the cells were at around 80% confluence, treatments were given for either 24 hours or 48 hours. After treatments were discarded, cells were gently washed with warm PBS to remove any treatment residue and discarded. Fresh DMEM was added and a sterile 1ml pipette tip was used to create a linear wound in each well including the control group. Six small cross shapes were marked on the lid on top of each well for the ease of finding the same spot every time the images were taken. Images were taken at one set corner of the cross shape after the wound was created and during recovery period up to 120 hours. Each treatment had triplicates in the same 6-well plate, and same treatment was repeated on other two plates at the same time as well.

## 2.3 3-(4, 5- DIMETHYLTHIAZOL-2-YL)-2, 5-DIPHENYLTETRAZOLIUM BROMIDE (MTT) ASSAY

Cells were grown in 96 well plate until around 80% confluence, the treatments were then added for 24 hours or 48 hours accordingly. After treatments, the treatment media was removed and 100µl fresh media without phenol red (21063- 029, Gibco, Life Technologies) was added in each well. 10µl of 12mM 3-(4,5- dimethylthiazol-2-yl)-2,5-diphenyltetrazolium bromide (MTT, V13154, Molecular Probes, Life Technologies) was added to each well and incubate the plate at 37°C incubator with 5% $CO_2$. After 4 hours of incubation, 85µl of mixed

solution was removed from each well, and 50µl of DMSO was added in each well, pipette up and down and left in the same incubator for 10 minutes. The plate was then read using a Model 680 XR microplate reader (Bio-Rad) at 550nm absorbance. A negative control of phenol red-free media with DMSO was also performed. Each treatment had at least triplicates in the same plate, and same treatment was repeated on other two plates at the same time as well.

Data from MTT assay were presented as 'cell viability', which was calculated as following formula:

*Cell viability = [(absorbance of treated cells – absorbance of negative control)/ (absorbance of control groups - absorbance of negative control)] x 100*

## 2.4 REACTIVE OXYGEN SPECIES (ROS) MEASUREMENT

The reactive oxygen species (ROS) was measured using fluorescent dye CM-$H_2$DCFDA (C6827, Invitrogen, Life technologies), and the experiment was performed according to protocol provided by manufacture. When this fluorescent dye CM-$H_2$DCFDA was exposed to the cells, it would be taken up by the cells and usually deacetylated by an intracellular enzyme. The oxidation of $H_2$DCF leads to fluorescent dichlorofluorescein which remain in the cells and could be detected.

Cells were seeded in black-walled 96 well plates 24 hours prior to the experiment. When cells reached about 90% confluence, treatments were added to the cells for different length of time according to experiment. Add 8.6µl

DMSO to each vial of CM-$H_2$DCFDA to get 10mM stock solution. Later 10mM stock solution would be diluted in HBSS to 5µM as working solution. The treatments were discarded and replaced with CM-$H_2$DCFDA working solution and incubated in the incubator for 60 minutes. The absorbance was read using a FLUORstar OPTIMA microplate reader at an excitation wavelength of 485nm and an emission wavelength of 520nm. A negative control of cells without fluorescent dye was also performed in each plate. Each treatment was at least triplicated in each plate and the treatment was repeated in other two plates at the same time.

## 2.5 IMMUNOCYTOCHEMISTRY

Cells were seeded on sterile 16mm circular glass coverslips (631-0152, VWR) in 12-well plates. After treatments, the cells were fixed with 4% paraformaldehyde (PFA, P/0840/53, Thermo Fisher Scientific) in PBS for 15 minutes at room temperature and followed by washing with PBS three times, 5 minutes each. Cells were then blocked with blocking buffer which contained 10ml PBS, 0.5g bovine serum albumin (BSA, 11423164. Sigma-Aldrich) and 50µl Triton X-100 (93420, Sigma-Aldrich) per 10ml solution. Selected primary antibody was diluted with the antibody dilution buffer which per 10ml contained 10ml PBS, 0.1g BSA and 30µl Triton X-100. Primary antibodies were diluted at 1:200 ratio by either slowly pipetting up and down or reversing the tube gently. After blocking for 60 minutes at room temperature, coverslips were then incubated with diluted primary antibody overnight at 4°C in a humidified chamber. The next morning the coverslips were washed with PBS three times,

5 minutes each. In the meantime, secondary antibodies were gently diluted with dilution solution at 1:500 ratio. After washing, coverslips were incubated in the same humidified chamber with secondary antibody for 2 hours in the dark at room temperature. After incubation, the coverslips were washed with PBS three times, 5 minutes each again before they were mounted on microscope glass slides (Adhesion slides, Polysine, VWR International) with Fluoroshield mounting medium with DAPI (ab104139, Abcam). The slides could then be used for imaging or stored at 4°C in the dark for long-term storage or at room temperature for short-term storage. Immunofluorescence microscopy was carried out using a Leica CTR 5000 digital microscope (Leica Microsystem) and images were taken using a Leica DFC420 microscope camera. Overlay images were generated using Leica Application Suite v.3.8 software. Any digital modifications were carried out in an identical manner for all sets of experiments. Three randomly chosen fields were captured per slide.

## 2.6 NUCLEAR EXTRACTION

Cells were seeded and cultured in a T75 flask. After treatments, cells were gently washed with ice-cold PBS, PBS was then discarded. 2ml fresh ice-cold PBS was added to the flask and cells were carefully scraped off then transferred to a 10ml tube. The tube was then placed in the centrifuge and spun at 10,000rpm for 5 minutes, the supernatant was discarded. The cells were washed with 5ml ice-cold PBS by gently pipetting up and down, then spun at 10,000rpm for 5 minutes, the supernatant was discarded. This washing process was repeated twice. The cell pellet was transferred to a pre-chilled eppendorf

and gently resuspended with 500µl 1xhypotonic buffer by pipetting up and down and incubated on ice for 15 minutes. After incubation, 25µl Triton X-100 was added and the eppendorf was vortexed at the highest setting for 10 seconds before being placed in the centrifuge and spun at 30,000rpm for 10 minutes at 4°C. The supernatant was cytoplasmic fraction, it was carefully pipetted into a pre-chilled eppendorf and stored at -80°C. The left nuclei pellet was resuspended in 50µl complete cell extraction buffer and incubated on ice for 30 minutes, vortexed every 10 minutes at the highest setting for 10 seconds. The complete cell extraction buffer was freshly prepared before the isolation by mixing every 5ml cell extraction buffer (FNN0011, Thermo Fisher Scientific) with 17µl 1mM phosphatase inhibitor and 250µl protease inhibitor cocktail to inhibit proteolysis in cell extracts. After the incubation, the nuclei mixture was spun at 14,000rpm at 4°C for 30 minutes in the centrifuge. The supernatant was nuclei fraction, it was carefully pipetted into a fresh ice-chilled eppendorf and stored at -80°C. Prior to running western blot analysis on the nuclei and cytoplasmic samples, an equal volume of 1xSDS was added to each sample to allow it to be run in a PAGE gel.

| **Reagent** | **Final concentration** |
|---|---|
| **Tris-HCL PH=7.4** | 20mM |
| **Sodium Chloride** | 10mM |
| **Magnesium Chloride** | 3mM |

**Table 2. 2 Reagents used for 1xhypotonic buffer.**

## 2.7 AGAROSE GEL ELECTROPHORESIS

Agarose gel electrophoresis was used to analyse the presence and size of the interested PCR products and nucleic acid in this project. Gel electrophoresis allowed DNA fragments and nucleic acid to be pulled through agarose gel matrix by 100V electric current and separated according to size. Therefore, the smallest sized fragment moved the fastest.

### 2.7.1 Making 1% (w/v) agarose gel

50xTAE buffer (H19109, Flowgen bioscience) was diluted into 1xTAE working solution by mixing with Elix water prior to agarose gel making process. Agarose powder (BP1356-500, Thermo Fisher Scientific) was measured and transferred to a clean conical flask, an appropriate volume of 1x TAE buffer was added to the conical flask to a final concentration of 1% (w/v) agarose solution. The conical flask was heated in a microwave at full power and gently swirled every 30 second. Once the agarose solution started to boil and turned clear, the conical flask was carefully taken out of the microwave and gently swirled with the top away from the body. The boiling agarose solution was quickly cooled down by running cold tap water over the conical flask base while continuing gently swirling the flask until the base could be handled. The cooled agarose solution was poured in RunOne Electrophoresis System' (Embi Tec) tray with appropriate comb placed towards the top of the gel tray and tape at the either end of the gel tray. The agarose gel was left at room temperature to set. Once the gel was set, the comb was removed, and the gel was stored with 1xTAE at 4°C sealed with clingflim.

### 2.7.2 Performing agarose gel electrophoresis

Before running the gel, tape was removed from the ends of the gel tray before the gel tray was submerged in 1xTAE buffer in the electrophoresis tank. 6x loading buffer (G190A, Promega UK) was used at final concentration of 1x to load sample volumes. Samples were kept on ice until used. A DNA ladder (Bio-33056, Bioline Meridian Bioscience) was loaded to the left end of the gel to provide a guide for the size of DNA. After running the gel at 100V for around 20 minutes or when the dye from the loading buffer had reached the bottom of the gel, the electrophoresis was turned off and the gel was transferred into ethidium bromide for at least 20 minutes. The gel was then transferred into clear water for another 20 minutes before it was read using ultraviolet (UV)-transilluminator (Gel Doc 2000, BioRad).

## 2.8 REAL TIME QUANTITATIVE PCR

### 2.8.1 Collecting cell samples for RNA extraction

Cells were seeded in T25 flasks or T75 flasks and incubated until around 80% confluence before treatments were given. After treatments, 10ml ice cold RNase-free PBS was added in each flask and a sterile 25cm cell scraper (83.1830, Sarstedt) was used to dislodge the attached cells. The cell-PBS mixture was then transferred to a sterile 30ml universal tube (128AP, Thermo Scientific) and was spun down to a cell pellet at 0°C. The cell pellet was resuspended with 1ml ice cold PBS and transferred to a 1.5ml eppendorf before

it was centrifuged again. After discarding the supernatant, the cell pellet was kept on ice before it was stored at -80°C.

### 2.8.2 RNA extraction

Total RNA was extracted from cells using a RNeasy Mini Kit (74104, Qiagen) following manufacture's protocol in a MACH-AIRE fume cupboard. To prepare for an RNA extraction, 10µl of β-mercaptoethanol (β-ME, M6250, Sigma-Aldrich) was added to every 1ml buffer RTL to obtain buffer RTL working solution, and four volumes of ethanol were added to buffer RPE and 550µl RNase-free water was added to Lyophilised DNase 1 (79254, Qiagen) to obtain DNase 1 stock solution. DNase 1 stock solution was mixed by gentle inversion and aliquoted to small volume and stored at -20°C.

350µl of buffer RTL working solution was added to each eppendorf with cell pellet, and a 1ml syringe (300013, BD Plastipak) with a 0.9 mm hypodermic needle (3301300, BD Plastipak) were used to homogenize the cells until they were uniformly homogeneous. The mixture was then spun down at 13,000rpm for 3 minutes in a Microfudge 22R microcentrifuge. After transferring the supernatant to a 1.5ml microcentrifuge tube, 350µl of 70% ethanol was added to the lysate and mixed immediately by pipetting the mixture up and down. 700µl of the mixture was transferred to a RNeasy spin column placed in a 2ml collection tube, and spun down at 12,000rpm for 15 seconds. The fluid in the collection tube was discarded. 350 µl buffer RW1 was added to the spin column and then spun down for 15 seconds at 12,000rpm. The fluid in the collection tube was discarded again. 10µl DNase 1 stock solution was added in 70µl buffer

RDD and mixed gently, then 80µl mixed solution was added to each spin column and incubated 15 minutes at room temperature. 350µl buffer RW1 was then added and spun down at 12,000rpm for 15 seconds, and the fluid in the collection tube was discarded. 500µl buffer RPE was added to the spin column membrane and spun down at 12,000rpm for 15 seconds, the fluid in the collection tube was discarded. 500µl buffer RPE was added to the spin column membrane again and spun down at 12,000rpm for 2 minutes in order to wash the membrane. The old collection tube was then discarded and a new collection tube was replaced. After spun down at 12,000rpm for 2 minutes, the collection tube was replaced by a 1.5ml eppendorf. 30µl RNase-free water was added directly to the column membrane and spun down at 10,000rpm for 1 minute to elute the RNA. RNA samples were then aliquoted 2µl for quality and quantity assessment, and the rest were stored at -80°C.

### 2.8.3 Total RNA quality and quantity

The concentrations of RNA were assessed using a NanoDrop 2000 spectrophotometer (Thermo Fisher Scientific) by pipetting 1.5µl RNA aliquots onto the pedestal and the absorbances were read. The purity of the samples was assessed by absorbance ratio at 260:280nm, and the closer the ratio is 2, the purer the RNA sample was. The RNA sample quality was further assessed by running each sample on 1% (w/v) agarose gel. RNA sample was mixed with 6x loading buffer by pipetting and loaded to each well of 1% (w/v) agarose gel. Intact RNA sample on agarose gel showed clear band for 18S and 28S ribosomal RNA at around 2:1 ratio of intensity. All RNA samples were then

diluted to 50ng/µl concentration with RNase-free water (10977035, Gibco, Life technologies) and stored in aliquots at -80°C.

### 2.8.4 cDNA synthesis

The first strand complimentary DNA (cDNA) was synthesised from RNA at 50ng/µl using RevertAid RT Kit (K1691, Thermo Fisher Scientific), following the protocol provided by the manufacturer.

As described in Table 2.3, 10µl 50ng/µl RNA was mixed with 1µl random Hexamer primer into a sterile, nuclease-free tube on ice, another 1µl Nuclease-free water was added to the tube. After being mixed gently and centrifuged briefly, the tubes were incubated at 65°C for 5 minutes in a GeneAmp PCR system 9700 (Thermo Fishes Scientific) followed by chilling on ice. The reagents described in Table 2.4 were added to each tube in the indicated order. After being mixed gently and centrifuged briefly, the tubes were transferred to a GeneAmp PCR system 9700 and incubated at 25°C for 5 minutes, followed by 42°C for 60 minutes. The reaction was terminated by heating up to 70°C for 5 min and cooled to 4°C. cDNA was diluted 1:5 by adding 80µl RNase-free distilled water to give a final volume of 100µl of neat cDNA. The neat cDNA samples were stored at -80°C for long-term storage.

| Reagent | Specification | Volume (µl) |
|---|---|---|
| **Template RNA (50ng/µl)** | 500ng total RNA | 10 |
| **Primer** | Random Hexamer primer | 1 |
| **Water** | Nuclease-free water | To 12 |
| **Total Volume** | | 12 |

**Table 2. 3 Step 1 of RevertAid RT Kit cDNA synthesis, mixture of reagents for each reaction.**

| Reagent | Volume (µl) |
|---|---|
| **5x Reaction Buffer** | 4 |
| **RiboLock RNase Inhibitor (20U/µl)** | 1 |
| **10mM dNTP Mix** | 2 |
| **RevertAid RT (200U/µl)** | 1 |
| **Total Volume** | 20 |

**Table 2. 4 Step 2 of RevertAid RT Kit cDNA synthesis, mixture of reagents for each reaction.**

### 2.8.5 Primer design

Primers were designed using Primer Express Software Version 3.0.1 (11983, Applied Biosystems). Table 2.5 shows the primer information of studied genes.

| Gene | Forward (F) and reverse (R) primer sequences (5’ to 3’) |
|---|---|
| GAPDH | F: ATATGATTCCACCCATGGCA<br>R: TGGAAGATGGTGATGGGATT |
| IL-18 | F: TGTAGAGATAATGCACCCCG<br>R: GCCATACCTCTAGGCTGGCT |
| TGFB1 | F: GTGGAAACCCACAACGAAAT<br>R: CGGAGCTCTGATGTGTTGAA |

**Table 2. 5 Real time PCR primers used for this study.**

### 2.8.6 Real time quantitative PCR (RTqPCR)

RTqPCR was performed using a Roche Lightcycler 480 (Roche Diagnostics), it was used to measure the relative mRNA transcript abundance for a gene in the sample. The primers used in RTqPCR were generated using Primer Express software 3.0.1 on exon-exon boundaries (Thermo Fisher Scientific) and were purchased from Sigma-Aldridge. Once the primers arrived, diluted the primers into 100μM stock solution according to the manufacturer's protocol, aliquot 10μl of the stock solution and further dilute to 10μM working solution to be used in RTqPCR experiment. All primers were tested via melt-curve analysis using Roche Lightcycler 480 and stored at -20°C. After generating first strand of cDNA, the primer designed specifically for each gene would amplify the targeted sequences of cDNA, generating a double stranded DNA product. LightCycler 480 SYBR Green I master (04887352001, Roche Dagnostics) was used to intercalate between double stranded DNA to generate a fluorescent signal, therefore enables further quantification. To prepare for RTqPCR, reagents listed in Table 2.6 were mixed to a master-mix for the total number of samples for each targeted transcript. When loaded to 384-plate, 10μl of the master-mix was loaded to each well followed by 5μl of neat cDNA sample performed in triplicate, including a negative control with only RNase-free distilled water. The template was used in RTqPCR was described in Table 2.7. The fluorescent signal could only be detected if it is increased above a threshold value, once it crossed the threshold, the cross point (Cp) value was marked. Cp value indicates the number of cycles taken for the signal to be detected,

therefore the lower the Cp value is, the higher level of targeted transcript is in the sample.

| | **Volume (µl)** |
|---|---|
| **SYBR Green I Master** | 7.5 |
| **Forward Primer** | 0.45 |
| **Reverse Primer** | 0.45 |
| **RNase-free distilled water** | 1.6 |
| **Total Volume** | 10 |

**Table 2. 6 Volumes of reagents used in RTqPCR in each reaction.**

| | Temperature (°C) | Time | Number of Cycles |
|---|---|---|---|
| **Initial Denaturation** | 95 | 10min | 1 |
| **Denaturation** | 94 | 45s | 30 |
| **Annealing** | 58 | 45s | |
| **Extension** | 72 | 45s | |
| **Final Extension** | 72 | 4min | 1 |
| **Cooling/Hold** | 4 | ∞ | 1 |

**Table 2. 7 RTqPCR program template used for Roche LightCycler 480.**

## 2.9 WESTERN BLOT

### 2.9.1 Western blot samples collection

Western blot analysis was used to quantify the specific protein level in the sample. A 10ml stock of 2xsodium dodecyl sulfate (SDS) solution was prepared prior to experiment as described in the Table 2.8. The stock 2xSDS was aliquoted and stored at -20°C. Cells were grown in 6-well plates and treated accordingly, each treatment was at least performed in triplites in at least three different plates. A tablet of inhibitor protease (04693124001, Roche) and phosphatase (04906845001, Roche) inhibitors were dissolved in 1ml RNase-free water and appropriate amount was added in 1x SDS working solution to a final dilution of 1x prior harvesting cells to prevent protein degradation by proteolytic enzymes. Media or treatment was completely removed from each well and 250µl of 1xSDS was added. Samples were scraped and pipetted into a labelled 1.5ml eppendorf and kept on ice during harvesting. Samples were stored at -20°C for short-term use or -80°C for long-term storage.

| | Volume (ml) | Product Code |
|---|---|---|
| **Glycerol** | 2 | G5516, Sigma-Aldrich |
| **1M Tris-HCl (pH 6.8)** | 1.25 | NA |
| **SDS Solution (10% w/v)** | 4 | NA |
| **1M DTT (0.154g/ml)** | 1 | D9779, Sigma-Aldrich |
| **Bromophenol Blue** | Tiny bit | 53H3640, Sigma-Aldrich |
| **RNase-free water** | 1.75 | NA |
| **Total** | 10 | |

**Table 2. 8 Volumes of reagents used to make 10ml 2xSDS solution.**

### 2.9.2 Quantification of protein concentration

The protein concentration of samples was quantified using 2D-quant kit (80-0483-56, GE Healthcare Life Sciences) according to the manufacturer's protocol. Prior to 2D quant analysis, samples were heated to 95°C for 5 minutes to denature the protein. Samples were spun down at 13,000rpm for 3 minutes Microfuge 22R microcentrifuge (Beckham Coulter) and left on ice. 1ml working solution of colour reagent was prepared for each sample by mixing one unit of Colour Reagent B with 100 unit of Colour Reagent A. A standard curve was generated by adding 0µl, 5µl, 10µl, 15µl, 20µl and 25µl of the supplied stock of

2mg/ml BSA standard solution to six clean microcentrifuge tubes, to generate final protein quantity of 0µg, 10µg, 20µg, 30µg, 40µg and 50µg. 10µl of each sample was pipetted in a clean 1.5ml microcentrifuge tube, 500µl Precipitant Solution was added to all samples including standard curve. Samples were vortexed briefly and incubated at room temperature for 2-3min. 500µl Co-precipitant Solution was added to every tube, vortexed briefly then centrifuged at 13,000rpm for 10 minutes at 0°C. A protein pellet should be visible after centrifuge. Supernatant was carefully removed from each tube. Samples were centrifuged again and the remaining supernatant was carefully removed. 100µl Copper Solution was added to each tube and followed by 400µl Elix water. The tubes were vortexed until the protein pellet was fully dissolved. 1ml working solution of colour reagent was added to each tube and mixed by inversion, then incubated at room temperature for 15 minutes. Each sample was then transferred to a cuvette (67.742, Sarstedt) and absorbance was read within 40min of the Colour reagent being added at 480nm on a UV/Vis Spectrophotometer (Ultrospec III, Pharmacia LKB). Elix water was used as a reference. The standard curve was generated in Microsoft Excel for protein quantity related to absorbance values, an equation was generated accordingly, therefore the concentration of samples was quantified. Samples were then normalised with 1xSDS and were stored at -20°C for short-term use or -80°C for long-term storage.

### 2.9.3 Polyacrylamide gel electrophoresis (PAGE)

Samples were thawed on ice prior to western blot analysis. 10X Tris-glycine-SDS PAGE Buffer (EC-870, National Diagnostics) was diluted 1:10 with Elix water for 1x running buffer. A 4-15% Criterion TGX Precast Midi Protein Gel (18-well: 5671084; 26-well: 5671085, BIO-RAD) was removed from the packaging, as well as the comb from the top and green tape from the bottom of the gel cassette. The precast gel was slotted securely and fully submerged in 1x running buffer within the gel tank. Equal amount of sample was loaded in each lane (30µl for 18-well and 15µl for 26-well) as well as 8µl of SDS protein standard (1610373, BIO-RAD) to provide a marker of protein sizes. The gel was run on a Bio-Rad Criterion Cell at 200V for 35 minutes or before the smallest protein marker run off the bottom of the gel.

Transfer buffer (described in Table 2.9) was made and thoroughly mixed with a magnetic flea and magnetic stirrer plate (HB502, BIPPY) while running polyacrylamide gel electrophoresis. Three sponges, an appropriately sized nitrocellulose membrane (Amersham Protran Supported 0.45 NC, 10600018, Amersham, GE Healthcare) and six pieces of sponge-sized filter paper were soaked in transfer buffer for 15 minutes prior using. Once PAGE stopped, the gel was carefully removed from the plastic cassette, the top right corner was cut to orientate the gel. A transfer cassette was set up in the following order: black side of the cassette, two sponges, three pieces of filter paper, PAGE gel, nitrocellulose membrane, three pieces of filter paper, a sponge and clear side of the cassette. After each layer was placed to the transfer cassette, small amount of transfer buffer was added on to each layer to prevent from drying

out, and bubbles were rolled out using a glass rod to prevent any interference during transfer. The transfer cassette was placed in the transfer tank filled up with transfer buffer, with gel placed closest to the negative electrode and nitrocellulose membrane closest to the positive electrode. A cooling system of two cooling coils was used to prevent overheating during transfer process. One of the coils was submerged in a box filled with ice and the other one was placed in the transfer tank. Running tap water was kept at a moderate speed throughout the transfer process and a magnetic stir bar was placed at the bottom of the transfer tank, keep spinning on top of a magnetic stirrer plate. The electric current for transfer was set to be at 0.5A for 2 hours.

| | **Quantity** | **Product Code** |
|---|---|---|
| **Glycine** | 60g | G8898, Sigma |
| **Tris Base** | 6g | BP152-1, Thermo Fisher Scientific |
| **Isopropanol** | 100ml | P7500, Thermo Fisher Scientific |
| **Elix Water** | Fill up to 2L | NA |

**Table 2. 9 Quantity of reagents used to make 2L transfer buffer.**

Once transfer process is finished, the transfer cassette was carefully taken out of the transfer tank. The nitrocellulose membrane was taken out and laid flat in a box and Ponceau-S stain was added to the membrane to check if the protein had been evenly transferred to the nitrocellulose membrane. The box was gently rocked forward and backward for about 2 minutes, and the excess Ponceau-S stain was poured back for future use. Stained nitrocellulose membrane was gently rinsed with Elix water until the Elix water run clear to remove excess Ponceau-S stain. The transferred protein was identified via the pink bands on the nitrocellulose membrane, excess nitrocellulose membrane was removed by a sharp scalpel blade and discarded.

10xTBS (described in Table 2.10) was made prior to the experiment, 1L 1xTBST working solution was made by 100ml 10xTBS solution, 1ml Tween-20 (P1379, Sigma Aldrich) and Elix water, and thoroughly mixed with a magnetic flea and magnetic stirrer plate.

The nitrocellulose membrane was then washed gently with 1xTBST on a rocker (SSL4, Stuart) for 10 minutes, repeated three times to remove the Ponceau-S stain. The nitrocellulose membrane was then blocked with 5% Marvel instant dried skimmed milk (Premier Brands UK) in 1xTBST for 1 hour at room temperature on the rocker at a low oscillation. Primary antibody was diluted to 1:1000 ratio with 5% milk in 1xTBST, the nitrocellulose membrane was incubated at 4°C overnight on a rocker. The next morning, primary antibody was replaced with 1xTBST and washed for 10 minutes, repeated at least three times. The nitrocellulose membrane was then incubated with the appropriate secondary antibody at 1:5000 ratio in 5% milk in 1xTBST for 1 hour at room

temperature on a rocker. The nitrocellulose membrane was then washed again with 1xTBST for 10 minutes, repeated three times.

| | Quantity | Product Code |
|---|---|---|
| **Sodium Chloride** | 90g | S/3169/65, Fisher Scientific |
| **Tris (1M, PH 7.5)** | 200ml | BP152-1, Fisher Scientific |
| **Elix Water** | Fill up to 1L | |

**Table 2. 10 Quantity of reagents used to make 1L of 10xTBS.**

ECL western blotting detection reagent (RPN2209, GE Healthcare) was used to detect the protein band. Lumino solution and peroxide solution were mixed in 1:1 ratio prior to adding to the nitrocellulose membrane. The nitrocellulose membrane was taken out of 1xTBST and placed on a plastic sheeting on a flat surface with protein side facing upward. Excess 1xTBST was gently dabbed off using a clean filter paper. Mixed detection reagent was pipetted on the nitrocellulose membrane evenly and the membrane was left at room temperature for 2 minutes. Excess detection reagent was removed gently, and the nitrocellulose membrane was placed in an X-ray cassette with taped plastic sheeting. The cassette was then taken to the dark room. High performance chemiluminescence film (28906836, GE Healthcare) was placed on the plastic sheeting in the cassette for various times in order to gain optimal exposure. The film was then removed from the cassette and place in the developer solution (1900943, GBX) for 2 minutes, then briefly washed with clean tap water before transferring to fixer solution (1758285, ILFORD HYPAM) for another minute. The film was then thoroughly rinsed with running tap water and dried in a drying cupboard (GelAir dryer, BIO-RAD). The nitrocellulose membrane was then washed with 1xTBST, the antibody could be stripped using restore plus western blot stripping buffer (46430, Thermo Scientifc). The membrane was then blocked again and labelled another antibody. Western blot film was imaged with Gel Doc XR+imaging system (Bio-Rad), relative band intensity was quantified by normalisation of integrated density for each sample to global background using Quantity One 4.6.8 Software.

## 2.10 ANIMAL EXPERIMENTS

### 2.10.1 Kidney processing and paraffin embedding

Fixed tissues were carefully washed three times with PBS for 20 minutes each, then left in 70% ethanol to dehydrate overnight at room temperature. The tissues were then transferred to 80%, 90% and 95% ethanol for 15 minutes each before they were transferred to 100% ethanol for 45 minutes at room temperature, fresh 100% ethanol was changed every 15 minutes. After dehydration, tissues were maintained in histo-clear (HS-202, Histo-Clear II, National Diagnostics) for 60 minutes, fresh histo-clear was replaced after the first 30 minutes. Histo-clear was then carefully removed by pipetting to leave as less histo-clear as possible, tissues were then maintained in liquefied paraffin wax at 60°C for 60 minutes twice. A small amount of liquid paraffin wax was place at the bottom of an appropriate sized mold and placed on the warm platform of a Leica EG1660 embedding centre (Leica Biosystems), the tissue was transferred to the mold and carefully oriented. A cassette was placed on top of the mold and fresh liquid paraffin wax was filled in until the top of the cassette was covered before transferring to the cold platform to allow the liquid wax to set. After approximately 15 minute or until the wax was completely solidified, the tissue block could be detached from the mold and stored at -4°C.

### 2.10.2 Kidney sectioning

The wax side of the tissue blocks were kept in ice for 20 minutes prior to section. A new microtome blade (3050835, MB35 premier disposable microtome blade,

Thermo Fisher Scientific) was placed securely on a Leica RM2235 manual microtome (Leica Biosystems Ltd.) and replaced when not sharp. For each new tissue block, microtome was set to trim 10µm wax off each time until tissue was exposed, then the microtome was set to trim 5µm tissue each time. The trimmed section was carefully transferred with brush and forceps to a glass plate with a few drops of 30% ethanol to mildly flatten the section before transferring to a Leica HI1210 water bath at 40°C (Leica Biosystems Ltd.). After a few seconds or until the section was completely flattened in the water bath, a microscope slide was used to mount the section on to the slide by vertically placing the slide close to the section, slowly moving towards the section and finally vertically moved away once section was mounted on. The slides were left vertically for about 5 minutes to drain the excess water before transferring to a 40°C Leica HI1220 flattening table (Leica Biosystems Ltd.) for 30 minutes to allow the slides to dry completely. The slides were then kept in microscope slide boxes and stored at room temperature.

### 2.10.3 Haematoxylin Eosin (H&E) staining

Haematoxylin and Eosin stain is a popular staining method in tissue histology in which the nuclei of the cells are stained blue by haematoxylin solution and other structures are stained light pink by eosin solution. The slides with targeted sections were deparaffinised in histo-clear in a staining dish for 30 minutes, fresh histo-clear was changed after first 15 minutes. Slides were submerged in 100%, 90%, 70% and 50% ethanol twice for 1 minute before repeating the same procedure in tap water. Slides were submerged in Harris haematoxylin

(230-D, Raymond A Lamb Ltd.) for 15 minutes and rinsed under running tap water for 15 minutes before differentiated in 1% acid ethanol (1% HCl in 70% ethanol) for 30 seconds. Slides were rinsed under tap water for 1 minute before submerged in eosin Y 0.5% alcoholic solution (102439, Merck Millipore Ltd.) for 15 minutes. Slides were rinsed under tap water for 1 minute followed by rinsing again with distilled water for 1 minute. 95% and 100% ethanol were used to dehydrate the sections by submerging slides in twice for 30 seconds each, followed by submerging slides in histo-clear twice for 5 minutes each. After carefully wiping off excess liquid around sections, 1-2 drops of DPX mountant (10050080, Fisher Scientific Ltd.) were applied on the tissue sections. An appropriately sized coverslip (MENZBB024050AZ, Menzel Glaser, VWR International Ltd.) was applied on top of the slides, and the slides were left to dry in the fume cupboard overnight. Dried slides were stored in microscope slide boxes at room temperature. H&E staining images were captured using a Leica DFC420 microscope camera and Leica Application Suite v.3.8 software. Five randomly chosen fields were captured per sample.

### 2.10.4 Immunohistochemistry

The immunohistochemistry procedures were performed as follows: slides with targeted sections were deparaffinised in histo-clear in a staining dish for 30 minutes, fresh histo-clear was changed after first 15 minutes before rehydrating in 100%, 90%, 70% ethanol and distilled water for 5 minutes each. Citrate buffer (pH=6.0) described in Table 2.11 was used as an antigen retrieval buffer. Antigen retrieval buffer was microwaved at full power until close to boiling

before submerging the slides in and steam together in a food steamer for 20 minutes at 800 watts. To prevent antigen retrieval buffer from evaporation, cling film with few holes was used to cover the top of the container. Slides were allowed to cool down in the antigen retrieval buffer for 20 minutes at room temperature before rinsing with PBST (PBS with 0.5% Tween 20) for 5 minutes. A Dako pen (S2002, Dako UK Ltd.) was used to draw a hydrophobic circle around the tissue section of each slide.

| | **Final Concentration** | **Product Code** |
|---|---|---|
| **Tri-sodium Citrate Dehydrate** | 10mM | 10112880, Fisher Scientific Ltd. |
| **Tween 20** | 0.5% | 27434-8, Sigma-Aldrich |

**Table 2.11 Reagents and concentrations to make citrate buffer.**

Tissue sections were blocked with secondary antibody host serum in 0.3% Triton X-100 and PBS mixed solution for 1 hour at room temperature following rinsing tissue sections in PBST twice 5 minutes each. Interested primary antibody was diluted at 1:200 in PBST then carefully pipetted on the tissue sections, and incubated the sections overnight in a humidified chamber at 4°C. The next morning slides were rinsed in PBST three times, 5 minutes each. Secondary antibody was diluted 1:500 in PBS containing 2% of secondary antibody host serum, then pipetted on to the tissue sections and incubated in a humidified dark chamber for 1 hour at room temperature. Slides were then rinsed in PBS three times, 5 minutes each before they were mounted in Vectashield Hardset containing DAPI with coverslips and were kept in the dark at 4°C for long term storage. Immunohistochemistry microscopy was carried out using a Leica CTR 5000 digital microscope (Leica Microsystem) and images were taken using a Leica DFC420 microscope camera. Overlay images were generated using Leica Application Suite v.3.8 software. Three randomly chosen fields were captured per slide.

The primary antibody and secondary antibody used in this study are described below:

| Primary Antibody | Secondary Antibody |
|---|---|
| **rabbit polyAb anti-six2** (Proteintech Euro 11582-1-AP) | **polyclonal swine anti-rabbit immunoglobulin FITC** (Dako 00092872) |
| **monoclonal anti-BrdU** (Sigma 057K4859) | **Alexa Fluor 488 donkey anti-mouse** (Molecular Probes, A21202) |
| **Pax2 antibody** (GeneTex EP3251) | **polyclonal swine anti-rabbit immunoglobulin FITC** (Dako 00092872) |

**Table 2.12 Primary and secondary antibody used for immunohistochemistry.**

## 2.11 STATISTICS

Statistics were performed using Statistical Package for the Social Sciences (SPSS) version 21.0. Details about the statistical analysis performed were explained in the following chapters. Data presented as Means ± standard error of the mean (SEM), only $p<0.05$ was considered as statistically significant.

# CHAPTER 3: EXPERIMENTAL MODEL DEVELOPMENT

## 3.1 INTRODUCTION

Acute kidney injury (AKI) has become a global health issue that affects more than 13 million people all over the world every year, especially in poor resource countries, AKI is connected with high morbidity and mortality (Patschan *et al.,* 2015). AKI is also a frequent and serious complication in hospitalised patients, survival often comes with long-term morbidity, and remains at risk of developing chronic kidney disease and end-stage renal disease (Coca *et al*., 2009). The major causes of AKI are ischemic-reperfusion injury, which is the tissue injury caused when the blood returns after a period of ischemia, and nephrotoxicity, which is caused by nephrotoxic drugs such as aristolochic acid and overdosing folic acid (Jonker *et al*., 2016).

Aristolochic acid is a chemical component that was mainly found in herbs belonging to the aristolochia. During ancient times, it was used to treat urinary problems, snakebites, and a variety of other ailments as it was also considered to be an effective contraceptive (Jadot et al., 2017; Bhattacharjee *et al*., 2017). However, in recent years AA was suspected to be the main cause of nephrotoxicity associated with interstitial fibrosis and carcinoma. Aristolochic acid-induced nephropathy (AAN) is initiated by the damage to proximal tubule cells when DNA adducts are formed, which triggers cell cycle arrest at G2/M checkpoint and an eventual induction of apoptosis (Romanov V *et al.*, 2015). In addition to the G2/M arrest, metabolic activation of AAI to Nhydroxyaristolactam I also results in the development of DNA adducts which leads to the transversion mutation A➔T in ras and p53 genes (Schmeiser *et al*., 1990; Slade *et al*., 2009). The presence of AA results in the elevation of ROS and

reactive nitrogen species (RNS), which may act as subcellular messengers altering signal transduction and genetic expression through mitogen activated protein kinase (MAPK) pathway and NF-κB pathway, as both pathways are characterised as oxidative stress sensitive (Cooke *et al*., 2003; Milligan *et al*., 1998; Cakir and Ballinger, 2005; Yu *et al*., 2011).

Folic acid is a member of the vitamin B family (B9), is essential for numerous bodily functions like DNA synthesis and repairing RNA. Excess folic acid might lead to folic acid-induced acute kidney injury because of the formation of luminal crystals, which have direct toxicity to renal cells; however, the precise mechanism behind it still remains unclear. It is worth noting that folic acid-induced kidney injury has similar syndromes as human AKI, it is considered as an experimental model for evaluation of epithelial regeneration and interstitial fibrosis.

Rodents, which mainly represent renal ischemia-reperfusion injury and nephrotoxicity, are commonly used as an AKI experimental model, and have provided crucial insight into the underlying pathophysiology. Male BALB/c mice were injected with AA at 5mg/kg of bodyweight by Yang and colleagues in order to investigate AA effected cycle analysis. C57BL/6 mice were treated with 5mg/kg AA or 10mg/kg AA for investigation of genetic pathways affected by AA induced necrosis (Wu *et al*., 2013; Baudoux *et al*., 2012; Xiao *et al*., 2009).

Some *in vitro* models like HK2 and HEK293 cell lines have been frequently used for kidney related research. As introduced in section 2.1.1 Cell lines, both cell lines adopt some renal characteristics, therefore provide the possibility for easy

and reliable studies of cellular mechanisms that may suggest potential pathophysiology and therapeutic agents that may treat the injury.

## 3.2 AIMS AND HYPOTHESIS

The aim of this chapter is to make use of nephrotoxic drugs like AA and FA to generate an experimental model that respond to nephrotoxic drugs but is able to recover after the acute injury. We followed a published protocol by Yang Li and colleagues injecting AA at 5mg/kg in BALB/c mice and observed an acute injury in proximal tubules and followed by tubular recovery (Yang *et al*., 2010). We also intended to make use of *in vitro* models that have renal characteristics such as HEK293 and HK2 cell line, by treating them with AA or FA to develop an *in vitro* model that showed damage and recovery response.

We hypothesised that 1) ICR mice would show similar damage and recovery response to BALB/c mice in the published protocol, enabling further pathway analysis during AA-induced damage and recovery. 2) HEK293 or HK2 would show significant damage in response to AA or FA induced acute damage, but be able to recover after damage, enabling further pathway analysis during AA induced damage and recovery.

## 3.3 METHODS AND MATERIALS

### 3.3.1 Animal study

#### 3.3.1.1 Animal study design

ICR (Imprinting control region) strain mice were used for this study. Mice were divided into two groups according to gender, however only males were used for analysis in this project. All males (n= 120) aged between 6-8 weeks were randomly divided into two groups: group A (n= 30) were pre-treated with PBS and administered PBS for 5 days; group B (n= 90) were pre-treated with PBS and administered aristolochic acid (5mg/kg of bodyweight) for 5 days. 24 hours before animals were humanly killed, BrdU (10mg/ml in PBS, 100mg per kg body weight) was injected in order to detect proliferative activity. Animals were humanely killed at 2, 7 and 35 to after AA administration to obtain kidneys from animals. All animal treatment was carried out, and tissue were harvested by Dr Simon Welham.

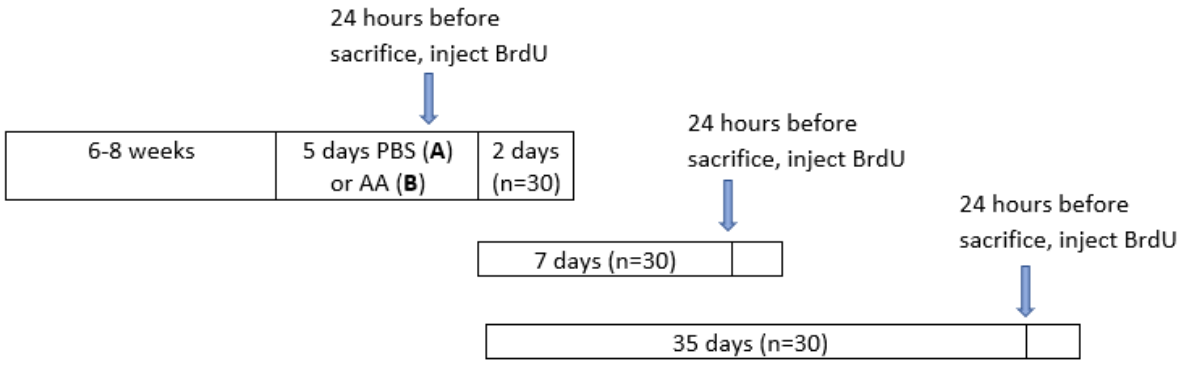


**Figure 3. 1 Experimental design and protocol.**

ICR male mice at age 6-8 weeks were treated with (A) PBS or (B) AA at 5mg/kg of body weight. Kidney tissues were humanely collected 2 days, 7 days and 35

days after AA administration. BrdU was injected to each mice 24 hours prior to sacrifice.

### 3.3.1.2 Kidney processing

The male mice were humanely killed, and the kidneys were embedded in paraffin wax for sectioning. The pre-fixed mouse kidney samples were processed following the protocol described in section 2.9.1. The tissue blocks were sectioned in 5µm thick section as described in section 2.9.2 Kidney sectioning.

### 3.3.1.4 Haematoxylin Eosin (H&E) staining

Animal kidney sections were stained using H&E staining method following the protocol described in section 2.9.3 Haematoxylin Eosin (H&E) staining. Three sections per animal were used and five randomly chosen fields were captured per section.

### 3.3.1.5 Immunohistochemistry

Immunohistochemistry was carried out following the protocol described in section 2.9.4 immunohistochemistry. Three sections per animal were used and three randomly chosen fields were captured per section. Phosphohistone H3 (PH3) was stained in red, which identifies only the cells that in late G2 and M

phase, BrdU was stained in green and it is a proliferating marker, which labelled cells that were either undergoing mitosis or had already finished the process .

#### 3.3.1.6 Wound area percentage calculation

H&E images were imported to NIS-Elements D 4.12.04 software to measure the area of selected wound in each unit. Five randomly chosen fields were captured per section per animal. The wound area percentage was calculated using following equation: *wound area percentage= (outlined wound area/outlined kidney section area) x100%.* All five images per sample were analyzed.

### 3.3.2 Cell culture

HK2 and HEK293 cells were seeded in DMEM at a density of 60,000 cells per well on a 6-well plate as described in section 2.1.4 Cell counting and seeding, the treatments were applied when cells reached around 80% confluence. Treatments were freshly prepared prior to each experiment as described in section 2.1.5 Cell culture treatments. Cell viability was determined via MTT assay (section 2.3 MTT assay) and cells were counted using a Hawkslay haemocytometer (section 2.1.4 Cell counting and seeding). Wound healing experiment was carried out using a 1ml pipette tip to create a linear wound on treated/control cell groups, pictures were taken at the same spot every 24h as described in section 2.2 Wound healing.

### 3.3.3 Statistics

Statistics were performed using Statistical Package for the Social Sciences (SPSS) version 21.0. Analysis was specified in each experiment and $p<0.05$ was considered as statistically significant.

## 3.4 RESULTS

### 3.4.1 ICR mice failed to respond to AA induced damage and recovery

#### 3.4.1.1 Expression of Pax2, Six2 and PH3 on male slides

The recovery of kidney structure and function after AKI is heavily dependent on the recovery of renal tubular epithelium (Kusch A *et al*., 2013). It has been proposed that the survival proximal tubular cells would migrate and replace the damaged tubular cells by proliferation (Bonventre *et al.,* 2011). Pax2, an embryonic gene, has been demonstrated to be re-expressed and play an important role during renal recovery after AKI (Huang *et al.*, 2012), therefore, this animal study was performed based on the protocol from Yang Li *et al.* in 2010 in order to 1) test Pax2 expression after AAN. 2) investigate the potential mechanism of how Pax2 re-expression contribute to renal recovery.

Male mice were randomly divided into four groups (n=30 in each group): sham, 2 days post AA injury, 7 days post AA injury and 35 days post AA injury. Pax2 expression in normal healthy kidneys is restricted in nuclei of the cells in collecting ducts (Qi *et al*., 2005), Pax2 protein were not detected in the renal structures (Figure 3.1 and Figure 3.2). It could be more clearly observed in Figure 3.3 and 3.4 that there was no Pax2 expressed in AA-treated animal tissues. The re-expression of Pax2 after AKI is a short, temporary process during renal recovery, however during all time points that ICR mice were treated with AA (2 days, 7 days and 35 days), there was no sign of Pax2 re-expression in the tissue sections.

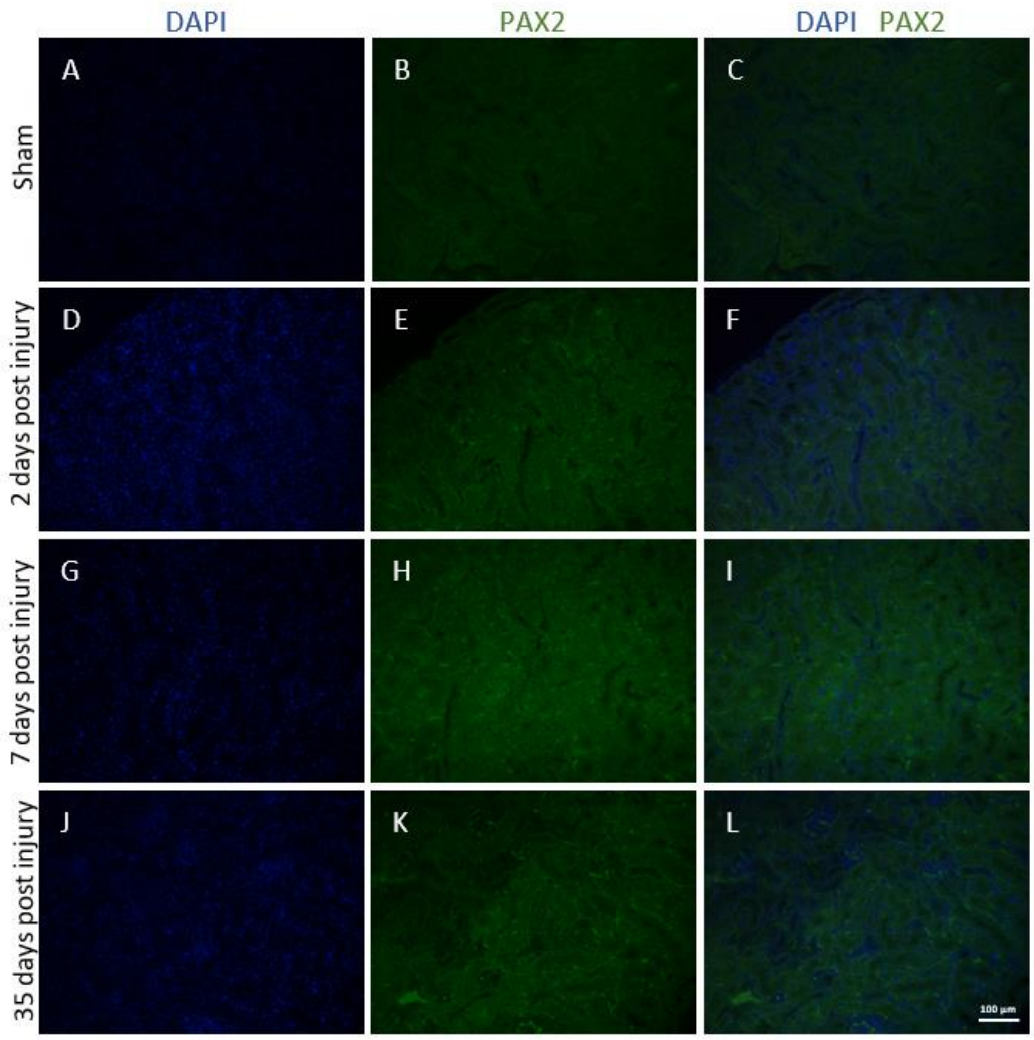


**Figure 3. 2 Pax2 labelling in mice kidney sections from sham, 2 days, 7 days and 35 days post injury groups.**

Kidney sections from sham (M28, A-C), 2 days post injury (M30, D-F), 7 days post injury (M117, G-I) and 35 days post injury (M92, J-L) were labbeled with DAPI (blue) and Pax2 (green). Images taken at 20x magnification. Scale bar = 100µm.

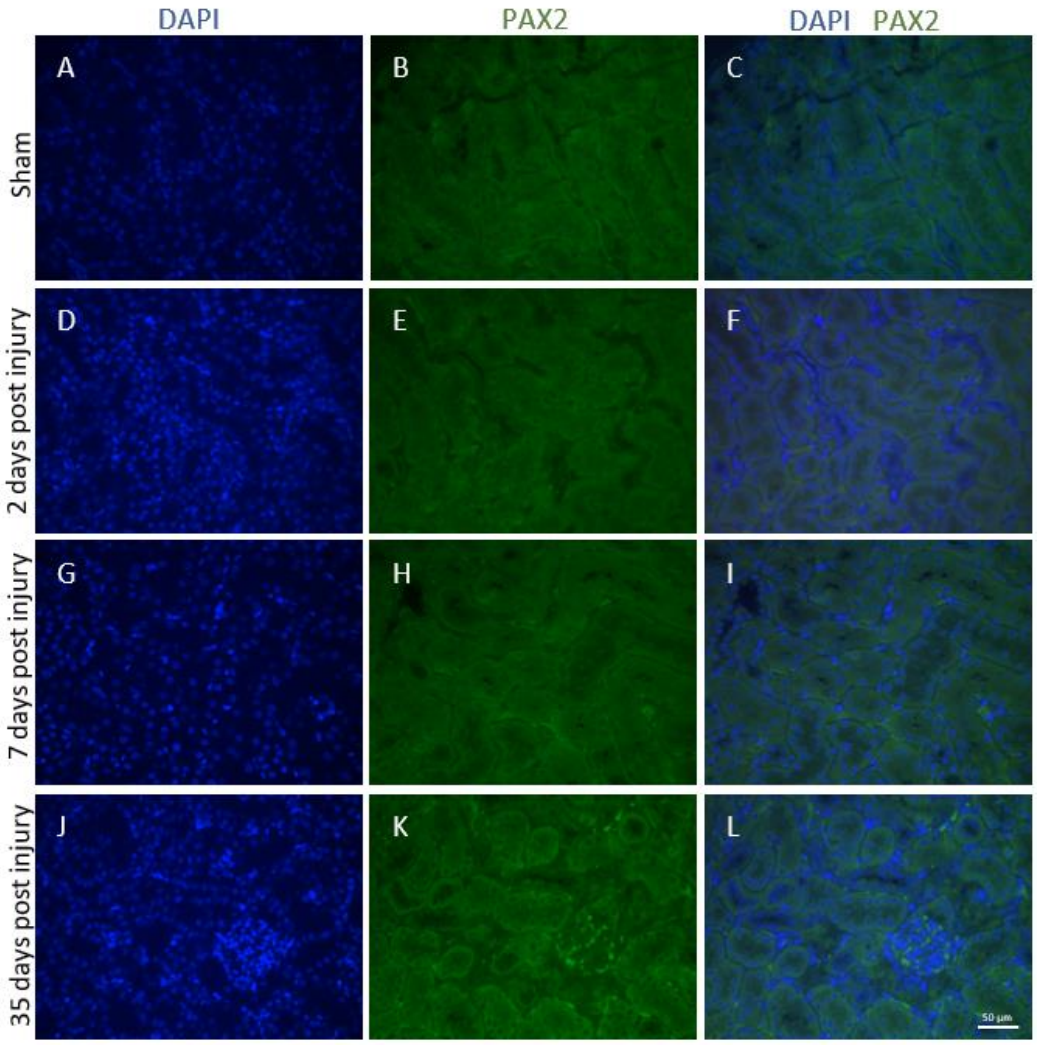


**Figure 3. 3 Pax2 labelling in mice kidney sections from sham, 2 days, 7 days and 35 days post injury groups.**

Kidney sections from sham (M28, A-C), 2 days post injury (M30, D-F), 7 days post injury (M117, G-I) and 35 days post injury (M92, J-L) were labbeled with DAPI (blue) and Pax2 (green). Images taken at 40x magnification. Scale bar = 50µm.

The sections were also labelled with BrdU and PH3 in order to reveal the proliferation process during recovery. PH3 was stained in red, which identifies only the cells that in late G2 and M phase (Hendzel *et al*., 1997); BrdU was in green and it is a proliferating marker, which labelled cells that were either undergoing mitosis or had already finished the process (Repka *et al*, 1992). BrdU and PH3 were detected in all treatments, and there were some cells that were co-localised with BrdU and PH3 (Figure 3.5, pointed by orange arrow), which indicated that those cells were proliferating but took longer to go through M phase. However, by comparing the BrdU, PH3 and the co-locolised cell count, there was no significant difference between control or aristolochic acid injected groups.

**1)**

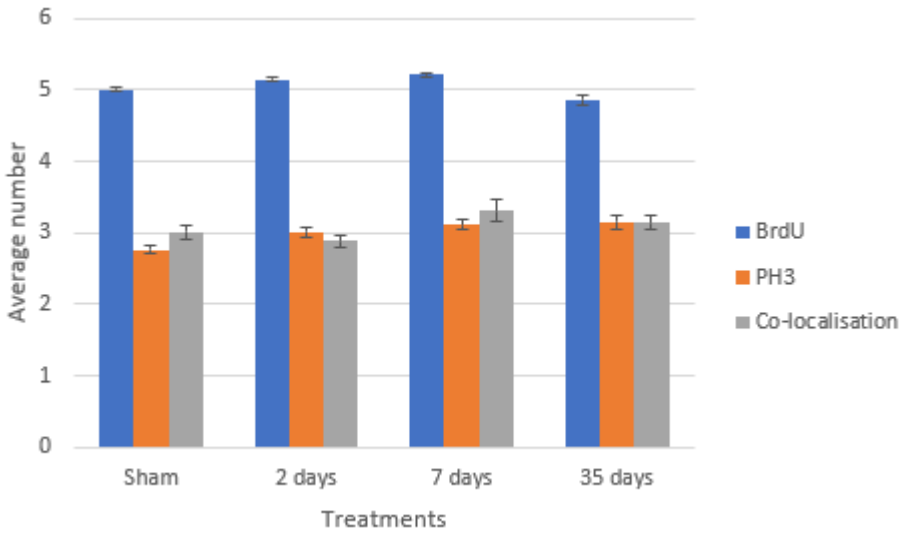
6
5
4
3
2
1
0
Average number
Sham
2 days
7 days
35 days
Treatments
BrdU
PH3
Co-localisation

**2)**

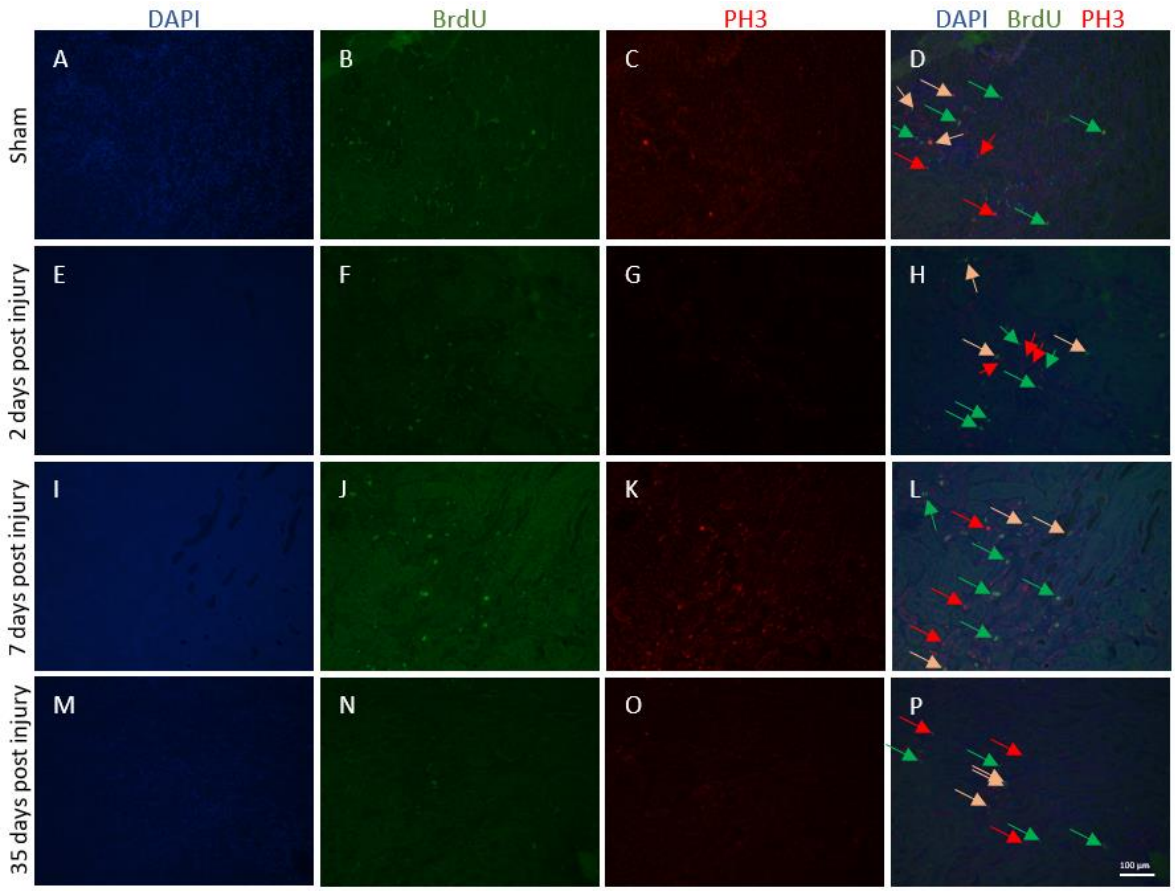


**Figure 3. 4 BrdU and PH3 labelling in mice kidney sections from sham, 2 days, 7 days and 35 days post injury groups.**

1) Average number of BrdU, PH3 and co-localised cells were shown. Three randomly chosen areas were used per section, and each sample was triplicated. 2) Kidney sections from sham (M40, A-D), 2 days post injury (M79, E-H), 7 days post injury (M78, I-L) and 35 days post injury (M43, M-P) were labbeled with DAPI (blue), BrdU (green) and PH3 (red). Arrows showed BrdU positive cells (green arrows), PH3 positive cells (red arrows) and co-locolisation of both (orange arrows). Images taken at 20x magnification. Scale bar = 100μm.

#### 3.4.1.2 AA treatment for the study did not create any measurable damage to the animals

Kidney sections at different recovery stages were stained with H&E in order to observe the damage of AA to the kidneys, however, there were no obvious morphological damages between sham and all the other recovery groups (Figure 3.6 and Figure 3.7). As shown by numerous studies, overdose of AA should cause significant proximal tubule damage and then lead to apoptosis, even necrosis; in this study, especially between sham and 2 days post injury groups, there were no distinct structural differences between the two groups, which lead to the suspicion that the administration of AA did not create sufficient damage to the animals, therefore, a wound area percentage analysis was performed. The wound area percentage of all four groups were relatively even, no significant difference was observed (Figure 3.8, $p=0.0891$). Combined with the previous H&E staining results, we could then draw the conclusion that the AA administration in this animal study unfortunately did not create enough damage to kidney to enable further analysis.

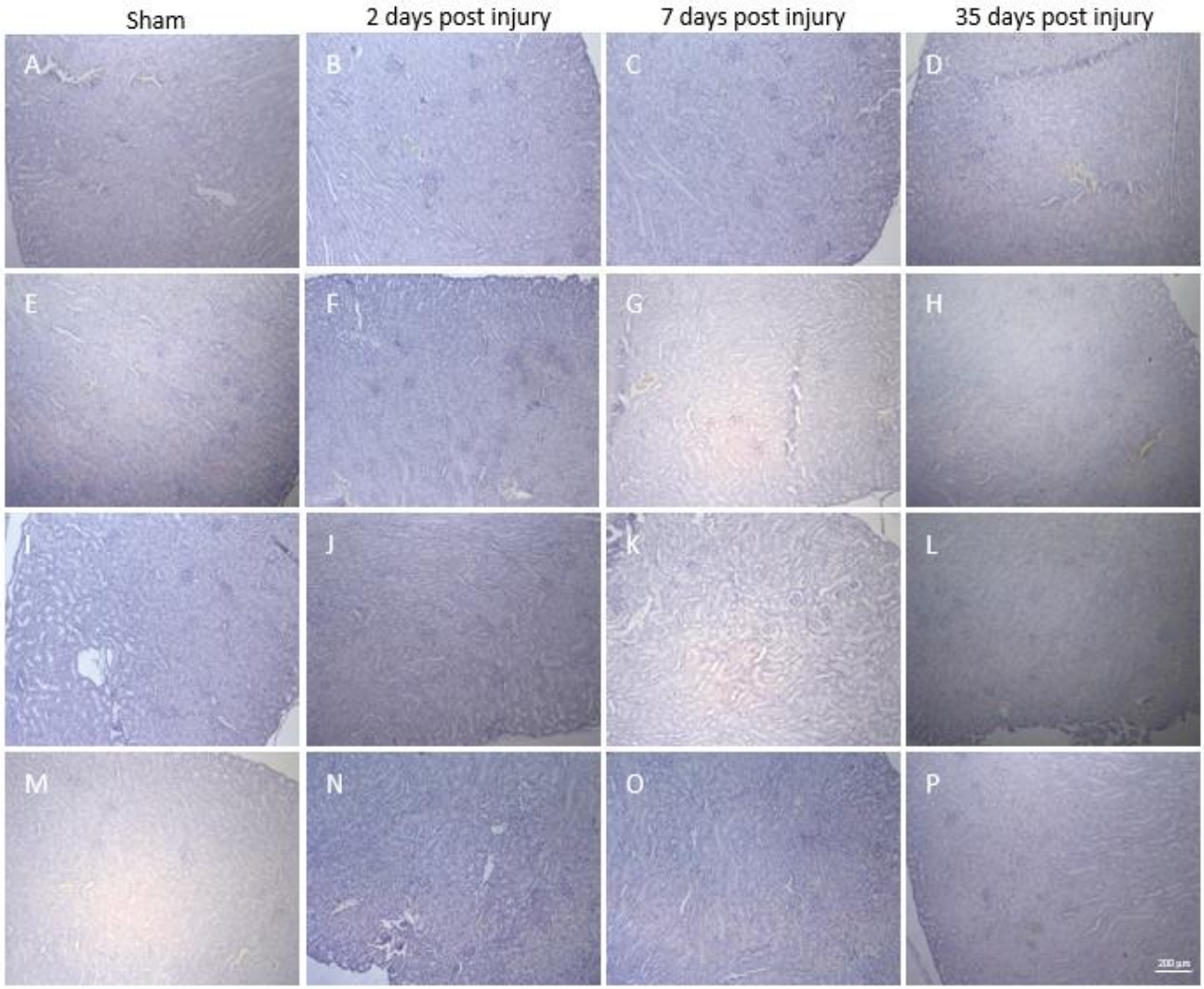


**Figure 3. 5 Representative images of H&E staining on kidney sections in control and different recovery stages.**

H&E staining was performed on sham, 2 days post injury, 7 days post injury and 35 days post injury. Sections shown were from: (A) M47 (B) M68 (C) M125 (D) M82 (E) M66 (F) M88 (G) M113 (H) M122 (I) M4 (J) M24 (K) M11 (L) M151 (M) M100 (N) M119 (O) M159 (P) M102. Images taken 10x magnification. Scale bar = 200μm.

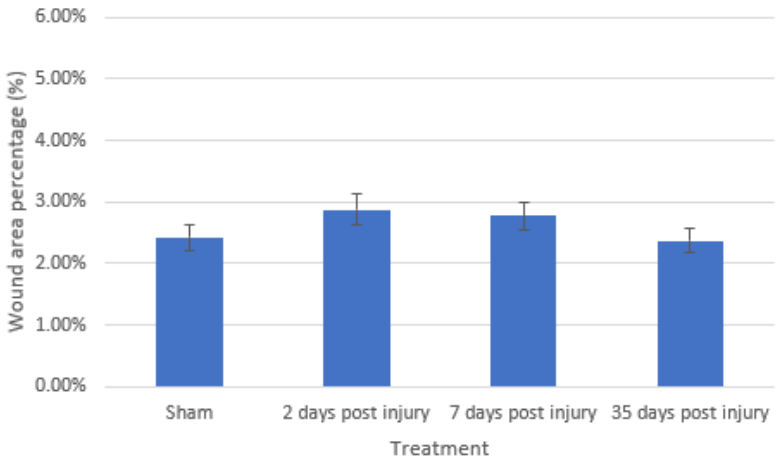


**Figure 3. 1 Wound area percentage calculated from H&E staining images on kidney sections at different recovery stages.**

Wounded area in H&E images taken from sham, 2 days post injury, 7 days post injury and 35 days post injury groups were outlined using NIS-Elements D 4.12.04 software. The wound area percentage was calculated as follow: *wound area percentage= (outlined wound area/outlined kidney section area) x100%.* Five replicates per section per animal were used. One-way ANOVA was performed and $p<0.05$ was considered as significant.

### 3.4.1.3 Expression of Pax2 on embryonic slides

As described in section 3.3.1.1 we failed to observe any Pax2 expression in mice kidney sections between sham, 2 days post injury, 7 days post injury and 35 days post injury groups, and the position of the kidney section that the antibody labelled was not Pax2-specific, therefore we tested the Pax2 antibody using E15 embryonic kidney sections due to its functions in the development of mammalian kidney.

In order to confirm that E15 embryonic kidney was still in the developmental stage, embryonic sections were labelled with a developmental marker Six2. Six2 positive cells were highlighted as bright green dots around the ureteric bud tips (Figure 3.9, image A and B, delineated by blue lines), which indicating the presence of the uninduced nephrogenic mesenchyme (Dressler G.R., 2009). Therefore, it was confirmed that E15 embryonic kidney was under development. As Pax2 first appears during the caudal descent of the nephric duct in the kidney development stage, when nephric duct arrives at somite 26, the ureteric bud emerges from the Wolffian duct and grows towards adjacent metanephric mesenchyme, which is orchestrated by Pax2 (Torban E *et al.*, 2006), thus, positive Pax2 signal was expected in kidney sections that were under development.

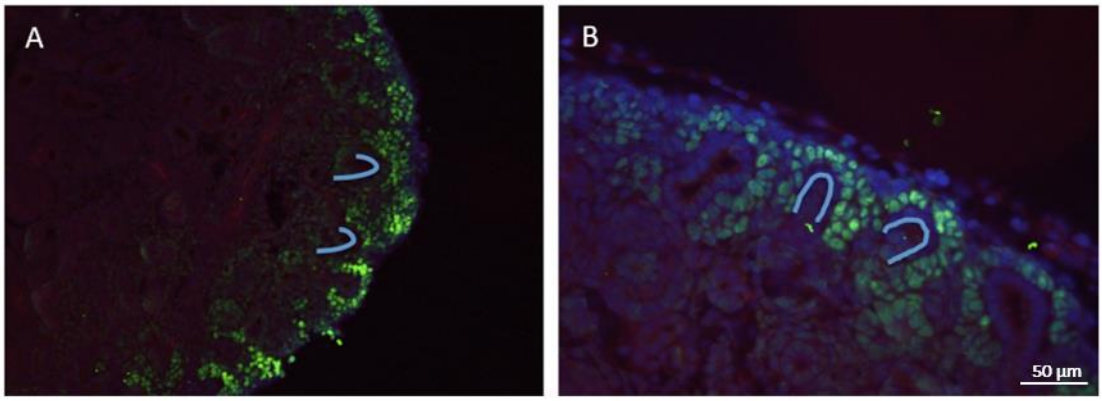


**Figure 3. 2 Six2 labelling in embryonic kidney sections (E15).**

Embryonic kidney sections from E15 were labelled with Six2 (green) and DAPI (blue). The Pale blue curves show the developmental ureteric buds. Nucleus stained with DAPI in blue. Image A was taken at 20x magnification, image B was taken at 40x magnification. Scale bar = 50µm.

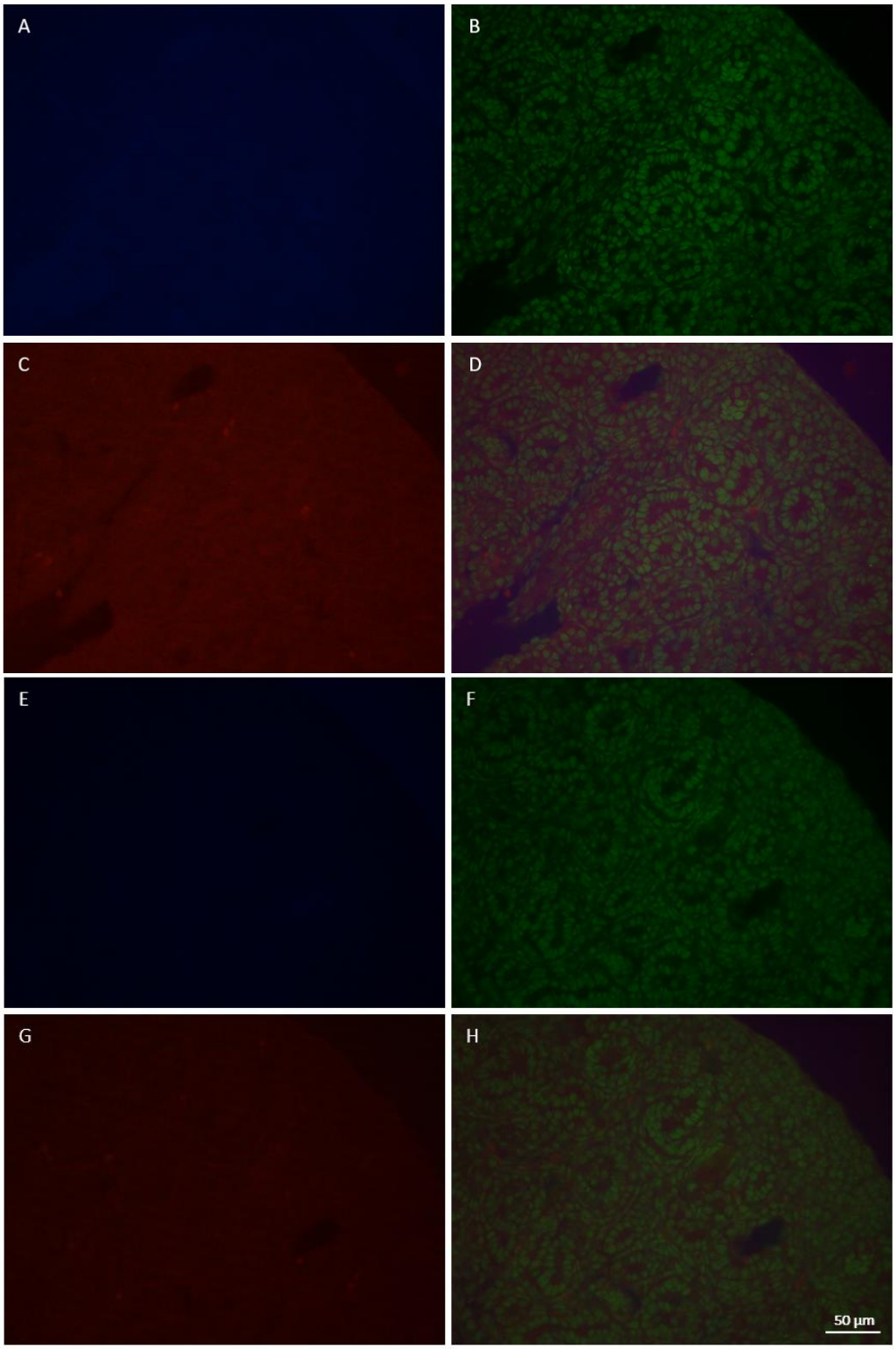


**Figure 3. 3 Representative images of Pax2 labelling in E15 kidney section.**

Developmental embryonic kidney section was labelled with DAPI (A&E), Pax2 (B&F) and PI (C&G), the overlay image was shown in image D and H. Images taken at 40x magnification. Scale bar = 50μm.

Pax2 nuclear expression was observed in the cells in the sections (Figure 3.10). Although it has been shown that Pax2 localized in mesenchyme and ureteric tip at E15.5 and plays an important role during kidney development (Saifudeen Z *et al.*, 2012), it is less likely that it exists in every cell. Pax2 expression was therefore further examined on proliferating cells in cell culture.

HEK293 and HK2 cells were cultured on coverslips while proliferating at high and low densities. The cytoplasm was highlighted in green when both cell lines were at high density (Figure 3.11 image A and B), whereas the positive signal colocalized with DAPI when cells were at low density (Figure 3.11 image C and D). This specific antibody was not only able to change its distribution when cell density changed, it could also change the position of where it was being labelled as well. Both characteristics do not match the characteristic of Pax2, therefore further evidence is needed to confirm the specificity of the antibody that was used.

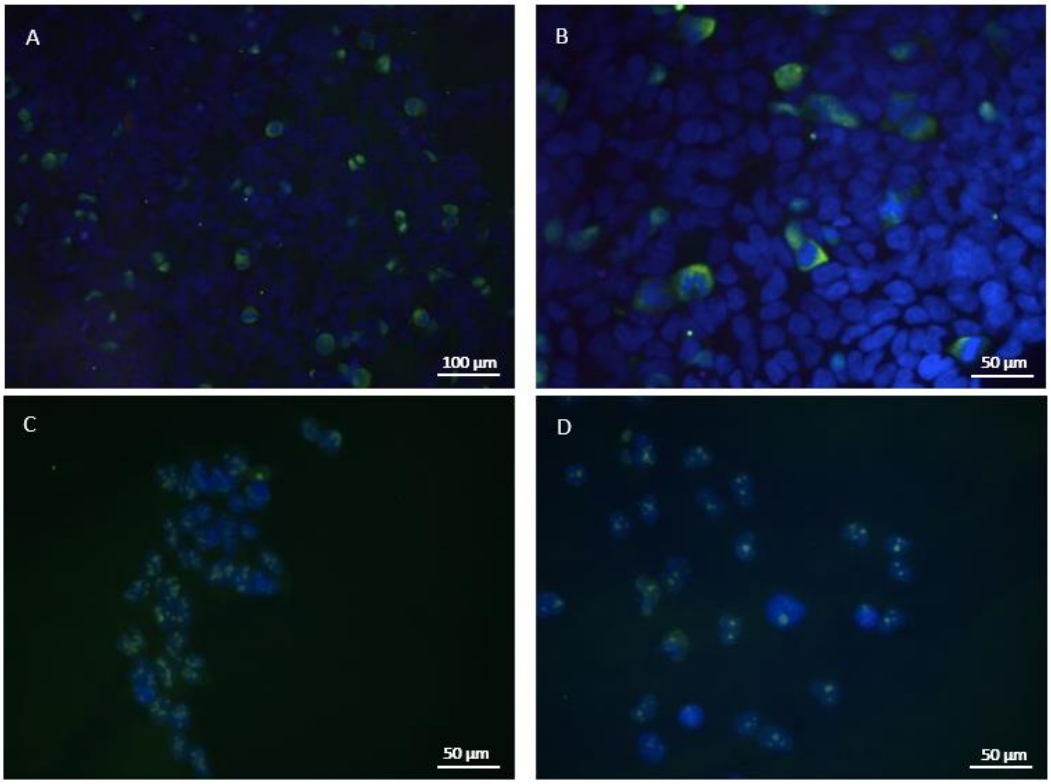


**Figure 3. 4 Pax2 expression on HK2 and HEK293 cells at high and low densities.**

HEK293 (A&C) and HK2 (B&D) cells at high (A&B) and low density (C&D) were labelled with Pax2 in green and DAPI in blue. Pax2 expressed in the cytoplasm when both cell types were at high density (A&B) and colocalized with DAPI when both cell types were at low density. Image A was taken at 20x magnification, image B, C, D were taken at 40x magnification. Scale bar of image A = 100µm, scale bar of image B, C, D = 50µm.

### 3.4.1.4 Test of Pax2 antibody

Western Blot analysis was applied on proliferating HK2 and HEK293 cell samples. HK2 cells and HEK293 cells were collected at 50% confluence following protocol in section 2.8.1. We observed a band for Pax2 expression (44kDa) in one of the HK2 samples (Figure 3.12), however the protein size that the antibody picked up was around 65kDa, suggesting that the antibody we used for Pax2 lacked specificity.

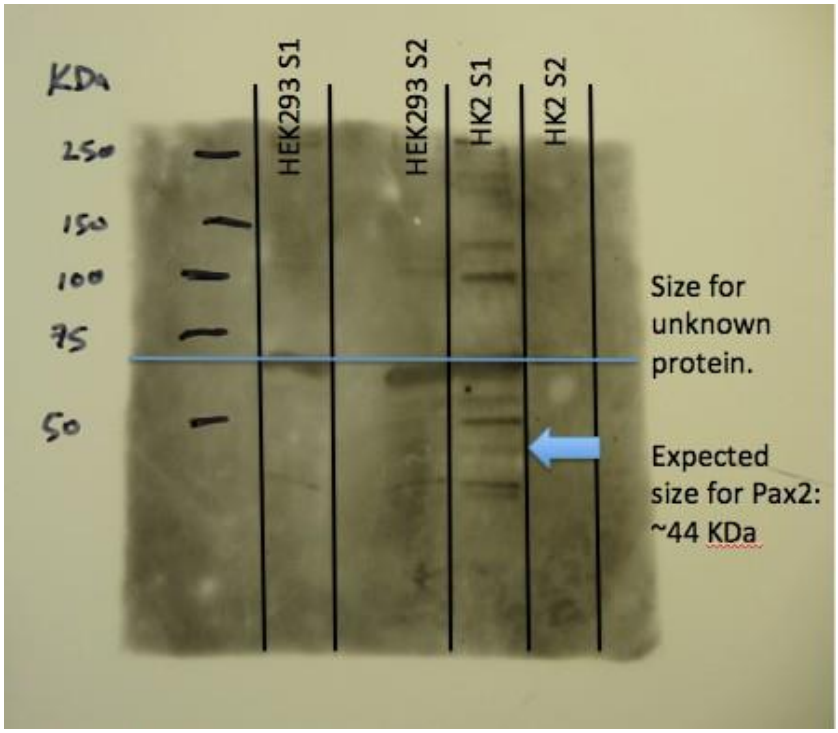


**Figure 3. 5 Western blot analysis of the unknown antibody on proliferating cell samples.**

Protein extracted from proliferating HK2 and HEK293 cells were used to test the antibody.

To conclude, the conducted ICR mice treated following the published protocol from Yang Li and colleagues could not be used for the following study. The Pax2 antibody used was not specific to Pax2 protein. Although proliferation process was observed in all experimental groups, the result from wound area calculation suggested that there was not enough damage induced by AA on the mice, therefore, a reliable experimental model such as cell models was needed to be generated to perform the remainder study.

### 3.4.2 HK2 cells showed nephrotoxic drugs induced damage and recovery response

#### 3.4.2.1 Cell viability significantly decreased after AA and FA treatment for 24 hours

In order to induce the nephrotoxic injury and post-damage recovery, both folic acid and aristolochic acid were tested on two different cell lines for the best result. AA or FA at various of concentrations were incubated with HK2 or HEK293 cells for 24 hours. MTT assay was carried out after the treatments and cell viability was calculated as an injury indicator.

A dose-dependent decrease on cell viability was observed after 24-hour treatment with increasing concentrations of AA (Figure 3.13 image A and C), with a significant difference at 30 μM and 44μM treatment compared to control group ($p<0.05$). A similar dose-dependent decrease trend was observed on 24-hour FA treatments; 14mM, 18mM and 23mM treatments had a significant impact on HK2 cell viability ($p<0.05$, Figure 3.13 image B and D). Same treatment was performed on HEK293 cells at the same time, however HEK293 cells were over-sensitive to serum-free treatment, therefore they are not considered as an appropriate cell model for this project (Figure 3.13 image E).

A

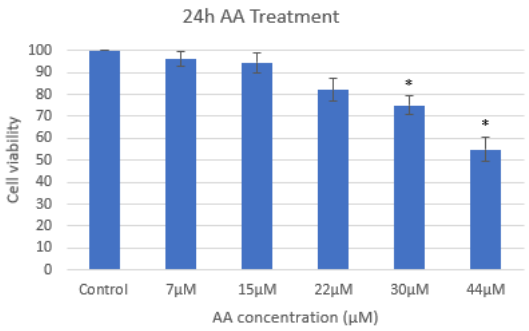
24h AA Treatment
Cell viability
100
90
80
70
60
50
40
30
20
10
0
Control
7μM
15μM
22μM
30μM
44μM
AA concentration (μM)
*
*

B

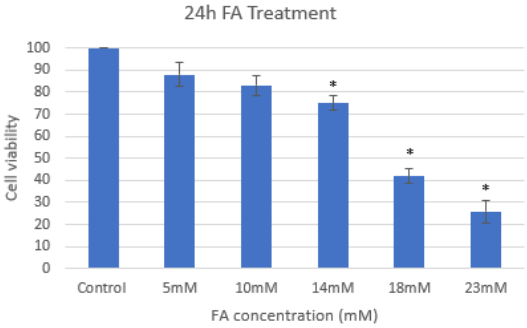
24h FA Treatment
Cell viability
100
90
80
70
60
50
40
30
20
10
0
Control
5mM
10mM
14mM
18mM
23mM
FA concentration (mM)
*
*
*

C

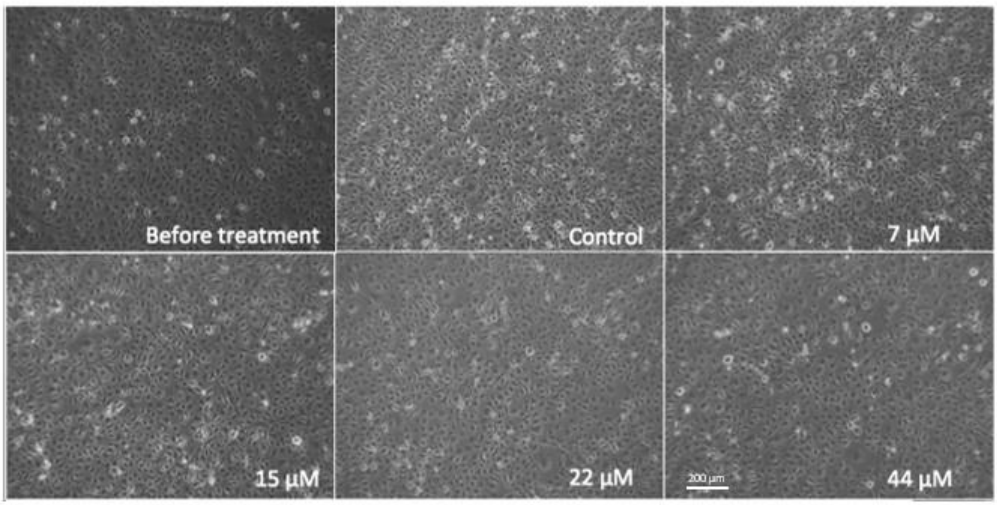
Before treatment
Control
7 μM
15 μM
22 μM
200 μm
44 μM

D

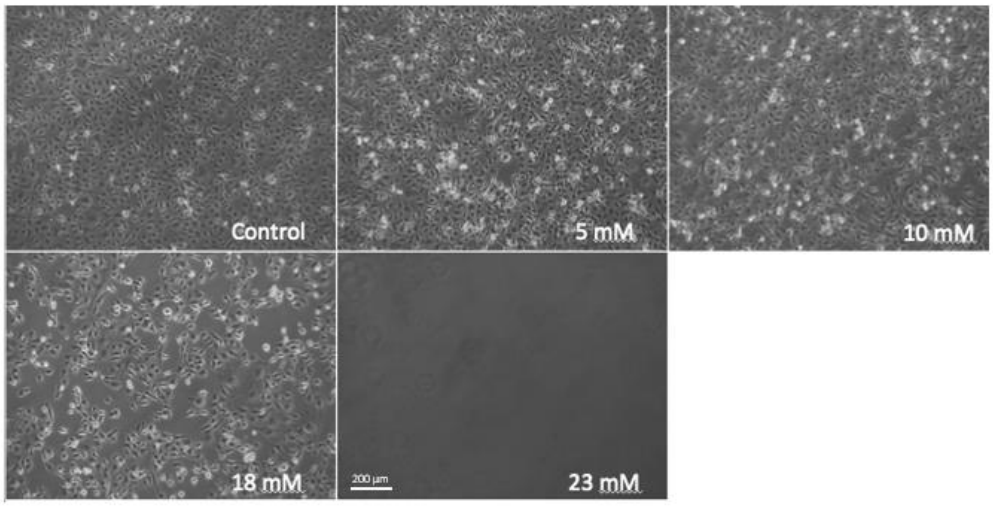
Control
5 mM
10 mM
18 mM
200 μm
23 mM

**E**

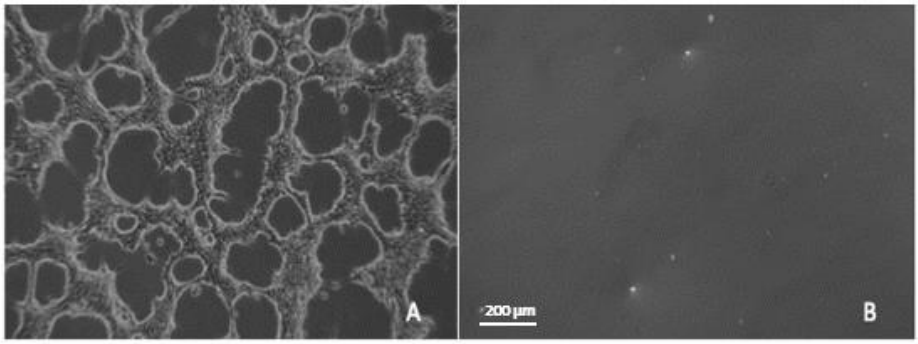


**Figure 3. 6 Effect of aristolochic acid and folic acid after 24-hour incubation with HK2 and HEK293 cells.**

Change of cell viability on HK2 cell line when incubated with aristolochic acid (image **A**) or folic acid (image **B**) at different concentrations after 24-hour. One-way ANOVA was used to analyse the data and followed by Dunnett's test, *$p<0.05$ was considered as significant. All data were shown as mean ± SEM. Images of HK2 cells incubated with AA or FA were shown in image **C** and **D**, images taken 10x magnification. HEK293 embryonic kidney cells under microscope (x10) after 24-hour incubation with serum-free medium only were shown in image **E**. Scale bar = 200µm.

### 3.4.2.2 Cell viability significantly decreased after AA and FA treatment for 48 hours

A time-dependent decrease on cell viability was observed after 48-hour AA treatment. Cell viability was significantly decreased after 48-hour AA treatment at lower concentration of 22μM (Figure 3.14 image A and C, $p<0.05$). Similar but worse damage was observed on FA 48-hour treatment: the cell viability dropped from 40% (24-hour treatment) to about 30% (48-hour treatment) at 18mM, and another sharp drop from roughly 25% (24-hour treatment) to 10% after 48-hour incubation with 23mM FA (Figure 3.14 image B and D, $p<0.05$). FA treated HK2 cells showed visible gaps between cells at 18mM after both 24-hour and 48-hour incubation; treatments at 23mM at both treatment timepoints seemed too strong for HK2 cells as it cleared the cell population. By contrast, AA treated cells did not show any visible damage to HK2 cells no matter concentrations and incubation time.

To conclude, both AA and FA were able to induce significant nephrotoxic injury to HK2 cells, and the severity of the injury (cell viability) was affected in both dose and time dependent manner.

**A**

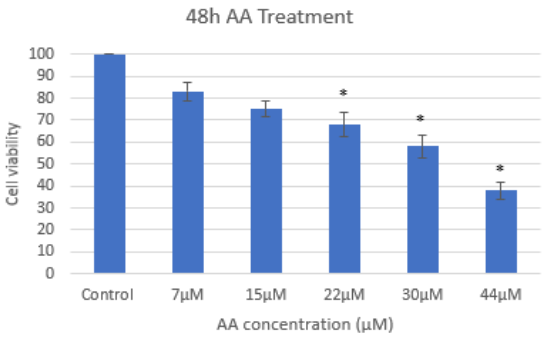
48h AA Treatment
Cell viability
100
90
80
70
60
50
40
30
20
10
0
Control
7μM
15μM
22μM
30μM
44μM
AA concentration (μM)

**B**

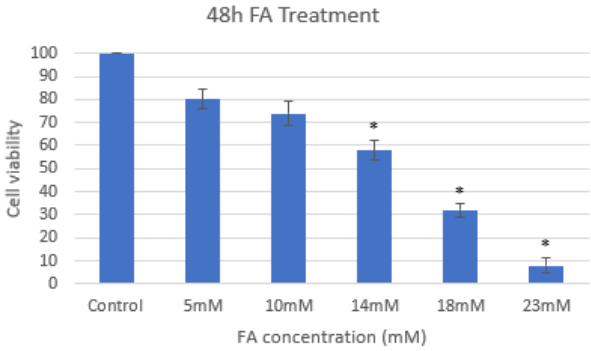
48h FA Treatment
Cell viability
100
90
80
70
60
50
40
30
20
10
0
Control
5mM
10mM
14mM
18mM
23mM
FA concentration (mM)

**C**

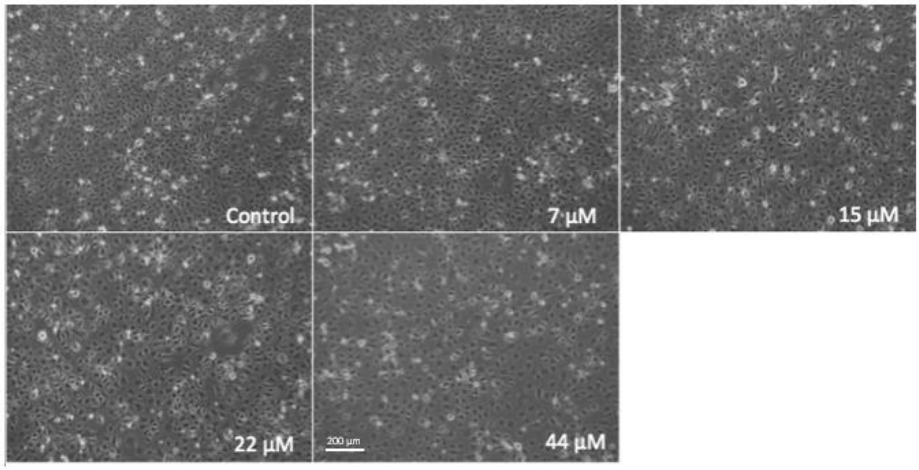
Control
7 μM
15 μM
22 μM
200 μm
44 μM

**D**

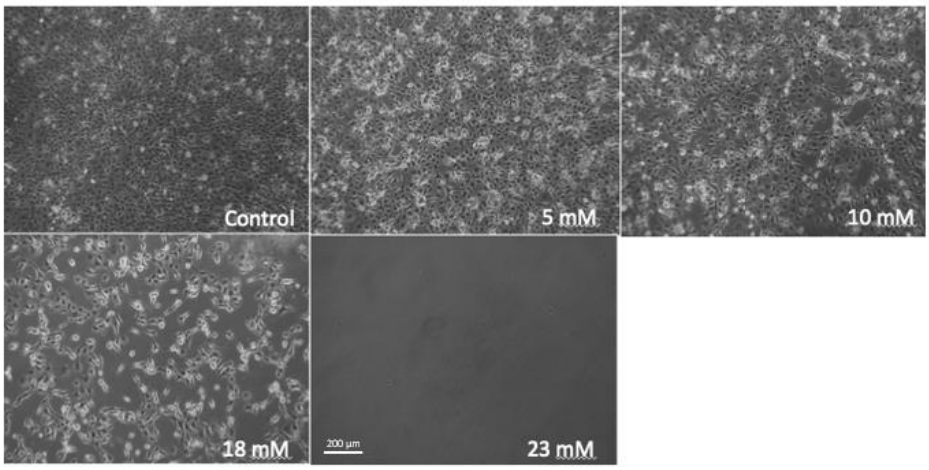
Control
5 mM
10 mM
18 mM
200 μm
23 mM

**Figure 3. 7 Effect of aristolochich acid and folic acid after 48-hour incubation with HK2 cell line.**

Change of cell viability on HK2 cell line when incubated with aristolochic acid (**A**) and folic acid (**B**) at different concentrations after 48-hour. Images of HK2 cells incubated with AA or FA were shown in image **C** and **D**, images taken 10x magnification. One-way ANOVA was used to analyse the data and followed by Dunnett's test, *$p<0.05$ was considered as significant. All data were shown as mean ± SEM. Scale bar = 200μm.

### 3.4.2.3 HK2 cells recovered after nephrotoxic injury

Wound healing experiments were carried out on AA or FA treated HK2 cells in order to investigate if HK2 cells were able to regenerate after treatments. 24-hour 88μM AA treated HK2 cells were able to gradually reduce the gap of the wound, and fully recover from injury after 120-hour recovery (Figure 3.15). 48-hour 88μM AA treated cells recovered more slowly compared to 24-hour treated cells. It started with a peak on wound area percentage after 24-hour recovery, which might due to the detachment of the dead cells from the bottom of the plate. The gap of the wound was slowly filled with proliferated cells during later recovery period. Although cells failed to fully recover in 120-hour recovery period, they still showed a strong recovery trend, which had more that 22% wound recovered after injury (Figure 3.15). Similar results were observed in Figure 3.16 image A and B, 24-hour 18mM FA treated HK2 cells were able to recover within 72-hour period. Both results suggested that HK2 cells were able to recover after been damaged by nephrotoxic drugs.

**A**

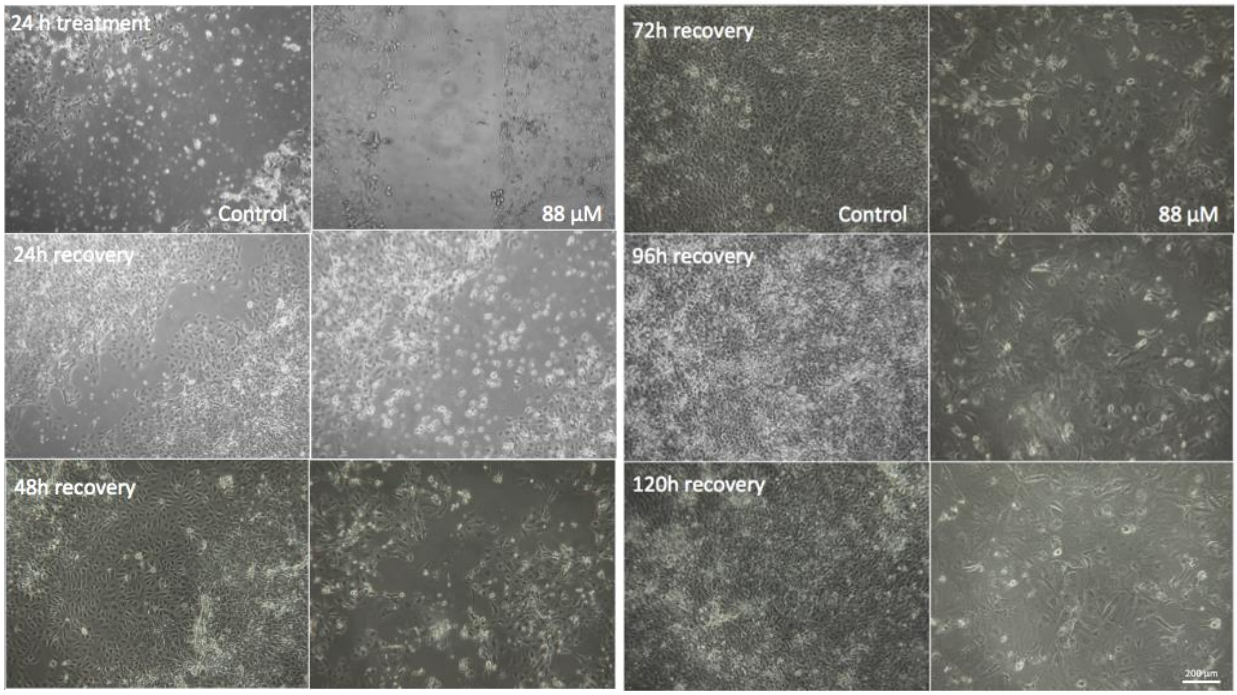
24 h treatment
Control
88 µM
72h recovery
Control
88 µM
24h recovery
96h recovery
48h recovery
120h recovery
200µm

**B**

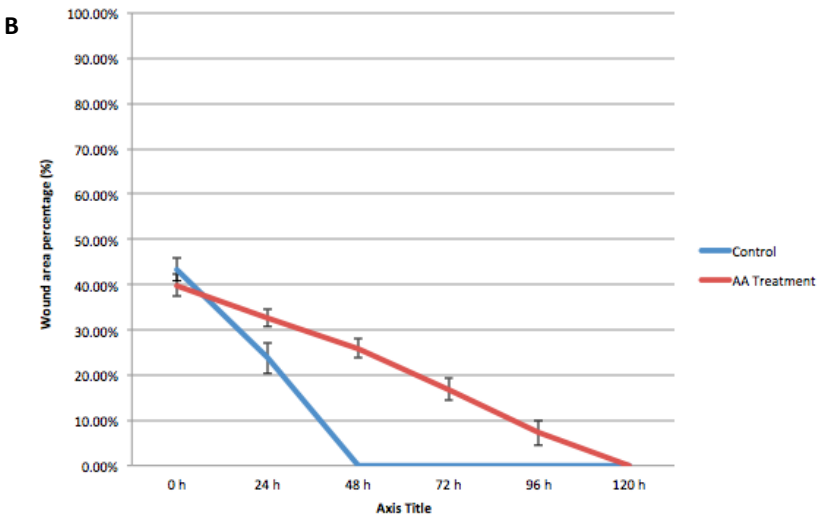
100.00%
90.00%
80.00%
70.00%
60.00%
50.00%
40.00%
30.00%
20.00%
10.00%
0.00%
Wound area percentage (%)
0 h
24 h
48 h
72 h
96 h
120 h
Axis Title
Control
AA Treatment

C

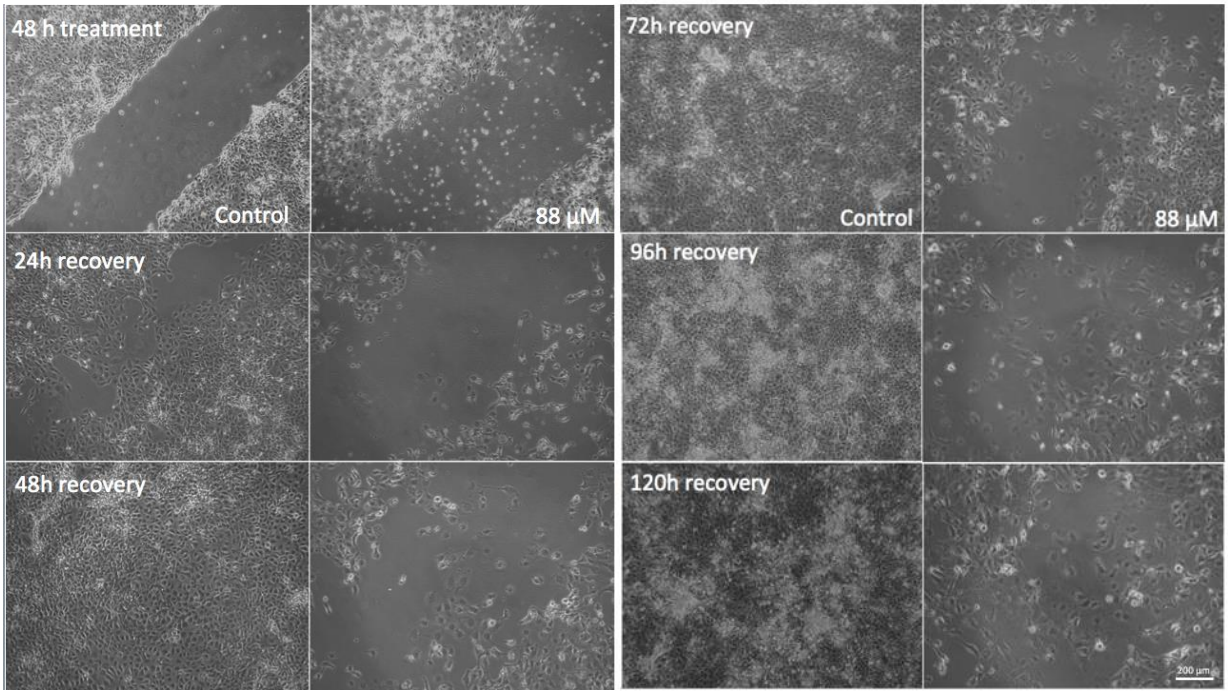


D

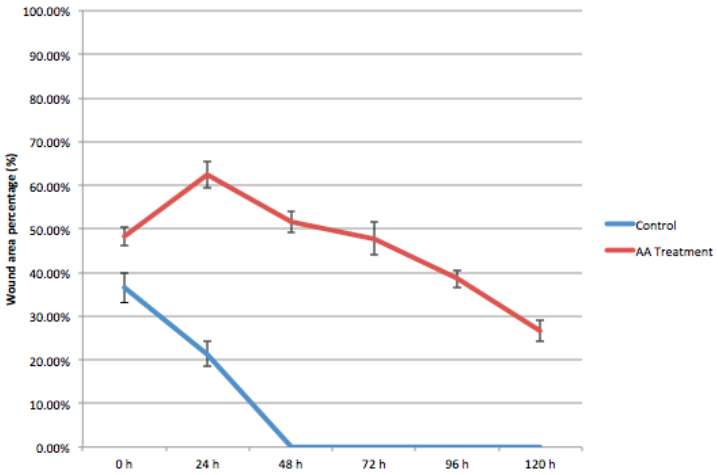


**Figure 3. 8 Wound healing experiment on AA treated HK2 cells.**

A wound was created on cells before treatments. Cells were incubated with AA for 24-hour (**A**) and 48-hour (**C**). Cells were washed three times by PBS, and fresh medium with 10% serum was added to allow recovery. (**B**) (**D**) Wound area percentage was measured within 120-hour time period. Wound area percentage was calculated by (sum of wound area)/total area x 100%. Scale bar = 200μm.

**A**

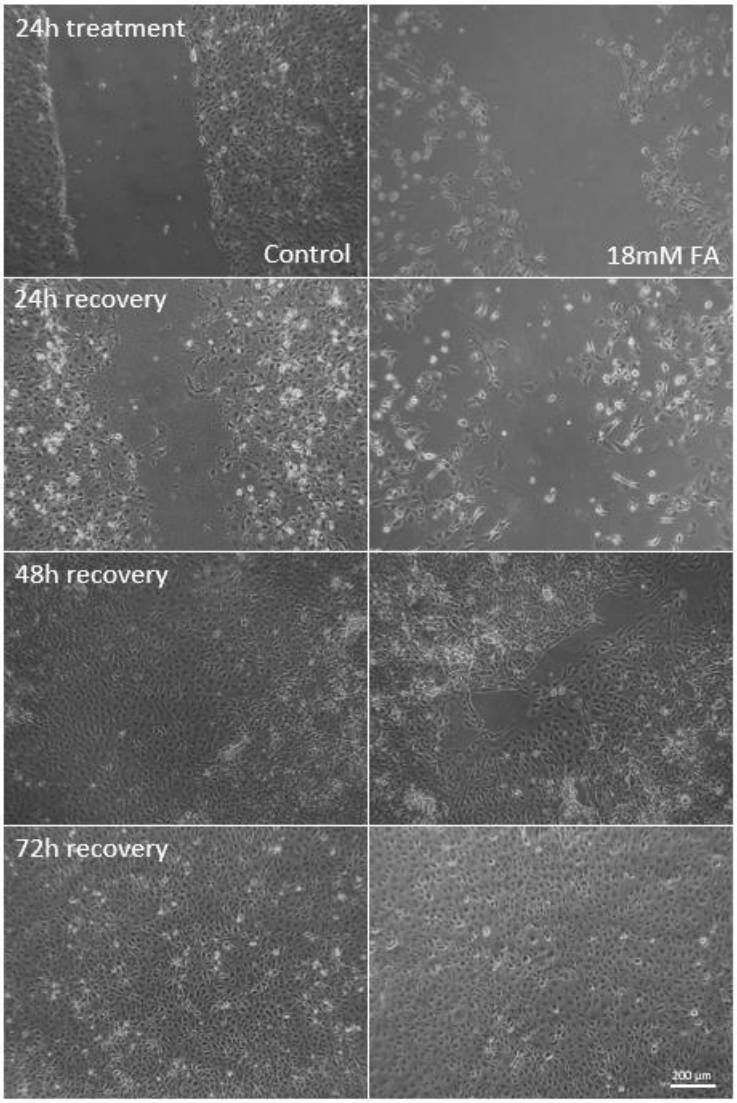
24h treatment
Control
18mM FA
24h recovery
48h recovery
72h recovery
200 µm

**B**

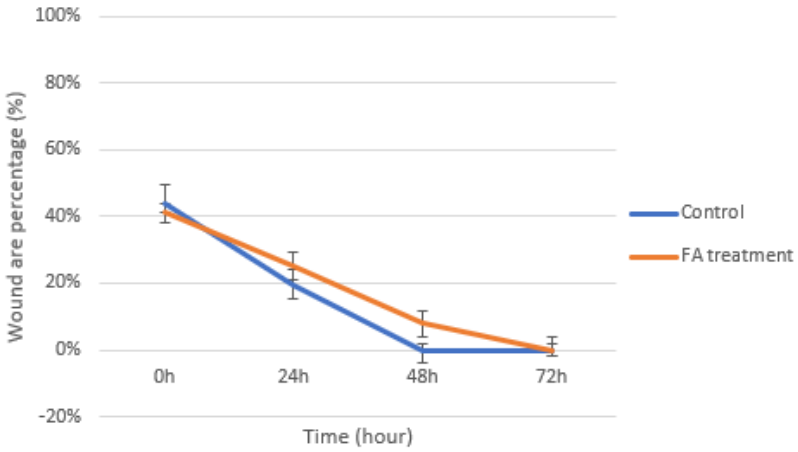
100%
80%
60%
40%
20%
0%
-20%
Wound are percentage (%)
0h
24h
48h
72h
Time (hour)
Control
FA treatment

**Figure 3. 9 Wound healing experiment on FA treated HK2 cells.**

A wound was created on cells before treatments. Cells were incubated with FA for 24 hours and fresh medium with 10% serum was added to allow recovery (**A**). (**B**) Wound area percentage was measured within 72-hour time period. Wound area percentage was calculated by (sum of wound area)/total area x 100%. Scale bar = 200μm.

Post-damage recovery was further assessed by cell viability change and cell number count during recovery. Cell viability measurements were performed in 96-well plates, cell counting assessments were carried out in 6-well plate. Both AA and FA showed significant damage 24-hour treatments (Figure 3.17, $p<0.05$). 117μM AA treatment showed significant 35% decreases in both cell viability and cell number after 24-hour treatments compared to the control group, 18mM FA created worse acute injury as it affected around half of the cell population ($p<0.05$). However, cells under both treatments were able to recover within 72 hours and showed no significant difference to the control group in terms of cell viability and cell numbers. In contrast, 48-hour treatments created more severe damage to the cells with a 60% decrease in cell viability for AA treatment and an 60% for FA treatment in terms of cell viability and cell numbers. Consequently, it took longer for the cells to recover.

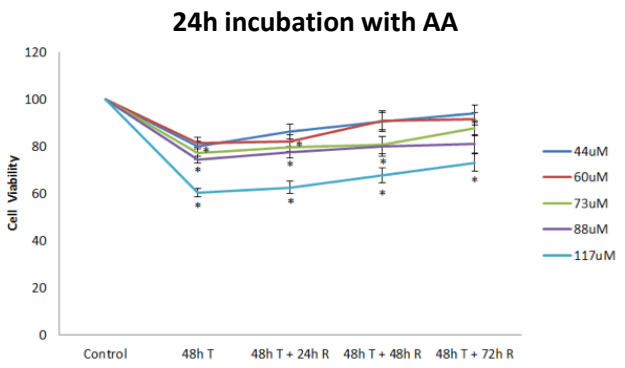
24h incubation with AA
Cell Viability
120
100
80
60
40
20
0
Control
48h T
48h T + 24h R
48h T + 48h R
48h T + 72h R
44uM
60uM
73uM
88uM
117uM

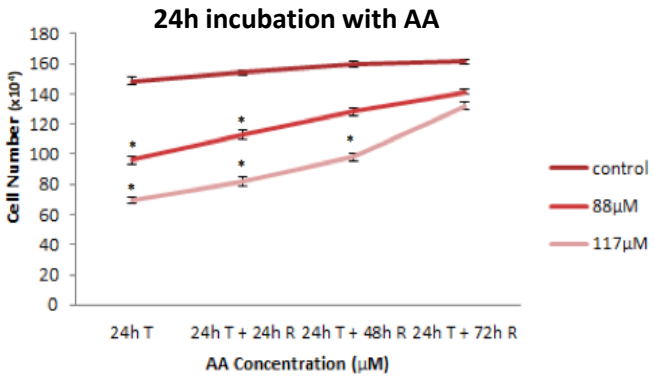
24h incubation with AA
Cell Number (x10⁴)
180
160
140
120
100
80
60
40
20
0
24h T
24h T + 24h R
24h T + 48h R
24h T + 72h R
AA Concentration (μM)
control
88μM
117μM

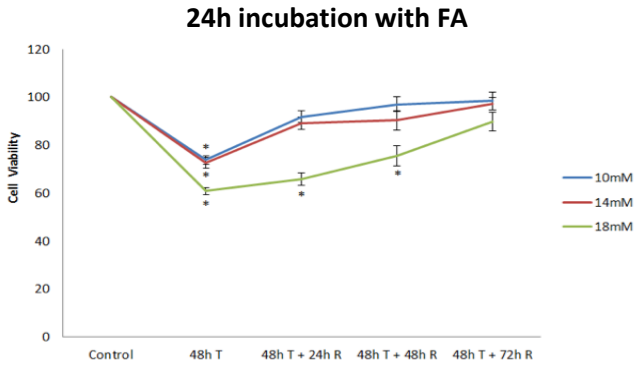
24h incubation with FA
Cell Viability
120
100
80
60
40
20
0
Control
48h T
48h T + 24h R
48h T + 48h R
48h T + 72h R
10mM
14mM
18mM

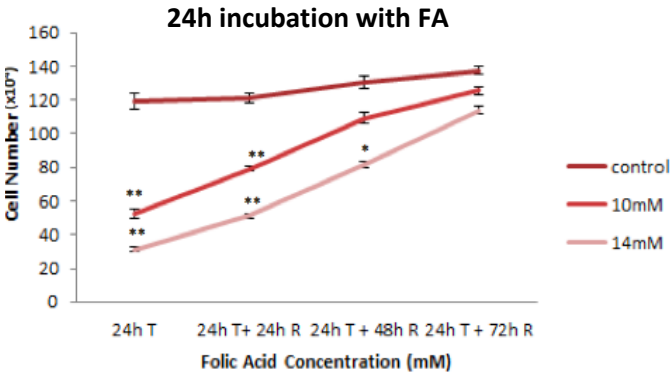
24h incubation with FA
Cell Number (x10⁴)
160
140
120
100
80
60
40
20
0
24h T
24h T+ 24h R
24h T + 48h R
24h T + 72h R
Folic Acid Concentration (mM)
control
10mM
14mM

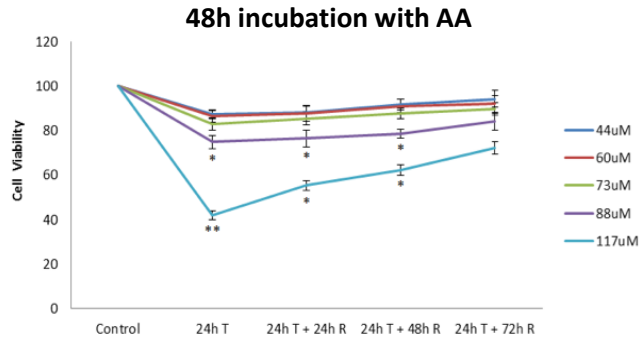
48h incubation with AA
Cell Viability
120
100
80
60
40
20
0
Control
24h T
24h T + 24h R
24h T + 48h R
24h T + 72h R
44uM
60uM
73uM
88uM
117uM

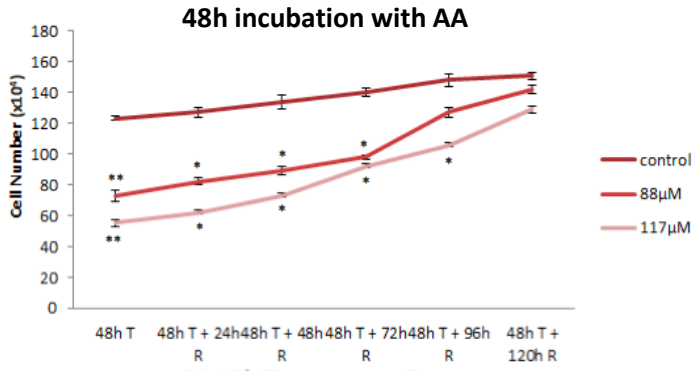
48h incubation with AA
Cell Number (x10⁴)
180
160
140
120
100
80
60
40
20
0
48h T
48h T + 24h R
48h T + 48h R
48h T + 72h R
48h T + 96h R
48h T + 120h R
control
88μM
117μM

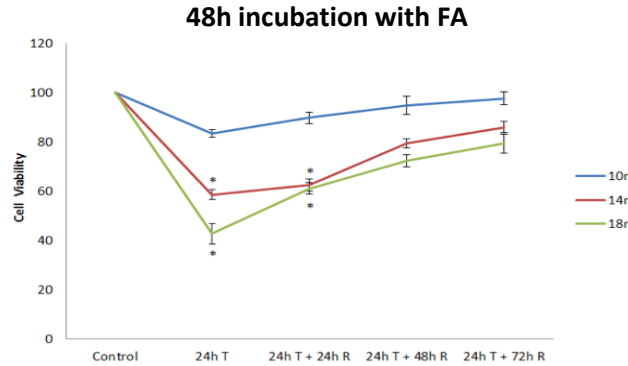
48h incubation with FA
Cell Viability
120
100
80
60
40
20
0
Control
24h T
24h T + 24h R
24h T + 48h R
24h T + 72h R
10mM
14mM
18mM

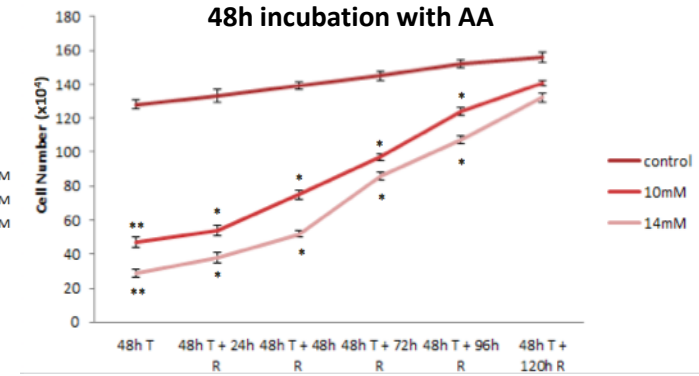
48h incubation with AA
Cell Number (x10⁴)
180
160
140
120
100
80
60
40
20
0
48h T
48h T + 24h R
48h T + 48h R
48h T + 72h R
48h T + 96h R
48h T + 120h R
control
10mM
14mM

**Figure 3. 10 HK2 cells were able to regenerate after being treated with AA.**

Cell viability was measured throughout the 72h recovering process. Cell counting also showed the same trend of recovery throughout 72h/120h recovery. Two-way ANOVA was used to analyse the data and followed by Tukey's test, *$p<0.05$ was considered as significant, all data were shown as mean ± SEM).

## 3.5 DISCUSSION AND CONCLUSION

This chapter intended to develop an experimental model which responded to nephrotoxic drug-induced acute injury and recovery, therefore enable transcriptional analysis during damage and recovery.

Firstly, we intended to use an animal model. ICR outbred mice were injected with 5mg/kg bodyweight of AA for 5 days in order to induce nephrotoxic injury. Kidney samples were collected 2 days. 7 days and 35 days post injury. The protocol was adapted from a published paper from Yang and colleagues where nephropathy was induced by intraperitoneal injection of AA to BALB/c mice, and their Masson's trichrome staining showed a significant increase of fibrotic outcomes 7 days post injury (Yang *et al.*, 2010). Unfortunately, although the same dose of AA was injected to the ICR mice, the H&E staining results did not show any significant tissue damage. Additionally, the tissue damaged area percentage results showed that there was no significant difference in terms of tissue damage between AA injected group and control group; therefore, the mice used in this study were not considered as a suitable experimental model. The lack of apparent damage in the tissue could be due to the different species of mice used. Yang and colleagues used BALB/c inbred mice as experimental model whereas ICR outbred mice were used in this animal study. Outbred mice have been commonly used in toxicological research, they are considered to be more accurate in mimicking the results would be found in human research due to their genetic heterogeneity. On the other hand, the main disadvantages of outbred mice are the lack of sensitivity to drugs and the high level of genetic heterogeneity increases the variation in response to a treatment and make the

outcomes less reproducible (Brekke *et al.*, 2018 and Festing *et al.*, 2010). In comparison to Yang and colleagues' animal study in 2010, the lack of sensitivity to AA and increased variation could be the key reasons why outbred ICR mice did not share the same outcome to inbred BALB/c mice. By increasing the dose of AA or increase the number of animals might help overcome this.

By contrast, acute damage incurred when either AA or FA was introduced to *in vitro* model HK2 cells. A significant ($p<0.05$) decrease in cell viability was observed after 24-hour incubation with AA at 117μM, and the cell viability dropped to around 50% after 48-hour 117μM AA treatment. FA shared a similar but worse injury trend on 24-hour treatment where the cell viability decreased to roughly 50% at 18mM. 48-hour 18mM FA treatment brought the cell viability to a 20%. These results showed that both AA and FA are able to induce acute damage to HK2 cells and the damage occurred in a dose and time dependent manner. Once the treatment was replaced with DMEM medium with 10% FBS, the damaged cells were able to recover in a short period of time. The wound recovery experiment, cell viability change and cell count during damage and recovery all showed that HK2 cells were able to repopulate after acute damage. These characteristics of HK2 cells enabled them to be used as an experimental model for the remainder of the project.

Comparing AA and FA treated cells, we also observed that dead cells after AA treatment tended to attach to the bottom of the flask/plate whereas FA treated cells did not appear to do so. It was obvious that although the cell viability of HK2 cells significantly reduced after 24-hour and 48-hour AA treatment (Figure 3.13 image C and D; Figure 3.14 image C and D, $p<0.05$), the dead cells were

only lifted and washed out after 24-hour recovery (Figure 3.15 image A and C). On the other hand, FA treated cells tended to detach from the plates after injury, making it easier to observe the recovery process after damage. Therefore, due to this observation as well as the fact that FA induced acute injury shares similar characteristics to human AKI, 18mM FA was chosen to induce acute injury to HK2 cells in the rest of the project.

To conclude, the ICR mice failed to respond to nephrotoxic drug AA, therefore they were not considered as a functional experimental model for this project. HK2 cells, on the other hand, were observed to show acute damage in cell viability when exposed to either AA or FA. For the reasons explained above, FA at concentration of 18mM was chosen for the remainder of the project.

# CHAPTER 4: HMGB1 AND AUTOPHAGY EXPRESSION DURING FA INDUCED DAMAGE AND RECOVERY

## 4.1 INTRODUCTION

High mobility group box 1 (HMGB1) belongs to the high mobility group nuclear protein family, it presents in mammalian cells in the nucleus, it has multiple biological functions, such as regulating gene transcription, DNA repair, proliferation and development (Yang *et al.*, 2011). It was reported to be passively released from the nuclei when cells were undergoing necrosis, acting as a proinflammatory cytokine that passes necrotic signal to the adjacent cells through cell-surface receptors; however when cells were undergoing apoptosis, HMGB1 was retained in the nuclei (Kang *et al.*, 2014; Degryse *et al*., 2001; Scaffidi *et al*., 2002). Studies have shown that HMGB1 may interact with a few receptors once released into the circulation, these receptors include receptor for advanced glycation end products (RAGE), toll-like receptor 2 (TLR2), toll-like receptor 4 (TLR4), Triggering receptor expressed on myeloid cells 1 (TREM1) and cluster of differentiation 24 (CD24) (Chen *et al*., 2009; El Mezayen *et al*., 2007; Kang *et al*., 2010; Park J.S., 2006). It was reported that the engagement between HMGB1 and receptors such as TLR2 and TLR4 might result in the induction of inflammatory responses and the release of proinflammatory cytokines, causing tissue damage in renal IRI (Wu *et al.*, 2010). A study performed on mice induced with kidney IRI showed a raise of HMGB1 expression in the kidney tubular epithelial cells at day 1 post IRI and day 5 post IRI compared with controls; however when mice were pre-treated with anti-HMGB1 antibodies (300μg per mouse) prior to IRI, the SCr level and signs of tubular injury such as loss of brush border and tubular necrosis were significantly reduced compared with IRI group (Wu *et al.*, 2010). It was also

reported that HMGB1 is released and secreted when cells were under oxidative stress received from $H_2O_2$ at 0.25mM. It was demonstrated that along with the release of HMGB1 after $H_2O_2$ induced acute injury, the interaction between chromosome region maintenance1 (CRM1) and HMGB1 significantly increased, suggesting that ROS induced HMGB1 release might be mediated by CRM1-dependent mechanism (Tang *et al*., 2007). Another study reported that treating mice with antioxidant ethyl pyruvate (EP) significantly suppressed signal transduction through NF-kB and p38 MAPK, along with the release and accumulation of HMGB1, suggesting that EP might mediate the release of HMGB1 by suppressing signal transduction through NF-kB and p38 MAPK (Ulloa *et al*., 2002).

Autophagy is a catabolic process of recycling and degrading old proteins and intracellular organelles, the recycled contents are then used to synthesize new proteins and made use for the cells; therefore, autophagy helps maintaining cellular homeostasis under normal conditions. On the hand, when cells are under stress condition such as hypoxia, starvation, oxidant injury, autophagy could still be induced as studies have reported that autophagy plays a crucial role in cell death, as upregulated autophagy increase the capability in response to stress; on the other hand, the reduction of activated autophagy promotes cell death (Kroemer and Levine, 2008; Kaushal G.P., 2012). Double membraned phagophores were formed in the cytoplasm. During the formation of the autophagosome, the protein complex ATG5–ATG12–ATG16L1 allows the conjugation of 1A/1B-light chain 3 II (LC3-II) to the membrane, which then disassociated from the membrane. As phagophores approach closure, the

autophagosomes are formed and then fuse with the lysosomes and their contents are degraded (Fig 4.1).

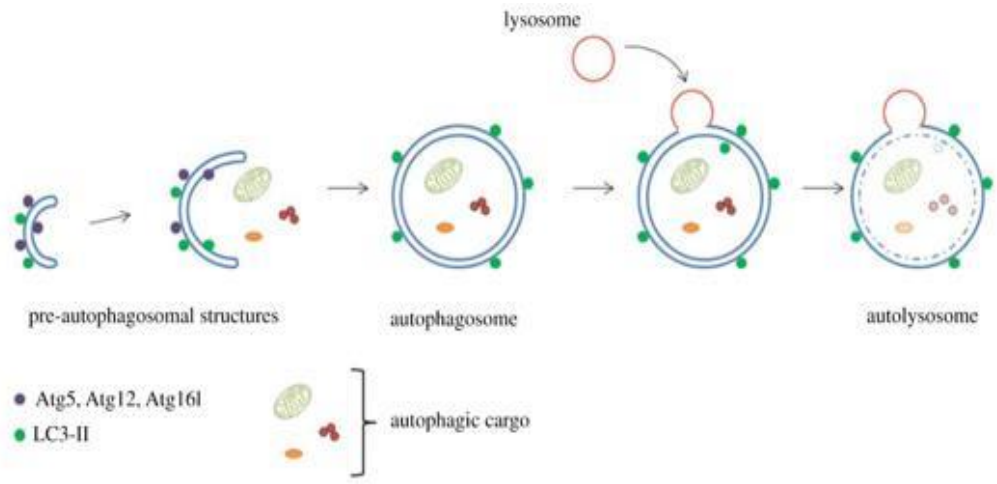


**Figure 4. 1 The process of autophagic flux.**

Image is taken from Lopez A., Fleming A., Rubinsztein D.C. (2008) Seeing is believing: methods to monitor vertebrate autophagy in vivo. Open Biol. 8(10).

Autophagy is also thought to participate in multiple biological processes: Some studies suggested that the inhibition of autophagy limits HMGB1 release, secretion and degradation (Dupond *et al*., 2011; Li *et al*., 2011). Studies also indicated that the deficit of HMGB1 limited exogenous $H_2O_2$-induced LC3-II expression and LC3 punctae formation, which suggested that HMGB1 might play an essential role in regulating oxidative stress-related autophagy activation (Tang *et al*., 2011).

The aim of this chapter is to make use of our *in vitro* model that was established from last chapter- by treating HK2 cells with FA for 24 hours to induce AKI, to enable the examination of gene expression of HMGB1, LC3B and GRP78 in the cells after FA damage and during recovery, which allows further understanding on 1) the mechanism of how FA damaged HK2 cells, 2) potential pathways by which HK2 cells took to prevent FA damage, 3) potential pathways by which HK2 cells recover from AKI.

We hypothesised that 1) the protein levels of HMGB1, LC3B and GRP78 increase after 24-hour FA treatment and decrease as the recovery progress, 2) the ROS level increase in the survived cells during 24-hour FA treatment and decrease as the recovery progress.

## 4.2 MATERIALS AND METHODS

HK2 cells were seeded in DMEM at a density of 60,000 cells per well on a 6-well plate as described in section 2.1.4 cell counting and seeding, the treatments were applied when cells reached around 80% confluence. Treatments were freshly prepared prior to each experiment as described in section 2.1.5 cell culture treatments. For immunocytochemistry experiment, sterilised coverslips were placed in all wells in 12-well plates, HK2 cells were seeded in DMEM at a density of 20,000 cells per well. Treatments were made freshly prior to each experiment and were given when cells reached around 80% confluence. Immunocytochemistry procedures were performed following section 2.5 Immunocytochemistry. Cell number were counted using a Hawkslay haemocytometer (section 2.1.4 cell counting and seeding) and ROS level was measured using fluorescent dye CM-$H_2$DCFDA (section 2.4 Reactive oxygen species measurement).

Bafilomycin A1 (B1793, Sigma-Aldrich) and chloroquine (C6628, Sigma-Aldrich), two common inhibitors for inhibiting fusion between autophagosomes and lysosomes (Redmann *et al*., 2017), were diluted to DMSO at 0.1 mg/ml or water at 50 mg/ml according to manufacturer's protocol, then further diluted with serum-free media into different treatments. The chosen working concentration for BA1 was 5ηM and the chosen working concentration for CQ was 20μM.

Statistics were performed using Statistical Package for the Social Sciences (SPSS) version 21.0. One-way ANOVA was performed and only $p<0.05$ was considered as statistically significant.

## 4.3 RESULTS

### 4.3.1 Treatment with FA increased the expression of total HMGB1

Immunocytochemistry was performed at 4 hours, 8 hours, 12 hours and 24 hours after HK2 cells were exposed to FA, and after 12 hours, 24 hours and 48 hours recovery. Immunofluorescence staining with HMGB1 (green), DAPI (blue) and F-actin was revealed by staining with phalloidin in red. An overlay image at each timepoint allow an overview of the expressions and detection of colocalization between cellular compartments.

The fluorescent HMGB1 protein could be observed as early as after 8-hour FA treatment (Figure 4.2 B3 and Figure 4.3 B3), then the fluorescent signal remained strong until early (12-hour) recovery stage (Figure 4.2 F3 and Figure 4.3 F3). The HMGB1 fluorescent signal slowly getting weaker during the cell recovery period and could be hardly observed after 48-hour recovery (Figure 4.2 H3 and Figure 4.3 H3). A clearer trend could be observed from Figure 4.4 and Figure 4.5 that the fluorescent signal of HMGB1 gradually increased during FA treatment, persisted at 24-hour treatment until 12-hour recovery period, then the signal slowly reduced following longer recovery.

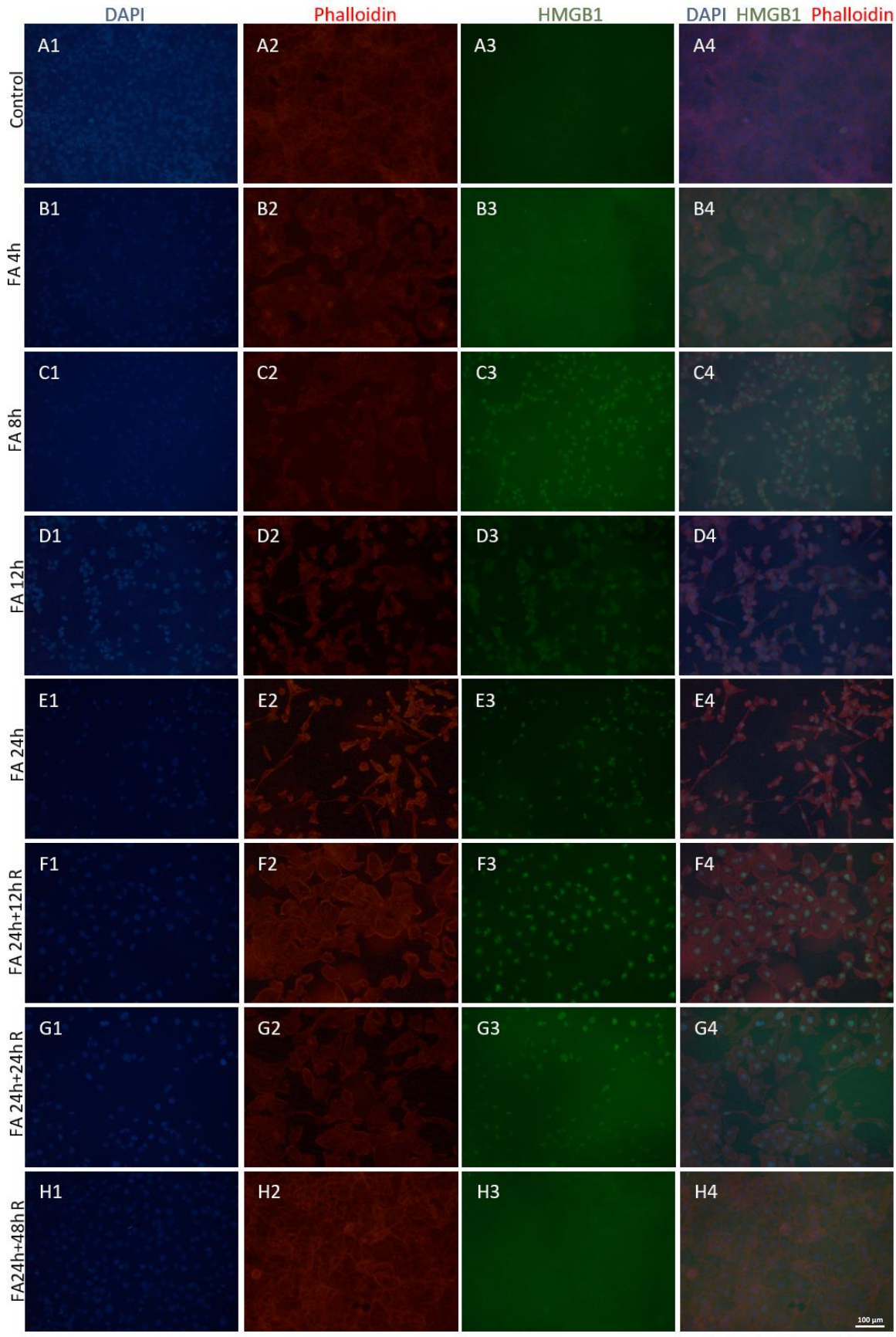
DAPI
Phalloidin
HMGB1
DAPI HMGB1 Phalloidin
Control
FA 4h
FA 8h
FA 12h
FA 24h
FA 24h+12h R
FA 24h+24h R
FA24h+48h R
A1
A2
A3
A4
B1
B2
B3
B4
C1
C2
C3
C4
D1
D2
D3
D4
E1
E2
E3
E4
F1
F2
F3
F4
G1
G2
G3
G4
H1
H2
H3
H4
100 μm

**Figure 4. 2 HMGB1 immunocytochemistry following FA treated and recovering HK2 cells.**

HK2 cells were fixed at different timepoints of exposure to FA and during recovery. Immunofluorescence staining with **DAPI** (A1, B1, C1, D1, E1, F1, G1, H1), **phalloidin** (A2, B2, C2, D2, E2, F2, G2, H2), **HMGB1** (A3, B3, C3, D3, E3, F3, G3, H3) and **overlay** (A4, B4, C4, D4, E4, F4, G4, H4). **Control**: HK2 cells were incubated in FBS-free media for a set of time. **FA 4h**: 4-hour incubation in FA treatment solution. **FA 8h**: 8-hour incubation in FA treatment solution. **FA 12h**: 12-hour incubation in FA treatment solution. **FA 24h**: 24-hour incubation in FA treatment solution. **FA 24h+12R**: 24-hour incubation in FA treatment solution followed with 12-hour recovery in DMEM media. **FA 24h+24R**: 24-hour incubation in FA treatment solution followed with 24-hour recovery in DMEM media. **FA 24h+48R**: 24-hour incubation in FA treatment solution followed with 48-hour recovery in DMEM media. Images were taken at 20x magnification. Scale bar = 100 μm. One field per slide and three slides per treatment group were performed for an n = 3.

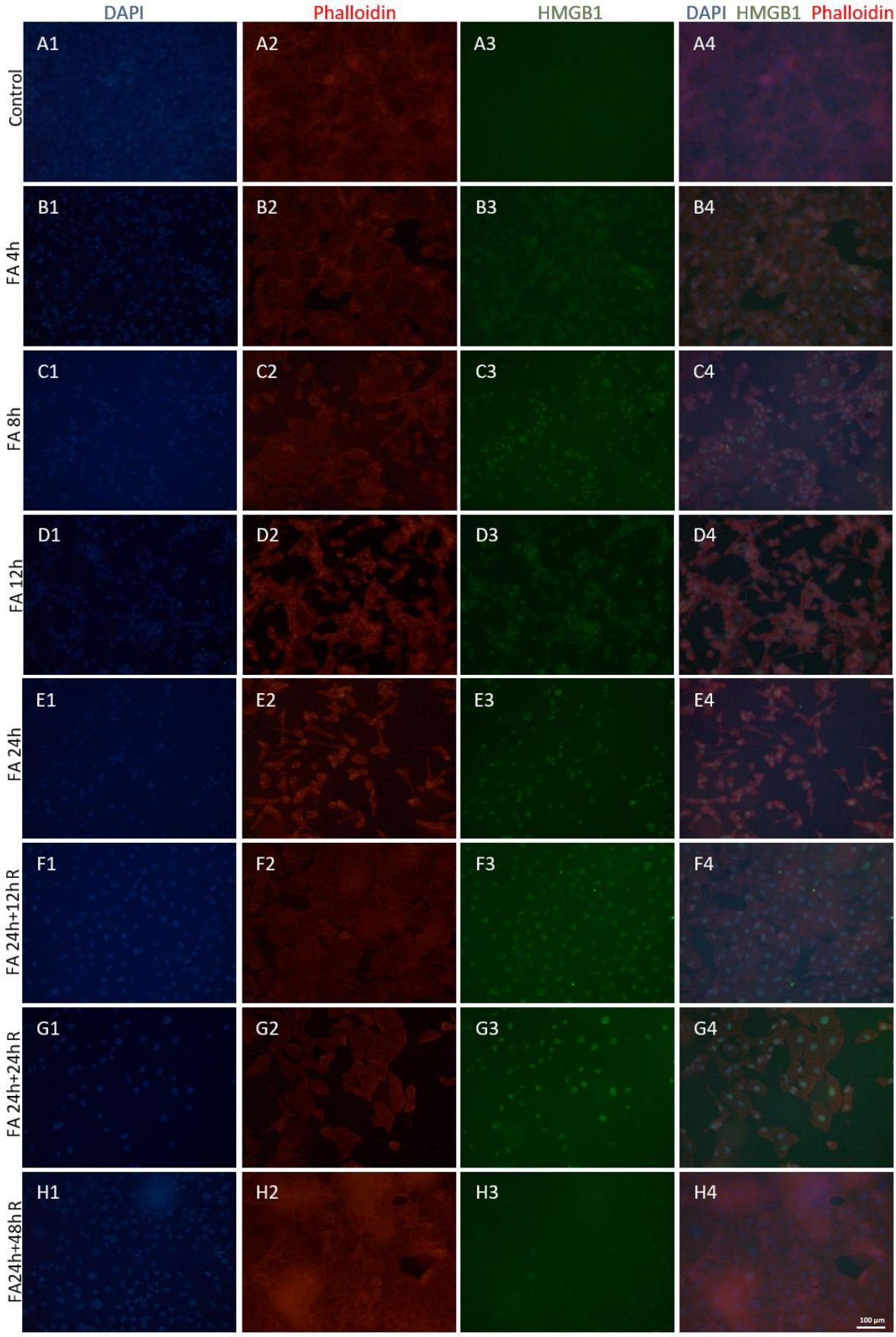
DAPI
Phalloidin
HMGB1
DAPI HMGB1 Phalloidin
Control
FA 4h
FA 8h
FA 12h
FA 24h
FA 24h+12h R
FA 24h+24h R
FA24h+48h R
A1
A2
A3
A4
B1
B2
B3
B4
C1
C2
C3
C4
D1
D2
D3
D4
E1
E2
E3
E4
F1
F2
F3
F4
G1
G2
G3
G4
H1
H2
H3
H4
100 µm

**Figure 4. 3 Repetitive images of HMGB1 immunocytochemistry following FA treated and recovering HK2 cells.**

HK2 cells were fixed at different timepoints of exposure to FA and during recovery. Immunofluorescence staining with DAPI (A1, B1, C1, D1, E1, F1, G1, H1), phalloidin (A2, B2, C2, D2, E2, F2, G2, H2), HMGB1 (A3, B3, C3, D3, E3, F3, G3, H3) and overlay (A4, B4, C4, D4, E4, F4, G4, H4). **Control**: HK2 cells were incubated in FBS-free media for a set of time. **FA 4h**: 4-hour incubation in FA treatment solution. **FA 8h**: 8-hour incubation in FA treatment solution. **FA 12h**: 12-hour incubation in FA treatment solution. **FA 24h**: 24-hour incubation in FA treatment solution. **FA 24h+12R**: 24-hour incubation in FA treatment solution followed with 12-hour recovery in DMEM media. **FA 24h+24R**: 24-hour incubation in FA treatment solution followed with 24-hour recovery in DMEM media. **FA 24h+48R**: 24-hour incubation in FA treatment solution followed with 48-hour recovery in DMEM media. Images were taken at 20x magnification, scale bar = 100 μm. One field per slide and three slides per treatment group were performed for an n = 3.

**A**

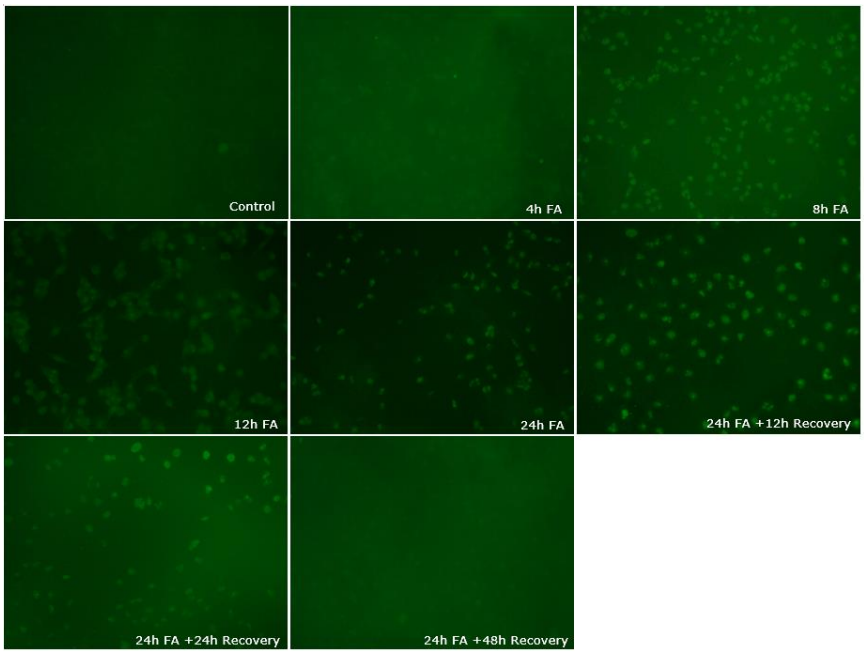


**B**

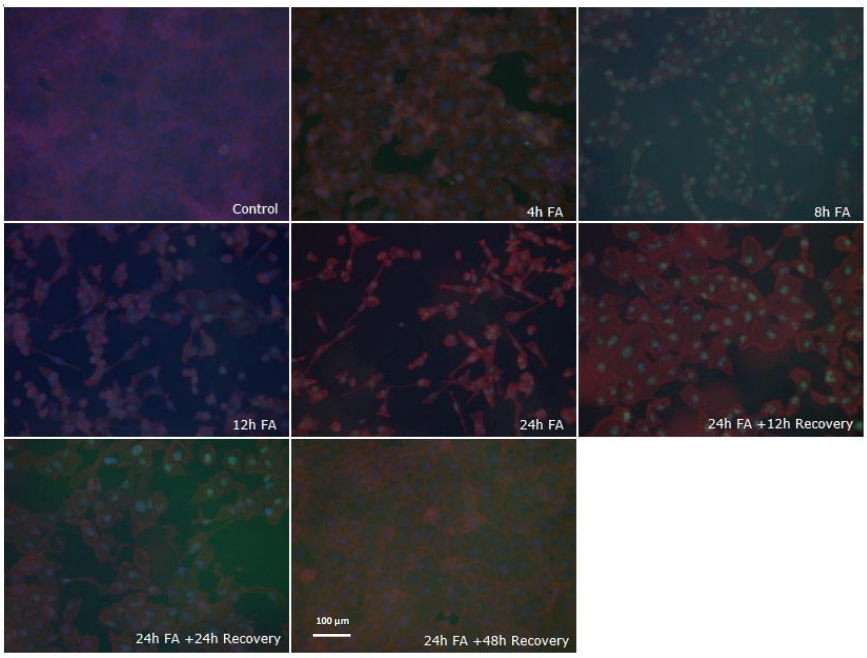


**Figure 4. 4 Immunocytochemistry following FA treated and recovering HK2 cells, HMGB1 and overlay only.**

HMGB1 (**A**) and overlay (**B**) images from Figure 4.2 were put together following the timepoints.

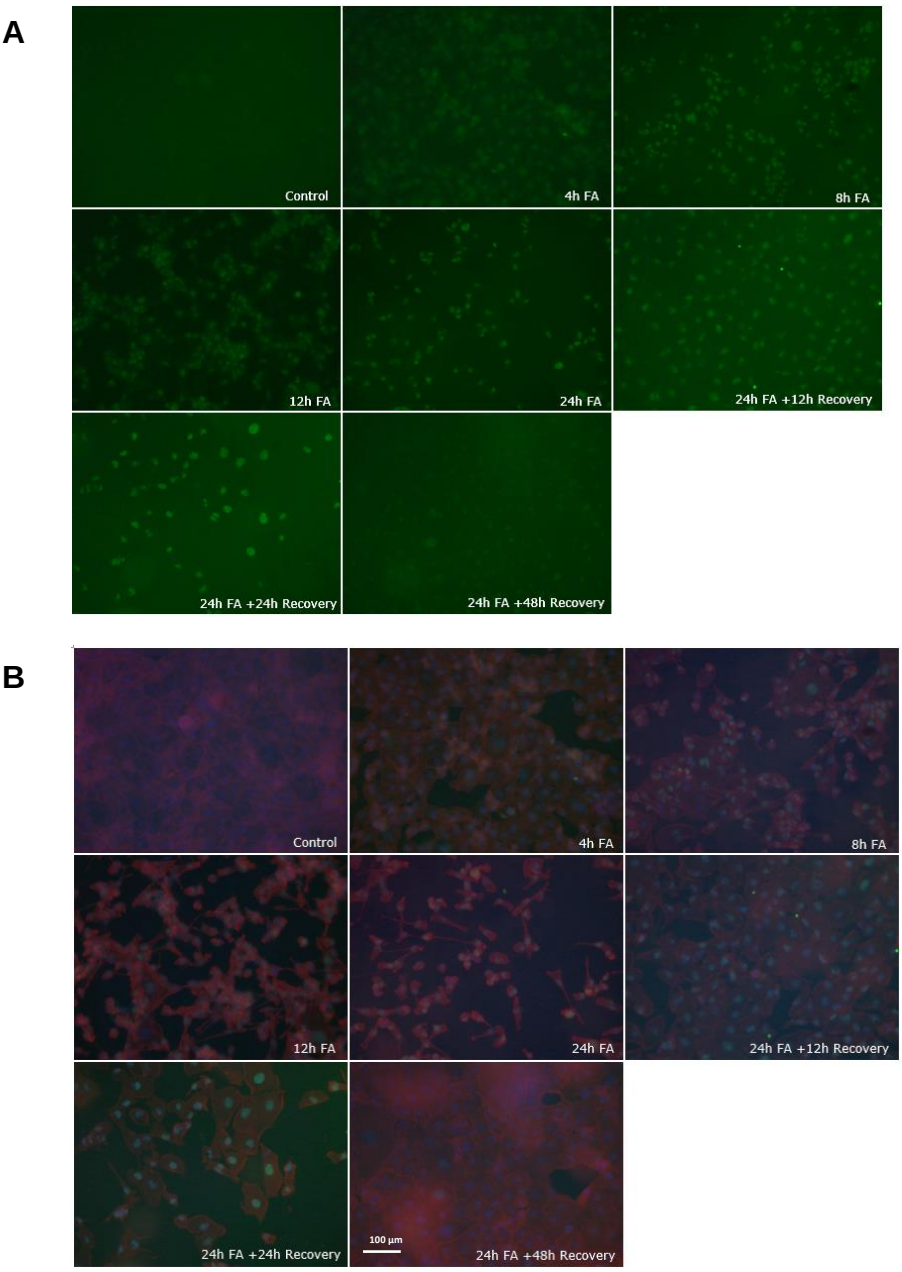


**Figure 4. 5 Repetitive images of immunocytochemistry following FA treated and recovering HK2 cells, HMGB1 and overlay only.**

HMGB1 (**A**) and overlay (**B**) images from Figure 4.3 were put together following the timepoints.

The expression of total HMGB1 was further confirmed by the results from western blot. HMGB1 showed a significant increase in expression after 24-hour FA treatment followed by a slight decrease after 12-hour recovery ($p<0.05$, Figure 4.6). The expression of total HMGB1 in cells showed no significant difference to the control during further recovery.

**A**

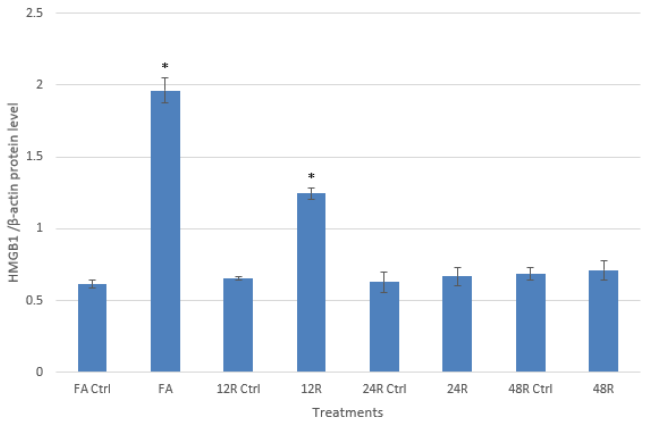


**B**

| | FA Control | FA | 12h Recovery Control | 12h Recovery | 24h Recovery Control | 24h Recovery | 48h Recovery Control | 48h Recovery |
|---|---|---|---|---|---|---|---|---|
| **HMGB1 (29KDa)** |  |  |  |  |  |  |  |  |
| **β -actin (42KDa)** |  | 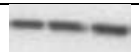 |  | 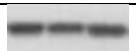 |  | 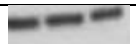 | 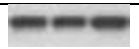 |  |

**Figure 4. 6 Total HMGB1 expression in FA induced damage and recovery.**

Total HMGB1 expression was analysed after 24-hour FA damage and during 48-hour recovery. (**A**) Relative protein levels of HMGB1. All data were shown as mean ± SEM for n=3 wells per treatment. One-way ANOVA was performed followed by Dunnett multiple comparison test, *p<0.05 was considered as significant. (**B**) Immunoblot of HMGB1 and β -actin in control, FA damage and recovery.

CM-$H_2$DCFDA was used to track the ROS level change during FA damage and recovery. As expected, after just 4 hours of incubation the ROS level in HK2 cells increased significantly compared to control group ($p<0.05$), and the ROS gradually increased during 24-hour FA treatment. Conversely, the ROS level gradually reduced when cells were allowed to recover from the damage. Noticeably, there was a significant difference between the latter recovery groups and the 24-hour FA treated group, indicating that cellular oxidative stress may reduce during recovery ($p<0.05$, Figure 4.7). Overall, the ROS level significantly increased during FA damage in a time-dependent manner and had a significant reduction at the end of 48-hour recovery, which matched HMGB1 protein pattern in Figure 4.2, 4.3 and 4.6, suggesting that HMGB1 was associated with ROS level during FA damage and recovery ($p<0.05$).

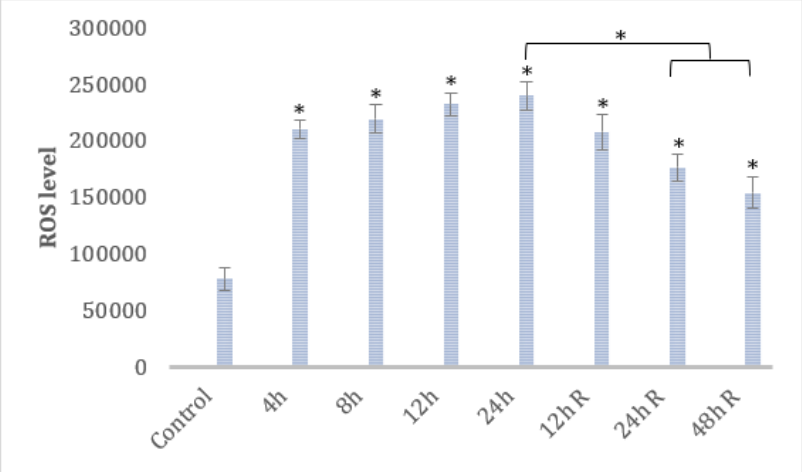


**Figure 4. 7 ROS level detection during cell damage and recovery.**

ROS level of control, 4-hour, 8-hour, 12-hour, 24-hour FA treated cells, as well as 12-hour, 24-hour and 48-hour recovery was detected using CM-$H_2$DCFDA. Means (n=3) ± SEM were shown, One-way ANOVA was performed followed by Tukey's test, $p<0.05$ was considered as significant.

### 4.3.2 Nuclear and cytoplasmic HMGB1 level increased in FA treated cells

The expression of nuclear HMGB1 significantly increased after 24-hour FA treatment compared to the control group (Figure 4.8 A and B, $p<0.05$). This was followed by a slight decrease in expression after 12-hour recovery, which also showed significant difference to its control group ($p<0.05$). After 24-hour recovery, the nuclear HMGB1 expression slightly reduced compared to 12-hour recovery but still had significant difference to its control group ($p<0.05$) until recovered for 48 hours ($p>0.05$). The expression of nuclear HMGB1 showed longer expression period than total HMGB1 as nuclear HMGB1 showed significant increase in expression in 24-hour recovery group compared to its control group, total HMGB1 did not show significant difference to its control group in 24-hour group, which suggested that HMGB1 remained activate in nucleus in recovery in response to FA damage, and its expression in recovery suggested that HMGB1 might play a role in promoting recovery after acute damage. Moreover, a significant 2.3-fold increase in cytoplasmic HMGB1 expression was observed after 24-hour FA treatment (Figure 4.8 C and D, $p<0.05$), and dropped to a similar level to its control group during recovery. Although studies have shown that HMGB1 was released from the nucleus to the cytoplasm in response to cell injury, and the migration of nuclear HMGB1 to cytoplasm might be a crucial step to allow HMGB1 play a proinflammatory role including activating inflammatory cells, promoting the secretion of inflammatory cytokines (Ruan *et al*., 2014; Zhan *et al.*, 2016; Wu *et al*., 2010; Doi *et al*., 2014; Zhan *et al*., 2016), the conclusion that HMGB1 had

nucleocytoplasmic translocation in response to FA damage could not be drawn until further histone H3 protein tested in the cytoplasmic samples.

**A**

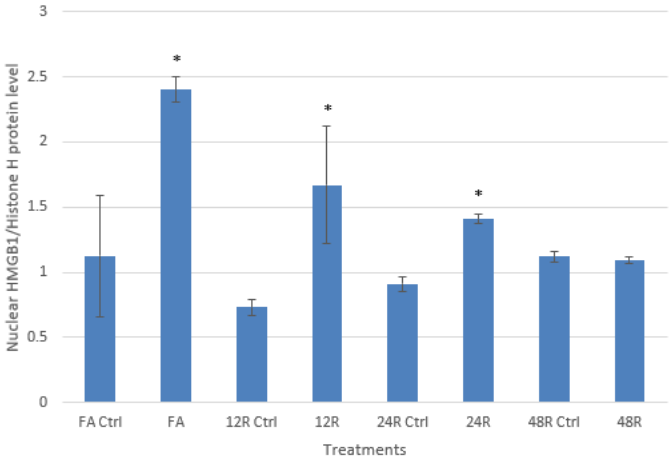


**B**

| | FA Control | FA | 12h Recovery Control | 12h Recovery | 24h Recovery Control | 24h Recovery | 48h Recovery Control | 48h Recovery |
|---|---|---|---|---|---|---|---|---|
| HMGB1 (Nuc) (29KDa) |  | 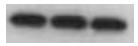 |  |  |  | 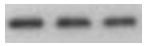 |  |  |
| Histone H3 (15KDa) | 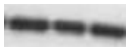 |  | 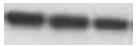 |  |  |  |  |  |

**C**

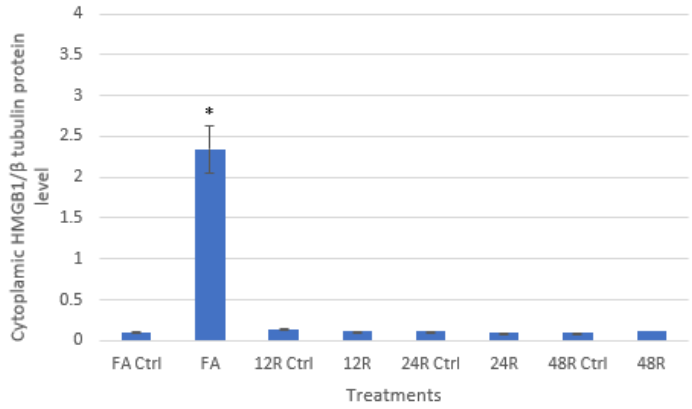


**D**

| | FA Control | FA | 12h Recovery Control | 12h Recovery | 24h Recovery Control | 24h Recovery | 48h Recovery Control | 48h Recovery |
|---|---|---|---|---|---|---|---|---|
| Cyto HMGB1 (29KDa) | | | | | | | | |
| β - tubulin (55KDa) | | | | | | | | |

**Figure 4. 8 Nuclear HMGB1 and cytoplasmic HMGB1 expression in FA induced damage and recovery.**

Nuclear HMGB1 expression was analysed after 24-hour FA damage and during recovery. (**A**) Relative protein levels of nuclear HMGB1 (**C**) Relative protein levels of cytoplasmic HMGB1, all data were shown as mean ± SEM for n=3 wells per treatment. One-way ANOVA was performed

followed by Dunnett multiple comparison test, *p<0.05 was considered as significant. (**B**) Immunoblot of nuclear HMGB1 and Histone H3 in treatments. (**D**) Immunoblot of cytoplasmic HMGB1 and β -tubulin in treatments.

### 4.3.3 By inhibiting HMGB1 with glycyrrhizin did not increase the survival rate after treating with FA.

Glycyrrhizin is the sweet-tasting compound of the root of Glycyrrhiza glabra, it has been reported as an inhibitor of extracellular HMGB1 cytokine (Mollica *et al*., 2007; Xiang *et al*., 2014; Li *et al*., 2017; Kim *et al*., 2015; Zhang *et al*., 2017). We intended to use glycyrrhizin to inhibit HMGB1 expression in order to detect its importance during FA damage. 20mg Glycyrrhizin (1405-86-3, Sigma) was dissolved in DMSO in order to prepare the stock solution at 20mg/ml, working solution was diluted from the stock solution with serum-free DMEM to 100μg/ml. A group of HK2 cells were pre-treated with glycyrrhizin for 24 hours prior to 24-hour FA treatment with other groups and cell number was counted using a haemocytometer. Pre-treating cells with glycyrrhizin did not have a significant influence on HMGB1 protein level compared to the group treated with FA only (Figure 4.9), both FA-treated group and glycyrrhizin treated group showed significant difference to the control group ($p<0.05$). In addition, FA created a significant cell number loss compared to control group (Figure 4.10, $p<0.05$); surprisingly, there was still a significant ($p<0.05$) cell loss over pre-treatment group, and there was no significant ($p>0.05$) difference between pre-treatment group and non-pre-treatment group in terms of cell number. Together it indicated that the activation of HMGB1 might not be the key to induce cell death under FA damage; pre-treatment with glycyrrhizin alone did not protect cells from death under FA treatment.

**A**

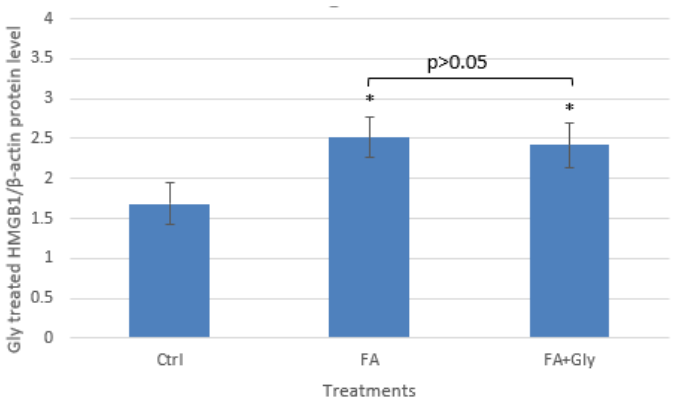


**B**

| | Control | 24h FA | 24h FA + glycyrrhizin |
|---|---|---|---|
| **HMGB1 (29KDa)** |  |  |  |
| **β -actin (42KDa)** |  |  |  |

**Figure 4. 9 HMGB1 expression with/without glycyrrhizin (Gly) in control and after 24-hour FA treatment.**

HMGB1 expression was analysed with/without Gly in control and after 24-hour FA damage. (**A**) Relative protein levels of HMGB1. All data were shown as mean ± SEM for n=3 wells per treatment. One-way ANOVA was performed followed by Tukey's test, *p<0.05 was considered as significant. (**B**) Immunoblot of HMGB1 and β -actin in control, FA damage with/without Gly.

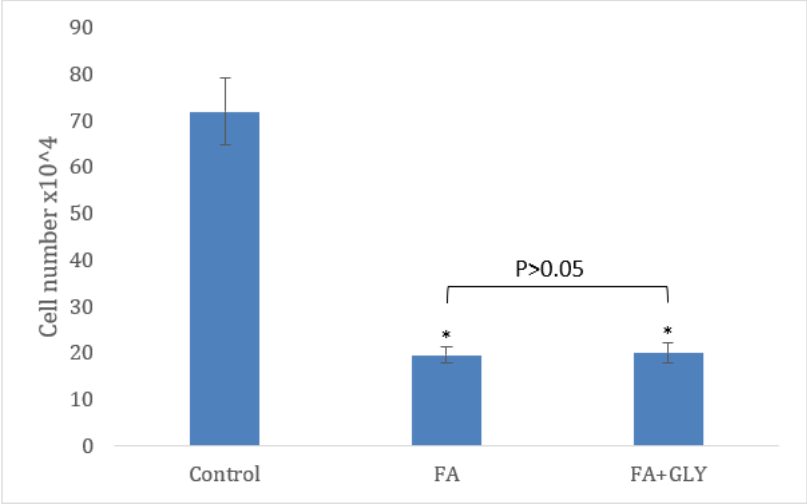


**Figure 4. 10 Cell number count comparison between control, FA treated and pre-treatment with glycyrrhizin.**

A group of HK2 cells were pre-treated with HMGB1 inhibitor glycyrrhizin for 24 hours before incubated with FA. Cell number was counted after 24-hour incubation with FA or FBS-free media. Means (n=3) ± SEM are shown, One-way ANOVA was performed followed by Tukey's test, *P<0.05 was considered as significant.

### 4.3.4 Treatment with FA increased the expression of LC3B and GRP78

Immunocytochemistry was performed on the control group, after 24-hour FA treatment, 12-hour recovery, 24-hour recovery and 48-hour recovery.

LC3B naturally expressed in HK2 cells and had a cytoplasmic punctate staining pattern (Figure 4.11 image B, Figure 4.12 image B). After 24-hour FA treatment, the signal of LC3B protein was stronger than control (Figure 4.11 image E Figure 4.12 image E). In comparison, the signal of LC3B decreased after 12-hour recovery (Figure 4.11 image H, Figure 4.12 image H), slightly increased after 24-hour recovery (Figure 4.11 image K, Figure 4.12 K) and sustained at similar expression level after 48-hour recovery (Figure 4.11 N, Figure 4.12 N).

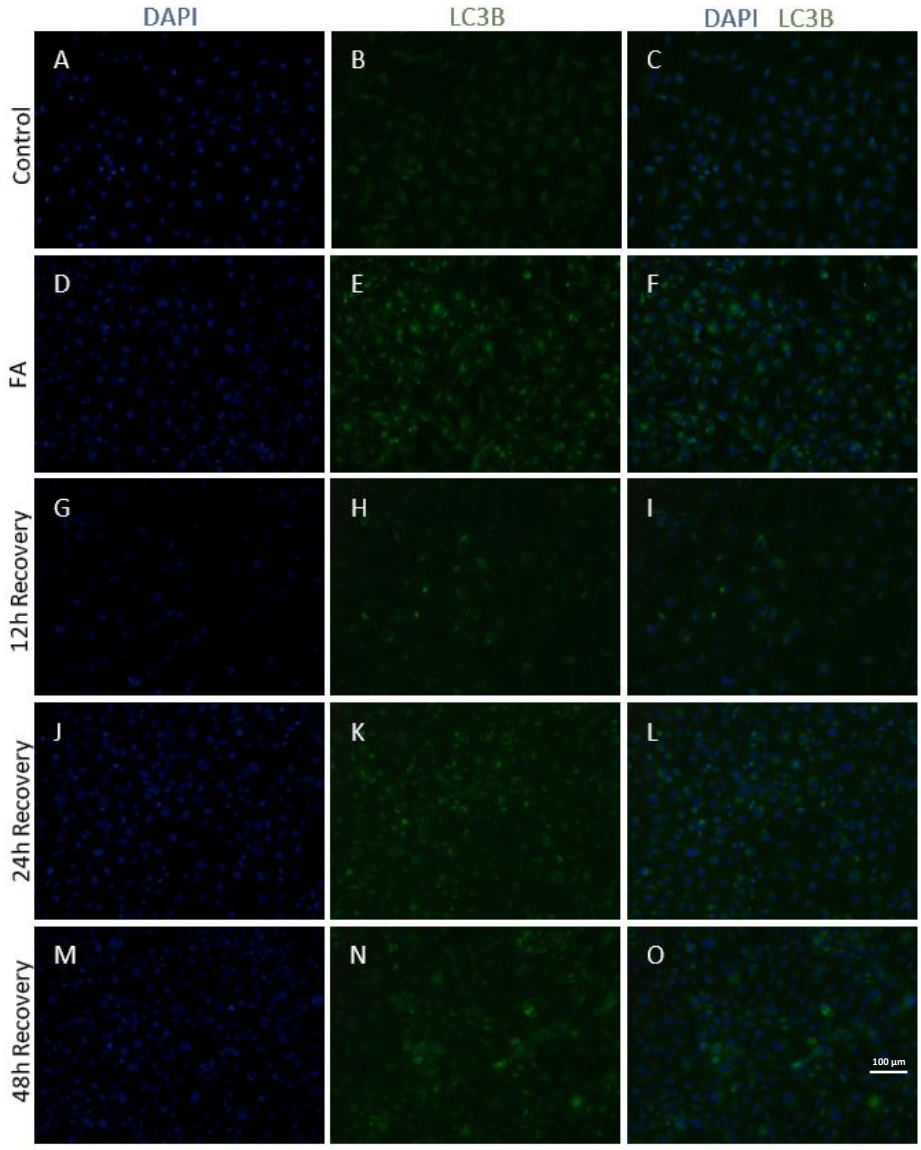


**Figure 4. 11 LC3B Immunocytochemistry after FA treatment and during recovery.**

HK2 cells were fixed at different time points of exposure to FA and during recovery. Nuclei was stained with DAPI in blue, LC3B was shown in green. Images were taken at 20x magnification. Scale bar = 100 µm. One field per slide and three slides per treatment group were performed for an n = 3.

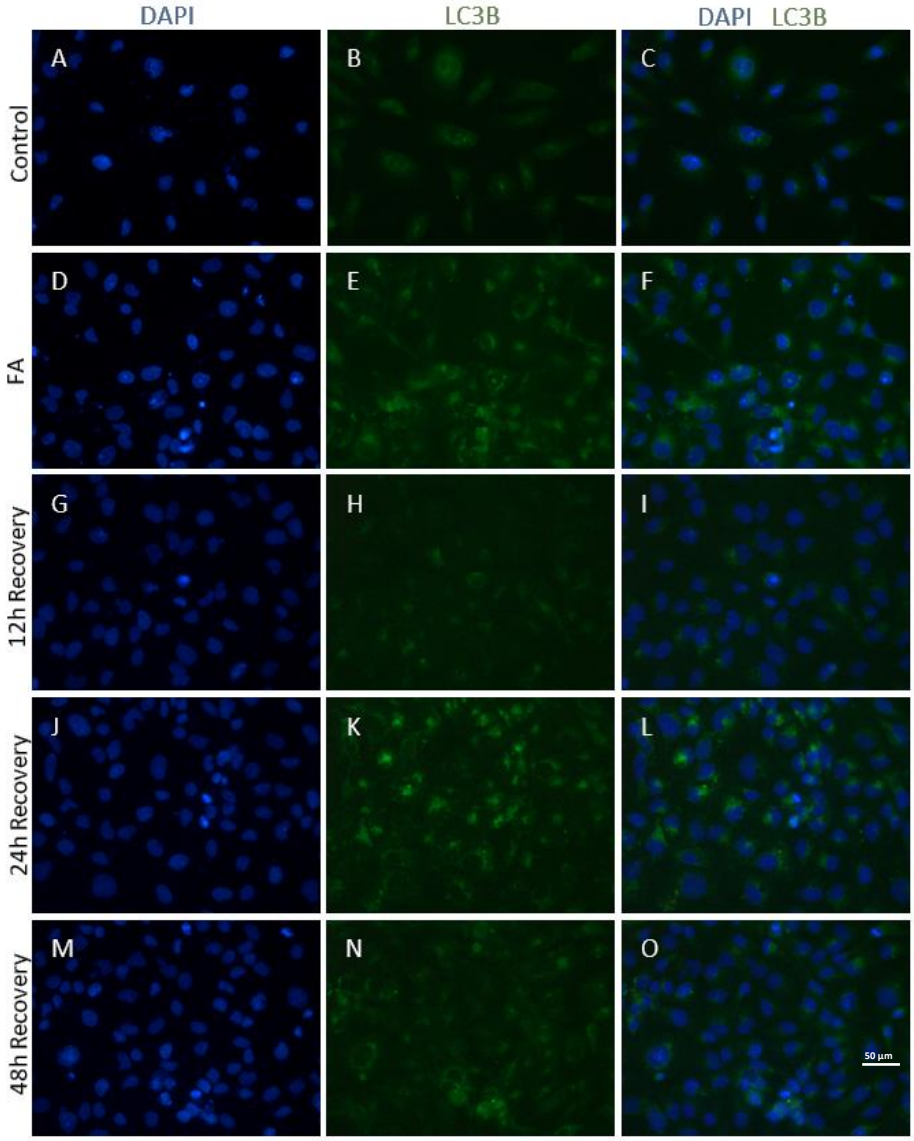


**Figure 4. 12 LC3B Immunocytochemistry after FA treatment and during recovery at higher power.**

HK2 cells were fixed at different time points of exposure to FA and during recovery. Nuclei was stained with DAPI in blue, LC3B was shown in green. Images were taken at 40x magnification, Scale bar = 50µm. One field per slide and three slides per treatment group were performed for an n = 3.

HK2 samples at 24-hour FA treatment, 12-hour recovery, 24-hour recovery, 48-hour recovery and the negative control group at all timepoints were also collected in order to quantify the protein level of LC3B, p62 and GRP78 during FA damage and recovery. There was a significant ($p<0.05$) increase in LC3B expression after 24-hour FA treatment, especially LC3B II, suggesting an upregulation of autophagy. The protein level of LC3B I and LC3B II significantly decreased after 12-hour recovery ($p<0.05$, Figure 4.13 image A and B).

GRP78 is one of the best-characterized chaperones in the endoplasmic reticulum (ER) protein folding machinery, which directs misfolded proteins toward ER-associated degradation, and it has been increasingly reported that GRP78 participates in multiple cell injuries (Zeeshan *et al.*, 2016). As expected, there was a significant ($p<0.05$) escalation of GRP78 expression in HK2 cells after 24-hour FA treatment (Figure 4.13 D and E), indicating that there was an increasing abundance of misfolding protein accumulation in the cells and potentially led to ER stress.

A

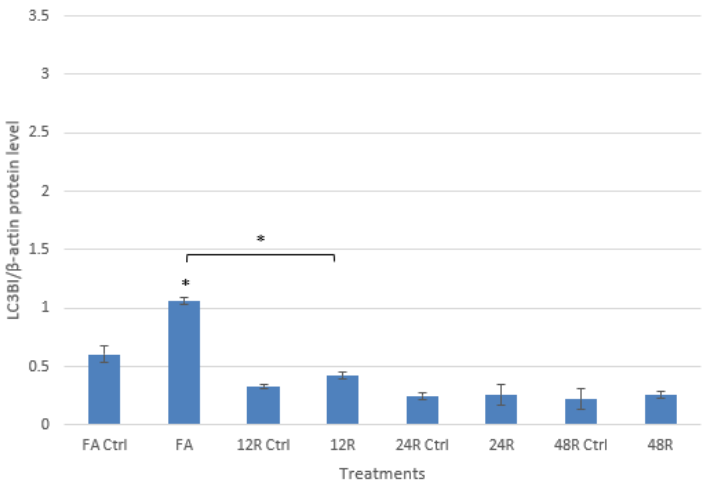


B

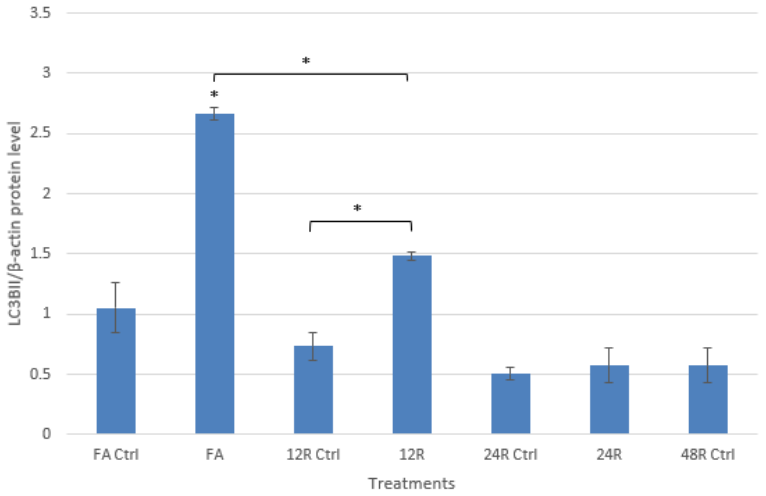


C

| | FA Control | FA | 12h Recovery Control | 12h Recovery | 24h Recovery Control | 24h Recovery | 48h Recovery Control | 48h Recovery |
|---|---|---|---|---|---|---|---|---|
| LC3BI and LC3BII (14KDa and 16KDa) |  | 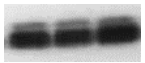 |  |  |  |  |  |  |
| β -actin (42KDa) |  |  |  |  |  |  |  | 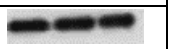 |

**D**

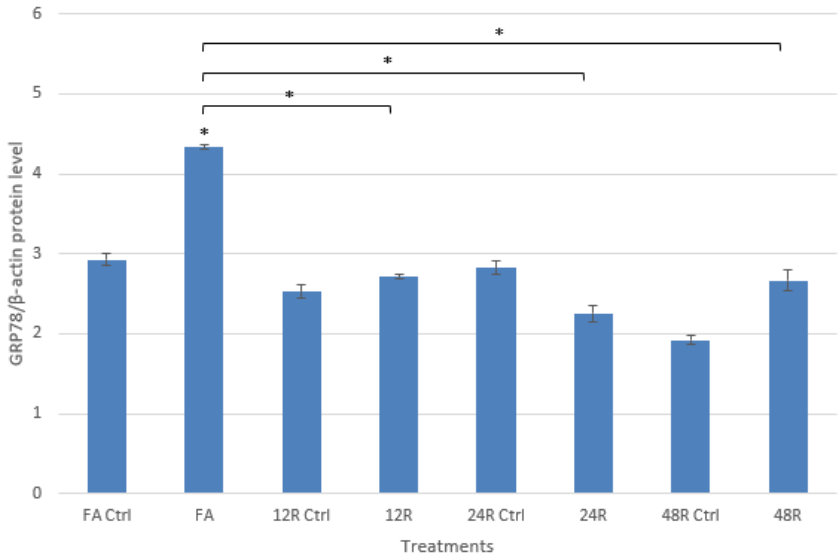


**E**

| | FA Control | FA | 12h Recovery Control | 12h Recovery | 24h Recovery Control | 24h Recovery | 48h Recovery Control | 48h Recovery |
|---|---|---|---|---|---|---|---|---|
| GRP78 (78KDa) | | | | | | | | |
| β -actin (42KDa) | | | | | | | | |

**Figure 4. 13 Western Blot analysis of LC3B and GRP78 expression after FA treatment and during recovery.**

HK2 cell samples were collected at 24-hour FA treatment, 12-hour recovery, 24-hour recovery, 48-hour recovery and the negative control group at all timepoints. (**A**) (**B**) Relative protein levels of LC3BI and LC3BII. (**D**) Relative protein levels of GRP78. All data were shown as mean ± SEM for n=3 wells per treatment. One-way ANOVA was performed followed by Tukey's test, *$p<0.05$ was considered as significant. (**C**) Immunoblot of LC3BI, LC3BII and β -actin. (**E**) Immunoblot of GRP78 and β -actin.

### 4.3.5 Inhibiting autophagy with BA1 did not prohibit HK2 cells from recovering after treated with FA

Bafilomycin A1 (BA1) is a known inhibitor of the late stage autophagy which restrains maturation of autophagic vacuoles by blocking fusion between autophagosomes and lysosomes (Yamamoto *et al*., 1998). Here we used BA1 to inhibit the function of autophagy in order to investigate the importance of autophagy during FA damage and recovery.

The working concentration of BA1 on HK2 cells was tested initially. 5ηM, 10ηM, 25ηM and 50ηM was chosen to test the effect of BA1 to LC3B as well as if the concentration difference would have different impact on LC3B protein level. There was a significant ($p<0.05$) increase in LC3B-I and LC3B-II level after 24-hour FA treatment (Figure 4.14 A and B); treating cells with 5ηM BA1 and FA significantly ($p<0.05$) increase the expression of LC3B-I and LC3B-II compared to FA treated group. On the other hand, the level of LC3B-I, LC3B-II and p63p protein was not affected by the increased concentration of BA1 ($p>0.05$, Figure 4.14 A, B, D). In addition, the cells did not show obvious difference in terms of morphology (Figure 4.14 F) between high and low concentrations of BA1. All results indicate that the effects of BA1 were the same for all concentrations tested on HK2 cells, therefore 5ηM BA1 was used for the following experiments.

**A**

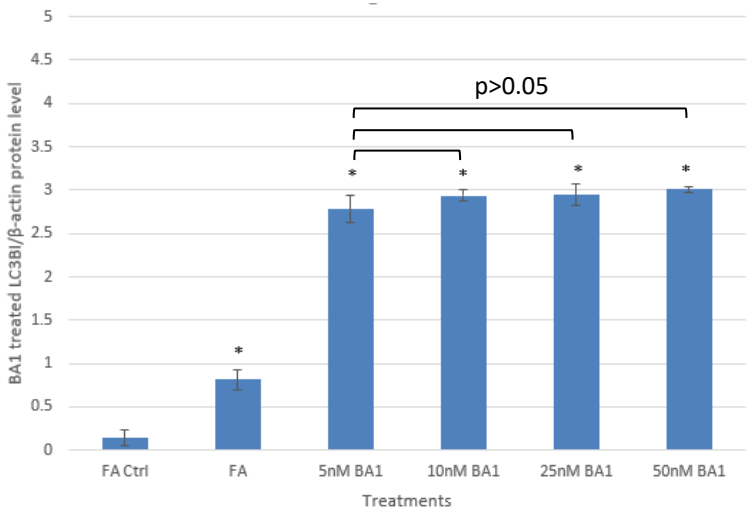


**B**

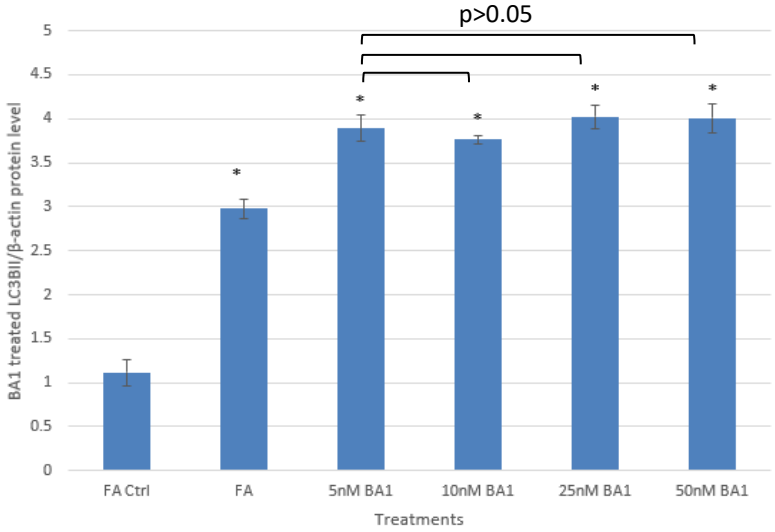


**C**

| | FA Ctrl | FA | 5nM BA1 | 10nM BA1 | 25nM BA1 | 50nM BA1 |
|---|---|---|---|---|---|---|
| LC3BI and LC3BII (BA1) (14KDa and 16KDa) | 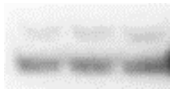 | 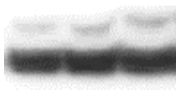 |  |  | 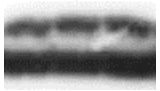 |  |
| β -actin (42KDa) | 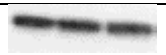 | 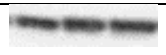 | 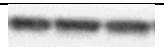 | 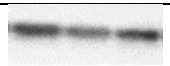 | 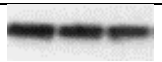 | 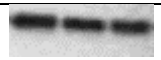 |

**D**

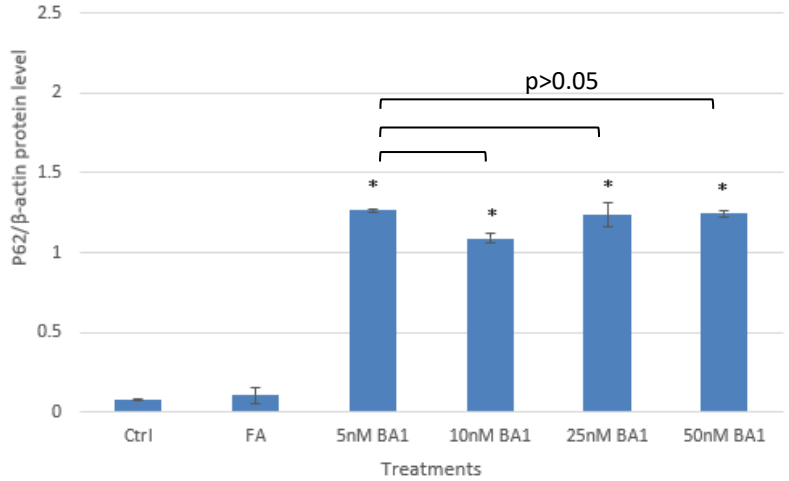


**E**

| | FA Ctrl | FA | 5nM BA1 | 10nM BA1 | 25nM BA1 | 50nM BA1 |
|---|---|---|---|---|---|---|
| p62 (BA1) (62KDa) | | | | | | |
| β -actin (42KDa) | | | | | | |

**F**

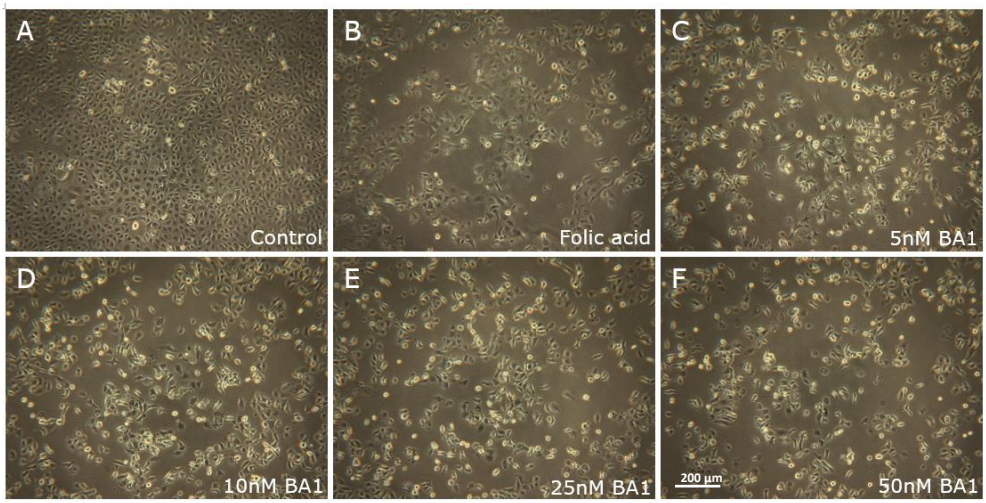


**Figure 4. 14 Effect of BA1 at various concentration on HK2 cells.**

HK2 cells were collected at 24-hour FA treatment, 24-hour FA treatment with BA1 at 5ηM, 10ηM, 25ηM and 50ηM. (**A**) (**B**) Relative protein levels of LC3BI and LC3BII after treating with BA1. (**D**) Relative protein levels of p62. All data were shown as mean ± SEM for n=3 wells per treatment. One-way ANOVA was performed followed by Tukey's test, *$p<0.05$ was considered as significant. (**C**) Immunoblot of LC3BI, LC3BII and β-actin after treating with BA1. (**E**) Immunoblot of p62 and β-actin after treating with BA1. Photographs were taken after each treatment. Photographs taken 6.7x magnification, scale bar = 200µm. One field per slide and three slides per treatment group were performed for an n = 3.

When cells were incubated with BA1 alone during treatment period, a slight reduction of cell number after 24-hour incubation was observed compared to the control group, which significantly slowed down the proliferation and recovery process (Fig 4.15 1 and 2), especially in the initial 24-hour recovery ($p<0.05$). However, it did not create long-term damage to the cells as the cell number recovered to a similar level to the control group after 72-hour recovery. The inhibition of autophagy on top of FA damage slowed down the progress of cell recovery. An extra 24 hours were needed for FA and BA1 treated cells to fully recover compared to the group that was treated with FA only. Incubation of cells with BA1 alone or FA and BA1 together did not increase cellular ROS level compared to either control or FA group respectively (Figure 4.15 3).

**1)**

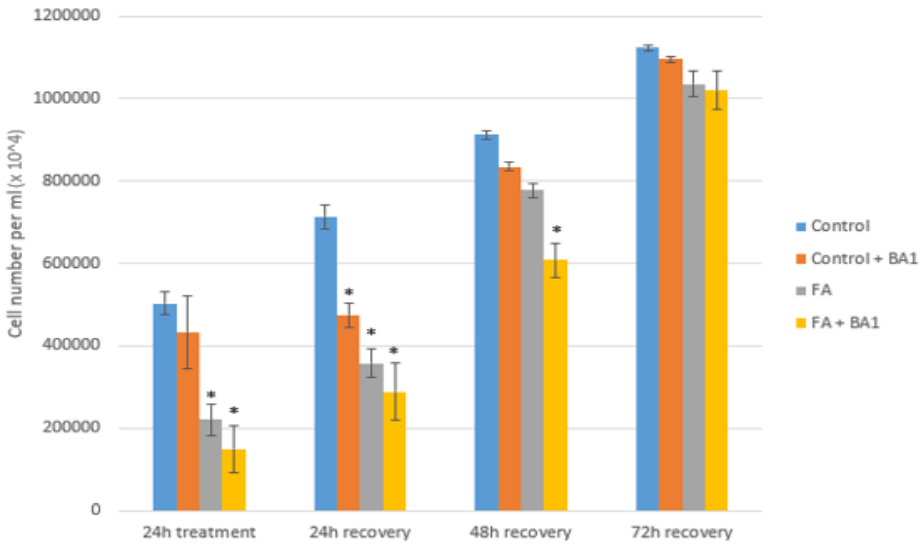
1200000
1000000
800000
600000
400000
200000
0
Cell number per ml (x 10^4)
24h treatment
24h recovery
48h recovery
72h recovery
Control
Control + BA1
FA
FA + BA1

**2)**

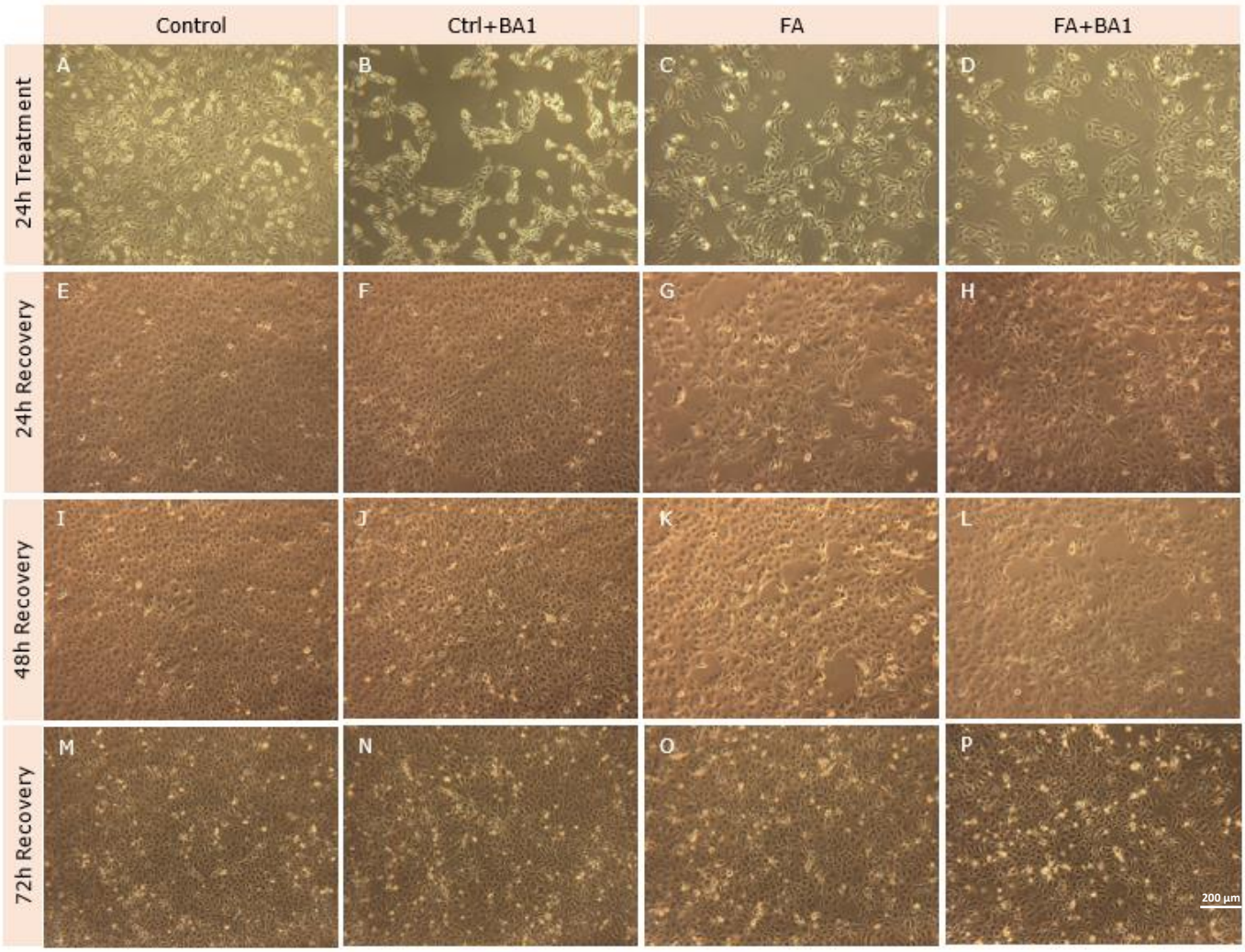
Control
Ctrl+BA1
FA
FA+BA1
24h Treatment
24h Recovery
48h Recovery
72h Recovery
A
B
C
D
E
F
G
H
I
J
K
L
M
N
O
P
200 µm

**3)**

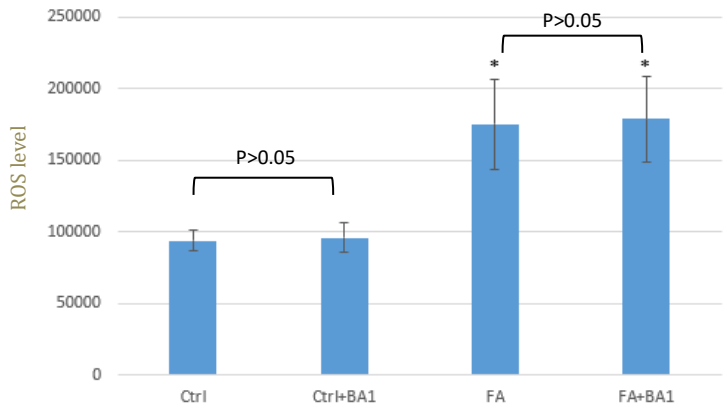


**Figure 4. 15 The effect of BA1 on HK2 cell recovery after FA induced injury.**

HK2 cells were divided into four groups: control, control with BA1, FA and FA with BA1. **(1)** Total cell count after 24-hour treatment, 24-hour recovery, 48-hour recovery and 72-hour recovery. Each treatment was carried out in triplicate, means ± SEM were shown, two-way ANOVA was used to analyse data and followed by Dunnett multiple comparison test **(2)** Images of HK2 cells after each treatment at different timepoints. Photos were taken at 6.7x magnification, scale bar = 200μm. (**3)** ROS level of HK2 cells after 24-hour treatment. The ROS level was measured using CM-$H_2$DCFDA. Each treatment was carried out in triplicate, means ± SEM were shown, One-way ANOVA was performed followed by Tukey's test, $p<0.05$ was considered as significant.

### 4.3.6 HK2 cells sustained normal mitochondrial morphology after inhibiting autophagy with BA1

The principle role for mitochondria is the generation of ATP, it is a dynamic organelle that could easily change its number and distribution in response to intracellular and extracellular regulation (Okamoto *et al.*, 2012). Mitophagy is a selective degradation of mitochondria by autophagy, it is a crucial mitochondrial quality control mechanism in order to maintain normal mitochondrial function and structure (Rambold *et al.*, 2011). Here we labelled mitochondria with mitotracker in order to track their morphology of mitochondria after inhibiting autophagy with BA1.

De Giorgi and colleagues (2000) and Skulache and colleagues (2001) suggested that mitochondria in mammalian cells can form physically interconnected networks under normal conditions in order to represent an efficient system to deliver energy, or calcium between cells (De Giorgi *et al*., 2000; Skulache *et al*., 2001). From immunocytochemistry images (Figure 4.16) there was no clear evidence of any morphological damage in response to FA, BA1 or the combination (Fig 4.16).

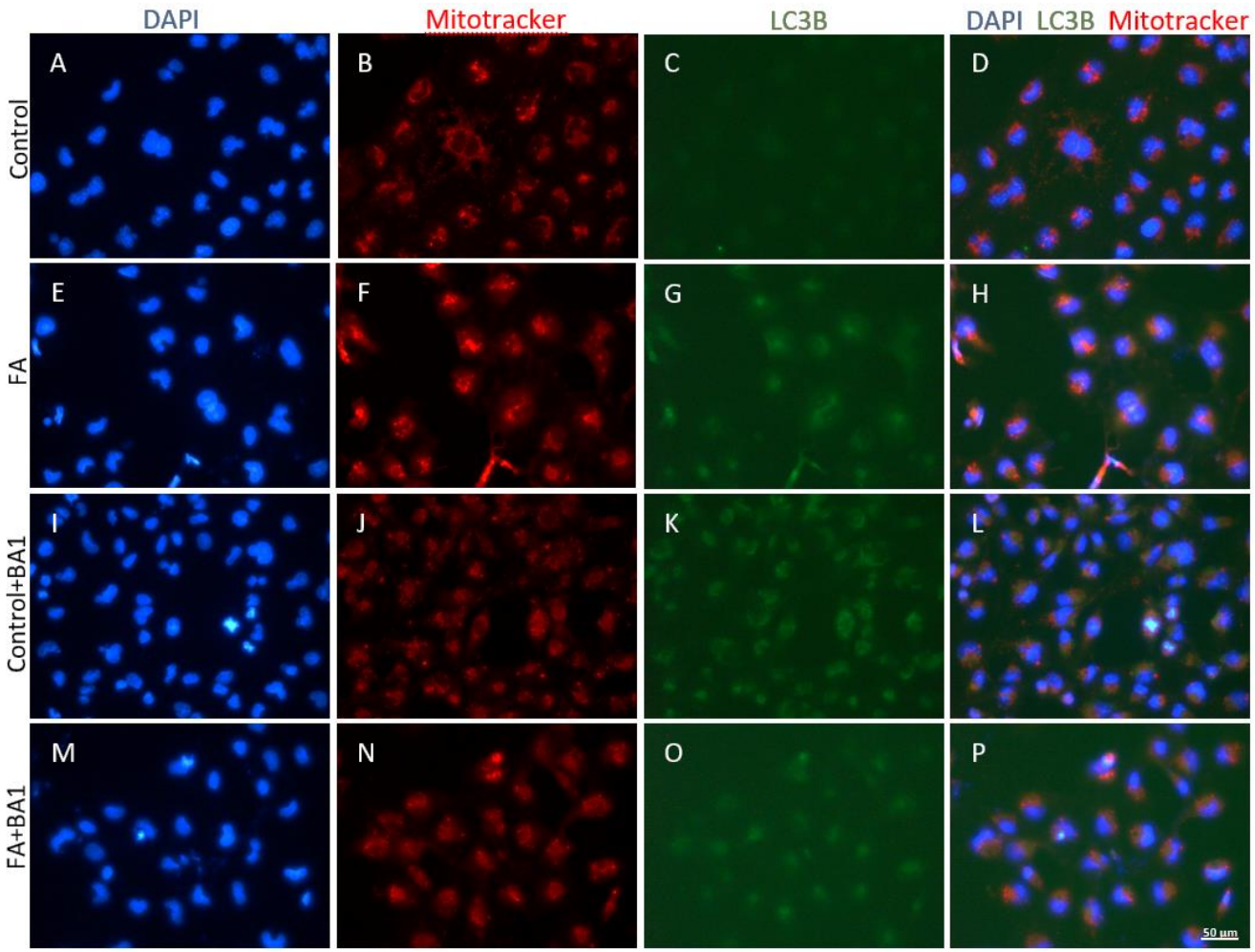


**Figure 4. 16 LC3B immunocytochemistry with mitotracker following BA1 incubated HK2 cells.**

HK2 cells were divided into four groups: control, FA, control+BA1 and FA+BA1. After 24-hour treatment, cells were fixed. Nuclei were stained with DAPI (blue), autophagy reflected by LC3B (green) and mitochondria were stained with mitotracker (red). Images taken at 40 magnification, scale bar = 50µm. One field per slide and three slides per treatment group were performed for an n = 3.

### 4.3.7 Inhibiting autophagy with CQ did not prohibit HK2 cells from recovering after treated with FA

Chloroquine (CQ) has a similar function to bafilomycin A1 as it inhibits fusion between autophagosomes and lysosomes. We intended to use CQ as an autophagy inhibitor to further explore the role of autophagy during FA damage and recovery.

The effect on cell number with CQ incubation was similar to that seen for BA1 incubation: the cell number slightly decreased after 24-hour incubation with CQ compared to the control group (Figure 4.17, 1 and 2,), incubation with FA for 24 hours significantly reduced the cell number compared to control ($p<0.05$), and by incubating cells with both FA and CQ slightly reduced the cell number compared to treating cell with FA only ($p>0.05$) . The group treated with CQ only showed significant difference in cell number after 24-hour recovery, suggesting that the inhibition of autophagy might slow down the proliferation rate in HK2 cell. FA damaged cells managed to recover after 48-hour recovery, however, cells treated with FA and CQ still showed a significant difference in terms of cell number compared to the control group ($p<0.05$), although cells from all treatment groups had recovered 72 hours after injury. Similar to the effect of BA1, by incubating cells with only CQ or incubating cells with both FA and CQ did not increase cellular ROS level compared to either control or FA group respectively (Figure 4.17 3).

**1)**

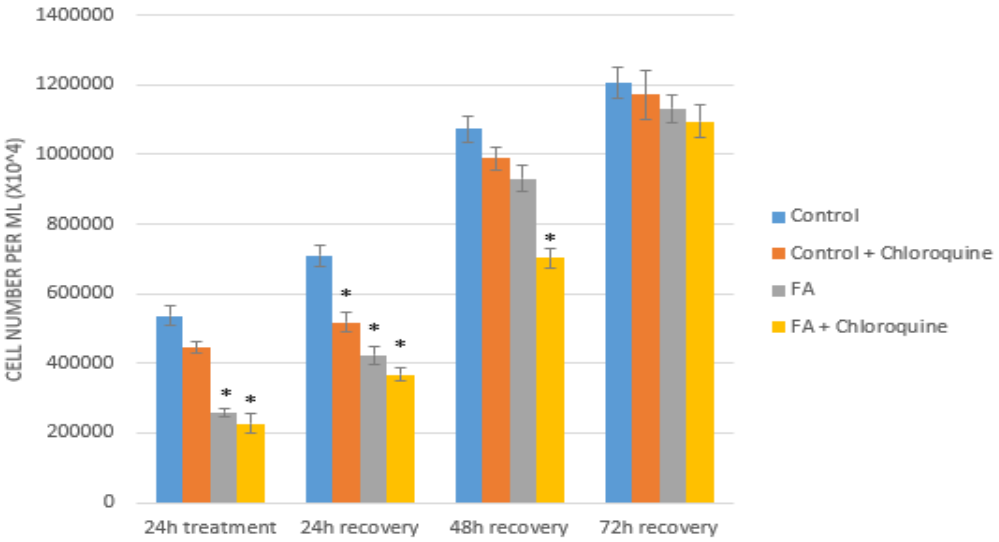
1400000
1200000
1000000
800000
600000
400000
200000
0
CELL NUMBER PER ML (X10^4)
24h treatment
24h recovery
48h recovery
72h recovery
Control
Control + Chloroquine
FA
FA + Chloroquine

**2)**

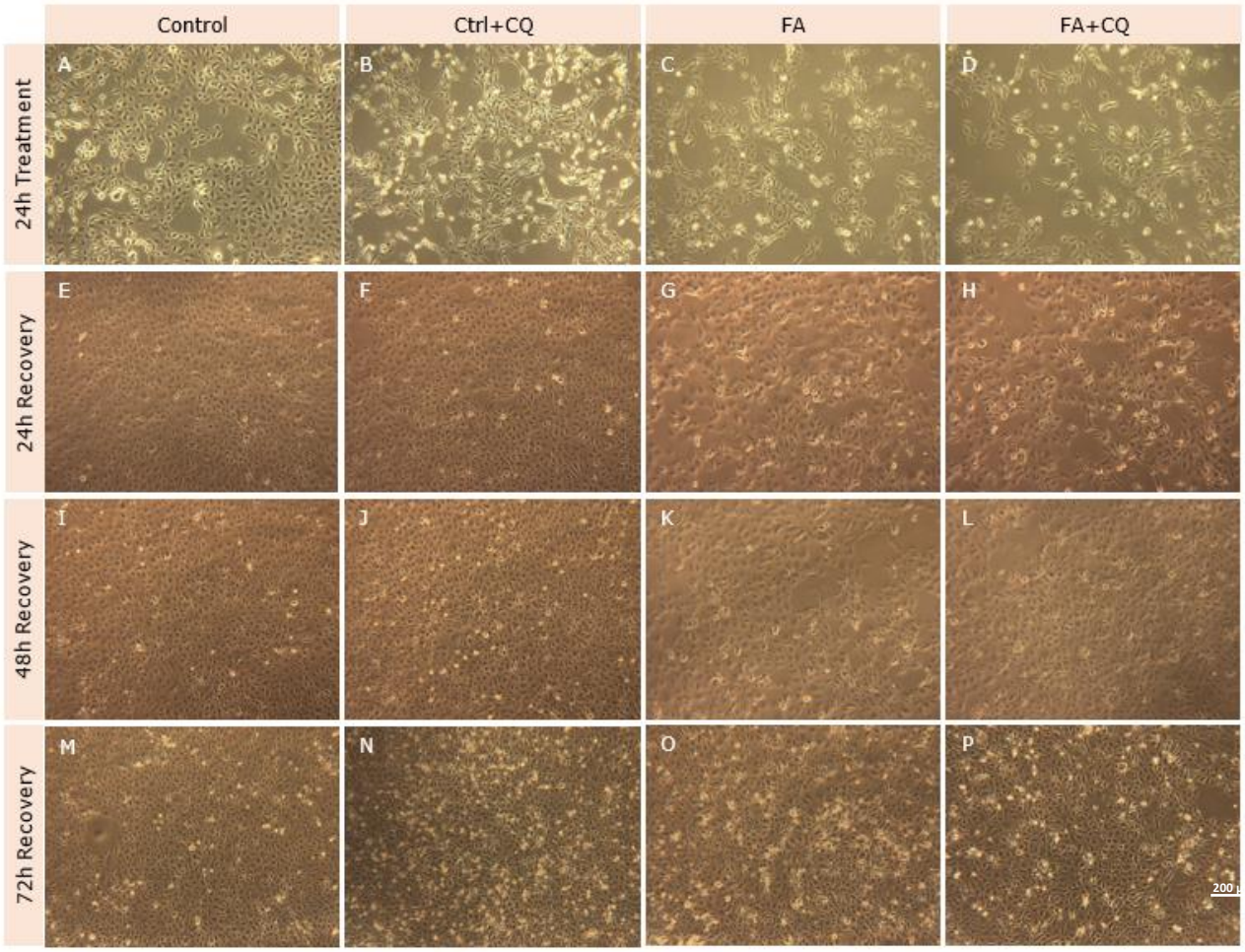
Control
Ctrl+CQ
FA
FA+CQ
24h Treatment
24h Recovery
48h Recovery
72h Recovery
A
B
C
D
E
F
G
H
I
J
K
L
M
N
O
P

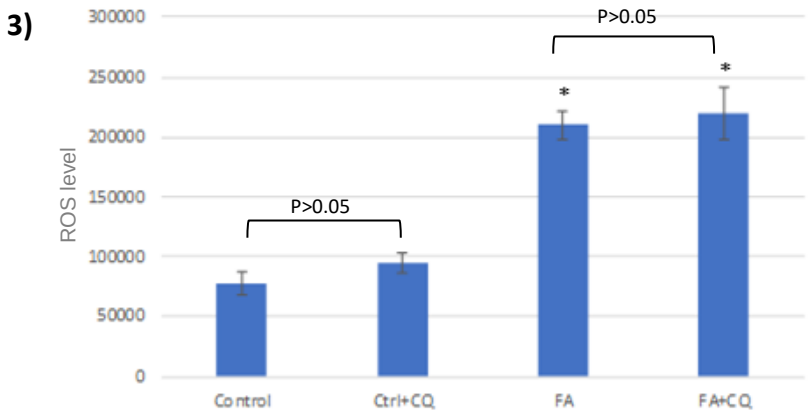


**Figure 4. 17 The effect of CQ on HK2 cell recovery after FA induced injury.**

HK2 cells were divided into four groups: control, control with CQ, FA and FA with CQ. **(1)** Total cell count after 24-hour treatment, 24-hour recovery, 48-hour recovery and 72-hour recovery. Two-way ANOVA was used to analyse data and followed by Dunnett multiple comparison test **(2)** Images of HK2 cells after each treatment. Images were taken at 6.7x magnification, scale bar = 200μm. **(3)** ROS level of HK2 cells after each treatment, One-way ANOVA was performed followed by Tukey's test. The ROS level was measured using CM-$H_2$DCFDA. Each treatment was carried out in triplicate, means ± SEM were shown, $p<0.05$ was considered as significant.

### 4.3.8 HK2 cells sustained normal mitochondrial morphology after inhibiting autophagy with CQ

There were no obvious changes in morphology in response to FA, CQ or the combination, as seen in Figure 4.18, which shared the same characteristic to BA1 treated cells. The immunocytochemistry images suggested that the mitochondria remained at the similar morphology after FA damage or inhibition of autophagy compared to the control group; however, further tests are needed to examine the fragmentation of mitochondria in order to investigate its function during FA damage and recovery.

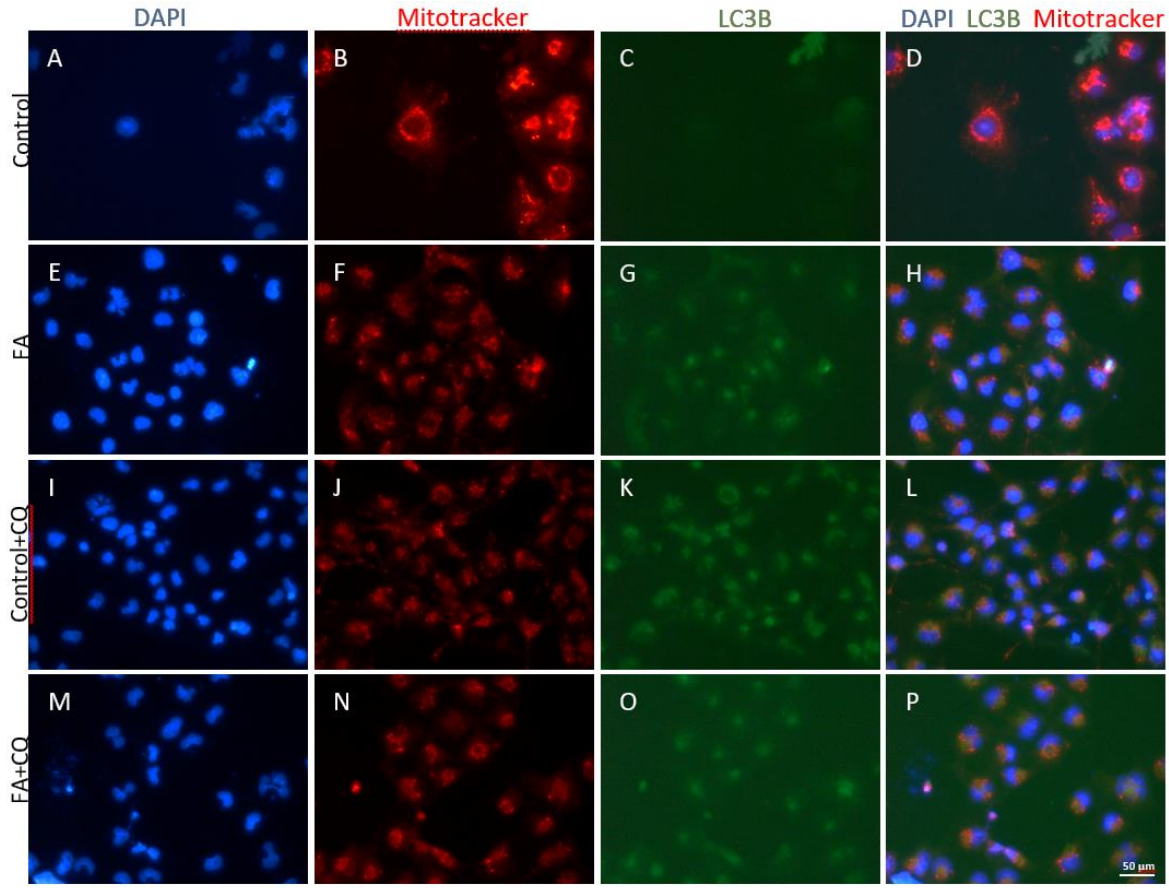


**Figure 4. 18 LC3B immunocytochemistry with mitotracker following CQ incubated HK2 cells.**

HK2 cells were divided into four groups: control, FA, control+BA1 and FA+BA1. After 24-hour treatment, cells were fixed. Nuclei was stained with DAPI (A, E, I, M) in blue, autophagy (C, G, K O) was stained with LC3B in green and mitochondria was stained with mitotracker (B, F, J, N) in red. Images were taken at 40 magnification, scale bar = 50µm One field per slide and three slides per treatment group were performed for an n = 3.

## 4.4 DISCUSSION AND CONCLUSION

Our results showed that the incubation of FA significantly increased the protein expression level of necrosis marker, HMGB1 ($p<0.05$), and FA incubation affected HMGB1 expression level in a time-dependent manner. During recovery, HMGB1 expression level decreased gradually, and reduced to similar levels as to the control group after 48-hour recovery. HMGB1 is a chromatin-binding nuclear protein participating in DNA replication, activation of autophagy, mitochondria quality control, transcription, and repair and promotes the activity of several transcription factors (Bianchi *et al*., 2000; Tang *et al*., 2011). HMGB1 can be released from necrotic or damaged cells and serves as a signal to trigger inflammation (Figure 4.19), it binds with several receptors including the RAGE, TLR2, TLR4, TREM1, and CD24, playing a role in regulating cell migration, cell activation, cell proliferation, and cell differentiation after injury. Similar upregulation of HMGB1 after acute injury was also observed in other studies (Tsung *et al*., 2005; Chung *et al*., 2008; Wu *et al*., 2007; Ilmakunnas *et al*., 2008). In a rat I/R injury study, HMGB1 protein was detected as early as 1 hour after reperfusion, and the expression level increased in a time-dependent manner. We also observed the significant increase of nuclear HMGB1 expression and cytoplasmic HMGB1 expression after 24-hour FA treatment ($p<0.05$). The increased expression of nuclear HMGB1 showed a longer response than total HMGB1, as nuclear HMGB1 was significantly increased after 24-hour recovery compared to its control group ($p<0.05$), whereas total HMGB1 was not. This suggested that HMGB1 remained activate in nucleus during recovery, and HMGB1 might play a role in recovery after acute damage. The increase of cytoplasmic HMGB1 only lasted when 24-hour FA treatment was applied, suggested that HMGB1 migrated from the

nucleus to the cytoplasm in response to FA induced injury. The HMGB1 nucleocytoplasmic translocation was also observed in several other studies (Ruan *et al*., 2014; Zhan *et al*., 2016) and recent studies demonstrated that the migration of nuclear HMGB1 to cytoplasm might be a crucial step to allow HMGB1 to play a proinflammatory role including activating inflammatory cells and promoting the secretion of inflammatory cytokines (Wu *et al*., 2010; Doi *et al*., 2014; Zhan *et al*., 2016)

The inhibition of HMGB1 activity with anti-HMGB1 antibody or pre-conditioning with HMGB1 prior to acute injury has been shown to reduce the damage (Tsung *et al*., 2005). In this study, we pre-treated cells with glycyrrhizin in order to inhibit HMGB1 expression during FA induced injury and therefore examine if the inhibition of HMGB1 could promote cell survival rate. Inhibition by glycyrrhizin did not change the total HMGB1 expression level. Additionally, there was no significant difference in terms of survived cell number between glycyrrhizin-inhibited group and FA treated group (Figure 4.9). Studies suggested that glycyrrhizin could bind directly to HMGB1 and therefore inhibit its chemoattractant and mitogenic activities, reduce the release and the level of expression of not only HMGB1 but also some proinflammatory cytokines (Mollica *et al*., 2007). Glycyrrhizin could also inhibit the binding between HMGB1 and RAGE and TLR4 receptors, therefore restrain the downstream MAPKs/NF-κB signalling pathway (Zhao *et al*., 2017). The HMGB1 expressions with/without glycyrrhizin showed no significant difference to each other suggested that the activation of HMGB1 might not be the key to induce cell death in FA damage, however, the precise role of HMGB1 needs to be examined via siRNA.

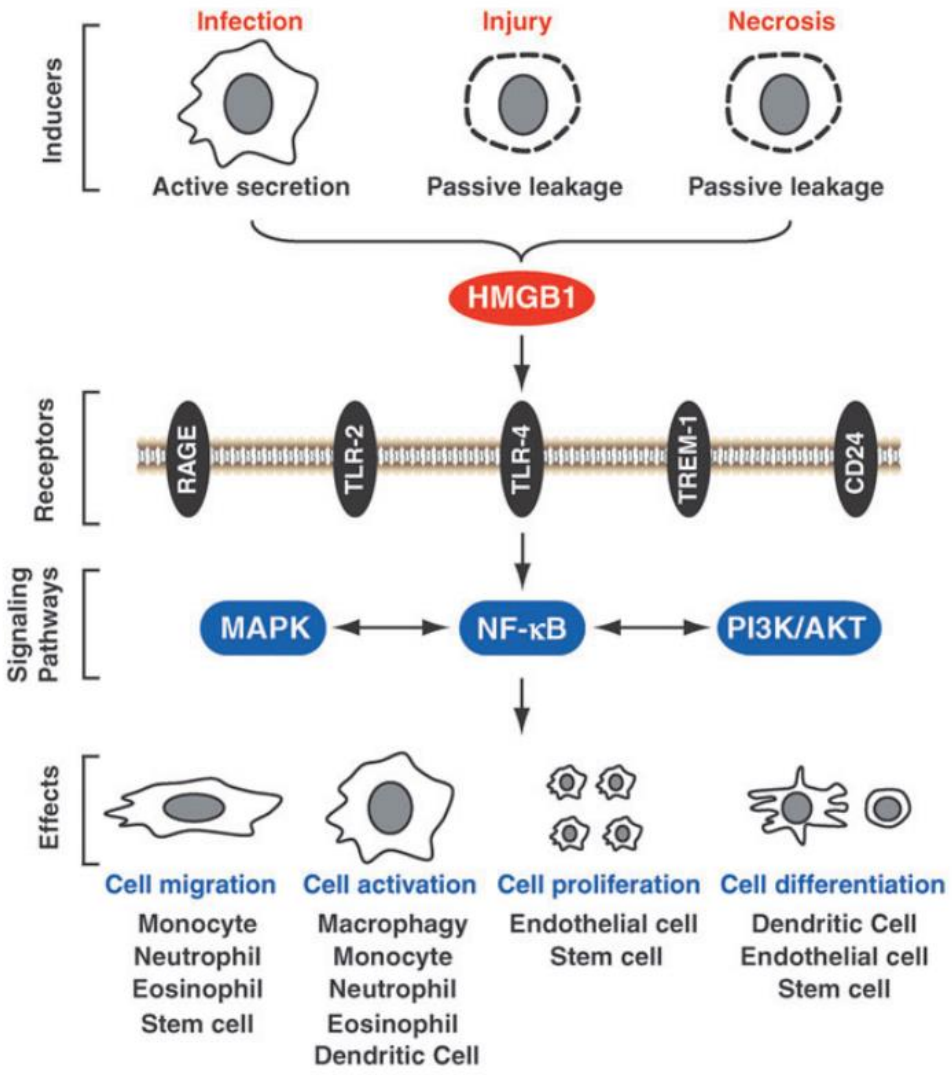


**Figure 4. 19 The function of extracellular HMGB1 acting as a damage-associated molecular pattern molecule.**

HMGB1 is passively released from injury and necrotic cells and is actively secreted by infected cells. It binds with several receptors including the receptor for advanced glycation end products (RAGE), Toll-like receptor 2 (TLR2), Toll-like receptor 4 (TLR4), triggering receptor expressed on myeloid cells1 (TREM1), and CD24, regulating the response to cell migration, cell activation, cell proliferation, and cell differentiation. Image was taken from Tang D., Kang

R., Zeh H., Lotze M. (2011) HMGB1, oxidative stress and disease. Antioxid Redox Signal 14: 1315–1335.

The ROS level shared a similar pattern to HMGB1 protein levels following FA damage and recovery. The ROS levels significantly increased after 4-hour incubation with FA and continued to increase in a time-dependent manner up to 24-hour incubation, then slowly reduced during recovery. ROS exists in normal cells as a product of cellular metabolism. $H_2O_2$ could be released from mitochondria in the cells and it is considered to be a main cause of oxidative damage, on top of that, it could initiate active and passive HMGB1 release in a time-dependent and dose-dependent manner (Tang *et al*., 2007). Under normal circumstances, $H_2O_2$ could induce HMGB1 translocation as soon as three hours. However, when $H_2O_2$ accumulates to a toxic concentration, it restricts cytotoxicity for macrophages and monocyte cell cultures, and then triggers both active and passive HMGB1 release (Tang *et al*., 2007). Additionally, it was demonstrated that $H_2O_2$ regulates the interaction between HMGB1 and chromosome region maintenance 1 (CRM1) protein homolog, suggesting that ROS might induce HMGB1 release through CRM1-dependent mechanism (Kayakawa *et al*., 2010).

It was also demonstrated that incubation with FA triggered autophagy activation. There was a significant increase in autophagosome indicator LC3B protein level after FA treatment ($p<0.05$); at the end of the recovery period, the expression level of LC3B significantly reduced compared to after FA incubation, suggesting the increasing autophagy activity during 24-hour FA treatment and the activity slowly went down as the recovery progressed (Figure 4.11, Figure 4.12, Figure 4.13). There are growing numbers of studies suggesting that upregulation of autophagy was observed during AKI in both in vivo and in vitro experimental models (Kaishal *et al*., 2008; Yang *et al*.,

2008; Jiang *et al*., 2010). By inhibiting autophagy formation during I/R injury in proximal tubule-specific autophagy-related genes 7 (Atg7) knockout mice, increased renal injury was observed compared with wild type group (Jiang *et al*., 2012), suggesting autophagy plays a pro-survival role in AKI. Atg7, along with Atg5, are essential for producing autophagosomes in proximal tubules; therefore, a pro-survival role of autophagy was also observed in proximal tubule specific Atg5 knockout mice (Takahashi *et al*., 2012). By contrast, the administration of rapamycin to mice, an inducer of autophagy, significantly reduced cisplatin-induced nephrotoxicity compared to control group ($p<0.05$), suggesting that over-expression of autophagy may have a protecting role in AKI (Takahashi *et al*., 2012).

HMGB1 protein levels were significantly increased after FA treatment ($p<0.05$), which was similar to LC3B protein, suggesting that the upregulation of HMGB1 may be linked with the activation of autophagy. Kang and colleagues (2010) proposed that HMGB1 interacts with the autophagy protein Beclin1 to stimulate autophagy activity (Kang *et al*., 2010). HMGB1 might take part in the regulation of Bcl-2 phosphorylation during autophagy through the extracellular signal regulated kinase (ERK) and the MAPK pathway, since ablation of HMGB1 diminishes starvation-induced phosphorylation of both ERK1/2 and Bcl-2 (Tang *et al*., 2010).

Mitochondria is the primary place to generate ATP, under normal conditions, a small amount of ROS are generated at the same time. When mitochondria are injured, large quantities of ROS might be released, which lead to impaired ATP production, oxidative stress, cellular damage, causing cell apoptosis and necrosis, inflammation and fibrosis (Figure 4.20). In addition, ROS may cause damage to mitochondria by damaging mitochondrial DNA, the damaged mitochondrial DNA could aggravate oxidative stress

by reducing electron transport-related protein, which leads to the organelle dysfunction (Van Houten *et al*., 2006); in addition, the increased ROS levels induce injury to the mitochondrial respiratory chain as well as mitochondrial membrane permeability and structure (Guo *et al*., 2013; Wei *et al*., 2011). Hence, it was proposed by Brook and colleagues that the mitochondrial fragmentation in the proximal tubule promoted the release of pro-apoptotic factors, thereby contributing to cell death when cells were under ischemic AKI (Brook *et al*., 2009). Although our immunocytochemistry images did not show any robust morphological damage to mitochondria during FA damage, the increased ROS might have influence on mitochondrial function by damaging mitochondrial structure and creating mitochondrial fragmentation.

To conclude, acute FA damage activated both HMGB1 and autophagy and their expression reduced to a normal level during recovery. HMGB1 showed nucleocytoplasmic translocation during FA treatment. FA significantly increased the ROS level in HK2 cells, suggested that FA may damage cells through elevation of ROS. It is unclear whether HMGB1 activated autophagy and whether it activated autophagy through the elevation of ROS, therefore further experiment involving siRNA might need to be carried out to find out the precise function of HMGB1 in cells and in the activation of autophagy.

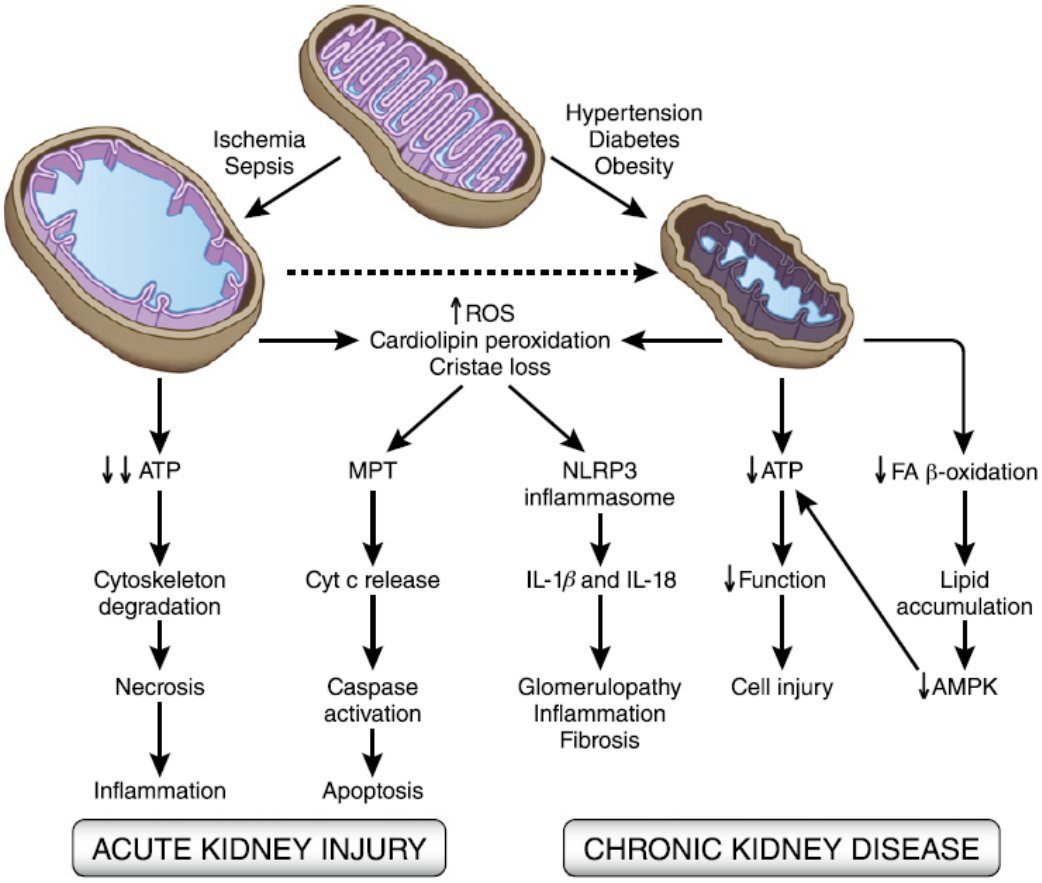


**Figure 4. 20 Mitochondrial changes in animal models of AKI and CKD.**

Stressors such as ischemia, sepsis, and toxins, cause mitochondrial matrix swelling and loss of cristae membrane. These structural changes are associated with impaired ATP production, oxidative stress, cellular demise, causing cell apoptosis and necrosis, inflammation, fibrosis etc. Image was taken from Szeto H.H. (2017) Pharmacologic Approaches to Improve Mitochondrial Function in AKI and CKD. J Am Soc Nephrol 28: 2856–2865.

# CHAPTER 5: NOVEL PATHWAYS INVOLVED IN FA INDUCED ACUTE KIDNEY INJURY

## 5.1 INTRODUCTION

Although there are three major ways of identifying AKI (section 1.2.2) and several biomarkers such as NGAL and IL-18 may increase the sensitivity and accuracy of AKI identification (section 1.2.4), more biomarkers that respond to FA induced AKI are still needed to help examine and facilitate experimental and clinical trials, therefore enable new clinical therapies that could treat AKI to be developed.

FA has shown to regulate expressions numerous of genes in different pathways in both in vitro and in vivo experiments. In this chapter, we would like to discuss genetic expression in three aspects: firstly, the genes that have been shown to be modulated in chapter 4 in response to FA treatment of HK2 cells, such as HMGB1 and LC3B, by confirming their mRNA expression with RNA-seq and investigate their potential related pathways that play a role in FA induced AKI; secondly, identify genes that are significantly increased during FA damage and recovery (such as MMP-7) and therefore investigate the potential pathways for FA induced damage and recovery; finally, genes that are expressed during development, silent in healthy adult tissue but re-expressed during recovery, such as Pax2, and find out potential related pathways that may help recovering.

The development of the kidney is slightly different from that of most organs in the body as it develops through three successive stages: pronephros, mesonephros and metanephros. However, the pronephros and the mesonephros are transient embryonic kidneys and will be degenerated throughout the kidney development. The metanephros, on the other hand, can form the adult mammalian kidneys (Saxin L., 1987). The pronephros appears about gestational day (GD) 22 in human when several

epithelial tubules appear within the nephrogenic cord, which are the connection to the pronephric duct. The human pronephric tubules regress about GD35, however the pronephric duct remains and become Woffian duct, which induces the development of the mesonephros (Smyth et al., 2017). During the mesonephros stage, Woffian duct induces a mesenchymal to epithelial transition of mesenchyme and form comma shaped bodies and S-shaped bodies. The S-shaped bodies elongates and induces epithelialization and the formation of blood vessels which indicates the start of glomerulogenesis. Later in the metanephros stage, ureteric buds are developed. The signals released from the ureteric buds induce the development of the renal proximal tubules, which later connect to the connecting duct system (Seely J.C., 2017).

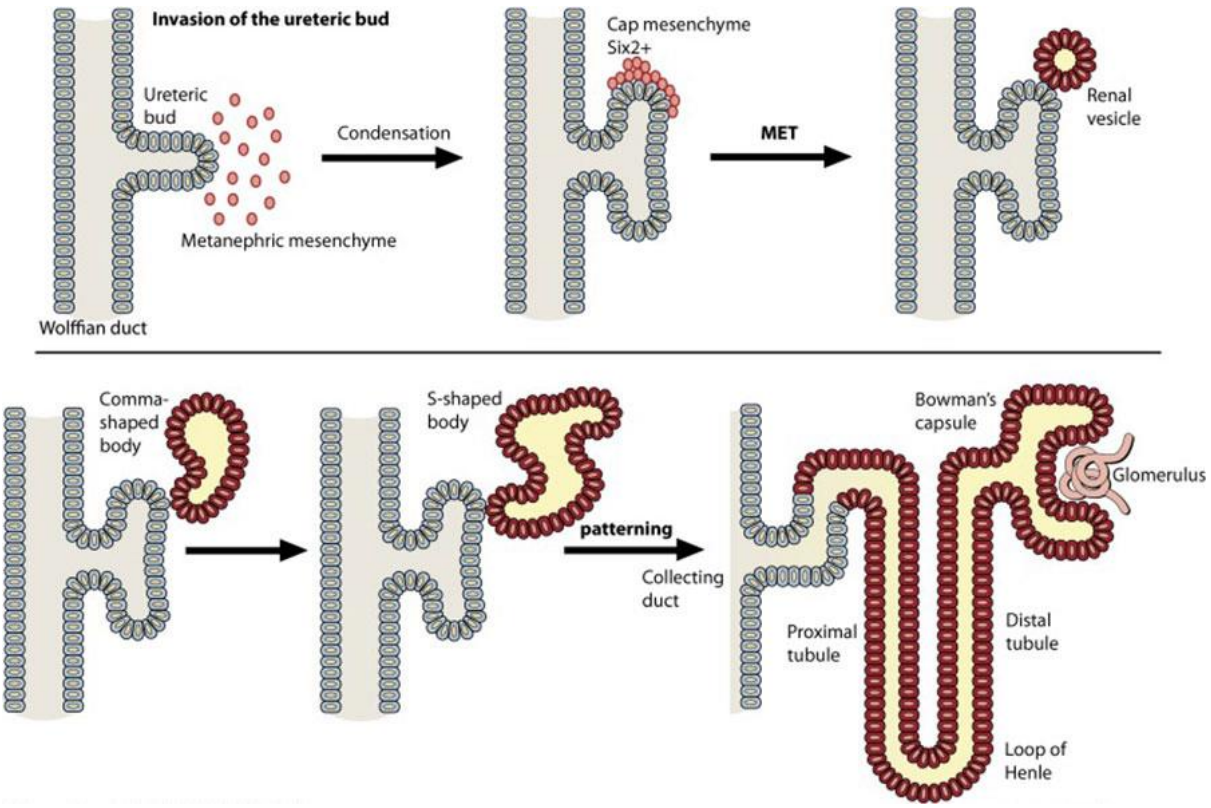


**Figure 5. 1 Kidney development.**

The ureteric bud extends from the Wolffian duct and form cap mesenchyme upon reaching metanephric mesenchyme, which then generate a renal vesicle. The renal

vesicle often continues to form the comma-shaped body which then develop to S-shaped body, followed by further development before a nature nephron is formed. Figure is taken from Hohenstein P., Pritchard-Jones K. Charlton J. (2015). The yin and yang of kidney development and Wilms' tumors. Genes Dev, 29, 467-482.

Matrix metalloproteinase7 (MMP7) expression has been recently discovered to markedly increase in renal tubular epithelium injury (Yang *et al*., 2017; Zhou *et al*., 2017). MMP-7 is one of the smallest members of its family and it is a zinc- and calcium-dependent endopeptidase (Tan *et al*., 2012; Ke *et al*., 2017). Some of the main functions of MMP-7 are breaking down the extracellular matrix by digesting casein, gelatins, fibronectin, and proteoglycan, as well as degrading E-cadherin ectodomain shedding, releasing tumour necrosis factor α (TNFα) and some other proteinases (Zhou et al., 2017; Grindel et al., 2014; He et al., 2012), therefore it is considered a potential factor that may control a wide-range of biological process including tissue apoptosis, inflammation and repairing (Tan *et al*., 2012; Surendran *et al*., 2004; Duarte *et al*., 2015). Compared to its markedly higher expression after tubular injury, MMP-7 expression in non-injured and non-inflamed kidneys could be barely detectable (Fu *et al*., 2019; Surendran *et al*., 2004). Several studies have shown that MMP-7 could be induced under CKD condition and worked as a biomarker of kidney injury (Zhou *et al*., 2017; Ho *et al*., 2016; Afkarian *et al*., 2015). A recent in vivo experiment treating MMP-7 knock-out mice with 250mg/kg FA showed that MMP-7 had a reno-protective role by limiting tubular cell apoptosis whilst promoting tubular regeneration (Fu *et al*., 2019); however, the exact role of MMP-7 in the pathogenesis of nephrotoxic AKI remains unclear.

The Pax gene family plays an irreplaceable role in embryogenesis. The members of the Pax gene family (Pax1 – Pax9) are tissue specific, they are associated with organogenesis and maintenance of stem cell populations during development (Chi *et al*, 2002). They function by encoding transcription factors that bind to DNA and regulate the expression of certain genes (Dziarmaga *et al*, 2006; Goulding *et al*, 1991 and Torban *et al*, 2006). The lack of Pax2 transcriptional regulator can lead to several consequences. Experiments carried out by Bouchard and his team (Bouchard *et al*, 2000) showed that Pax2-/- embryos could form pronephros and mesonephros in nephrogenesis but failed to form matanephros, which is mainly due to the function of Pax2 in nephric duct maintenance. On the other hand, a mild reduction of Pax2 expression in Pax2+/- may allow the formation of matanephros but results in a hypoplastic kidney which only has the size of 60-75% of a normal kidney (Sanyanusin *et al*, 1996). Pax2 protein was also detected during renal regeneration. Imgrund and his colleagues (Imgrund *et al*, 1999) first found that Pax2 protein re-appeared in the proximal tubule cells after renal injury. Later on Maeshima and her coworkers (Maeshima *et al*, 2012) used renal ischemia/reperfusion injury mice model to further confirm that Pax2 is re-expressed during regeneration, which shows that Pax2 gene could potentially influence renal regeneration; they also found other transcription factors and growth factors that re-appeared such as Wnt1, Wnt4 and Pax8. Then they continuously found that the peak of Pax2 expression happens before the peak of bromodeoxyuridine (BrdU)– positive cells, which illustrate the cells that are under proliferation; additionally, they showed that by inhibiting Pax2 expression the proliferation rate significantly decreased. Therefore, they concluded that the expression of Pax2 could drive the proliferation of tubular cells. In 2004, Zhang and

colleagues showed the expression of Pax2 could prevent cell death (Zhang *et al.*, 2004). They used immortalized renal proximal tubular cells (IRPTC) to show that the cells lacking Pax2 expression are 2.4 times more likely to enter apoptosis than control group, and the proliferation rate of those cells decreased about 50%. However, the mechanism of Pax2 in the repair process after AKI is still not fully understood yet.

The aim of this chapter is to investigate the potential pathways that were activated when HK2 cells were undergoing damage and recovery using an RNAseq approach.

## 5.2 METHOD

Methods for collecting cell samples, RNA extraction, total quantity and quantity, please refer to section 2.7.1, 2.7.2 and 2.7.3. 10ng total RNA per sample was sent for RNA-seq test. Each treatment (control, 24h FA and 24h recovery) was triplicated. The raw full dataset was kindly analysed by Nigel Mongan from the Vet School.

Genes with log2(FC) ≤ -1 and log2(FC) ≥ 1 were considered as upregulated or downregulated respectively in this project. Gene Ontology (GO) analysis was performed using Protein ANalysis THrough Evolutionary Relationships (PANTHER) Classification System 14.1. Statistics were performed using Statistical Package for the Social Sciences (SPSS) version 21.0.

## 5.3 RESULTS

### 5.3.1 Functionality groups of gene regulated by treatments

In order to examine mRNA expression changes in renal damage and recovery, RNAseq was performed in HK2 cells in control, 24-hour FA treatment and 24-hour recovery groups (n=3 per treatment). A total of 5898 genes showed significant changes with 24-hour FA treatment group when compared with controls ($p<0.05$). There were 2086 genes which showed significant changes in the 24-hour recovery group compared with the control group ($p<0.05$). In addition, we found that 4899 genes showed significant changes in the 24-hour recovery group compared with 24-hour FA treatment group ($p<0.05$).

The upregulated genes and downregulated genes were assigned to several functional groups including molecular functions, cellular components and biological processes (Table 5.1).

| Functions | | Treatment groups | | |
|---|---|---|---|---|
| | | Control vs FA | Control vs Recovery | FA vs Recovery |
| Molecular Functions | Binding | 421 | 103 | 305 |
| | Catalytic activity | 390 | 84 | 293 |
| | Molecular function regulator | 88 | 18 | 73 |
| | Molecular transducer activity | 80 | 26 | 52 |
| | Structural molecule activity | 31 | 6 | 27 |
| | Transcription regulator activity | 70 | 23 | 59 |
| | Translation regulator activity | 2 | 1 | 4 |
| | Transporter activity | 91 | 22 | 73 |
| Cellular Component | Cell junction | 9 | 3 | 3 |
| | Cell | 469 | 102 | 351 |
| | Extracellular region | 94 | 25 | 51 |
| | Membrane | 116 | 36 | 83 |
| | Organelle | 296 | 75 | 235 |
| | Protein-containing complex | 118 | 29 | 101 |
| | Supramolecular complex | 5 | 1 | 5 |
| | Synapse | 1 | N/A | 3 |
| Biological process | Biological adhesion | 46 | 13 | 31 |
| | Biological phase | 2 | 2 | N/A |
| | Biological regulation | 259 | 70 | 195 |
| | Cell proliferation | 9 | 2 | 4 |
| | Cellular component organization or biogenesis | 18 | 5 | 18 |
| | Cellular process | 512 | 128 | 387 |
| | Developmental process | 30 | 7 | 35 |
| | Immune system process | 47 | 19 | 40 |
| | Localization | 185 | 43 | 145 |
| | Metabolic process | 304 | 66 | 242 |
| | Multicellular organismal process | 105 | 29 | 82 |
| | Pigmentation | 1 | N/A | N/A |
| | Reproduction | 12 | 6 | 13 |
| | Response to stimulus | 91 | 23 | 96 |
| | Rhythmic process | 2 | N/A | 2 |
| | Signalling | 1 | N/A | 3 |

**Table 5. 1 Functional groups of genes regulated in all treatment groups.**

The number of up- and down- regulated genes in molecular function, cellular component and biological process in all treatment groups. N/A: not applicable.

In control compared to 24-hour FA group, out of all genes were involved in molecular function, around 40% of them were related to binding and a similar number were associated with catalytic activities, others were related to structural molecule activity and molecular transducer activity (Table 5.1). We observed 296 organelle related genes was altered, others were cell membrane and protein-containing complex associated. Cellular process and metabolic process were two main functions that genes were involved in biological process, in which 512 and 304 genes were significantly altered ($p<0.05$). It was followed by biological regulation and localization, in which 259 and 185 genes were altered respectively. Similar biological process was observed in the comparison between control and 24-hour recovery group and 24-hour FA compared with 24-hour recovery. In the genes related to molecular functions, there were 103 genes and 305 genes associated with binding in control compared to 24-hour recovery group and 24-hour FA compared to 24-hour recovery group, following by the number of genes involved in catalytic activity, in which 84 genes involved in control compared to 24-hour recovery group and 293 genes involved in 24-hour FA compared to 24-hour recovery group. In the genes associated with cellular component, there were 75 genes related to organelle in in control compared to 24-hour recovery group and 235 genes related to 24-hour FA compared to 24-hour recovery group, other altered genes mainly focus on membrane and protein-containing complex in both groups.

Cross comparing the number of genes in functional groups in all treatment groups, most genes were altered in control compared to 24-hour FA group, followed by 24-hour FA compared to 24-hour recovery group and in control compared to 24-hour recovery group. In biological process group in particular, the number of genes were

regulated in control compared to 24-hour FA group was noticeably higher than those in the other two groups, especially the genes regulated in cellular process, localization, biological regulation and metabolic process function, the number of genes were noticeably higher than control compared to 24-hour recovery group.

### 5.3.2 Top novel pathways regulated by treatments

There was a total of 109 pathways impacted by 24-hour FA treatment, covering a wide range of molecular responses such as oxidative stress, p53 activity and HIF mediated functions (Table 5.2). The top pathway was inflammation mediated by chemokine and the cytokine signalling pathway (Table 5.2). Several components of the pro-inflammatory pathway showed significant elevation in their expressions (Table 5.3 A $p<0.05$). Comparing FA treated cells to the control group, IL-1A and IL-1B showed 6.94-fold and 7.66-fold increase ($p<0.05$), MKK3 showed 2.52-fold elevation in expression ($p<0.05$), JNK and CHOP showed 2.28-fold and 2.09-fold increase in expression ($p<0.05$).

| Pathway | Number of genes involved |
|---|---|
| Inflammation mediated by chemokine and cytokine signalling pathway | 29 |
| Wnt signalling pathway | 27 |
| Angiogenesis | 23 |
| CCKR signalling map | 19 |
| PDGF signalling pathway | 19 |
| Integrin signalling pathway | 19 |
| Gonadotropin-releasing hormone receptor pathway | 17 |
| Huntington disease | 17 |
| FGF signalling pathway | 15 |
| Alzheimer disease-presenilin pathway | 14 |
| EGF receptor signalling pathway | 14 |
| Endothelin signalling pathway | 13 |
| T cell activation | 12 |
| Heterotrimeric G-protein signalling pathway-Gi alpha and Gs alpha mediated pathway | 12 |
| Cadherin signalling pathway | 12 |
| B cell activation | 12 |
| Apoptosis signalling pathway | 11 |
| VEGF signalling pathway | 11 |
| p53 pathway | 10 |
| TGF-beta signalling pathway | 10 |
| Nicotinic acetylcholine receptor signalling pathway | 10 |
| Heterotrimeric G-protein signalling pathway-Gq alpha and Go alpha mediated pathway | 10 |
| PI3 kinase pathway | 8 |
| Ionotropic glutamate receptor pathway | 8 |
| Interleukin signalling pathway | 8 |
| p53 pathway feedback loops 2 | 8 |
| Ras Pathway | 8 |
| Axon guidance mediated by netrin | 7 |
| Transcription regulation by bZIP transcription factor | 7 |
| Parkinson disease | 7 |
| Muscarinic acetylcholine receptor 1 and 3 signalling pathway | 7 |
| Cytoskeletal regulation by Rho GTPase | 7 |
| Blood coagulation | 7 |
| 5HT2 type receptor mediated signalling pathway | 7 |
| Alzheimer disease-amyloid secretase pathway | 6 |
| Oxidative stress response | 6 |
| Metabotropic glutamate receptor group III pathway | 6 |
| Thyrotropin-releasing hormone receptor signalling pathway | 6 |

| | |
|---|---|
| Oxytocin receptor mediated signalling pathway | 6 |
| General transcription regulation | 6 |
| Histamine H1 receptor mediated signalling pathway | 6 |
| Axon guidance mediated by Slit/Robo | 5 |
| Plasminogen activating cascade | 5 |
| Insulin/IGF pathway-protein kinase B signalling cascade | 5 |
| Hypoxia response via HIF activation | 5 |
| Alpha adrenergic receptor signalling pathway | 4 |
| Ubiquitin proteasome pathway | 4 |
| Notch signalling pathway | 4 |
| Metabotropic glutamate receptor group I pathway | 4 |
| p38 MAPK pathway | 4 |
| Cortocotropin releasing factor receptor signalling pathway | 4 |
| Cell cycle | 4 |
| Axon guidance mediated by semaphorins | 3 |
| Heme biosynthesis | 3 |
| Toll receptor signalling pathway | 3 |
| De novo purine biosynthesis | 3 |
| Coenzyme A biosynthesis | 3 |
| Muscarinic acetylcholine receptor 2 and 4 signalling pathway | 3 |
| Androgen/estrogene/progesterone biosynthesis | 3 |
| Insulin/IGF pathway-mitogen activated protein kinase kinase/MAP kinase cascade | 3 |
| p53 pathway by glucose deprivation | 3 |
| Heterotrimeric G-protein signalling pathway-rod outer segment phototransduction | 3 |
| Opioid proopiomelanocortin pathway | 3 |
| Opioid proenkephalin pathway | 3 |
| Nicotine pharmacodynamics pathway | 3 |
| General transcription by RNA polymerase I | 3 |
| Angiotensin II-stimulated signalling through G proteins and beta-arrestin | 3 |
| Beta3 adrenergic receptor signalling pathway | 3 |
| De novo pyrimidine ribonucleotides biosythesis | 2 |
| Metabotropic glutamate receptor group II pathway | 2 |
| Interferon-gamma signalling pathway | 2 |
| P53 pathway feedback loops 1 | 2 |
| Opioid prodynorphin pathway | 2 |
| Enkephalin release | 2 |
| Dopamine receptor mediated signalling pathway | 2 |
| FAS signalling pathway | 2 |
| Cholesterol biosynthesis | 2 |
| Beta2 adrenergic receptor signalling pathway | 2 |
| Beta1 adrenergic receptor signalling pathway | 2 |

| | |
|---|---|
| 5HT4 type receptor mediated signalling pathway | 2 |
| 5HT1 type receptor mediated signalling pathway | 2 |
| 5-Hydroxytryptamine degredation | 2 |

**Table 5. 2 Name of the pathways involved in control compared to 24-hour FA group and the number of genes involed in.**

Another highlighted pathway was the Wnt signalling pathway. The Wnt signalling pathway regulates a number of crucial cellular aspects such as cell migration and cell proliferation, it also works as an important mediator of patterning decisions during embryonic development (Komita *et al*., 2008). On the other hand, although the Wnt signalling pathway was detected as the second pathway that was highlighted after FA damage (Table 5.2), however key components involved in the pathway such as adenomatosis polyposis coli (APC), glycogen synthase kinase 3 (GSK3) and casein kinase 1α (CK1α) did not show significant fold change during treatment, only drosophila dishevelled (DSH) had a significant 2.30-fold increase in expression ($p<0.05$).

Angiogenesis signalling pathway was the third most involved pathway (Table 5.2). The mRNA expression level of VEGF in HK2 cells after 24-hour FA treatment significantly increased by 11.2-fold compared to the control group (Table 5.3 B, $p<0.05$); in addition, the expression of HIF1-α mRNA significantly increased by 2.25-fold after FA treatment ($p<0.05$). Similar elevation in expression were also observed in AKT and

PLCγ mRNA, they had significant 2.35-fold and 4.72-fold increase respectively ($p<0.05$).

**A**

| **Inflammation mediated by chemokine and the cytokine signalling pathway** | | | |
|---|---|---|---|
| **Genes** | **Abbreviation** | **Expression level** | **Significance** |
| Interleukin 1 | IL-1A | ↑ 6.94 | p<0.05 |
| | IL-1B | ↑ 7.66 | p<0.05 |
| Mitogen-activated protein kinase kinase 3 | MKK3 | ↑ 2.52 | p<0.05 |
| c-Jun N-terminal kinases | JNK | ↑ 2.28 | p<0.05 |
| C/EBP homologous protein | CHOP | ↑ 2.09 | p<0.05 |

**B**

| **Angiogenesis** | | | |
|---|---|---|---|
| **Genes** | **Abbreviation** | **Expression level** | **Significance** |
| Vascular endothelial growth factor | VEGF | ↑ 11.20 | p<0.05 |
| Hypoxia-inducible factor 1- α | HIF1-α | ↑ 2.25 | p<0.05 |
| RAC-alpha serine/threonine-protein kinase | AKT | ↑ 2.35 | p<0.05 |
| Phospholipase C | PLCγ | ↑ 4.72 | p<0.05 |

**Table 5. 3 Genetic expression in inflammatory and angiogenesis pathway.**

The change of gene expression in (**A**) inflammation mediated by chemokine and the cytokine signalling pathway and (**B**) angiogenesis pathways. ↑ indicates the elevation of gene expression. $p<0.05$ was considered as significance.

There were a total of 66 pathways highlighted comparing 24-hour recovery group to the control group, the top two pathways were inflammation mediated by chemokine and cytokine signalling pathway and Wnt signalling pathway (Table 5.4), however except for the expression of Wnt9A and VEGF mRNA being significantly increased by 2.17-fold and 2.63-fold respectively ($p<0.05$), other key components involved in the pathways did not show significant fold change during treatment.

The third most involved pathway involved was integrin signalling pathway (Table 5.4). The expression level of ERK and cell division cycle 42 (CDC42) mRNA both were significantly decreased by 2.57-fold and 2.17-fold respectively ($p<0.05$), but the expression of other components in the pathway did not show significant fold change.

| | |
|---|---|
| Inflammation mediated by chemokine and cytokine signalling pathway | 7 |
| Wnt signalling pathway | 6 |
| Integrin signalling pathway | 5 |
| PDGF signalling pathway | 5 |
| CCKR signalling map | 5 |
| Angiogenesis | 4 |
| Interleukin signalling pathway | 4 |
| Vitamin D metabolism and pathway | 4 |
| FGF signalling pathway | 4 |
| EGF receptor signalling pathway | 4 |
| Oxidative stress response | 4 |
| Blood coagulation | 4 |
| B cell activation | 4 |
| Gonadotropin-releasing hormone receptor pathway | 4 |
| Heterotrimeric G-protein signalling pathway-Gq alpha and Go alpha mediated pathway | 3 |
| Heterotrimeric G-protein signalling pathway-Gi alpha and Gs alpha mediated pathway | 3 |
| TGF-beta signalling pathway | 3 |
| Metabotropic glutamate receptor group III pathway | 2 |
| Apoptosis signalling pathway | 2 |
| Alpha adrenergic receptor signalling pathway | 2 |
| Huntington disease | 2 |
| VEGF signalling pathway | 2 |
| Ras Pathway | 2 |
| FAS signalling pathway | 2 |
| Plasminogen activating cascade | 2 |
| Endothelin signalling pathway | 2 |
| PI3 kinase pathway | 2 |
| Notch signalling pathway | 2 |
| Nicotinic acetylcholine receptor signalling pathway | 2 |
| Cadherin signalling pathway | 2 |
| Enkephalin release | 2 |

**Table 5. 4 Name of the pathways involved in control compared to 24-hour recovery group and the number of genes involved in.**

There were 109 pathways highlighted comparing FA-treated group to 24-recovery group, the top of which was Wnt signalling pathway. Wnt7b and Wnt16 exhibited a 3.64 fold and 6.12 fold decrease respectively in recovery compared to FA damage ($p<0.05$). Wnt7b is a signalling protein that functions in many developmental processes including kidney development. During kidney development, the major role of Wnt7b is to create the cortico-medullary axis of epithelial organization, it promotes kidney medulla formation by mediating orientation of cell divisions in kidney medullary collecting duct epithelium (Yu *et al*., 2009). Wnt16 is associated with several developmental processes as well as regulating cell fate and patterning in embryogenesis (Nalesso *et al*., 2017). The expression of Wnt16 is highly associated to the expression of NF-κB. Whilst the expression of Wnt16 decreased by 6.12 fold during recovery, the expression of NF-κB was decreased by 2.51-fold.

| | |
|---|---|
| Wnt signalling pathway | 22 |
| Inflammation mediated by chemokine and cytokine signalling pathway | 20 |
| Angiogenesis | 16 |
| Gonadotropin-releasing hormone receptor pathway | 14 |
| Integrin signalling pathway | 14 |
| FGF signalling pathway | 13 |
| Nicotinic acetylcholine receptor signalling pathway | 12 |
| Heterotrimeric G-protein signalling pathway-Gi alpha and Gs alpha mediated pathway | 12 |
| Cadherin signalling pathway | 12 |
| Apoptosis signalling pathway | 11 |
| CCKR signalling map | 11 |
| PDGF signalling pathway | 11 |
| Huntington disease | 11 |
| Parkinson disease | 10 |
| VEGF signalling pathway | 9 |
| Heterotrimeric G-protein signalling pathway-Gq alpha and Go alpha mediated pathway | 9 |
| T cell activation | 8 |
| EGF receptor signalling pathway | 8 |
| B cell activation | 8 |
| Endothelin signalling pathway | 7 |
| p53 pathway | 6 |
| TGF-beta signalling pathway | 6 |
| Oxidative stress response | 6 |
| Ras Pathway | 6 |
| Cytoskeletal regulation by Rho GTPase | 6 |
| 5HT2 type receptor mediated signalling pathway | 6 |
| Transcription regulation by bZIP transcription factor | 5 |
| Muscarinic acetylcholine receptor 2 and 4 signalling pathway | 5 |
| Insulin/IGF pathway-protein kinase B signalling cascade | 5 |
| Insulin/IGF pathway-mitogen activated protein kinase kinase/MAP kinase cascade | 5 |
| Thyrotropin-releasing hormone receptor signalling pathway | 5 |
| Oxytocin receptor mediated signalling pathway | 5 |
| Axon guidance mediated by netrin | 4 |
| Alzheimer disease-presenilin pathway | 4 |
| Alzheimer disease-amyloid secretase pathway | 4 |
| PI3 kinase pathway | 4 |
| Muscarinic acetylcholine receptor 1 and 3 signalling pathway | 4 |
| Ionotropic glutamate receptor pathway | 4 |
| Interleukin signalling pathway | 4 |
| p53 pathway feedback loops 2 | 4 |

| | |
|---|---|
| Hypoxia response via HIF activation | 4 |
| General transcription regulation | 4 |
| FAS signalling pathway | 4 |
| Axon guidance mediated by semaphorins | 3 |
| Toll receptor signalling pathway | 3 |
| De novo pyrimidine ribonucleotides biosythesis | 3 |
| De novo purine biosynthesis | 3 |
| Synaptic vesicle trafficking | 3 |
| Interferon-gamma signalling pathway | 3 |
| Nicotine degradation | 3 |
| Dopamine receptor mediated signalling pathway | 3 |
| Pyruvate metabolism | 3 |
| Histamine H1 receptor mediated signalling pathway | 3 |
| Beta3 adrenergic receptor signalling pathway | 3 |
| Beta2 adrenergic receptor signalling pathway | 3 |
| Beta1 adrenergic receptor signalling pathway | 3 |
| Alpha adrenergic receptor signalling pathway | 2 |
| Adrenaline and noradrenaline biosynthesis | 2 |
| Ubiquitin proteasome pathway | 2 |
| Heme biosynthesis | 2 |
| Notch signalling pathway | 2 |
| Metabotropic glutamate receptor group I pathway | 2 |
| Metabotropic glutamate receptor group III pathway | 2 |
| Androgen/estrogene/progesterone biosynthesis | 2 |
| p53 pathway by glucose deprivation | 2 |
| p38 MAPK pathway | 2 |
| Glycolysis | 2 |
| Nicotine pharmacodynamics pathway | 2 |
| Angiotensin II-stimulated signalling through G proteins and beta-arrestin | 2 |
| Cortocotropin releasing factor receptor signalling pathway | 2 |
| Circadian clock system | 2 |
| 5HT4 type receptor mediated signalling pathway | 2 |
| 5HT3 type receptor mediated signalling pathway | 2 |
| 5-Hydroxytryptamine degredation | 2 |

**Table 5. 5 Name of the pathways involved in 24-hour FA compared to 24-hour recovery group and the number of genes involved in.**

A number of genes regulated in response to NF-κB activation showed significant changes comparing 24-hour recovery group to 24-hour FA group, these genes included BCL2 interacting protein 3 (BNIP3), superoxide dismutase 1 (SOD1), C-X-C motif chemokine ligand 2 (CXCL2), C-X-C motif chemokine ligand 11 (CXCL11), C-C motif chemokine ligand 5 (CCL5) and proteasome subunit beta 9 (PSMB9). The protective SOD1 and CXCL11 were decreased by 50.27 and 43.98 times respectively (Tablw 5.6). Conversely BNIP3, a BCL2 family member, was significantly increased by 6.26-fold in recovery compared to FA treated cells ($p<0.05$). The expression of CXCL2, CCL5 and PSMB9 were significantly increased by 4.57, 5.09 and 2.63-fold respectively ($p<0.05$).

The angiogenesis pathway was highlighted as the expression of several main components such as HIF1-α, significantly decreased by 3.37-fold and the expression of VEGF significantly decreased by 4.25-fold after 24-hour recovery ($p<0.05$). C-C motif chemokine ligand 2 (CCL2), a small cytokine that attracts monocytes and dendritic cells to an inflamed area (Carr *et al*., 1994) was significantly decreased by 2.55-fold compared to that in 24-hour FA treatment ($p<0.05$).

**Title:** PI3K-AKT-NFKB pathway
**Availability:** CC BY 2.0
**Organism:** Rattus norvegicus

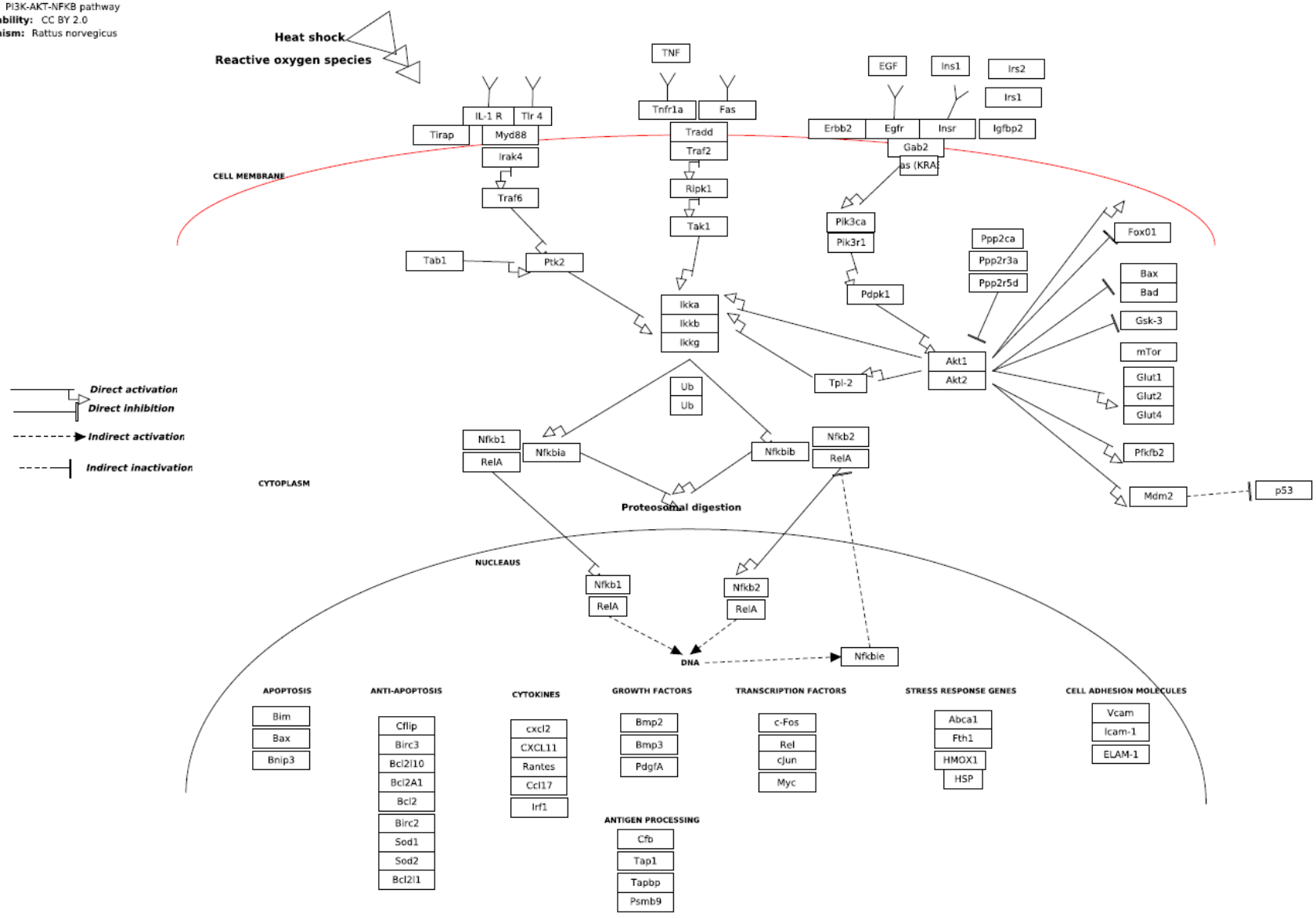

**Figure 5. 2 PI3K-AKT-NFκB pathway and the expressions of downsteam genes.**

Major activators and transcriptive genes involved in PI3K-AKT-NFκB pathway as well as downsteam genes that were mediated by the pathway. Figure is taken from Reddy M.S., Willighagen E., Pico A., Digles D., Kutmon M. (2016) PI3K-AKT-NFκB pathway.

| | |
|---|---|
| **Apoptosis** | |
| Bnip3 | ↑ 6.26 |
| **Anti-apoptosis** | |
| SOD1 | ↓ 50.27 |
| **Cytokines** | |
| CXCL2 | ↑ 4.57 |
| CXCL11 | ↓ 43.98 |
| CCL5 | ↑ 5.09 |
| **Antigen Processing** | |
| Psmb9 | ↑ 2.63 |

**Table 5. 6 The expression of downsteam genes comparing 24-hour recovery to 24-hour FA.**

↑ indicated the gene expression increased during recovery compared to FA treatment;

↓ indicated gene expression decreased during recovery compared to FA treatment.

### 5.3.3 Confirmation of biomarkers of renal injury and recovery through qPCR

The expression of TGFβ-1 and IL-18 mRNA both showed a significant elevation when cells were treated with FA (Figure 5.3, $p<0.05$). TGFβ-1 in particular, showed a 3.6 fold increase in mRNA expression after 24-hour FA treatment compared to control group (Figure 5.3, imgae A); IL-18, on the other hand, showed a 1.8-fold increase after FA treatment (Figure 5.3, imgae B). The mRNA expression of both were reduced after 24-hour recovery.

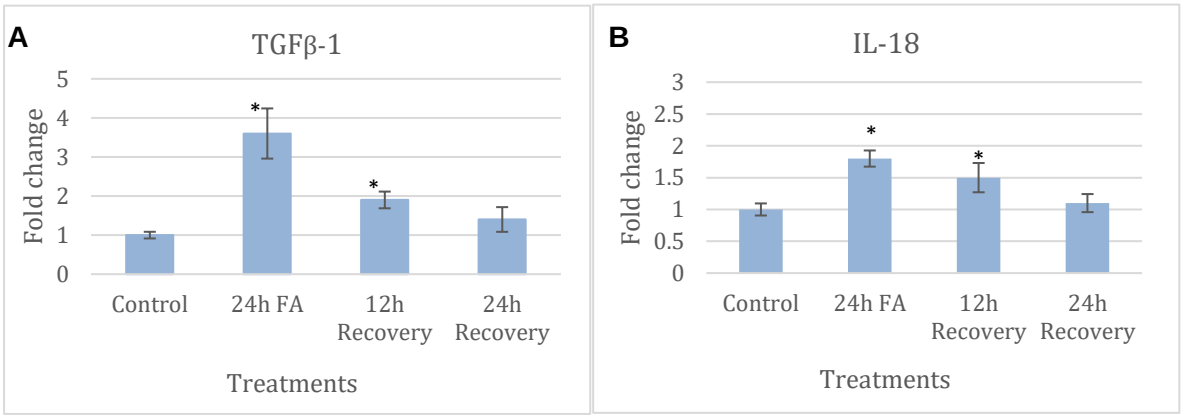


**Figure 5. 3 Fold changes of TGFβ-1 and IL-18 identified by qPCR.**

Fold change of (**A**) TGFβ-1 and (**B**) IL-18 in control, FA treatment and 12-hour, 24-hour recovery, β-actin was used as house keeping gene. Each group of treatment was triplicated (n=3), means ± SEM were shown, *$p<0.05$ was considered as significant.

To confirm the mRNA expressions of TGFβ-1 and IL-18 in RNA-seq, relative fold changes were presented in Figure 5.4. After 24-hour FA treatment, the expression of TGFβ-1 significantly increased by 4.75-fold compared to control group ($p<0.05$); TGFβ-1 expression significantly decreased by 3.86 fold during recovery compared to the expression after FA treatment ($p<0.05$). IL-18 showed a significant 2.23-fold increase after FA damage compared to control group and a significant 3.33-fold reduction during recovery compared to FA treatment group ($p<0.05$). TGFβ-1 and IL-18 did not show significant fold changes comparing control group to recovery group. It also worth mentioning that NGAL showed a significant 2.34 increase in its expression in recovery compared to FA treated group, and in the previous experiment NGAL mRNA expression showed a significant 3.6-fold increase in 24-hour FA treated cells compared to the control group ($p<0.05$).

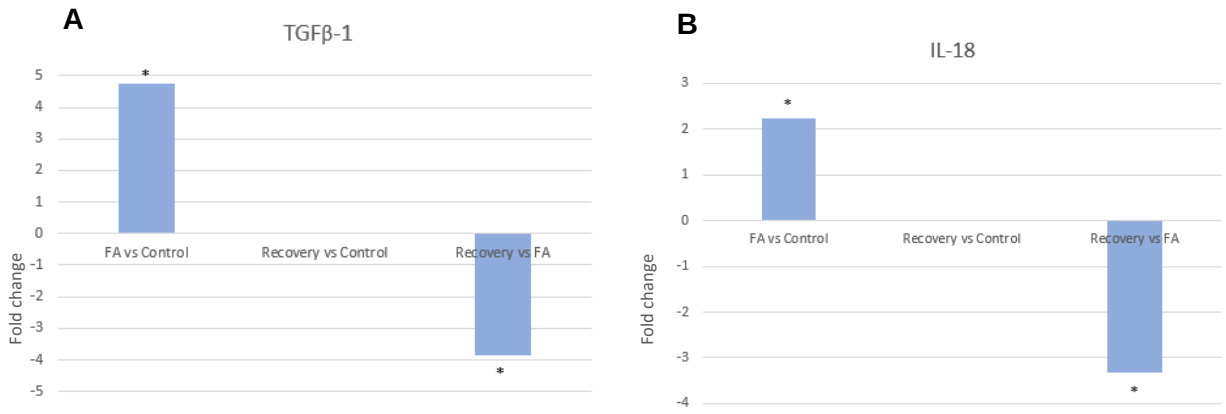


**Figure 5. 4 Relative fold change of TGFβ-1 and IL-18 mRNA identified by RNA-seq.**

Relative fold change of (**A**) TGFβ-1 and (**B**) IL-18 mRNA in treatments: FA compared to control, recovery compared to control and recovery compared to FA. Positive fold change indicated an increase in the mRNA expression, negative fold change indicated a reduction of mRNA expression. *p<0.05 was considered as significant.

### 5.3.4 Potential pathways that HMGB1 was involved in FA damage and recovery

#### 5.3.4.1 HMGB1 expression in FA damage and recovery

In previous expriments, incrasd protein expression of HMGB1 was observed within 8 hours of treatment with FA and retained high up to 24 hours of treatment (Section 4.3.1, Figure 4.1, image E3). After FA damage, the protein expression of HMGB1 remained strong until 24-hour recovery (Figure 4.1, image G3), then it was weakened during further recovery. HMGB1 did not show a significant change in the RNAseq data, however the expression of several HMGB1 pseudogenes did show some significant

changes (Figure 5.5, $p<0.05$). Pseudogenes are copies of a gene that have coding-sequence deficiencies such as premature codons, but the function of the copies are similar to its original gene (Tutar Y., 2012). Comparing the expression of HMGB1 pseudogenes in FA treated group to the control group showed expression to be highly variable with some, such as HMGB1p1, showing a significant increase (2.07-fold, $p<0.05$), whilst others, such as HMGB1p20, HMGB1p21, HMGB1p24, HMGB1p31, HMGB1p44 were greatly reduced (136.78, 9.11, 12.24, 3.61 and 31.76-fold respectively). Comparing the expression of HMGB1 pseudogenes in 24-hour recovery group to the FA treatment group, the HMGB1p44 expression had a significant 31.76-fold increase with recovery ($p<0.05$), while other pseudogenes HMGB1p20, HMGB1p21, HMGB1p24, HMGB1p31 and HMGB1p49 were all significantly increased 5.56, 17.08, 10.39, 3.65 and 4.78-fold respectively ($p<0.05$). The elevation of HMGB1 pseudogenes expression suggested that they may be involved in the cell recovery process, although pseudogenes may often be dysfunctional versions of the original; more importantly, in our model, HMGB1 seemed targeted mainly on translation instead of transcription, as HMGB1 protein was detected in the previous results (Figure 4.1) but HMGB1 RNA was not detected in RNA-seq data.

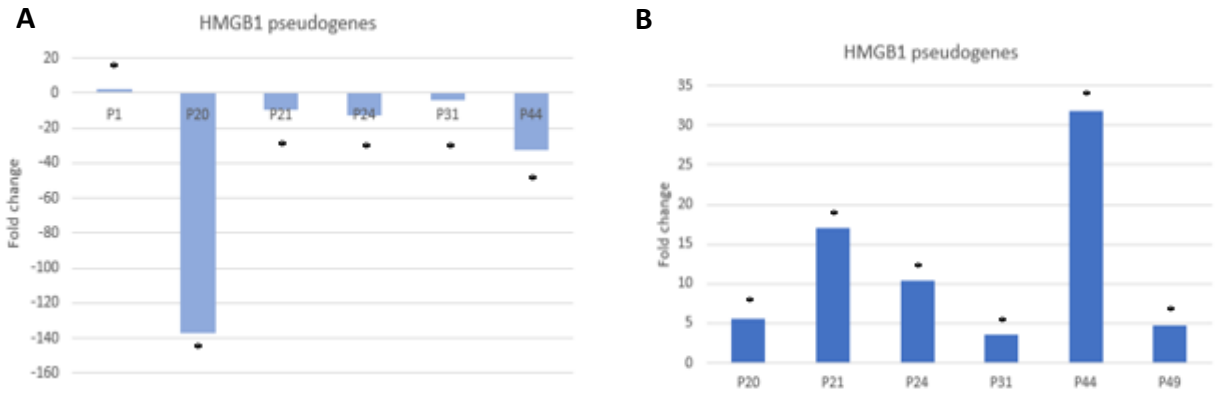


**Figure 5. 5 HMGB1 pseudogenes mRNA expression was increased in recovery group compared with FA treatment group and decreased in FA treated group compared to the control group.**

The relative fold change of HMGB1 pseudogenes including (**A**) HMGB1p1, HMGB1p20, HMGB1p21, HMGB1p24, HMGB1p31, HMGB1p44 in FA treated group in comparison to the control group and (**B**) HMGB1p20, HMGB1p21, HMGB1p24, HMGB1p31, HMGB1p44 and HMGB1p49 in 24-hour recovery group in comparison to 24-hour FA treatment group. Positive fold change indicated an increase in the expression, negative fold change indicated a reduction of expression. $p<0.05$ was considered as significant.

### 5.3.4.2 Cytoplasmic and nuclear HMGB1 expression in FA damage and recovery and its related pathways

In the cytoplasm, the function of HMGB1 is via partly stimulating the activation of autophagy and maintaining the balance between autophagy and apoptosis (Tang *et al*., 2010). In section 4.3.4, we showed an increase in the expression of LC3 in HK2 cells after 24-hour FA incubation, following with a slight decrease in expression after 12-hour recovery and an increase after 24-hour recovery, the expression level of LC3 remained the same after 48-hour recovery. Our RNA-seq data indicated that LC3 showed a significant 3.14-fold increase in FA treatment group compared to control group ($p<0.05$), and a significant 11.94-fold increase in recovery group compared to control group ($p<0.05$), as well as a significant 3.8-fold increase in recovery compared to FA treatment ($p<0.05$).

HMGB1 interacts with Bcl2-Beclin1 complex and binds to beclin 1 by leaving Bcl2 using cysteine 23 and 45 (Figure 5.6) in the cytoplasm. The expression of Bcl2 showed a significant 2.86-fold increase in FA treatment group compared to control group ($p<0.05$); it also increased significantly by 2.27-fold in recovery group compared with control group ($p<0.05$). The elevation of Bcl2 and LC3 expression suggested cytoplasmic HMGB1 might induce autophagy via the interaction with Bcl2-Beclin1 complex.

A number of studies propose that nuclear HMGB1 is associated with replication, transcription, DNA repair as well as improving inflammatory response to infection (Yuan *et al*., 2004; Prasad *et al*., 2007; Avgousti *et al*., 2016). Nuclear HMGB1 induces autophagy by mediating the expression of HSPB1 (Figure 5.6; Kwak *et al*., 2013).

However the expression of HSPB1 mRNA did not have a significant fold change in any treatment, the expression of PTEN-induced kinase 1 (PINK1) mRNA, on the other hand, showed a significant 3.22-fold increase in the recovery group compared to FA treated group (Table 5.7, $p<0.05$). Other main cytokines did not show any significant change.

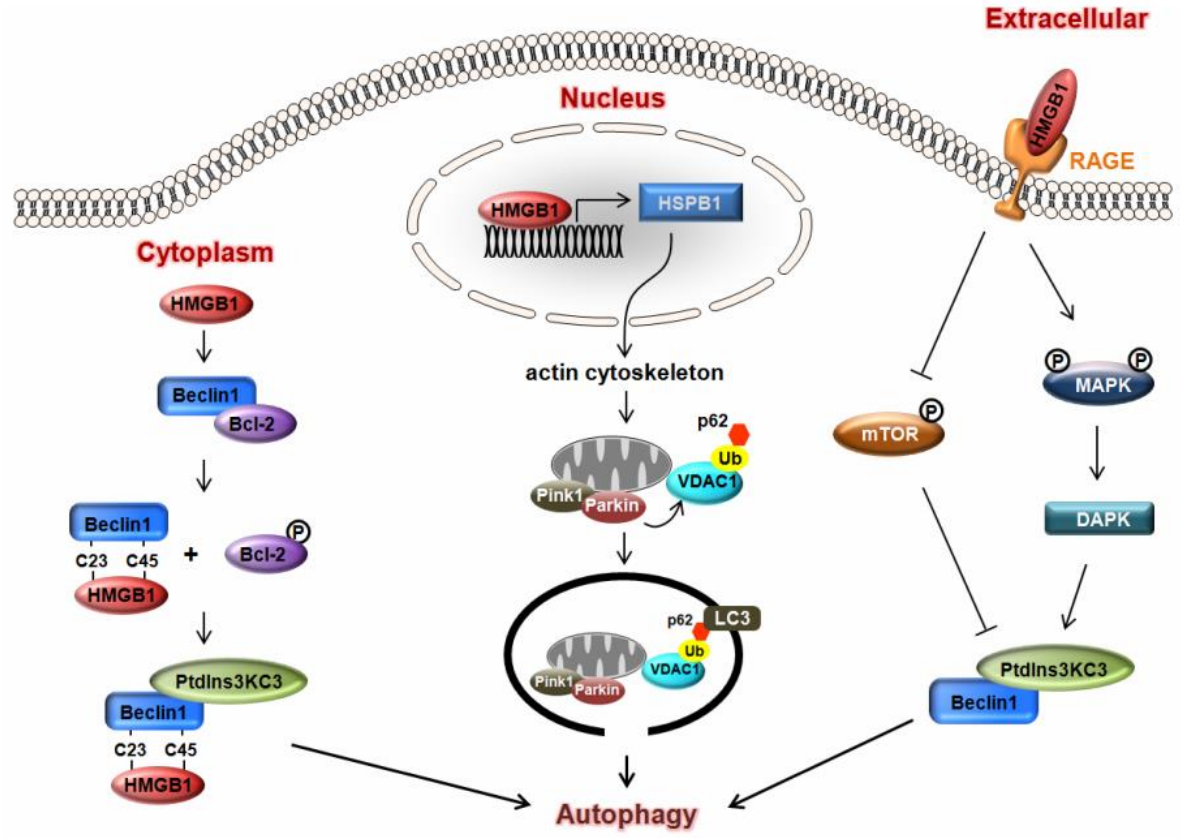


**Figure 5. 6 HMGB1 regulates autophagy in cytoplasm, nucleus and extracellular matrix.**

HMGB1 induces autophagy by interacting with Bcl2-Beclin1 complex (cytoplasm), heat shock protein β-1 (HSPB1, nucleus) and RAGE (extracellular matrix). Figure is taken from Kwak

M.S., Shin J.S. (2013) Current Understanding of HMGB1-mediated Autophagy. Journal of Bacteriology and Virology. 43(2): 148-154.

### 5.3.4.3 Extracellular HMGB1 expression in FA damage and recovery and its related pathways

HMGB1 could be secreted by cells that undergo necrosis and apoptosis. Necrotic cell released HMGB1 acts as danger associated molecular pattern (DAMP) molecule which passes on the signals to the adjacent cells, triggering an immune response (Scaffidi *et al*., 2002). This has also been observed for most cells undergoing apoptosis (Bell *et al*., 2006; Qin *et al*., 2006).

HMGB1 release results in HMGB1 binding to cell surface receptors and signal transduction pathways are activated (Figure 5.7). HMGB1 binding to the TLR2 receptor leads to the MyD88-dependent response which regulates the kinase activity of IRAK complex (IRAK4, IRAK1 and IRAK2). The IRAK complex stimulates TRAF6, followed by the activation of TAK1, TAB2, TAB3 and IKKs. The IKKs degrade IκBα through phosphorylation, which leads to NF-κB, JNK and p38 translocation, therefore stimulating proinflammatory cytokines (Lin *et al*., 2010; Johnson *et al*., 2002; Kawai *et al*., 2007). Despite the expression of TLR2 mRNA being significantly increased by 2.08-fold in the recovery group compared to FA treatment (Table 5.7, $p<0.05$), other main cytokines did not show significant fold change during treatments. In addition, the expression of IκBα mRNA showed a significant 2.51-fold increase during recovery compared to FA ($p<0.05$); furthermore, the expression of AP1 mRNA was increased 3.23-fold during FA treatment (Table 5.7, $p<0.05$).

HMGB1, along with C-X-C motif chemokine 12 (CXCL12) bind CXC receptor 4 (CXCR4) and initiate signals that are associated with chemotaxis, cell survival and gene transcription (Teicher *et al*., 2010). The expression of CXCL12 mRNA showed a significant 42.74-fold increase when cells were treated with FA compared to those in control group ($p<0.05$), but no significant changes in expression was observed in other treatments (Table 5.7). CXCR4 mRNA showed a significant 2-fold increase in the FA group compared with the recovery group (Table 5.7, $p<0.05$).

| | FA vs Ctrl | Recovery vs Ctrl | Recovery vs FA |
|---|---|---|---|
| **TGFβ-1** | ↑4.75* | | ↓3.86* |
| **IL-18** | ↑2.23* | | ↓3.33* |
| **NGAL** | ↑3.6* | ↑2.34* | |
| **LC3** | ↑3.14* | ↑11.94* | ↑3.8* |
| **Bcl2** | ↑2.86* | ↑2.27* | |
| **PINK1** | | | ↑3.22* |
| **TLR2** | | | ↑2.08* |
| **IκBα** | | | ↑2.51* |
| **AP1** | ↑3.23* | | |
| **CXCL12** | ↑42.74* | | |
| **CXCR4** | | | ↑2* |

**Table 5. 7 Fold change of mRNA in different treatments.**

↑ indicates the elevation of gene expression, ↓ indicates the reduction of gene expression. *$p<0.05$ was considered as significance.

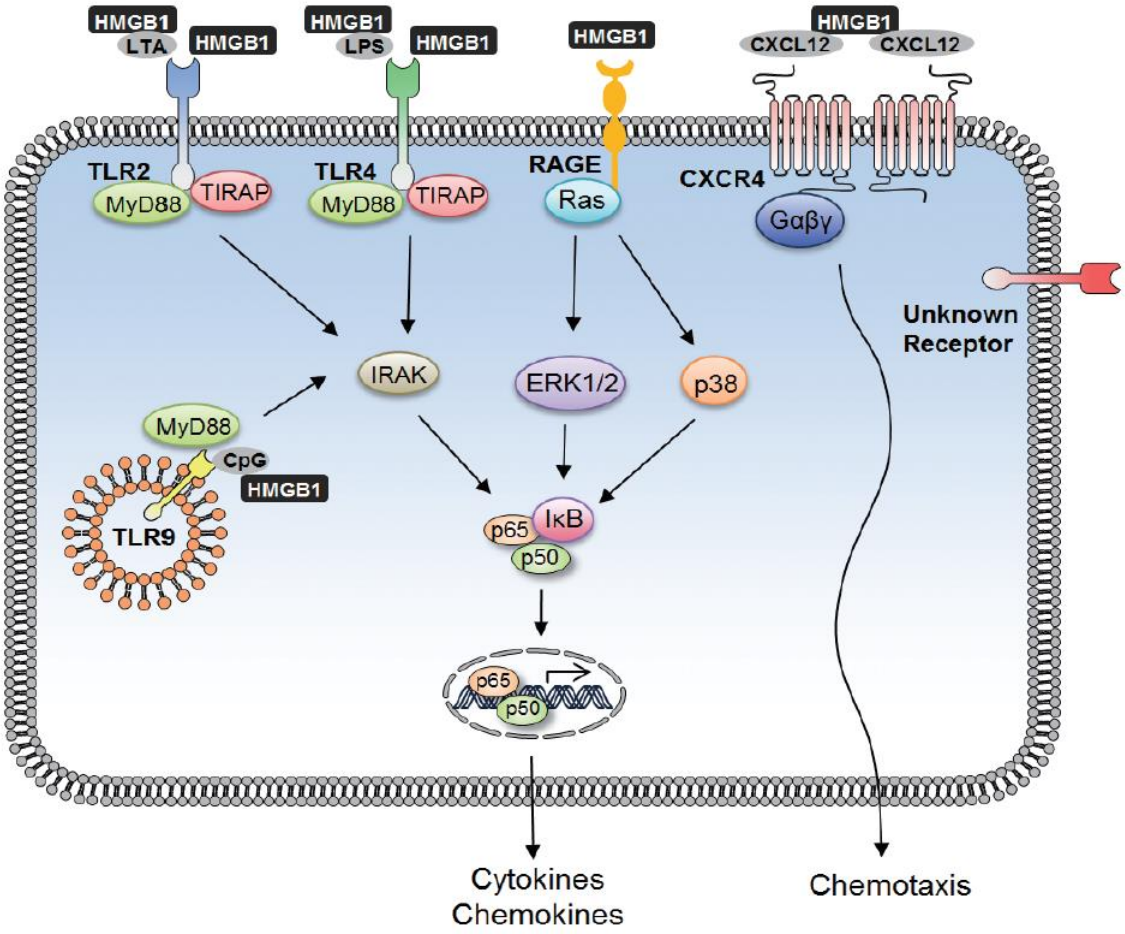


**Figure 5. 7 HMGB1 initiates signal transduction pathways by binding to receptors.**

Secreted HMGB1 interacts with TLR2, TLR4, RAGE receptors and leads to the activation of NF-κB, the activated NF-κB then translocate into the nucleus and form p65/p50 heterodimer by binding to DNA. Secreted HMGB1 interacts with CXCR4 by binding to CXCL12. Inflammatory responses are triggered once interaction of HMGB1 and receptors are induced. Figure is taken from Lee S.A., Kwak M.S., Shin J.S. (2014) The Role of High Mobility Group Box 1 in Innate Immunity. Yonsei Med J 55(5):1165-1176.

### 5.3.5 Potential pathways that Pax2 was involved in FA damage and recovery

Pax2 mRNA was also detected in FA treated HK2 cells during both damage and recovery period (Figure 5.8). Comparing the Pax2 mRNA expression in the control group, there was a significant 2.24-fold increase when cells were treated with FA ($p<0.05$), and a significant 2.35-fold decrease during recovery ($p<0.05$). A significant 5.26-fold reduction in Pax2 expression was observed in recovery compared to FA treated cells ($p<0.05$). The cell proliferation marker Ki67, on the other hand, had a significant 3.49-fold decrease in its expression in 24-hour FA treatment group compared to the control group ($p<0.05$), and a significant 3.61-fold increase in expression in 24-hour recovery group compared to 24-hour FA treatment group ($p<0.05$).

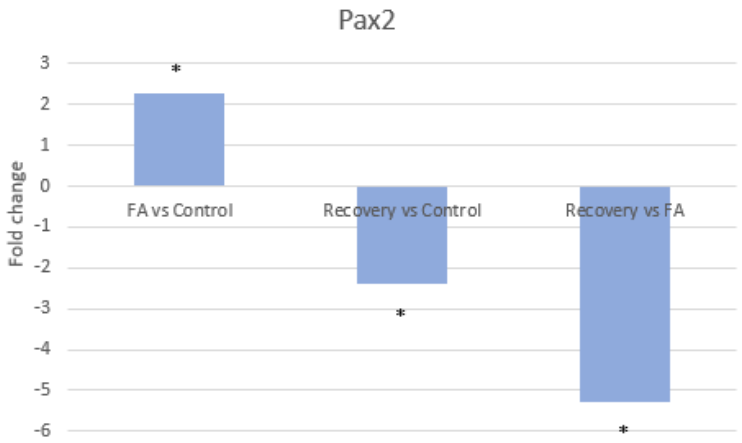


**Figure 5. 8 Pax2 mRNA fold change in treatments.**

Relative fold change of Pax2 in treatments: FA compared to control, recovery compared to control and recovery compared to FA. Positive fold change indicated an increase in the expression, negative fold change indicated a reduction of expression. *$p<0.05$ was considered as significant.

There were numerous research on genes that could mediate the expression of Pax2 or vice versa. Gene such as angiotensin II (Ang II) are reported to upregulate Pax2 expression following kidney injury through angiotensin II type 2 receptor (AT2R) and the JAK2/STAT pathways (Figure 5.11; Zhang *et al*., 2004; Guo *et al*., 2004); in our model, we observed a significant decrease of Ang II receptor (AGTR2) mRNA expression by 3.94-fold in FA treated group than the control group ($p<0.05$), as well as a significant 2.36-fold increase in expression comparing recovery group to FA treated group (Table 5.8, $p<0.05$). The expression of AT2R, JAK2, STAT3 and STAT5 mRNA did not have significant changes in any treatments. Chen and colleagues proposed that NF-κB mediated Pax2 mRNA expression, and the change of NF-κB mRNA expression matched the mRNA expression of Pax2 (Chen *et al*., 2006): NF-κB 1A, 1B and 1D showed significant increase in mRNA expression by 3.71, 3.09 and 3.53-fold after cells received FA treatment compared to the control group ($p<0.05$), and significant reduction in NF-κB expression were noticed by 2.51, 2.37 and 2.89-fold respectively in recovery group compared to FA treated group (Table 5.8 , $p<0.05$). Sonic hedgehog (SHH) mRNA expression decreased in the recovery group compared to the FA treated group, it was illustrated to promote the mRNA expression of Pax2 and the mRNA expression of which significantly decreased by 2.09-fold in recovery compared to FA treated cells (Table 5.6, $p<0.05$ ; Zhao *et al*., 2010). The mRNA expression of activin A, a downregulator of Pax2, was observed to have a significant 3.55-fold elevation in FA treated cells compared to the cells in control group ($p<0.05$); furthermore, its expression significantly increased by 2.54-fold in recovery group compared to the control group (Table 5.6 , $p<0.05$). There are two pathways mediated by the action of activin A (Figure 5.11), the Smad-dependent pathway and Smad-

independent pathway. The Smad-dependent pathway starts with the binding of activin A and receptor, leading to the phosphorylation of Smad2 or Smad3, forming a Smad complex with Smad4 which regulates the expression of Pax2 (Lindoso *et al*., 2009). The Smad-independent pathway is mediated by TAK1 which triggers the p38 MAPK signalling pathway (Zhang *et al*., 2005); however, the mRNA expression of the key components in both pathways did not show significant changes in any treatment groups.

| Genes | FA vs Control | Recovery vs Control | Recovery vs FA |
|---|---|---|---|
| **Angiotensin II receptor (AGTR2)** | ↓ 3.94* | - | ↑ 2.36* |
| **Nuclear factor kappa B (NF-kB)** | 1A ↑ 3.71*; 1B ↑ 3.09*; 1D ↑ 3.53* | - | 1A ↓ 2.51*; 1B ↓ 2.37*; 1D ↓ 2.89* |
| **Sonic hedgehog (SHH)** | - | - | ↓ 2.09* |
| **Activin A** | ↑ 3.55* | ↑ 2.54* | - |
| **Glial cell line-derived neurotrophic factor (GDNF)** | ↑ 5.81* | - | ↓ 11.61* |
| **Transglutaminase 4 (TGM4)** | | ↑ 2.73* | ↑ 2.33* |

| | | | |
|---|---|---|---|
| **Secreted frizzled related protein 2 (SFRP2)** | ↑ 3.84* | - | ↓ 3.12* |

**Table 5. 8 Fold change of mRNA that regulate Pax2 mRNA and involved in downstream pathway.**

The change of mRNA mediates the expression of Pax2 mRNA and downstream pathway. ↑ indicates the elevation of gene expression, ↓ indicates the reduction of gene expression. *p<0.05 was considered as significance.

Pathways downstream of Pax2 were also influenced by FA exposure including those involving glial-derived neurotrophic factor (GDNF), transglutaminase 4 (TGM4) and secreted frizzled related protein (SFRP2). The mRNA expression of GDNF could be upregulated by Pax2 (Brophy *et al*., 2001), and its mRNA expression had a significant 5.81-fold elevation in FA treated group compared to the control group ($p<0.05$), followed by a significant 11.61-fold decrease in expression in recovery group compared to FA treated cells (Table 5.8, $p<0.05$). The increase in Pax2 expression was shown to decrease TGM4 mRNA expression (Tamimi *et al*., 2008), and the mRNA expression of TGM4 significantly increased by 2.73-fold in recovery compared to the control group ($p<0.05$), and a further significant 2.33-fold increase in recovery compared to FA treated group (Table 5.6, $p<0.05$). The mRNA expression of SFRP2 is strongly associated with the activation of Pax2 (Brophy *et al*., 2003), and its mRNA expression was observed a significant 3.84-fold increase in FA treated group compared to the control group, and a significant 3.12-fold decrease in recovery group

compared to FA treated cells (Table 5.8, $p<0.05$). Epidermal growth factor (EGF) was illustrated to extend the Pax2 half-life in the cells through PI3K and AKT (Figure 5.9) without directly mediating Pax2 expression.

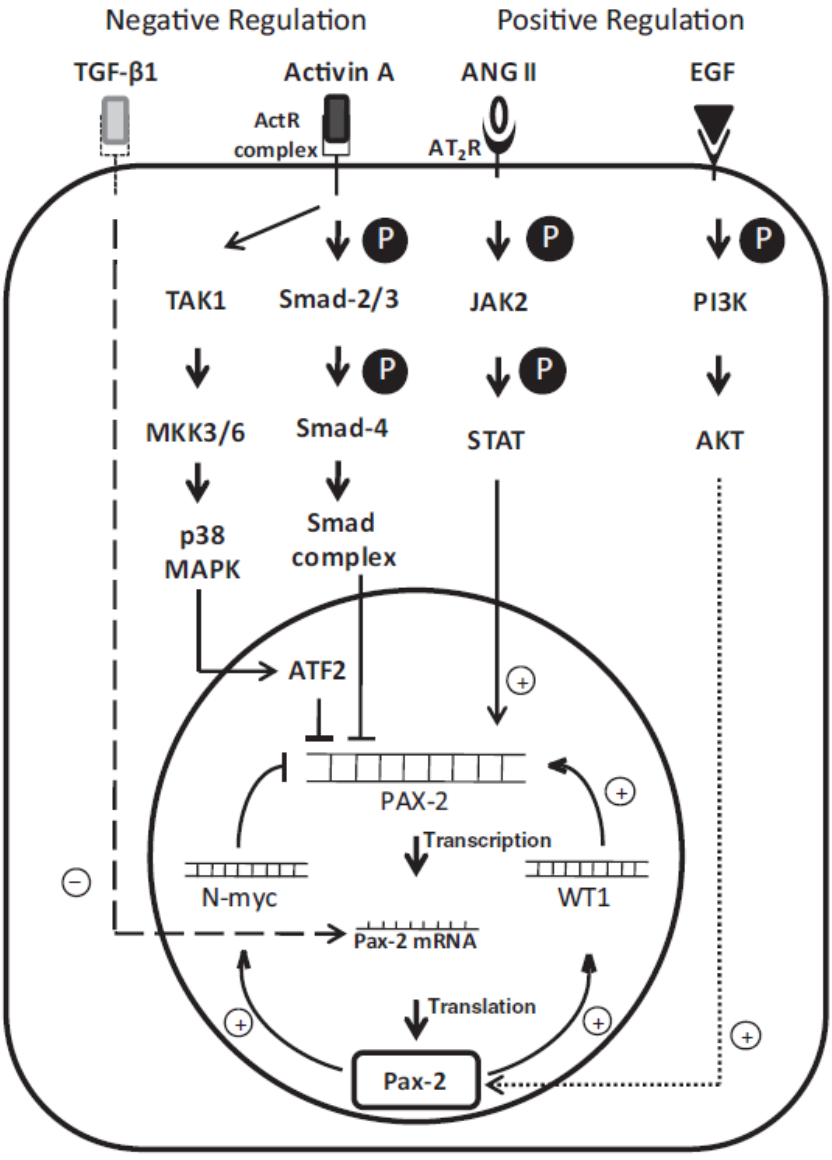


**Figure 5. 9 Pax2 involved signalling pathways.**

Positive and negative regulation pathways of Pax2 expression. Figure is taken from Lindoso R.S., Verdoorn K.S., Einicker-Lamas M. (2009) Renal recovery after injury: the role of Pax-2. Nephrol Dial Transplant. 24: 2628–2633.

### 5.3.6 Potential pathways that MMP7 was involved in FA damage and recovery

MMP7 mRNA expression was observed a significant 6.86-fold decrease in cells treated with FA compared to those in the control group ($p<0.05$), as well as a significant 2.16-fold decrease in the recovery group compared to the control group (Figure 5.10, $p<0.05$). However, the mRNA expression of MMP7 increased significantly by 3.18-fold compared the recovery group to the FA treated group ($p<0.05$). MMP7 was demonstrated to protect proximal tubules from progressing apoptosis and inducing cell regeneration (Fu *et al*., 2019), partially due to the direct degradation to fas ligand (FasL). FasL belongs to the tumor necrosis factor (TNF) family and the binding to its receptor induces cell apoptosis, therefore the degradation of FasL by MMP7 protects tubular cells from apoptosis. The mRNA expression of FasL had a significant 7.69-fold increase in FA treated cells compared to the control group ($p<0.05$), and a significant 7.77-fold decrease in expression was observed in the recovery group compared to FA treated cells ($p<0.05$).

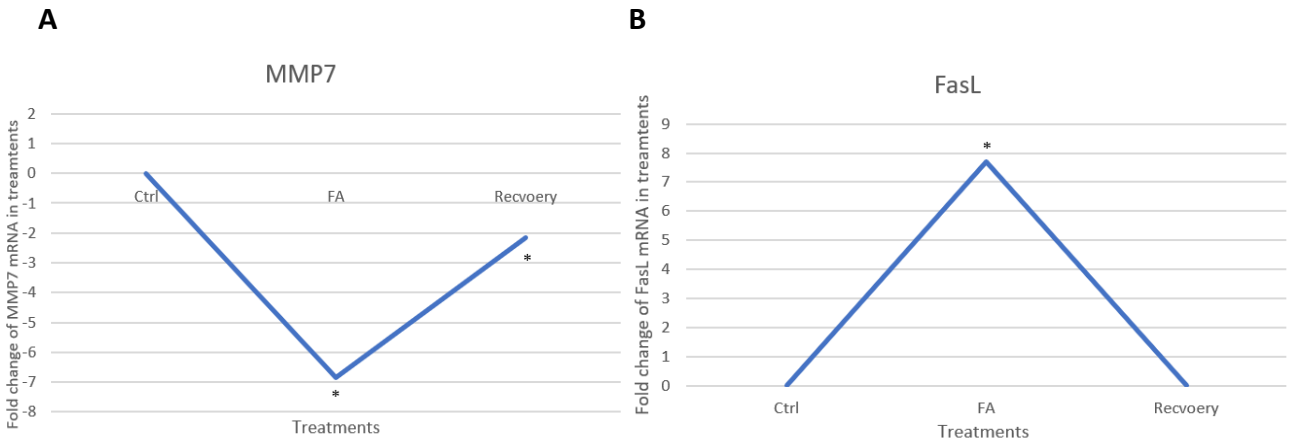


**Figure 5. 10 Pax2 fold change in treatments.**

Relative fold change of (**A**) MMP7 and (**B**) FasL: FA compared to control, recovery compared to control and recovery compared to FA. Positive fold change indicated an increase in the expression, negative fold change indicated a reduction of expression. *p<0.05 was considered as significant.

### 5.3.7 Developmental related transcription factors re-expressed in FA treated HK2 cells.

A few developmental related transcription factors re-expressed during FA induced acute damage and recovery. Pax2, Pax8, GDNF, c-ret, VRGF as well as some members of Hox and WNT family showed significant increase in mRNA expression in response to FA treatment by 2.24-fold, 3.34-fold, 5.81-fold, 2.39-fold, 11.2-fold respectively; Hoxa and Hoxc13 showed significant 2.36-fold and 3.19-fold increase in mRNA expression, Wnt9a, Wnt7b and Wnt16 showed significant 2.55-fold, 5.98-fold and 3.33-fold increase in mRNA expression after 24-hour FA treatment. c-ret and VEGF showed significant 2.39-fold and 2.63-fold increase in mRNA expression after 24-hour recovery (Table 5.9).

| | Kidney Development | | | | | | |
|---|---|---|---|---|---|---|---|
| **Genes** | **Function** | **Location** | **REF** | **Re-expressed in FA induced damage and recovery (Y/N)** | **FC (FA vs Ctrl)** | **FC (Recovery vs Ctrl)** | **FC (Recovery vs FA)** |
| Bone morphogenetic proteins (BMP) | activate IM specific genes and lateral plate markers | metanephritic mesenchyme | Obara-Ishihara et al., 1999 | Y | BMP8b ↓2.84* | BMP8b ↓2.38*; BMP4 ↓4.39* | BMP4 ↓3.25* |
| Odd-skipped related gene (OSR1) | markers of the LPM | metanephric mesenchyme | James et al., 2006 | N | - | - | - |
| Paired box gene 2 (PAX2) | development of the renal epithelium | Wolffian duct, the ureteric bud, the collecting ducts. metanephric blastema at early stages of metanephrogenesis | Dressler et al., 1999 | Y | ↑ 2.24* | ↓2.35* | ↓5.26* |
| Paired box gene 8 (PAX8) | regulator of the first steps of pronephric development | S-shaped body and in the early proximal tube | Buisson et al., 2015 | Y | ↑ 3.34* | - | ↓3.31* |
| LIM Homeobox 1 (LHX1) | markers of the LPM | intermediate mesoderm | Tsang et al., 2000 | N | - | - | - |
| Homeobox (HOX) | regional specification and patterning of the axial skeleton | metanephric mesenchyme | Wellik et al., 2007 | Y | Hoxa ↑ 2.36*; Hoxc13 ↑ 2.19*; Hoxd8 ↓2.64*; Hoxb9 ↓2.4* | Hoxa5 ↓2.35* | Hoxd4 ↑ 2.39*; Hoxc13 ↓2.56*; Hoxd12 ↓37.8* |

| | | | | | | | |
|---|---|---|---|---|---|---|---|
| Wilms' tumor suppressor gene1 (WT1) | regulation of the process of Mesenchymal-Epithelial-Transition and in the development and maturation of podocytes | metanephric mesenchyme, vesicles, in comma-shaped bodies, and at the proximal part of S-shaped bodies | Fanni et al., 2011 | N | - | - | - |
| Glial cell line-derived neurotrophic factor (GDNF) | promote growth and branching of the ureteric bud | metanephric mesenchyme | Kobayashi et al., 2008 | Y | ↑ 5.81* | - | ↓11.61* |
| sina oculis-related homeobox 2 (SIX2) | maintain a nephron progenitor population | metanephric mesenchyme | Chi et al., 2009 | Y | - | ↓2.23* | - |
| c-RET | induce epithelial cell rearrangement and migration | metanephric mesenchyme | Seely et al., 2017 | Y | ↑ 2.39* | ↑ 2.58* | - |
| Sprouty homolog 1 (SPRY1) | limits the intensity or duration of RET signalling, | condensing mesenchyme | Basson et al., 2005 | N | - | - | - |
| Fibroblast growth factor | regulate ureteric bud epithelium | metanephric mesenchyme | Powers et al., 2000 | Y | FGFR2 ↓6.72*; FGFR3 ↓4.32* | FGFR2 ↓3.51*; FGFR3 ↓2.13* | FGFR3 ↑ 2.03* |

| | | | | | | | |
|---|---|---|---|---|---|---|---|
| receptors (FGFR) | | | | | | | |
| Hepatocyte growth factor (HGF) | regulate cell growth, cell motility and morphogenesis | mesenchymal cells, distal tubules and collecting ducts, | Woolf et al., 1995 | N | - | - | - |
| Vascular endothelial growth factor (VEGF) | regulate endothelial cell proliferation, migration, and differentiation | metanephric mesenchyme | Ferrara N., 2004 | Y | ↑ 11.2* | ↑ 2.63* | ↓4.25* |
| Platelet-derived growth factor (PDGF) | promote differentiation of mesangial cells and promote glomerular vasculogenesis | metanephric mesenchyme | Lindahl et al., 1998 | Y | PDGFA ↓2.62*; PDGFC ↓2.61*; PDGFD ↓2.07* | - | - |
| insulin-like growth factor (IGF) | regulation of cell growth, proliferation, survival | metanephric mesenchyme | Hammerman et al., 1987 | N | - | - | - |
| Ang II receptors 2 (AT2R) | Regulate renal blood flow and formation of the embryonic ureter by the promotion of the mesenchymal cell apoptosis | mesenchymal cells adjacent to the UB stalk | Keiser et al., 1992 | N | - | - | - |

| | | | | | | | |
|---|---|---|---|---|---|---|---|
| WNT | inducer of the metanephric mesenchyme | branching ureteric bud | Carroll et al., 2005 | Y | WNT5a ↓2.55*; WNT9a ↑ 2.24*; WNT7b ↑ 5.98*; WNT16 ↑ 3.33* | WNT9a ↑2.17*; WNT10b ↓2.09* | WNT7b ↓3.64*; WNT16 ↓6.12* |
| EYA Transcriptional Coactivator And Phosphatase 1 (Eya-1) | essential for early metanephric mesenchyme specification | metanephric mesenchyme | Abdelhak et al., 1997 | N | - | - | - |
| forkhead box C1 (Foxc1) | regulate cell proliferation, cell fate determination, and differentiation. | metanephric mesenchyme | Kume et al., 2000 | N | -- | - | - |
| Sal-like 1 (Sall 1) | required for the metanephric mesenchyme to attract the ureteric bud | metanephric mesenchyme | Nishinakamura et al., 2001 | N | - | - | - |

**Table 5. 9 List of transcription factors involved in kidney development and their fold changes in FA treatment and recovery.**

Some of the developmental related transcription factors re-expressed in HK2 cells in response to FA treatment and/or recovery. ↑ indicates the elevation of gene expression, ↓ indicates the reduction of gene expression. *p<0.05 was considered as significance.

## 5.4 DISCUSSION AND CONCLUSION

There were total 109 pathways significantly altered comparing 24-hour FA treatment to the control group ($p<0.05$); the top three involved were pro-inflammatory pathway, Wnt signalling pathway and angiogenesis pathway. The mRNA expression of components such as IL-1A, IL-1B, MKK3, JNK and CHOP were significantly increased in pro-inflammatory pathway ($p<0.05$), suggested that the pro-inflammatory pathway was activated after FA treatment and the components might be stimulated through the activation of JNK and CHOP. We have noticed significantly elevated expression of components of the angiogenesis pathway ($p<0.05$), including VEGF, HIF1- α, AKT and PLCγ mRNA. Angiogenesis is a developmental process that is related to endothelial cell proliferation, migration and tube formation; in cancer, angiogenesis contributes to the formation of new blood vessels from existing vessels in order to supply tumour growth (Loizzi *et al*., 2017). The angiogenesis pathway could be initiated by hypoxia, cellular stress and inflammation, which leads to the release of VEGF and other pro-angiogenetic molecules. Despite inducing angiogenesis pathway, VEGF also functions in inhibiting cell apoptosis, stimulating endothelial cell growth and proliferation. HIF1-α is also involved in the angiogenesis pathway assisting in promoting oxygen delivery to hypoxic regions as well as inducing transcription of genes promoting cell proliferation and survival (Lee *et al*., 2004). HIF1-α could activate VEGF to assist cell regeneration and recovery after axon injury (Cho *et al*., 2015; Mahar *et al*., 2018). The activation of such pathway indicated that HK2 cells were under proliferation and regeneration during FA treatment.

Comparing 24-hour recovery group to 24-hour FA treated group, the expression of Wnt7b, Wnt 16 and NF-κB mRNA were significantly decreased in the recovery group ($p<0.05$). The reduction in expression of NF-κB mRNA also triggered inflammation stimulated by chemokine and cytokine signalling pathway. NF-κB could not only be activated by IL-1 and lead to the induction of pro-inflammatory gene expression, but also by several growth factors or cellular stress. The reduction of these components suggested a decrease of expression of pro-inflammatory cytokines and a reduction of expression of developmental-related genes in the recovery stage.

Comparing the recovery group to the control group, despite the activation of Wnt signalling pathway and pro-inflammatory pathway, the integrin pathway was the third most involved pathway with ERK and CDC42 mRNA showed significant upregulation in recovery group compared to the control group ($p<0.05$). Integrins are receptors located at the cell surface. They interact with various targets to regulate a number of cellular processes such as cell migration, proliferation and apoptosis (Cary *et al*., 1999). After ligand binding to integrin receptors, the phosphorylated focal adhesion kinase (FAK) activates phosphoinositide 3-kinase (PI3K) and growth factor receptor bound protein 7 (GRB7), leading to the activation of Akt signalling (Zhao *et al*., 2011). The Akt pathway is a signal transduction pathway which improves cell survival, growth, proliferation and angiogenesis in response to extracellular signals (Osaki *et al*., 2004). The activation of its critical kinase Akt requires the phosphorylation of Ser473, which can be regulated by phosphoinositide-dependent kinase 2 (PDK2), integrin-linked kinase (ILK), mammalian target of rapamycin complex

(mTORC) and DNA-dependent protein kinase (DNA-PK) (Osaki *et al*., 2004; Hemmings *et al*., 2012; Vanhaesebroeck *et al*., 2000).

CXCL2 has been shown to promote wound healing and angiogenesis (AL-Alwan *et al*., 2013), while CCL5 has been demonstrated to induce proliferation and activation of certain natural killer (NK) cells (Maghazachi *et al*., 1996). PSMB9, a subunit contributing to the complete assembly of the proteasome complex, it was proven to contribute to recognize degraded and damaged proteins (Coux *et al*., 1996). The change of expressions suggested that although FA treatment triggered inflammatory pathway, HK2 cells were undergoing recovery by diminishing free radicals created by FA damage, as well as reducing cell death and increasing cell development and proliferation.

We also further confirmed the expression of some biomarkers for renal injury and recovery. The expression of TGFβ-1 and IL-18 were elevated after FA treatment and reduced during recovery in both qPCR and RNA-seq results. TGFβ-1 is a 25 kDa polypeptide member of the transforming growth factor beta superfamily, it was proven to play a role in wound healing (Assoian *et al*., 1983) as well as regulating several cell activities including cell growth, proliferation, differentiation and apoptosis (Letterio *et al*., 1998). IL-18 is a sensitive biomarker of AKI, it could be easily detected in urine when kidneys are undergoing acute injuries (Section 1.2.4.2). The upregulation of both biomarkers after FA treatment suggested FA induced damage to HK2 cells and the surviving cells might be under proliferation.

The induction of HMGB1 protein was observed 4-hours after incubated with FA, the expression of HMGB1 protein remained strong during FA treatment for 24-hours and gradually reduced during recovery (Section 4.3.1, Figure 4.1). Similar expression was observed in the Western Blot result (Figure 4.5) where the expression of HMGB1 protein was significantly elevated after 24-hour FA treatment ($p<0.05$), slightly reduced after 12-hour recovery and showed no significant difference to the control group after 24-hour recovery. In our RNA-seq data, we observed HMGB1 mRNA did not show significant fold change in any treatment other than its pseudogenes, which demonstrated that HMGB1 was more translation regulated in FA induced AKI in HK2 cells instead of transcription regulated. In addition, multiple studies have shown the upregulation of HMGB1 protein expression during acute renal injury (Wu *et al*., 2010; Zakiyanov *et al*., 2013; Wu *et al*., 2010). However, it would be better to run a few more RNA-seq analysis to confirm this result.

Our results also showed that the upregulation of cytosolic HMGB1 protein might be associated with the activation of autophagy, which could be reflected by the increased expression of LC3B protein. The secreted cytoplasmic HMGB1 plays a role in separating beclin1 and Bcl2, therefore allow the bind between HMGB1 and beclin1. The formed BECN1-PtdIns3KC3 complex stimulates autophagosome maturation and the activation of autophagy. This theory was also demonstrated by Huang and colleagues and Kwak and colleagues (Huang *et al*., 2012; Kwak *et al*., 2013). HMGB1 also works as DAMP molecules when released by necrotic cells, it functions as a mediator of inflammation in innate immune system by mediating the maturation and migration of dendritic cells

and activates T-cells by interacting with RAGE (Dumitriu *et al*., 2005; Yang *et al*., 2007; Messmer *et al*., 2004), however, we have also shown that due to the changes in expression of other vital components, HMGB1 did not regulate autophagy activation through RAGE. Similar to extracellular HMGB1, although the expression of TLR2 significantly increased by 2.08-fold in recovery group compared to FA treatment group ($p<0.05$), it could only suggest that HMGB1 might induce proinflammatory cytokines through TLR2 signalling pathway in HK2 cells suffered from FA induced AKI, however TLR2 signalling pathway was not the primary way of inducing proinflammatory cytokines.

In our data, we observed a significant fold increase in Pax2 expression in 24-hour FA treatment group compared to the control group ($p<0.05$), a significant downregulation of Pax2 expression in the 24-hour recovery group compared to the control group ($p<0.05$), followed by a significant decreased in expression in 24-hour recovery group compared to 24-hour FA treatment ($p<0.05$). The upregulation of SHH, which expression functioned in the formation of sonic hedgehog protein, played a role in cell growth. GDNF functions as a mesenchyme-derived signal in kidney development and encourages ureteric branching (Airaksinen *et al*., 2002), whereas SFRP2 is required for anteroposterior axis elongation and somitogenesis in the thoracic region during mouse embryogenesis (Satoh *et al*., 2006). The expression of these genes shown in other studies to be influenced by Pax2 expression were appropriately altered in our study. Pax2 can be found in the caudal mesonephric duct, ureteric bud and mesenchymal condensates during renal development stage, and the expression fades out as the epithelial cells differentiate (Chi *et al*., 2002; Eccles

*et al*., 1992; Torres *et al*., 1995); thus Pax2 only expresses in collecting ducts in healthy adult kidneys (Torban *et al*., 2000). However, one of the major functions of Pax2 during kidney development is to restrain the programmed cell death in ureteric bud cells, therefore Pax2 has been hypothesised the re-express of Pax2 may minimise the apoptosis during renal injury. Imgrund and colleagues, however, were first to find the re-expression of Pax2 in mice kidneys after FA-induced necrosis (Imgrund *et al*., 1999). Nonetheless, Maeshima and colleagues confirmed the re-expression of Pax2 in I/R model, along with some other transcription factors involved in development such as Pax8 and WT1 (Maeshima *et al*., 2002), suggesting that Pax2 might not only promote development during embryonic stage, but also played a role during renal recovery after acute injury. Accordingly, numerous researchers believe that the re-expression of Pax2 and other developmental related genes in matured but damaged proximal tubules is an introduction of cell atavistic transition, which mocks the tubular developmental process in embryonic stage. In the same study that Maeshima carried out in I/R model, they found that the peak of Pax2 expression was prior to the peak of BrdU expression, IHC analysis showed Pax2 colocalised with BrdU in the cells; on top of that, by inhibiting Pax2 with inhibitor, the proliferation rate of survived cells significantly decreased. All evidence illustrated that the re-expression of Pax2 promoted the proliferation rate of survived cells (Maeshima *et al*., 2002). Further evidence was reported by Zhang and colleagues that around 50% proliferation rate was affected by blocking the expression of Pax2 in the immortalised renal proximal tubular cells; in addition, cells lacked Pax2 were 2.4-time more likely to suffer

from apoptosis than the control group (Zhang *et al*., 2004). Further directed experiments would be necessary to confirm whether PAX2 is the upstream gene of those genes in this model. These findings along with the significant decrease of Ki67 expression in 24-hour FA treatment group compared to the control group ($p<0.05$), as well as the significant elevation in Ki67 expression in 24-hour recovery compared to the 24-hour FA group suggested 1) A few Pax2 related and developmental related genes re-expressed during FA induced AKI model, promoting cell growth and recovery. 2) Pax2 re-expressed in FA treatment group compared to the control suggested Pax2 played a role during cell injury, whether Pax2 had a role in promoting proliferation needed to be further tested by inhibiting the expression of Pax2.

GDNF is a member of the TGF-β superfamily which is produced by the metanephric mesenchyme, it functions in ureteric budding during kidney development (Sariola *et al*., 1999). Studies suggested that in the absence of Pax2 in mouse embryos, the development of ureteric bud was interrupted (Torres *et al*., 1995); on top of that, Gong and colleagues (2007) demonstrated that Pax2 can form a complex by binding Hox11 and Eya1, therefore regulate the expression of GDNF in the metanephric mesenchyme. The mRNA expression of both significantly increased during 24-hour FA treatment in HK2 cells, which suggested that Pax2 and GDNF might play a role during acute damage in reforming ureteric bud. Similar to Pax2, Pax8 also play a part in kidney development by contributing in collecting duct branching (Imgrund *et al*., 1999), the re-expression of Pax8 after FA treatment also suggested it might contribute in the recovery of the injury. The upregulation of VEGF has also been

reported in response to kidney injury. Gnudi and colleagues (2015) reported that VEGF could attract endothelial progenitors from the surrounding stroma and induce the generation of glomerular capillaries. The upregulation of VEGF mRNA during 24-hour FA treatment and during 24-hour recovery suggested that the re-expression of VEGF might contribute in promoting recovery.

Ang II was demonstrated to promote the expression of Pax2 in tubular cells during embryonic kidney development (Wolf *et al.,* 2002; Zhang *et al*., 2004). Moreover, Jiang and colleagues found that the expression of Pax2 was proportional to the time cells exposed to Ang II and the dose of Ang II, and the expression of which regulated Pax2 and relative CD24 expression (Jiang *et al*., 2014). On the contrary, we noticed the decrease in expression of angiotensin II receptor (AGTR2) in FA treated cells compared to the control group, however its expression increased during recovery compared to FA treated group; the expression of CD24 and Pax2 both showed significant decrease in expression in recovery compared to the control group as well as recovery compared to FA treated group ($p<0.05$), based on the theory proposed by Jiang and colleagues, the expression of Pax2 was related to CD24 but not Ang II. On the other hand, the expression of Pax2 increased in FA treated group compared to the control group, followed by a reduction in expression in recovery compared to the control group as well as recovery compared to FA treated group, this tendency was also reflected by the expression of downstream genes such as GDNF and SFRP2.

With the FA treatment, the expression level of MMP7 significantly decreased compared to the control group ($p<0.05$), which subsequentially increased the

expression level of FasL due to the direct degradation. FasL was proved to play a crucial role in receptor-mediated apoptosis pathway (Villa-Morales *et al*., 2012), the elevation of FasL expression in 24-hour FA treatment group compared to the control group suggested MMP7 might not have sufficient protective role in FA-induced AKI on HK2 cells by inhibiting the death receptor-mediated apoptosis pathway. Fu and colleagues who demonstrated on both I/R injury and cisplatin-induced AKI, they found that the expression of FarL showed a significant elevation when MMP7 was inhibited ($p<0.05$), and the downstream apoptotic pathway was activated (Fu *et al*., 2019). On the other hand, several studies pointed out that the FasL induced by MMP7 promoted interstitial fibroblasts apoptosis (Powell *et al*., 1999; Zhou *et al*., 2013). This difference was highlighted between cell injury phase and cell recovery phase, thus, it was proposed that MMP7 had a renal protective function over tubular cells from apoptosis, which could be achieved by degrading FasL during cell injury phase; it might also help promoting fibroblasts apoptosis by inducing FasL during cell recovery phase (Zhou *et al*., 2013).

To conclude, we found that in the top three pathways were involved in 24-hour FA compared to the control, Wnt signalling pathway, proinflammatory pathway and angiogenesis pathway were highlighted in the analysis and the key components of each pathways were further demonstrated in our data; on top of that, in 24-hour recovery compared to control, neither key components in each pathway were found significantly influenced by the treatment; finally, in the 24-hour recovery compared to the 24-hour FA treatment group, the top three pathways involved were Wnt signalling pathway, proinflammatory pathway and

angiogenesis pathway the mRNA level of key components of each pathways were further demonstrated in our data. Moreover, the RNA-seq data matched TGFβ1 and IL-18 expression involved in the injury and recovery that we found using qPCR. HMGB1 targeted on the translation in FA treated HK2 cells and it may activate autophagy through binding beclin 1 and Bcl2, it may also induce proinflammatory cytokines through TLR2 signalling pathway. Pax2 indicated the FA induced damage to HK2 cells and might have a protective role over FA induced acute injury. Furthermore, Pax2 had impact on downstream pathways through GDNF and SFRP2. Additionally, MMP7 was not upregulated after 24-hour FA injury and so appears not to have a protective role by inhibiting the expression of FasL.

# Chapter 6: Discussion and Conclusion

AKI continues to be a global concern that troubles over 13 million people, especially to hospital patients, causing around 1.7 million death every year (Zuk *et al*., 2016; Mehta *et al*., 2015; Bellomo *et al*., 2012). The majority of survivors suffer from long-term outcomes of AKI including developing CKD and end-stage renal disease, leading to poor health and high costs of care (Chawla *et al*., 2014; Coca *et al*., 2012). Thus, effective ways of identifying AKI to minimise the outcomes and treatments are needed in order to decrease the mortality rate and promote recovery. This study is the first to use FA to induce acute injury on HK2 cells and make use of RNA sequencing analysis to identify the pathways involved during FA induced injury and recovery, therefore understanding the mechanisms of how FA damage impacts on cells, and pathways that are most significantly regulated during damage and recovery to enable targeted therapy.

### 6.1 The role of HMGB1 and its pathways in FA induced acute injury

In this study, we demonstrated that HMGB1 protein and nuclear HMGB1 protein showed significant increase in expression when exposed to FA ($p<0.05$), nuclear HMGB1 in particular, showed significant difference to its control group even after 24-hour recovery (section 4.3.2, $p<0.05$). As recovery period progressed, the level of HMGB1 protein decreased and dropped back to the control level. Although cytoplasmic HMGB1 showed a significant increase in protein level, the conclusion that HMGB1 had nucleocytoplasmic translocation in response to FA damage could not be drawn until further histone H3 protein tested in the cytoplasmic samples. Altogether these results suggested HMGB1 played a crucial role in nucleus when HK2 cells were under acute FA damage,

and its impact gradually disappeared when cells were undergoing recovery. HMGB1 could be passively released from the nuclei when cells were undergoing necrosis, acting as a pro-inflammatory cytokine that passes necrotic signals to adjacent cells through cell-surface receptors which plays a vital role in mediating immune response to acute injury (VanPatten *et al*., 2018; Pandi-Perumal *et al*., 2008). A number of studies demonstrated the upregulation the HMGB1 expression in response to acute injury (Tsung *et al*., 2005; Chung *et al*., 2008; Wu *et al*., 2007; Ilmakunnas *et al*., 2008) and HMGB1 nucleocytoplasmic translocation was also observed in several other studies (Ruan *et al*., 2014; Zhan *et al*., 2016). Recent studies reported that the migration of nuclear HMGB1 to cytoplasm might be a crucial step to allow HMGB1 play a proinflammatory role including activating inflammatory cells, promoting the secretion of inflammatory cytokines (Wu *et al*., 2010; Doi *et al*., 2014; Zhan *et al*., 2016); on the other hand, inhibiting the translocation of HMGB1 significantly reduced the damage from FA induced acute injury in tubular epithelial cells (Zhu *et al*., 2017). Although HMGB1 downstream signalling pathway is not thoroughly studied yet, Palumbo and colleagues as well as Penzo and colleagues have illustrated that NF-κB activation was involved in the HMGB1 downstream regulation (Palumbo *et al*., 2009; Penzo *et al*., 2010). The activation of NF-κB then promotes the transcription of Cxcl12 gene, and HMGB1 prevent CXCL12 from degradation (Penzo *et al*., 2010; Campana *et al*., 2009). We found the change in expression of NF-κB mRNA matched the expression of HMGB1 mRNA in our RNA-seq data, as well as the mRNA expression of CXCL12 and its receptor CXCR4. These findings may

suggest that HMGB1 stimulates an inflammatory response by interacting with CXCL12 via its receptor CXCR4 (Figure 5.7). Furthermore, the increase of TLR2 expression also suggested that HMGB1 might induce proinflammatory cytokines through TLR2 signalling pathway. Nevertheless, the lack of significant fold change of other main components of TLR2 signalling pathway, it could only suggest that TLR2 signalling pathway was involved in the HMGB1 not the main way of inducing proinflammatory cytokines.

We also found that FA treatment activated LC3B, which expression significantly increased during 24-hour FA treatment ($p<0.05$) and gradually reduced during the recovery period. Several studies have suggested that the activation of autophagy in response to injury has a link to the activation of HMGB1 (Huang *et al*., 2012; Kwak *et al*., 2013): cytoplasmic HMGB1 interacts with Bcl2-Beclin1 complex which stimulates autophagosome maturation and therefore promotes the activation of autophagy. The expression of Bcl2 mRNA had a significant increase after 24-hour FA treatment ($p<0.05$), suggesting a potential role for this in our system. However, the activation of autophagy was not the key mechanism to promote HK2 cell survival after FA induced damage. This was indicated by the fact that significant subset of cells survived FA induced injury, despite blockade of autophagy using BA1 or CQ (section 4.3.5 and section 4.3.7)

Our RNA-seq results suggested that after 24-hour incubation with FA, the HMGB1 mRNA expression was not significant to those in the control group, only HMGB1 pseudogenes were found instead. On the contrary, our protein-related result suggested the level of HMGB1 protein was significantly increased

after 24-hour FA treatment ($p<0.05$). Both results together indicated that HMGB1 might mainly be regulated by translation instead of transcription. Therefore, the lack of altered HMGB1 mRNA expression could be explained due to the fast turnover between transcription and translation.

### 6.2 The role of Pax2 and other developmental related genes in FA-induced damage and recovery

Pax2 is heavily downregulated once nephrogenesis is finished and it is not normally expressed in the mature proximal tubule cells (Jiang *et al*., 2014). The re-expression of developmental related genes such as Pax2 and GDNF in matured proximal tubule cells is considered as mimicking but reverse the process of nephrogenesis, which allow the matured proximal tubule cells regain the characteristics of progenitor cells (Jiang *et al.*, 2013). It was shown that the expression of Pax2 mRNA was elevated only in the FA treated group compared to the control group, the expression of which remained lower than the control group and 24-hour FA treatment group after the 24-hour recovery. These data suggest that the re-expression of Pax2 after FA-induced injury might have a functional link with kidney epithelium acute injury. Alongside of re-expression of Pax2, the expression of other developmental related genes such as SHH, GDNF and SFRP2 were all up-regulated during 24-hour FA treatment (compared to the control group), followed by a reduction of expression in both 24-hour recovery compared to the control group and 24-hour recovery compared to 24-hour FA treatment group. These suggested that the re-expression of developmental associated genes might promote cell growth and

recovery during FA damage. In addition, the expression of several upstream genes that regulate Pax2 mRNA such as NF-κB and SHH were similarly altered, suggesting a role for them in control of Pax2 expression during FA induced damage and recovery; additionally, the expression of two downstream genes that are regulated by Pax2 mRNA, GDNF and SFRP2 also showed significant increase in mRNA expression, suggested that the expression of Pax2 was stimulated by NF-κB and SHH, and its expression then induced the expression of GDNF and SFRP2.

Similar to Pax2, Wnt expression is downregulated in matured kidneys, studies suggest that Wnt involved pathway could be re-activated during renal recovery (Kuure *et al*., 2007; Cirio *et al*., 2015). Terada and colleagues (2003) reported that on I/R mice model, the mRNA level of Wnt4 significantly increased as early as 6 hours post injury and reduced to around the baseline around 24 hours post injury. They also reported the increased protein level of Wnt4 corelated with the increased protein level of CyclinD1 and CyclinA, which suggested that Wnt4 might be promoting tubular cell proliferation by supressing cylins.

The mRNA expression of VEGF significantly increased after 24-hour FA treatment as well as after 24-hour recovery, suggested VEGF played a role in protecting cells from FA-induced damage or contributed in recovery. Evidence suggested that VEGF could act as a survival factor and protect cells from apoptosis via stimulation of VEGF R-2-mediated signaling cascade involving PI3K/Akt pathway (Gerber et al., 1998). Kim and colleagues (2000) reported that in response to toxin-induced AKI, the re-expression of VEGF promote the recovery of microvasculature and better renal function. Although the mRNA

expression increased in response to FA-induced damage and recovery (Table 5.9), and such recovery process mimicked the development of kidneys, the re-expression of certain genes and pathways is not equivalent to the recapitulation of kidney development, as the there are other genes uniquely present during kidney development that are not involved in tubular repair postnatally.

### 6.3 How did FA damage the HK2 cells?

An elevation of oxidative stress is common in cells or tissue undergoing AKI, which causes oxidative damage to renal tubular cells (Ni *et al*., 2018). Animal studies verified the significant damage caused by raised oxidative damage and subsequent reduction of antioxidant status following renal I/R injury or nephrotoxic injury (Paller *et al*., 1984; Baliga *et al*., 1999). ROS are often related to the principle of oxidative stress, the increased level of ROS causes the peroxidation of lipids, oxidation of proteins, damage to nucleic acid and specific enzyme inhibition, which lead to the programmed cell death (Lemineur *et al*., 2006). In our cell model, the level of ROS significantly increased when HK2 cells were exposed to FA after as little as 4 hours ($p<0.05$), and the level peaked at 24-hour FA treatment, then slowly reduced during the recovery period. Such results matched the loss of cell number after 24-hour FA treatment and the restoration of the cell number when cells were undergoing recovery (Figure 3.17).

A protein critical for mediation of the unfolded protein response, GRP78, remains inactive in the endoplasmic reticulum membrane under normal condition (Clarke *et al*., 2011; Clarke *et al*., 2012). The release of GRP78 is directly associated with the accumulation of unfolded or misfolded proteins in the endoplasmic reticulum. The accumulation of misfolded protein disturbs the ER homeostasis which then causes ER stress, and the cellular response to ER stress is initiating unfolded protein response in order to restore the normal function of ER and degrade misfolded proteins (Bravo *et al*., 2013; Cook *et al*., 2016). The elevation of GRP78 in 24-hour FA treatment suggested an elevation of unfolded or misfolded protein accumulated in ER (Figure 4.12).

Together this demonstrates that the FA induced damage in HK2 cells may be mediated by elevated ROS levels which impacts an array of cellular processes and organelles. The significant elevation of the GRP78 ER stress protein strongly supports the idea that FA exposure whether directly or via ROS production ($p<0.05$), results in considerable protein mis-folding and survival requires appropriate defence measures to be put in place by the cell.

## 6.4 Conclusion

In conclusion, folic acid induced damage in HK2 cells may be mediated by ROS damage and results in HMGB1 induction and nuclear translocation within a few hours of exposure. Whilst the cells in which this translocation is observed survive, they also induce the expression of pro-inflammatory cytokines potentially through the CXCL12 or TLR2 signalling pathways. The autophagy

response is activated after FA injury which may be induced independently or through an HMGB1 mediated process, but it is not solely responsible for enabling the survival seen in FA exposed HK2 cells. The processes identified in this thesis may be helpful in understanding further the paths of damage and potential recovery in nephrotoxic injury.

# CHAPTER 7: LIMITATIONS AND FUTURE WORK

## 7.1 LIMITATIONS

The conclusions were drawn based on the results found in HK2 cells. HK2 cells are immortalized human proximal kidney cell line that have characteristics of renal cells, they were shown to be suitable to use in *in vitro* nephrotoxicity studies (Gunness *et al*., 2010; Ryan *et al*., 1994), however for certain transporters such as uptake transporters', protein expression is limited (Jenkinson *et al*., 2012), which suggests HK2 cell line has certain limitations in cellular response; therefore the results we found in HK2 cells may not be broadly applicable to animals or human. Freshly isolated primary proximal tubule cells may solve this issue and provide more broadly applicable results.

We followed a published method from Yang and colleagues who used male BALB/c mice as an experimental model, induced injection of 5mg/kg bodyweight AA as the treatment group for 5 days. Other studies that used the same concentration in BALB/c and other mice models also showed significant damage in mice kidney tissues (Zhou *et al*., 2010; Dai *et al*., 2016; Sabbisetti *et al*., 2013; Novitskaya *et al.*, 2014), however some studies used a higher concentration of 10mg/kg bodyweight to induce acute kidney injury in mice models including BALB/c (Zeng *et al*., 2014; Lebeau *et al*., 2005; Meng *et al*., 2014). We followed Yang's protocol and used 5mg/kg bodyweight on ICR mice to induce AKI, however, the AA injected group showed no significant renal damage compared to the control group, suggesting that 5mg/kg bodyweight of AA did not induce AKI in ICR mice. The use of outbred mice is common in scientific research. Considering the genetic contribution to diseases, the outbred mice provide diverse genetic pool which offers more generalizability of

responses across populations, therefore supposedly mimic what is more likely to find in human. However, the main disadvantage of outbred mice in toxicology research is the lack of sensitivity to drugs, and the genetic heterogeneity leads to an increased variation to the research (Brekke *et al.,* 2018 and Festing *et al*., 2010). The increased population might reduce variation and an increased drug concentration might induce similar damage to which induced with low concentration in inbred mice.

## 7.2 FUTURE WORK

1. We have discussed the pathways that HMGB1 might have functioned in during FA induced damage and recovery in Chapter 5, however a HMGB1 knock-out *in vitro* study would be helpful to investigate the importance of HMGB1 in FA induced damage and recovery. This could be achieved by using HMGB1 inhibitor ethyl pyruvate (EP), which inhibits the release of HMGB1 in cells, or using small interfering RNA (SiRNA) to silence the expression of HMGB1 to enable further analysis.
2. More time points of FA treatment need to be tested in order to examine the accurate expression HMGB1 mRNA. Time points to be tested could include 2-hour treatment, 4-hour treatment and 8-hour treatment, as ROS level significantly increased after 4-hours of treatment, and HMGB1 protein started to show in immunostaining after 8-hour FA treatment.
3. Pax2 protein was not examined in the *in vitro* model, therefore a reliable Pax2 antibody is needed to enable IHC and Western blot analysis. A

Pax2 knock-out *in vitro* study would be crucial to understand the full function of Pax2 during proximal tubule damage and recovery.

4. Use a reliable animal model to analyse pathways involve in FA induced damage and recovery would be better to observe a more broadly applicable result.

# CHAPTER 8: REFERENCES

## References

Abdelhak S., Kalatzis V., Heilig R., Compain S., Samson D., Vincent C., Weil D., Cruaud C., Sahly I., Leibovici M., Bitner-Glindzicz M., Francis M., Lacombe D., Vigneron J., Charachon R., Boven K., Bedbeder P., Van Regemorter N., Weissenbach J., Petit C. (1997) A human homologue of the Drosophila eyes absent gene underlies branchio-oto-renal (BOR) syndrome and identifies a novel gene family. Nat Genet. 15(2):157-64.

Advancement as a Potential Drug Target. J. Med. Chem. 61: 5093−5107.

Afkarian M., Zelnick L.R., Ruzinski J., Kestenbaum B., Himmelfarb J., Boer I.H., Mehrotra R. (2015) Urine matrix metalloproteinase-7 and risk of kidney disease progression and mortality in type 2 diabetes. J Diabetes Complications. 29:1024–1031.

Airaksinen, M. S., Saarma, M. (2002). The GDNF family: signalling, biological functions and therapeutic value. Nat. Rev. Neurosci. 3: 383-394.

Al-Alwan L.A., Chang Y., Mogas A., Halayko A.J., Baglole C.J., Martin J.G., Rousseau S., Eidelman D.H., Hamid Q. (2013). Differential roles of CXCL2 and CXCL3 and their receptors in regulating normal and asthmatic airway smooth muscle cell migration. Journal of Immunology. 191 (5): 2731–41.

Ali T, Khan I, Simpson W. (2007) Incidence and outcomes in acute kidney injury: a comprehensive population-based study. J Am Soc Nephrol 18: 1292–98.

Al-Merani S.A., Brooks D.P., Chapman B.J., Munday K.A. (1978) The half-lives of angiotensin II, angiotensin II-amide, angiotensin III, Sar1-Ala8-angiotensin II and renin in the circulatory system of the rat. J Physiol. 278: 471–490.

Amin A.P., Salisbury A.C., McCullough P.A. (2012) Trends in the incidence of acute kidney injury in patients hospitalized with acute myocardial infarction. Arch Intern Med 172: 246–53.

Arlt V.M., Pfohl-Leszkowicz A., Cosyns J., Schmeiser H.H. (2001) Analyses of DNA adducts formed by ochratoxin A and aristolochic acid in patients with Chinese herbs nephropathy. Mutat Res. 494(1–2): 143-150.

Assadi F., Sharbaf F.G. (2019) Urine KIM-1 as a Potential Biomarker of Acute Renal Injury After Circulatory Collapse in Children. Pediatr Emerg Care 35(2):104-107.

Assoian R.K., Komoriya A., Meyers C.A., Miller D.M., Sporn M.B. (1983). Transforming growth factor-beta in human platelets. Identification of a major storage site, purification, and characterization. J. Biol. Chem. 258 (11): 7155–7160.

Avgousti D.C., Herrmann C., Kulej K., Pancholi N.J., Sekulic N., Petrescu J., Molden R.C., Blumenthal D., Paris A.J., Reyes E.D., Ostapchuk P., Hearing P., Seeholzer S.H., Worthen G.S., Black B.E., Garcia B.A., Weitzman M.D. (2016) A core viral protein binds host nucleosomes to sequester immune danger signals. Nature. 535(7610):173-177.

Baliga R., Ueda N., Walker P.D., Shah S.V. (1999) Oxidant mechanisms in toxic acute renal failure. Drug Metab Rev. 31(4): 971-997.

Basile D.P., Anderson M.D., Sutton T.A. (2014) Pathophysiology of Acute Kidney Injury. Compr Physiol 2(2): 1303–1353.

Bastin A.J., Ostermann M., Slack A.J., Diller G.P., Finney S.J., Evans T.W. (2013) Acute kidney injury after cardiac surgery according to risk/injury/failure/loss/end-stage, acute kidney injury network, and kidney disease: Improving global outcomes classifications. J. Crit. Care 28, 389–396.

Baudoux T.E., Pozdzik A.A., Arlt V.M., De Prez E.G., Antoine M.H., Quellard N., Goujon J.M., Nortier J.L. (2012) Probenecid prevents acute tubular necrosis in a mouse model of aristolochic acid nephropathy. Kidney Int. 82(10):1105-1113.

Bazzano L.A. (2011) No effect of folic acid supplementation on cardiovascular events, cancer or mortality after 5 years in people at increased cardiovascular risk, although homocysteine levels are reduced. Arch. Intern. Med. 170: 1622-1631.

Beker B.M., Corleto M.G, Fieiras C. and Musso C.G. (2018) Novel acute kidney injury biomarkers: their characteristics, utility and concerns. International Urology and Nephrology 50:705–713.

Bell C.W., Jiang W., Reich C.F. 3rd, Pisetsky D.S. (2006) The extracellular release of HMGB1 during apoptotic cell death. Am J Physiol Cell Physiol. 291: 1318-1325.

Bellomo R., Kellum J. A., Ronco C. (2012). Acute kidney injury. The Lancet, 380(9843), 756-766.

Bellomo R., Ronco C., Kellum J.A., Mehta R.L., Palevsky P. (2004) Acute renal failure—Definition, outcome measures, animal models, fluid therapy and information technology needs: The second international consensus conference of the Acute Dialysis Quality Initiative (ADQI) group. Crit. Care 8, R204–R212.

Bhattacharjee P., Bera I., Chakraborty S., Ghoshal N., Bhattacharyya D. (2017) Aristolochic acid and its derivatives as inhibitors of snake venom L-amino acid oxidase. Toxicon. 138:1-17.

Bianchi M.E, Beltrame M. (2000) Upwardly mobile proteins. Workshop: the role of HMG proteins in chromatin structure, gene expression and neoplasia. EMBO Rep 1: 109 –114.

Bieler C.A., Stiborova M., Wiessler M., Cosyns J.P., Ypersele van de Strihou C., Schmeiser H.H. (1997) 32P-post-labelling analysis of DNA adducts formed by aristolochic acid in tissues from patients with Chinese herbs nephropathy. Carcinogenesis. 18(5): 1063-1067.

Blaine J., Chonchol M., Levi M. (2015) Renal control of calcium, phosphate, and magnesium homeostasis. Clinical Journal of the American Society of Nephrology, 10(7), 1257-1272.

Bonventre J.V. (1993) Mechanisms of ischemic acute renal failure. Kidney Int. 43:1160-78.

Bonventre J.V., Yang L. (2011) Cellular pathophysiology of ischemic acute kidney injury. The Journal of Clinical Investigation, 121, 4210-4221.

Bose S.K., Gibson W., Giri S., Nath N., Donald C.D. (2009) Angiotensin II up-regulates PAX2 oncogene expression and activity in prostate cancer via the angiotensin II type I receptor. The Prostate. 69 (12): 1334–1342.

Bouchard M., Pfeffer P., Busslinger M. (2000) Functional equivalence of the transcription factors Pax2 and Pax5 in mouse development. Development 127(17): 3703-3713.

Bravo R., Parra V., Gatica D., Rodriguez A.E., Torrealba N., Paredes F., Wang Z.V., Zorzano A., Hill J.A., Jaimovich E., Quest A.F., Lavandero S. (2013) Endoplasmic reticulum and the unfolded protein response: dynamics and metabolic integration. Int Rev Cell Mol Biol. 301: 215-290.

Briggs, J.P., Kriz, W., Schnermann, J.B. (2014) Overview of kidney function and structure. In: Gilbert, S. and Weiner, D. E. (Eds.) National kidney foundation primer on kidney diseases, 6th edition. 1: 1-18.

Brooks C., Wei Q., Cho S.G., Dong Z. (2009) Regulation of mitochondrial dynamics in acute kidney injury in cell culture and rodent models. J Clin Invest 119: 1275–1285.

Brophy P.D., Lang K.M., Dressler G.R. (2003) The secreted frizzled related protein 2 (SFRP2) gene is a target of the Pax2 transcription factor. J Biol Chem. 278, 52401–52405.

Brophy P.D., Ostrom L., Lang K.M., Dressler G.R. (2001) Regulation of ureteric bud outgrowth by Pax2-dependent activation of the glial derived neurotrophic factor gene. Development. 128, 4747–4756.

Bruce M., Koeppen M.D. (2013) Structure and Function of the Kidneys. Renal Physiology (Fifth Edition). 2: 15-26.

Buettner G.R. (1993) The pecking order of free radicals and antioxidants: Lipid peroxidation, alpha-tocopherol, and ascorbate. Arch. Biochem. Biophys. 300, 535–543.

Buisson I., Le Bouffant R., Futel M., Riou J.F., Umbhauer M. (2015) Pax8 and Pax2 are specifically required at different steps of Xenopus pronephros development. Dev Biol. 15;397(2):175-90.

Bunel V., Antoine M.H., Stévigny C., Nortier J., Duez P. (2016) New in vitro insights on a cell death pathway induced by magnolol and honokiol in aristolochic acid tubulotoxicity. Food Chem Toxicol. 87: 77-87.

Byrnes K.A., Ghidoni J.J., Suzuki M., Thomas H., Mayfield Jr E.D. (1972) Response of the rat kidney to folic acid administration. II. Morphologic studies. Lab Invest 26:191–200.

Cakir Y., Ballinger S.W. (2005). Reactive species-mediated regulation of cell signaling and the cell cycle: the role of MAPK. Antioxid. Redox Signal. 7: 726–740.

Calkins M.J., Manczak M., Mao P., Shirendeb U., Reddy P.H. (2011) Impaired mitochondrial biogenesis, defective axonal transport of mitochondria, abnormal

mitochondrial dynamics and synaptic degeneration in a mouse model of Alzheimer's disease. Hum Mol Genet 20:4515–4529.

Campana L., Bosurgi L., Bianchi M.E., Manfredi A.A., Rovere- Querini P. (2009) Requirement of HMGB1 for stromal cell-derived factor-1/ CXCL12-dependent migration of macrophages and dendritic cells. J. Leukoc. Biol. 86: 609–615.

Canaud G., Bonventre J.V. (2015) Cell cycle arrest and the evolution of chronic kidney disease from acute kidney injury. Nephrol Dial Transplant. 30: 575-583.

Cao M., Jiang J., Du Y., Yan P. (2012) Mitochondria-targeted antioxidant attenuates high glucose-induced P38 MAPK pathway activation in human neuroblastoma cells. Mol Med Rep 5:929–934.

Carr A.C., Frei B. (1999) Toward a new recommended dietary allowance for vitamin C based on antioxidant and health effects in humans. Am. J. Clin. Nutr. 69, 1086–1107.

Carr M.W., Roth S.J., Luther E., Rose S.S., Springer T.A. (1994). Monocyte chemoattractant protein 1 acts as a T-lymphocyte chemoattractant. Proceedings of the National Academy of Sciences of the United States of America. 91 (9): 3652–3656.

Carroll T.J., Park J.S., Hayashi S., Majumdar A., McMahon A.P. (2005) Wnt9b plays a central role in the regulation of mesenchymal to epithelial transitions underlying organogenesis of the mammalian urogenital system. Dev Cell. 9(2):283-92.

Cary L.A., Han D.C., Guan J.L. (1999) Integrin-mediated signal transduction pathways. Histol Histopathol. (3):1001-1009.

Case, J., Khan, S., Khalid, R. and Khan, A. (2013) Epidemiology of acute kidney injury in the intensive care unit. Critical Care Research and Practice (4):479730.

Chakraborty S., Kaur S., Guha S. and Batra S.K. (2012) The multifaceted roles of neutrophil gelatinase associated lipocalin (NGAL) in inflammation and cancer. Biochim Biophys Acta 1826(2) 129-169.

Chander V., Chopra K. (2006) Protective effect of nitric oxide pathway in resveratrol renal ischemia-reperfusion injury in rats. Arch Med Res. 37(1):19–26.

Chau W., Ross R., Li J.Y.Z., Yong T.Y., Klebe S., Barbara J.A. (2011) Nephropathy associated with use of a Chinese herbal product containing aristolochic acid. Med J Aust. 194: 367-368.

Chawla L.S., Eggers P.W., Star R.A., Kimmel P.L. (2014) Acute kidney injury and chronic kidney disease as interconnected syndromes. N. Engl. J. Med. 371:58–66.

Chen G.Y., Tang J., Zheng P., Liu Y. (2009) CD24 and Siglec-10 selectively repress tissue damage-induced immune responses. Science. 323: 1722– 1725.

Chen Y.W., Liu F., Tran S., Zhu Y., Hébert M.J., Ingelfinger J.R., Zhang S.L. (2006) Reactive oxygen species and nuclear factor-kappa B pathway mediate high glucose-induced Pax-2 gene expression in mouse embryonic mesenchymal epithelial cells and kidney explants. Kidney Int 70: 1607–1615.

Chertow G., Burdick E., Honour M., Bonventre J., Bates D. (2005) Acute kidney injury, mortality, length of stay, and costs in hospitalized patients. J. Am. Soc. Nephrol. 16, 3365–3370.

Chi N., Epstein J.A. (2002) Getting your Pax straight: Pax proteins in development and disease. Trends Genet 18: 41–47.

Chi N., Epstein J.A. (2002) Getting your Pax straight: Pax proteins in development and disease. Trends Genet. 18: 41–47.

Chi X., Michos O., Shakya R., Riccio P., Enomoto H., Licht J.D., Asai N., Takahashi M., Ohgami N., Kato M., Mendelsohn C., Costantini F. (2009) Ret-dependent cell rearrangements in the Wolffian duct epithelium initiate ureteric bud morphogenesis. Dev Cell. 17(2):199-209.

Cho Y., Shin J.E., Ewan E.E., Oh Y.M., Pita-Thomas W., Cavalli V. (r 2015). Activating Injury-Responsive Genes with Hypoxia Enhances Axon Regeneration through Neuronal HIF-1α. Neuron. 88 (4): 720–34.

Cirio M.C., de Groh E.D., Caestecker M.P., Davidson A.J., Hukriede N.A. (2015) Kidney Regeneration: Common Themes From the Embryo to the Adult. Pediatr Nephrol. 2014 Apr; 29(4): 553–564.

Coca S.G., Singanamala S., Parikh C.R. (2012) Chronic kidney disease after acute kidney injury: a systematic review and meta-analysis. Kidney Int. 81:442–448.

Coca S.G., Yusuf B., Shlipak M.G., Garg A.X., Parikh C.R. (2009) long-term risk of mortality and other adverse outcomes after acute kidney injury: a

systematic review and meta-analysis. American Journal of Kidney Disease 53: 961-973.

consequences of defective mitochondrial respiration and impaired antioxidant enzyme system. Chin J Physiol. 44(1):1–11.

Cook K.L., Soto-Pantoja D.R., Clarke P.A., Cruz M.I., Zwart A., Wärri A., Hilakivi-Clarke L., Roberts D.D., Clarke R. (2016) Endoplasmic Reticulum Stress Protein GRP78 Modulates Lipid Metabolism to Control Drug Sensitivity and Antitumor Immunity in Breast Cancer. Cancer Res. 76(19): 5657-5670.

Copeland NG, Gilbert DJ, Jenkins NA, Scully S, Lacey DL,

Cosyns J., Jadoul M., Squifflet J.P., Van Cangh P., van Ypersele de Strihou C. (1994) Urothelial malignancy in nephropathy due to Chinese herbs. Lancet. 344: 188.

Cosyns J.P., Dehoux J.P., Guiot Y., Goebbels R.M., Robert A., Bernard A.M., van Ypersele de Strihou C. (2001) Chronic aristolochic acid toxicity in rabbits: a model of Chinese herbs nephropathy? Kidney Int. 59(6):2164-2173.

Coux O., Tanaka K., Goldberg A.L. (1996). Structure and functions of the 20S and 26S proteasomes. Annual Review of Biochemistry. 65: 801–47.

Dai X.Y., Huang X.R., Zhou L., Zhang L., Fu P., Manthey C., Nikolic-Paterson D.J., Lan H.Y. (2016) Targeting c-fms kinase attenuates chronic aristolochic acid nephropathy in mice. Oncotarget. 7(10): 10841-10856.

D'Amico G., Bazzi C. (2003) Pathophysiology of proteinuria. Kidney International. 63(3), 809-825.

De Giorgi F, Lartigue L and Ichas F (2000) Electrical coupling and plasticity of the mitochondrial network. Cell Calcium 28: 365–370

Debelle F.D., Nortier J.L., De Prez E.G. (2002) Aristolochic acids induce chronic renal failure with interstitial fibrosis in salt-depletedrats. J Am Soc Nephrol 13: 431-436.

Degryse B., Bonaldi T., Scaffidi P., Muller S., Resnati M., Sanvito F., (2001) The high mobility group (HMG) boxes of the nuclear protein HMG1 induce chemotaxis and cytoskeleton reorganization in rat smooth muscle cells. J Cell Biol. 152: 1197–1206.

Dennis J.M. and Witting P.K. (2017) Protective role for antioxidants in acute kidney disease *Nutrients* 9, 718.

Devarajan P. (2010) The promise of biomarkers for personalized renal cancer care. Kidney Int. 77:755–757.

Dinarello C.A. (2007) Interleukin-18 and the pathogenesis of inflammatory diseases. Semin Nephron 27(1):98–114.

Doi K., Ishizu T., Tsukamoto-Sumida M., Hiruma T., Yamashita T., Ogasawara E., Hamasaki Y., Yahagi N., Nangaku M., Noiri E. (2014) The high mobility group protein B1-Toll-like receptor 4 pathway contributes to the acute lung injury induced by bilateral nephrectomy. Kidney Int. 86: 316–326.

Doi K., Okamoto K., Negishi K., Suzuki Y., Nakao A., Fujita T., Toda A., Yokomizo T., Kita Y., Kihara Y., Ishii S., Shimizu T., Noiri E. (2006) Attenuation

of folic acid-induced renal inflammatory injury in platelet-activating factor receptor-deficient mice. Am J Pathol. 168(5):1413-24.

Downey J.M., Miura T., Eddy L.J., Chambers D.E., Mellert T., Hearse D.J., Yellon D.M. (1987) Xanthine oxidase is not a source of free radicals in the ischemic rabbit heart. J Mol Cell Cardiol. 19:1053–1060.

Dressler G.R. (2009) Advances in early kidney specification, development and patterning. Development. 136: 3863-3874.

Dressler G.R1., Woolf A.S. (1999) Pax2 in development and renal disease. Int J Dev Biol. 43(5):463-8.

Du J., Cullen J.J., Buettner G.R. (2012) Ascorbic acid: Chemistry, biology and the treatment of cancer. Biochim. Biophys. Acta 1826, 443–457.

Duarte S., Baber J., Fujii T., Coito A.J. (2015) Matrix metalloproteinases in liver injury, repair and fibrosis. Matrix Biol. 44–46:147–156.

Dumitriu I.E., Baruah P., Valentinis B., Voll R.E., Herrmann M., Nawroth P.P. (2005) Release of high mobility group box 1 by dendritic cells controls T cell activation via the receptor for advanced glycation end products. J Immunol. 174:7506-15.

Dupont N., Jiang S., Pilli M., Ornatowski W., Bhattacharya D., Deretic V. (2011) Autophagy-based unconventional secretory pathway for extracellular delivery of IL-1beta. EMBO J. 30 (23), 4701–4711.

Dziarmaga A., Hueber P.A., Iglesias D. (2006) Neuronal apoptosis in- hibitory protein (NAIP) is expressed in development kidney and is regulated by PAX2. Am J Physiol Renal Physiol 291: 913– 920.

Eccles M.R., Wallis L.J., Fidler A.E. (1992) Expression of the Pax2 gene in human fetal kidney andWilms' tumor. Cell Growth Differ. 3: 279–289.

El Mezayen R., El Gazzar M., Seeds M.C., McCall C.E., Dreskin S.C., Nicolls M.R. (2007) Endogenous signals released from necrotic cells augment inflammatory responses to bacterial endotoxin. Immunol Lett. 111: 36–44.

El-Shafei R.A.; Saleh R.M. (2016) Pharmacological effects of vitamin C & E on diclofenac sodium intoxicated rats. Biomed. Pharmacother. 84, 314–322.

Endo T., Nakamura J., Sato Y., Asada M., Yamada R., Takase M., Takaori K., Oguchi A., Iguchi T., Higashi A.Y., OHbayashi T., Nakamura T., Muso E., Kimura K., Yanagita M. (2015) Exploring the origin and limitations of kidney regeneration. J Pathol 236: 251–263.

Fan J., Li Y., Levy R.M., Fan J.J., Hackam D.J., Vodovotz Y., Yang H., Tracey K.J., Billiar T.R., Wilson M.A. (2007) Hemorrhagic shock induces NAD(P)H oxidase activation in neutrophils: role of HMGB1-TLR4 signaling. J Immunol 178: 6573–6580.

Fanni D., Fanos V., Monga G., Gerosa C., Locci A., Nemolato S., Van Eyken P., Faa G. (2011) Expression of WT1 during normal human kidney development. J Matern Fetal Neonatal Med. 2:44-7.

Farooqi, S. and Dickhout, J. G. (2016) Major comorbid disease processes associated with increased incidence of acute kidney injury. World Journal of Nephrology, 5(2), 139-146.

Ferrara N. (2004) Vascular endothelial growth factor: basic science and clinical progress. Endocr Rev. 25(4):581-611.

Fink M., Henry M., Tange J.D. (1987) Experimental folic acid nephropathy. Pathology. 19(2):143-149.

Fu H.Y., Zhou D., Zhu H.L., Liao J.L., L L., Hong X., Hou F.F., Liu Y.H. (2019) Matrix metalloproteinase-7 protects against acute kidney injury by priming renal tubules for survival and regeneration. Kidney International 95: 1167–1180.

Fu H.Y., Zhou D., Zhu H.L., Liao J.L., Lin L., Hong X., Hou F.F., Liu Y.H. (2019) Matrix metalloproteinase-7 protects against acute kidney injury by priming renal tubules for survival and regeneration. Kidney International. 95: 1167–1180.

Gerber H.P., Dixit V., Ferrara N. (1998) Vascular endothelial growth factor induces expression of the antiapoptotic proteins Bcl-2 and A1 in vascular endothelial cells. J Biol Chem. 22; 273(21):13313-6.

Ghatanatti R., Teli A., Tirkey S.S., Bhattacharya S., Sengupta G., Mondal A. (2014) Role of renal biomarkers as predictors of acute kidney injury in cardiac surgery. Asian Cardiovasc Thorac Ann 22(2):234–241.

Gillani, S.; Cao, J.; Suzuki, T.; Hak, D.J. (2012) The effect of ischemia reperfusion injury on skeletal muscle. Injury 43, 670–675.

Gnudi L., Benedetti S., Woolf A.S., Long D.A. (2015) Vascular growth factors play critical roles in kidney glomeruli. Clin Sci (Lond) 129: 1225– 1236.

Gong K.Q., Yallowitz A.R., Sun H., Dressler G.R., Wellik D.M. (2007) A Hox-Eya-Pax complex regulates early kidney developmental gene expression. Mol Cell Biol. 27:7661–7668.

Goulding M.D., Chalepakis G., Deutsch U. (1991) Pax-3, a novel murine DNA binding protein expressed during early neurogenesis. EMBO J 10: 1135–1147.

Graham F.L., Smiley J., Russell W.C., Nairn R. (1977) Characteristics of a Human Cell Line Transformed by DNA from Human Adenovirus Type 5. *The Journal of General Virology*, 36(1), 59–74.

Granger D.N., Rutili G., McCord J.M. (1981) Superoxide radicals in feline intestinal ischemia. Gastroenterology. 81:22–29.

Granger N.D., Kvietys P.R. (2015) Reperfusion injury and reactive oxygen species: The evolution of a concept. Redox Biology. 6: 524–551.

Grindel B.J., Martinez J.R., Pennington C.L., Muldoon M., Stave J., Chung L.W., Farach-Carson M.C. (2014) Matrilysin/matrix metallo proteinase-7 (MMP7) cleavage of perlecan/HSPG2 creates a molecular switch to alter prostate cancer cell behavior. Matrix Biol. 36:64–76.

Groebler L.K., Wang X.S., Kim H.B., Shanu A., Hossain F., McMahon A.C., Witting P.K. (2012) Cosupplementation with a synthetic, lipid-soluble polyphenol and vitamin C inhibits oxidative damage and improves vascular

function yet does not inhibit acute renal injury in an animal model of rhabdomyolysis. Free Radic. Biol. Med. 52, 1918–1928.

Grollman A.P., Shibutani S., Moriya M., Miller F., Wu L., Moll U., Suzuki N., Fernandes A., Rosenquist T., Medverec Z. (2007) Aristolochic acid and the etiology of endemic (Balkan) nephropathy. Proc Natl Acad Sci USA. 104: 12129-12134.

Gunness P., Aleksa K., Kosuge K., Ito S., Koren G. (2010) Comparison of the novel HK-2 human renal proximal tubular cell line with the standard LLC-PK1 cell line in studying drug-induced nephrotoxicity. Can J Physiol Pharmacol. 88(4):448-455.

Guo C., Sun L., Chen X., Zhang D. (2013) Oxidative stress, mitochondrial damage and neurodegenerative diseases. Neural Regen Res. 8(21): 2003-2014.

Guo J., Zhang S.L., Moini B., Ingelfinger J.R. (2004) Angiotensin II stimulates Pax-2 in rat kidney proximal tubular cells: impact on proliferation and apoptosis. Kidney Int. 66(6):2181-2192.

Gupta A., Puri V., Sharma R., Puri S. (2010) Folic acid induces acute renal failure (ARF) by enhancing renal prooxidant state. Exp Toxicol Pathol. 64(3):225-232.

Haase M., Bellomo R., Devarajan P. (2009) Accuracy of neutrophil gelatinase-associated lipocalin (NGAL) in diagnosis and prognosis in acute kidney injury: a systematic review and metaanalysis. Am J Kidney Dis. 54:1012–24.

Haase M., Mertens P.R. (2015) Biomarkers: more than just markers Nephrol Dial Transplant 30(1):33–38.

Halbert C.L., Demers G.W., Galloway D.A. (1991) The E7 gene of human papillomavirus type 16 is sufficient for immortalization of human epithelial cells. *J Virol* (65), 473-478.

Hammerman M.R., Rogers S. (1987) Distribution of IGF receptors in the plasma membrane of proximal tubular cells. Am J Physiol. 253(5 Pt 2):841-7.

Han W. K., Wagener G., Zhu Y., Wang S., Lee H. T. (2009) Urinary biomarkers in the early detection of acute kidney injury after cardiac surgery. Clinical Journal of the American Society of Nephrology 5: 873–882.

Hawley-Nelson P., Vousden K.H., Hubbert N.L., Lowy D.R., Schiller I.T. (1989) HPV16 E6 and E7 proteins cooperate to immortalize human foreskin keratinocytes. *EMBO J* (8), 3905-3910.

Hayakawa K., Arai K., Lo E.H. (2010) Role of ERK map kinase and CRM1 in IL-1beta-stimulated release of HMGB1 from cortical astrocytes. Glia. 58(8):1007-15.

He W., Tan R.J., Li Y. (2012) Matrix metalloproteinase-7 as a surrogate marker predicts renal Wnt/beta-catenin activity in CKD. J Am Soc Nephrol. 23: 294–304.

He W., Tan R.J., Li Y., Wang D., Nie J., Hou F.F., Liu Y. (2012) Matrix metalloproteinase-7 as a surrogate marker predicts renal Wnt/beta-catenin activity in CKD. J Am Soc Nephrol. 23:294–304.

Hemmings B.A., Restuccia D.F. (2012). PI3K-PKB/Akt Pathway. Cold Spring Harb Perspect Biol. 4 (9): a011189.

Hendzel M.J., Wei Y., Mancini M.A., Van Hooser A., Ranalli T., Brinkley B.R., Bazett-Jones D.P., Allis C.D. (1997) Mitosis-specific phosphorylation of histone H3 initiates primarily within pericentromeric heterochromatin during G2 and spreads in an ordered fashion coincident with mitotic chromosome condensation Chromosoma. 106: 348-360.

Hirsch R., Dent C., Pfriem H. (2007) NGAL is an early predictive biomarker of contrast-induced nephropathy in children. Pediatr Nephrol. 22:2089–2095.

Ho J., Rush D.N., Krokhin O., Antonovici M., Gao A., Bestland J., Wiebe C., Hiebert B., Rigatto C., Gibson I.W., Wilkins J.A., Nickerson P.W. (2016) Elevated urinary matrix metalloproteinase-7 detects underlying renal allograft inflammation and injury. Transplantation. 100:648–654.

Hohenstein P., Pritchard-Jones K., Charlton J. (2015). The yin and yang of kidney development and Wilms' tumors. Genes Dev, 29, 467-482.

Holthoff J.H., Wang Z., Seely K.A., Gokden N., Mayeux P.R. (2012) Resveratrol improves renal microcirculation, protects the tubular epithelium, and prolongs survival in a mouse model of sepsis-induced acute kidney injury. Kidney Int. 81(4):370–378.

Horbelt D., Denkis A., Knaus P. (2012) A portrait of Transforming Growth Factor β superfamily signalling: Background matters. Int. J. Biochem. Cell Biol. 44(3), 469–74.

Hoste E.A., Clermont G., Kersten A., Venkataraman R., Angus D.C., De Bacquer D., Kellum J.A. (2006) RIFLE criteria for acute kidney injury are associated with hospital mortality in critically ill patients: A cohort analysis. Crit. Care 10, R73.

Hoste E.A., Clermont G., Kersten A., Venkataraman R., Angus D.C., De Bacquer D. (2006) RIFLE criteria for acute kidney injury are associated with hospital mortality in critically ill patients: a cohort analysis. Crit Care 10: R73.

Hsu C.Y. (2012) Yes, AKI truly leads to CKD. J Am Soc Nephrol 23: 967–969.

Hsu D.Z., Li Y.H., Chu P.Y., Periasamy S., Liu M.Y. (2011) Sesame oil prevents acute kidney injury induced by the synergistic action of aminoglycoside and iodinated contrast in rats. Antimicrob Agents Chemother. 55(6):2532–2536.

Hsu D.Z., Liu C.T., Li Y.H., Chu P.Y., Liu M.Y. (2010) Protective effect of daily sesame oil supplement on gentamicin-induced renal injury in rats. Shock. 33(1):88–92.

Huang B., Pi L., Chen C., Yuan F., Zhou Q., Teng J., Jiang T. (2012) WT1 and Pax2 re-expression is required for epithelial-mesenchymal transition in 5/6 nephrectomized rats and cultured kidney tubular epithelial cells. Cells Tissues Organs 195: 296–312.

Huang J., Liu K., Yu Y., Xie M., Kang R., Vernon P., Cao L., Tang D., Ni J. (2012) Targeting HMGB1-mediated autophagy as a novel therapeutic strategy for osteosarcoma. Autophagy. 8(2):275-7.

Husain-Syed F., Ronco C. (2018) The odyssey of risk stratification in acute kidney injury. Nat. Rev. Nephrol.

Hvidberg V., Jacobsen C., Strong R.K., et al (2005) The endocytic receptor megalin binds the iron transporting neutrophil-gelatinase-associated lipocalin with high affinity and mediates its cellular uptake. FEBS Lett 579:773–777.

Ichimura T., Bonventre J.V., Bailly V. (1998) Kidney injury molecule-1 (KIM-1), a putative epithelial cell adhesion molecule containing a novel immunoglobulin domain, is up-regulated in renal cells after injury. J Biol Chem 273: 4135–4142.

Ilmakunnas M., Tukiainen E.M., Rouhiainen A., Rauvala H., Arola J., Nordin A., Makisalo H., Hockerstedt K., Isoniemi H. (2008) High mobility group box 1 protein as a marker of hepatocellular injury in human liver transplantation. Liver Transpl 14: 1517–1525.

Imgrund M., Grone E., Grone H.J. (1999) Re-expression of the development gene Pax-2 during experimental acute tubular necrosis in mice. Kidney Int 56: 1423–1431.

Ishimoto Y. and Inagi R. (2016) Mitochondria: a therapeutic target in acute kidney injury Nephrol Dial Transplant 31: 1062–1069.

Jadot I., Decleves A.E., Nortier J., Caron N. (2017) An Integrated View of Aristolochic Acid Nephropathy: Update of the Literature. Int. J. Mol. Sci. 18: 297-321.

Jadot I., Declèves A.E., Nortier J., Caron N. (2017) An Integrated View of Aristolochic Acid Nephropathy: Update of the Literature. Int J Mol Sci. 18(2): 297.

James R.G., Kamei C.N., Wang Q., Jiang R., Schultheiss T.M. (2006) Odd-skipped related 1 is required for development of the metanephric kidney and regulates formation and differentiation of kidney precursor cells. Development. 133(15):2995-3004.

Jang H.R., Rabb H. (2009) The innate immune response in ischemic acute kidney injury. Clin Immunol 130:41-50.

Jankauskas S.S., Matsievsky D.D., Andrianova N.A., Savchenko E.S., Alieva I.B., Plotnikov E.Y., Zorov D.B. (2016) Mitochondria-targeted antioxidant skqr1 pevents endothelial dysfunction during ischemic acute kidney injury. Nephrology Dialysis Transplantation 31(1): 143.

Jankauskas S.S., Plotnikov E.Y., Morosanova M.A., Pevzner I.B., Zorova L.D., Skulachev V.P., Zorov D.B. (2012) Mitochondria-targeted antioxidant SkQR1 ameliorates gentamycin-induced renal failure and hearing loss. Biokhimiya 77: 818-823.

Jelakovic B., Karanovic S., Vukovic-Lela I., Miller F., Edwards K.L., Nikolic J., Tomic K., Slade N., Brdar B., Turesky R.J. (2012) Aristolactam-DNA adducts are a biomarker of environmental exposure to aristolochic acid. Kidney Int. 81: 559-567.

Jenkinson S.E., Chung G.W., van Loon E., Bakar N.S., Dalzell A.M., Brown C.D. (2012) The limitations of renal epithelial cell line HK-2 as a model of drug transporter expression and function in the proximal tubule. Pflugers Arch. 464(6):601-611.

Jiang M., Liu K., Luo J. (2010) Autophagy is a renoprotective mechanism during in vitro hypoxia and in vivo ischemia-reperfusion injury. Am J Pathol. 176: 1181–1192.

Jiang M., Wei Q., Dong G. (2012) Autophagy in proximal tubules protects against acute kidney injury. Kidney Int. 82: 1271–1283.

Jiang Y., Jiang T., Ouyang J., Zhou Q., Liang Y., Cui Y., Chen P., Huang B. (2014) Cell Atavistic Transition: Paired Box 2 Re-Expression Occurs in Mature Tubular Epithelial Cells during Acute Kidney Injury and Is Regulated by Angiotensin II. PLoS One. 9(4): e93563.

Jiang Y.S., Jiang T., Huang B., Chen P.S., Ouyang J. (2013) Epithelial-mesenchymal transition of renal tubules: divergent processes of repairing in acute or chronic injury? Med Hypotheses.81(1):73-75.

Jiang Y.S., Jiang T., Ouyang J., Zhou Q.S Liang Y.L., Cui Y.P., Chen P.S., Huang B. (2014) Cell Atavistic Transition: Paired Box 2 Re-Expression Occurs in Mature Tubular Epithelial Cells during Acute Kidney Injury and Is Regulated by Angiotensin II. PLoS One. 9(4): e93563.

Johnson G. L., Lapadat R. (2002) Mitogen-activated protein kinase pathways mediated by ERK, JNK, and p38 protein kinases. Science. 298, 1911–1912.

Jonker S.J., Menting T.P., Warlé M.C., Ritskes-Hoitinga M., Wever K.E. (2016) Preclinical Evidence for the Efficacy of Ischemic Postconditioning against Renal Ischemia-Reperfusion Injury, a Systematic Review and Meta-Analysis. PLoS ONE 11(3): e0150863.

Joseph Meltzer (2013) Pharmacology and Physiology for Anesthesia. 32: 561-573.

Kalogeris T., Bao Y.M., Korthuis R.J. (2014) Mitochondrial reactive oxygen species: A double edged sword in ischemia / reperfusion vs preconditioning. Redox Biology. 2: 702–714.

Kang R., Chen R., Zhang Q., Hou W., Wu S., Cao L., Tang D. (2014). HMGB1 in health and disease. *Mol Aspects Med*, 40, 1-116.

Kang R., Livesey K.M., Zeh H.J., Loze MT., Tang D. (2010) HMGB1: A novel Beclin 1-binding protein active in autophagy. Autophagy 6: 1209–1211.

Kang R., Tang D., Schapiro N.E., Livesey K.M., Loughran P., Bierhaus A., Lotze M.T., Zeh H.J. (2010) The receptor for advanced glycation end products (RAGE) sustains autophagy and limits apoptosis, promoting pancreatic tumor cell survival. Cell Death Differ. 17: 666–676.

Katsuki M., Asashima M., Yokota T. (2001) Murine homolog of SALL1 is essential for ureteric bud invasion in kidney development. Development 128: 3105–3115.

Kaushal G.P. (2012) Autophagy protects proximal tubular cells from injury and apoptosis. Kidney International. 82: 1250–1253.

Kaushal G.P., Kaushal V., Herzog C. (2008) Autophagy delays apoptosis in renal tubular epithelial cells in cisplatin cytotoxicity. Autophagy. 4: 710–712.

Kawai T., Akira S. (2007) Signaling to NF-kB by toll-like receptors. Trends Mol. Med. 13, 460–469.

Ke B., Fan C., Yang L., (2017) Matrix metalloproteinases-7 and kidney fibrosis. Front Physiol. 8:21-27.

Keiser J.A., Bjork F.A., Hodges J.C., Tayor D.Q. Jr. (1992) Renal hemodynamic and excretory response to PD123319 and losartan, nonpeptide AT1 and AT2 subtype-specific angiotensin II ligands. J Pharmacol Exp Ther. 263:1154–1160.

Kellum, J. A., Unruh, M. L., & Murugan, R. (2011). Acute kidney injury. BMJ clinical evidence, 2011, 2001.

Kennedy D.O. (2016) B Vitamins and the Brain: Mechanisms, Dose and Efficacy. Nutrients. 8(2):68.

Kennedy T.P., Rao N.V., Hopkins C., Pennington L., Tolley E., Hoidal J.R. (1989) Role of reactive oxygen species in reperfusion injury of the rabbit lung. J Clin Investig. 83:1326–1335.

Khwaja A. (2012) KDIGO clinical practice guideline for acute kidney injury. Nephron Clin. Pract. 120, 179–184.

Kim Y.G., Suga S.I., Kang D.H., Jefferson J.A., Mazzali M., Gordon K.L., Matsui K., Breiteneder-Geleff S., Shankland S.J., Hughes J., Kerjaschki D., Schreiner G.F., Johnson R.J. (2000) Vascular endothelial growth factor accelerates renal

recovery in experimental thrombotic microangiopathy. Kidney Int. 58(6):2390-9.

Kim Y.M., Kim H.J., Chang K.C. (2015) Glycyrrhizin reduces HMGB1 secretion in lipopolysaccharide-activated RAW 264.7 cells and endotoxemic mice by p38/Nrf2-dependent induction of HO-1. Int Immunopharmacol. 26(1): 112-118.

Kobayashi A., Valerius M.T., Mugford J.W., Carroll T.J., Self M., Oliver G., McMahon A.P. (2008) Six2 defines and regulates a multipotent self-renewing nephron progenitor population throughout mammalian kidney development. Cell Stem Cell. 3(2): 169–181.

Kokkoris S., Pipili C., Grapsa E., Kyprianou T., Nanas S. (2013) Novel biomarkers of acute kidney injury in the general adult ICU: a review. Ren Fail 35(4):579–591.

Komiya Y., Habas R. (2008) Wnt signal transduction pathways. Organogenesis. 4:2, 68-75.

Korkmaz A., Kolankaya D. (2009) The protective effects of ascorbic acid against renal ischemia-reperfusion injury in male rats. Ren. Fail. 31, 36–43.

Koul V., Kaur A., Singh A.P. (2015) Investigation of the role of nitric oxide/soluble guanylyl cyclase pathway in ascorbic acid-mediated protection against acute kidney injury in rats. Mol. Cell. Biochem. 406, 1–7.

Krawczeski CD, Woo JG, Wang Y, Bennett M.R., Ma Q., Devarajan P. (2011) Neutrophil gelatinase-associated lipocalin concentrations predict development

of acute kidney injury in neonates and children after cardiopulmonary bypass. J Pediatr (6) 1009–1015.

Kroemer G., Levine B. (2008). Autophagic cell death: the story of a misnomer. Nat. Rev. Mol. Cell Biol. 9 (12), 1004–1010.

Krumme B., Endmeir R., Vanhaelen M., Walb D. (2001) Reversible Fanconi syndrome after ingestion of a Chinese herbal “remedy” containing aristolochic acid. Nephrol Dial Transplant. 16: 400-402.

Kumar D., Singla S.K., Puri V., Puri S. (2015) The Restrained Expression of NF-kB in Renal Tissue Ameliorates Folic Acid Induced Acute Kidney Injury in Mice. PLoS One. 10(1):e115947.

Kume T., Deng K., Hogan B.L. (2000) Murine forkhead/winged helix genes Foxc1 (Mf1) and Foxc2 (Mfh1) are required for the early organogenesis of the kidney and urinary tract. Development 127: 1387–1395.

Kusch A., Hoff U., Bubalo G., Zhu Y., Fechner M, Schmidt-Ullrich R., Marko L., Muller D.N., Schmidt-Ott K.M., Gurgen D., Blum M., Schunck W.H., Dragun D. (2013) Novel signalling mechanisms and targets in renal ischaemia and reperfusion injury. Acta Physiol (Oxf).

Kuure S., Popsueva A., Jakobson M., Sainio K., Sariola H. (2007) Glycogen synthase kinase-3 inactivation and stabilization of beta-catenin induce nephron differentiation in isolated mouse and rat kidney mesenchymes. J Am Soc Nephrol. 18:1130–1139.

Kwak M.S., Shin J.S. (2013) Current Understanding of HMGB1-mediated Autophagy. Journal of Bacteriology and Virology. 43(2): 148 – 154.

Lameire N., Van Biesen W., Vanholder R. (2005) Acute takes failure. Lancet 365: 417-430.

Lebeau C., Debelle F.D., Arlt V.M., Pozdzik A., De Prez E.G., Phillips D.H., Deschodt-Lanckman M.M., Vanherweghem J.L., Nortier J.L. (2005) Early proximal tubule injury in experimental aristolochic acid nephropathy: functional and histological studies. Nephrol Dial Transplant. 20(11):2321-2332.

Lee H.L., Chen C.L., Yeh S.T., Zweier J.L., Chen Y.R. (2012) Biphasic modulation of the mi- tochondrial electron transport chain in myocardial ischemia and reperfusion. American Journal of Physiology: Heart and Circulatory Physiology. 302: 1410-1422.

Lee J.W., Bae S.H., Jeong J.W., Kim S.H., Kim K.W. (2004). Hypoxia-inducible factor (HIF-1) alpha: its protein stability and biological functions. Experimental & Molecular Medicine. 36 (1): 1–12.

Lee S., Lee T., Lee B., Choi H., Yang M., Ihm C., Kim M., (2004) Fanconi's syndrome and subsequent progressive renal failure caused by a Chinese herb containing aristolochic acid. Nephrology. 126-129.

Lee S.A., Kwak M.S., Shin J.S. (2014) The Role of High Mobility Group Box 1 in Innate Immunity. Yonsei Med J. 55(5):1165-1176.

Lemineur T., Deby-Dupont G., Preiser J.C. (2006) Biomarkers of oxidative stress in critically ill patients: what should be measured, when and how? Curr Opin Clin Nutr Metab Care. 9(6): 704-710.

Letterio J.J., Roberts A.B. (1998). Regulation of immune responses by TGF-beta. Annu. Rev. Immunol. 16: 137–161.

Li C., Peng S., Liu X., Han C., Wang X., Jin T., Liu S., Wang W., Xie X., He X., Zhang H., Shan L., Fan C., Shan Z., Teng W. (2017) Glycyrrhizin, a Direct HMGB1 Antagonist, Ameliorates Inflammatory Infiltration in a Model of Autoimmune Thyroiditis via Inhibition of TLR2-HMGB1 Signaling. Thyroid. 27(5): 722-731.

Li H., Bian C., Liao L., Li J., Zhao R.C. (2011) miR-17-5p promotes human breast cancer cell migration and invasion through suppression of HBP1. Breast Cancer Res. Treat. 126 (3), 565–575.

Li W., Zhu S., Li J., Assa A., Jundoria A., Xu J., Fan S., Eissa N.T., Tracey K.J., Sama A.E., Wang H. (2011) EGCG stimulates autophagy and reduces cytoplasmic HMGB1 levels in endotoxin-stimulated macrophages. Biochem. Pharmacol. 81 (9), 1152–1163.

Li Y.C., Tsai S.H., Chen S.M., Chang Y.M., Huang T.C., Huang Y.P., Chang C.T., Lee J.A. (2012) Aristolochic acid-induced accumulation of methylglyoxal and N-(carboxymethyl)lysine: An important and novel pathway in the pathogenic mechanism for aristolochic acid nephropathy. Biochem Biophys Res Commun. 423: 832-837.

Lin S.C., Lo Y.C., Wu H. (2010) Helical assembly in the MyD88- IRAK4-IRAK2 complex in TLR/IL-1R signalling. Nature. 465, 885–890.

Lindahl P., Hellström M., Kalén M., Karlsson L., Pekny M., Pekna M., Soriano P., Betsholtz C. (1998) Paracrine PDGF-B/PDGF-Rbeta signaling controls mesangial cell development in kidney glomeruli. Development. 125(17):3313-22.

Liu K.E., Frazier W.A. (2015). Phosphorylation of the BNIP3 C-Terminus Inhibits Mitochondrial Damage and Cell Death without Blocking Autophagy. PLOS ONE. 10 (6): e0129667.

Loizzi V., Del Vecchio V., Gargano G., De Liso M., Kardashi A., Naglieri E., Resta L., Cicinelli E., Cormio G (2017) Biological Pathways Involved in Tumor Angiogenesis and Bevacizumab Based Anti-Angiogenic Therapy with Special References to Ovarian Cancer. Int J Mol Sci. 14: 18(9).

Long D.A., Woolf A.S., Suda T., Yuan H.T. (2001) Increased renal angiopoietin-1 expression in folic acid-induced nephrotoxicity in mice. J Am Soc Nephrol. 12:2721–2731.

Lord G.M., Hollstein M., Arlt V.M., Roufosse C., Pusey C.D., Cook T., Schmeiser H.H. (2004) DNA adducts and p53 mutations in a patient with aristolochic acid-associated nephropathy. Am J Kidney Dis. 43: e18.1-e18.7.

Lord G.M., Tagore R., Cook T., Gower P., Pusey C.D. (1999) Nephropathy caused by Chinese herbs in the UK. Lancet 354: 481-482.

Lu Y.C., Yeh W.C., Ohashi P.S. (2008) LPS/TLR4 signal transduction pathway. Cytokine. 42: 145–151.

Luo X., Jiang L., Du B. Wen Y., Wang M., Xi X. (2014) A comparison of different diagnostic criteria in acute kidney injury in critically ill patients. Crit. Care 18, R144.

Macedo E., Malhotra R., Claure-Del Granado R., Fedullo P., Mehta R.L. (2011) Defining urine output criterion for acute kidney injury in critically ill patients. Nephrol. Dial. Transplant. 26, 509–515.

Maeshima A., Maeshima K., Noiima Y. (2002) Involvement of Pax-2 in the action of activin A on tubular cell regeneration. J Am Soc Nephrol 13: 2850–2859.

Maghazachi A.A., Al-Aoukaty A., Schall T.J. (1996). CC chemokines induce the generation of killer cells from CD56+ cells. Eur. J. Immunol. 26 (2): 315–9.

Mahar M., Cavalli V. (2018). Intrinsic mechanisms of neuronal axon regeneration. Nature Reviews. Neuroscience. 19 (6): 323–337.

Malek M., Nematbakhsh M. (2015) Renal ischemia/reperfusion injury; from pathophysiology to treatment. J Renal Inj Prev 4(2): 20-27.

McLeod L.L., Alayash A.I. (1999) Detection of a ferrylhemoglobin intermediate in an endothelial cell model after hypoxia-reoxygenation. Am J Physiol. 277: 92-99.

Mehta R.L., Cerda J., Burdmann E.A., (2015) International Society of Nephrology's 0by25 initiative for acute kidney injury (zero preventable deaths by 2025): a human rights case for nephrology. *Lancet* 385:1–28.

Mehta R.L., Kellum J.A., Shah S.V., Molitoris B.A., Ronco C., Warnock D.G., Levin A. (2007) Acute Kidney Injury Network: Report of an initiative to improve outcomes in acute kidney injury. Crit. Care 11, R31.

Melnikov V.Y., Ecder T., Fantuzzi G., (2001) Impaired IL-18 processing protects caspase-1 deficient mice from ischemic acute renal failure. J Clin Invest 107:1145–1152.

Meng F., Li Z., Yan J., Manjanatha M., Shelton S., Yarborough S., Chen T. (2014) Tissue-specific microRNA responses in rats treated with mutagenic and carcinogenic doses of aristolochic acid. Mutagenesis. 29(5): 357-365.

Messmer D., Yang H., Telusma G., Knoll F., Li J., Messmer B. (2004) High mobility group box protein 1: an endogenous signal for dendritic cell maturation and Th1 polarization. J Immunol. 173: 307-13.

Meyer M.M., Chen T.P., Bennett W.M. (2000) Chinese herb nephropathy. Proc. (Bayl. Univ. Med. Cent.) 13: 334-337.

Michl J., Jennings H.M., Kite G.C., Ingrouille M.J., Simmonds M.S.J., Heinrich M. (2013) Is aristolochic acid nephropathy a widespread problem in developing countries: A case study of Aristolochia indica L. in Bangladesh using an ethnobotanical-phytochemical approach. J. Ethnopharmacol. 149: 235-244.

Michos O., Cebrian C., Hyink D., Grieshammer U., Williams L., D'Agati V., Jonathan Licht J.D., Martin G.R., Costantini F. (2010) Kidney Development in the Absence of Gdnf and Spry1 Requires Fgf10. PLoS Genet 6(1): e1000809.

Milligan S.A., Owens M.W., Grisham M.B. (1998). Differential regulation of extracellular signal-regulated kinase and nuclear factor-kappa B signal transduction pathways by hydrogen peroxide and tumor necrosis factor. Arch. Biochem. Biophys. 352: 255–262.

Mishra J., Dent C., Tarabishi R. (2005) Neutrophil gelatinase-associated lipocalin (NGAL) as a biomarker for acute renal injury following cardiac surgery. Lancet. 365:1231–121238.

Mishra J., Ma Q., Prada A., Mitsnefes M., Zahedi K., Yang J., Barasch J., Devarajan P. (2003) Identification of neutrophil gelatinase-associated lipocalin as a novel early urinary biomarker for ischemic renal injury. J Am Soc Nephrol 14(10): 2534-43.

Mishra J., Ma Q., Prada A., Mitsnefes M., Zahedi K., Yang J., Barasch J., Devarajan P. (2003) Identification of neutrophil gelatinase-associated lipocalin as a novel urinary biomarker for ischemic injury. J Am Soc Nephrol. 4:2534–2543.

Mishra J., Mori K., Ma Q., Kelly C., Barasch J., Devarajan P. (2004) Neutrophil Gelatinase-Associated Lipocalin (NGAL): a novel urinary biomarker for cisplatin nephrotoxicity. Am J Nephrol. 24:307–315.

Mitsnefes M., Kathman T., Mishra J. (2007) Serum NGAL as a marker of renal function in children with chronic kidney disease. Pediatr Nephrol. 22:101–108.

Mollica L., De Marchis F., Spitaleri A., Dallacosta C., Pennacchini D., Zamai M., Agresti A., Trisciuoglio L., Musco G., Bianchi M.E. (2007) Glycyrrhizin binds to high-mobility group box 1 protein and inhibits its cytokine activities. Chem Biol. 14(4): 431-441.

Nalesso G., Thomas B.L., Sherwood J.C., Yu J., Addimanda O., Eldridge S., Thorup A.S., Dale L., Schett G., Zwerina J., Eltawil N., Pitzalis C., Dell'Accio F. (2017) WNT16 antagonises excessive canonical WNT activation and protects cartilage in osteoarthritis. Ann Rheum Dis. 76(1):218-226.

Ni D., Jiang D., Kutyreff C.J., Lai J., Yan Y., Barnhart T.E., Yu B., Im H.J., Kang L., Cho S.Y., Liu Z., Huang P., Engle J.W., Cai W. (2018) Molybdenum-based nanoclusters act as antioxidants and ameliorate acute kidney injury in mice. Nat Commun. 21;9(1): 5421.

Nishinakamura R, Matsumoto Y, Nakao K, Nakamura K, Sato A, Nisula S., Kaukonen K.M., Vaara S.T., Korhonen A.M., Poukkanen M., Karlsson S., Haapio M., Inkinen O., Parviainen I., Suojaranta-Ylinen R. (2013) Incidence, risk factors and 90-day mortality of patients with acute kidney injury in Finnish intensive care units: The FINNAKI study. Intensive Care Med. 39, 420–428.

Nortier J.L., Pozdzik A., Roumeguere T., Vanherweghem J.L. (2015) Aristolochic acid nephropathy ("Chinese herb nephropathy") Nephrol Ther. 11(7): 574-88.

Novitskaya T., McDermott L., Zhang K.X., Chiba T., Paueksakon P., Hukriede N.A., de Caestecker M.P. (2014) A PTBA small molecule enhances recovery and reduces postinjury fibrosis after aristolochic acid-induced kidney injury. Am J Physiol Renal Physiol. 306(5): 496-504.

Obara-Ishihara T., Kuhlman J., Niswander L., Herzlinger D. (1999) The surface ectoderm is essential for nephric duct formation in intermediate mesoderm. Development. 126(6):1103-8.

Obermüller N., Geiger H., Weipert C., Urbschat A., Obermüller N., Geiger H., Weipert C., Urbschat A. (2014) Current developments in early diagnosis of acute kidney injury. Int Urol Nephrol 46(1):1–7.

Okamoto K., Kondo-Okamoto N. (2012) Mitochondria and autophagy: critical interplay between the two homeostats *Biochim Biophys Acta* 1820(5):595-600.

Osaki M., Oshimura M., Ito H. (2004). The PI3K-Akt pathway: Its functions and alterations in human cancer. Apoptosis. 9 (6): 667–676.

Palipoch S. (2013) A Review of Oxidative Stress in Acute Kidney Injury: Protective Role of Medicinal Plants-Derived Antioxidants. Afr J Tradit Complement Altern Med. 10(4): 88–93.

Paller M.S., Hoidal J.R., Ferris T.F. (1984) Oxygen free radicals in ischemic acute renal failure in the rat. J Clin Invest. 74(4): 1156-1164.

Palumbo R. F., De Marchis T., Pusterla A., Conti M., Alessio M.E. (2009) Src family kinases are necessary for cell migration induced by extracellular HMGB1. J. Leukoc. Biol. 86: 617–623.

Pandi-Perumal S.R., Trakht I., Srinivasan V., Spence D.W., Maestroni G.J., Zisapel N. Cardinali D.P. (2008) Physiological effects of melatonin: role of melatonin receptors and signal transduction pathways. Prog Neurobiol 85: 335-353.

Parikh C.R., Abraham E., Ancukiewicz M. (2005) Urine IL-18 is an early diagnostic marker for acute kidney injury and predicts mortality in the intensive care unit. J Am Soc Nephrol. 16:3046–3052.

Parikh C.R., Philbrook H.T. (2011) Statistical considerations in analysis and interpretation of biomarker studies 2: 25-37.

Park J.S. (2006) High mobility group box 1 protein interacts with multiple toll-like receptors. Am J Physiol Cell Physiol. 290: C917–C924.

Patanwala I., King M.J., Barrett D.A., Rose J., Jackson R., Hudson M., Philo M., Dainty J.R., Wright A.J., Finglas P.M., Jones D.E. (2014) Folic acid handling by the human gut: implications for food fortification and supplementation. Am. J. Clin. Nutr. 100(2): 593-599.

Penzo M., Molteni R., Suda T., Samaniego S., Raucci A., Habiel D.M., Miller F., Jiang H.P., Li J., Pardi R., (2010). Inhibitor of NF-kappa B kinases alpha and beta are both essential for high mobility group box 1- mediated chemotaxis. J. Immunol. 184: 4497–4509.

Perry T.E., Muehlschlegel J.D., Liu K.Y. (2010) Plasma neutrophil gelatinase-associated lipocalin and acute postoperative kidney injury in adult cardiac surgical patients. Anesth Analg. 110:1541–1547.

Plotnikov E.Y., Chupyrkina A.A., Jankauskas S.S., Pevzner I.B., Silachev D.N., Skulachev V.P., Zorov D.B. (2011) Mechanisms of nephroprotective effect of mitochondria-targeted antioxidants under rhabdomyolysis and ischemia/reperfusion. Biochim Biophys Acta 1812(1):77–86.

Plotnikov E.Y., Kazachenko A.V., Vyssokikh M.Y., Vasileva A.K., Tcvirkun D.V., Isaev N.K., Kirpatovsky V.I., Zorov D.B. (2007) The role of mitochondria in oxidative and nitrosative stress during ischemia/reperfusion in the rat kidney. Kidney International. 72: 1493–1502.

Powell W.C., Fingleton B., Wilson C.L. (1999) The metalloproteinase matrilysin proteolytically generates active soluble Fas ligand and potentiates epithelial cell apoptosis. Curr Biol. 9:1441–1447.

Powers C.J., McLeskey S.W., Wellstein A. (2000) Fibroblast growth factors, their receptors and signaling. Endocr Relat Cancer. 7(3):165-97.

Pozdzik A.A., Salmon I.J., Debelle F.D., Decaestecker C., van den Branden C., Verbeelen D., Deschodt-Lanckman M.M., Vanherweghem J.L., Nortier J.L. (2008) Aristolochic acid induces proximal tubule apoptosis and epithelial to mesenchymal transformation. Kidney Int. 73: 595-607.

Pozzoli S., Simonini M., Manunta P. (2017) Predicting acute kidney injury: current status and future challenges. J Nephrol. 31(2):209-223.

Prasad R., Liu Y., Deterding L.J., Poltoratsky V.P., Kedar P.S., Horton J.K., Kanno S., Asagoshi K., Hou E.W., Khodyreva S.N., Lavrik O.I., Tomer K.B., Yasui A., Wilson S.H. (2007) HMGB1 is a cofactor in mammalian base excision repair. Mol Cell. 27(5):829-841.

Qi C., Dmitrieva N.I., Ferraris J.D., Brooks H.L., van Balkom B.W.M., Burg M. (2005) Proc Natl Acad Sci U S A. 11; 102(2): 503–508.

Qin S., Wang H., Yuan R., Li H.., Ochani M, Ochani K., Rosas-Ballina M., Czura C.J., Huston J.M., Miller E., Lin X., Sherry B., Kumar A., Larosa G., Newman W., Tracey K.J., Yang H. (2006) Role of HMGB1 in apoptosis-mediated sepsis lethality. J Exp Med 203: 1637-1642.

Rabadi M.M., Xavier S., Vasko R., Kaur K., Goligorksy M.S., Ratliff B.B. (2015) High-mobility group box 1 is a novel deacetylation target of Sirtuin1. Kidney International. **87**, 95–108;

Rambold A.S., Lippincott-Schwartz J. (2011) Mechanisms of mitochondria and autophagy crosstalk *Cell Cycle.* 10(23): 4032–4038.

Reddy T.P., Manczak M., Calkins M.J., Mao P., Reddy A.P., Shirendeb U., Park B., Reddy P.H. (2011) Toxicity of neurons treated with herbicides and neuroprotection by mitochondria-targeted antioxidant SS31. Int J Environ Res Public Health 8:203–221.

Redmann M., Benavides G.A., Berryhill T.F., Wani W.Y., Ouyang X.S., Johnson M.S., Ravi S., Barnes S., Darley-Usmar, V.M., Zhang J.H. (2017) Inhibition of

autophagy with bafilomycin and chloroquine decreases mitochondrial quality and bioenergetic function in primary neurons. Redox Biol. 11: 73–81.

Repka A.M., Adler R. (1992) Accurate determination of the time of cell birth using a sequential labeling technique with [3H]-thymidine and bromodeoxyuridine ("window labeling"). J Histochem Cytochem. 40(7): 947-53.

Rhoden E., Teloken C., Lucas M., Rhoden C., Mauri M., Zettler C., Bello-Klein A. and Barros E. (2000) Protective effect of allopurinol in the renal ischemia-reperfusion in uninephrectomized rats. General Pharmacology, 35(4): 189-193.

Rodrigues F.B., Bruetto R.G., Torres U.S., Otaviano A.P., Zanetta D.M., Burdmann E.A. (2013) Incidence and mortality of acute kidney injury after myocardial infarction: A comparison between KDIGO and RIFLE criteria. PLoS ONE 8, e69998.

Romanov V., Whyard T.C., Waltzer W.C., Grollman A.P., Rosenquist T. (2015) Aristolochic acid-induced apoptosis and G2 cell cycle arrest depends on ROS generation and MAP kinases activation. Arch Toxicol. 89: 47-56.

Rosenquist T.A., Grollman A.P. (2016) Mutational signature of aristolochic acid: Clue to the recognition of a global disease. DNA Repair (Amst.) 44: 205-211.

Ruan Y., Wang L., Zhao Y., Yao Y., Chen S., Li J., Guo H., Ming C., Chen S., Gong F., Chen G. (2014) Carbon monoxide potently prevents ischemia-induced high-mobility group box 1 translocation and release and protects against lethal renal ischemia-reperfusion injury. Kidney Int. 86: 525–537.

Ryan M.J., Johnson G., Kirk J., Fuerstenberg S.M., Zager R.A., Torok-Storb B. (1994) HK-2: An immortalized proximal tubule epithelial cell line from normal adult human kidney. *Kidney International*, (45), 48-57.

Ryan M.J., Johnson G., Kirk J., Fuerstenberg S.M., Zager R.A., Torok-Storb B. (1994) HK-2: an immortalized proximal tubule epithelial cell line from normal adult human kidney. Kidney Int. 45(1):48-57.

Sabbisetti V.S., Ito K., Wang C., Yang L., Mefferd S.C., Bonventre J.V. (2013) Novel assays for detection of urinary KIM-1 in mouse models of kidney injury. Toxicol Sci. 131(1): 13-25.

Saifudeen Z., Liu J., Dipp S., Yao X., Li Y., McLaughlin N., Aboudehen K., El-Dahr S.S. (2012) A p53-Pax2 Pathway in Kidney Development: Implications for Nephrogenesis. PLoS ONE 7(9): e44869.

Salmon A.B., Richardson A., Pérez V.I. (2010) Update on the oxidative stress theory of aging: does oxidative stress play a role in aging or healthy aging? Free Radic Biol Med. 48:642–655.

Sands J.M., Layton H.E. (2009) The physiology of urinary concentration: An update. Seminars in Nephrol. 29(3), 178-195.

Sanyanusin P., Schimmenti L.A., McNoe L.A., Ward T.A., Pierpont M.E., Sullivan M.J., Dobyns W.B., Eccles M.R. (1996) Mutation of the PAX2 gene in a family with optic nerve colobomas, renal anomalies and vesicoureteral reflux. Nat Genet 9: 358 –364.

Sariola H., Saarma M. (1999) GDNF and its receptors in the regulation of the ureteric branching. Int J Dev Biol 43: 413–418.

Satoh W., Gotoh T., Tsunematsu Y., Aizawa S., Shimono A. (2006) Sfrp1 and Sfrp2 regulate anteroposterior axis elongation and somite segmentation during mouse embryogenesis. Development. 133: 989-999.

Saxén L. (1987) Organogenesis of the kidney. Developmental and cell biologu 19th addition. (1) 1-18.

Scaffidi P., Misteli T., Bianchi M.E. (2002) Release of chromatin protein HMGB1 by necrotic cells triggers inflammation. Nature. 418: 191-195.

Schmeiser H.H., Janssen J.W., Lyons J., Scherf H.R., Pfau W., Buchmann A., Bartram C.R., Wiessier M. (1990) Aristolochic acid activates ras genes in rat tumors at deoxyadenosine residues. Cancer Res. 50: 5464–5469.

Schmeiser H.H., Schoepe K.B., Wiessler M. (1988) DNA adduct formation of aristolochic acid I and II in vitro and in vivo. Carcinogenesis. 9(2): 297-303.

Seely J.C. (2017) A brief review of kidney development, maturation, developmental abnormalities, and drug toxicity: juvenile animal relevancy. J Toxicol Pathol. 30(2): 125–133.

Sener G., Tuğtepe H., Yüksel M., Cetinel S., Gedik N., Yeğen B.C. (2006) Resveratrol improves ischemia/reperfusion-induced oxidative renal injury in rats. Arch Med Res. 37(7):822–829.

Sharfuddin A.A., Molitoris B.A. (2011) Pathophysiology of ischemic acute kidney injury. Nat Rev Nephrol 7: 189–200.

Sharfuddin, A.A., Molitoris, B.A. (2008) Chapter 76. Pathophysiology of acute kidney injury. In: Alpern, R.J. and Hebert, S.C. (Eds.) Seldin and Giebisch's the kidney: Physiology and pathophysiology. New York: Lippincott Williams and Wilkins.

Shibutani S., Dong H., Suzuki N., Ueda S., Miller F., Grollman A.P. (2007) Selective toxicity of aristolochic acids I and II. Drug Metab Dispos. 35: 1217-1222.

Silvester W., Bellomo R., Cole L. (2001) Epidemiology, management, and outcome of severe acute renal failure of critical illness in Australia. Crit. Care Med. 29, 1910–1915.

Skulachev VP (2001) Mitochondrial filaments and clusters as intracellular power-transmitting cables. Trends Biochem. Sci. 26: 23–29

Slade N., Moll U.M., Brdar B., Zoric A., Jelakovic B. (2009) P53 mutation as fingerprints for aristolochic acid; an environmental carcinogen in endemic (Balkan) nephropathy. Mutation Res. 663: 1–6.

Slocum J.L., Heung M., Pennathur S. (2012) Marking renal injury: can we move beyond serum creatinine? Transl Res 159(4):277–289.

Smith A.D., Kim Y.I., Refsum H. (2008) Is folic acid good for everyone? Am. J. Clin. Nutr. 87: 517-533.

Smyth I.M., Cullen-McEwen L.A., Caruana G., Black M.J., Bertram J.F. (2017) Development of the Kidney: Morphology and Mechanisms. Fetal and Neonatal Physiology (Fifth Edition). Volume 2, 953-964.

Sorg O. (2004) Oxidative stress: a theoretical model or a biological reality? C R Biol. 327:649–662.

Stallons L.J., Whitaker R.M., Schnellmann R.G. (2014) Suppressed Mitochondrial Biogenesis in Folic Acid-Induced Acute Kidney Injury and Early Fibrosis. Toxicol Lett. 224(3): 326–332.

Stengel B., Jones E. (1998) End-Stage Renal Insufficiency Associated with Chinese Herbal Consumption in France. Nephrologie 19: 15-20.

Stiborova M., Frei E., Wiessler M. and Schmeiser H.H. (2001). Human enzymes involved in the metabolic activation of carcinogenic aristolochic acids: evidence for reductive activation by cytochromes P450 1A1 and 1A2. Chem Res Toxicol 14: 1128-37.

Supavekin S., Zhang W., Kucherlapati R., Kaskel F.J., Moore L.C., Devarajan P. (2003) Differential gene expression following early renal ischemia-reperfusion. Kidney Int. 63:1714–1724.

Surendran K., Simon T.C., Liapis H., McGuire J.K. (2004) Matrilysin (MMP-7) expression in renal tubular damage: Association with Wnt4. Kidney International. 65: 2212–2222.

Szeto H.H. (2017) Pharmacologic Approaches to Improve Mitochondrial Function in AKI and CKD. J Am Soc Nephrol 28: 2856–2865.

Szeto H.H., Liu S., Soong Y., Wu D., Darrah S.F., Cheng F.Y., Zhao Z., Ganger M., Tow C.Y., Seshan S.V. (2011) Mitochondriatargeted peptide accelerates ATP recovery and reduces ischemic kidney injury. J Am Soc Nephrol 22:1041–1052.

Takahashi A., Kimura T., Takabatake Y. (2012) Autophagy guards against cisplatin-induced acute kidney injury. Am J Pathol. 180: 517–525.

Tamimi Y., Ekuere U., Laughton N., Grundy P. (2008) WNT5A is regulated by PAX2 and may be involved in blastemal predominant Wilms tumorigenesis. Neoplasia. 10, 1470–1480.

Tan RJ, Liu Y. Matrix metalloproteinases in kidney homeostasis and diseases. Am J Physiol Renal Physiol. 2012; 302: 1351–1361.

Tanaka A., Nishida R., Maeda K., Sugawara A., Kuwahara T. (2000) Aristolochic acid—Induced Fanconi's syndrome and nephropathy presenting as hypokalemic paralysis. Clin Nephrol. 39: 521116.

Tang D., Kang R., Livesey K.M., Cheh C.W., Farkas A., Loughran P., Hoppe G., Bianchi M.E., Tracey K.J., Zeh H.J., Lotze M.T. (2010) Endogenous HMGB1 regulates autophagy. J Cell Biol 190: 881–892.

Tang D., Kang R., Livesey K.M.m Zeh H.J., Lotze M.T. (2011) High mobility group box (HMGB1 activates an autophagic response to oxidative stress. Antioxid Redox Signal. 15(8): 2185-2195.

Tang D., Kang R., Zeh H., Lotze M. (2011) HMGB1, oxidative stress and disease. Antioxid Redox Signal 14: 1315–1335.

Tang D., Shi Y., Kang R., Li T., Xiao W., Wang H., Xiao X. (2007) Hydrogen peroxide stimulates macrophages and monocytes to actively release HMGB1. J Leukoc Biol 81: 741–747.

Tang D., Shi Y., Kang R., Li T., Xiao W., Wang H., Xiao X. (2007) Hydrogen peroxide stimulates macrophages and monocytes to actively release HMGB1. J Leukoc Biol 81: 741–747.

Tang D.L., Kang R., Livesey K.M., Kroemer G., Billiar T.R., van Houten B. (2011) High mobility group box1 is essential for mitochondrial quality control. Cell Metab 13:701–11.

Teicher B.A., Fricker S.P. (2010) CXCL12 (SDF-1)/CXCR4 Pathway in Cancer. Clin Cancer Res. 16(11); 2927–3291.

Thadhani R., Pascual M., Bonventre J.V. (1996) Acute renal failure. N Engl J Med 334: 1448–1460.

Thomas M.E., Blain, C., Dawnay A., Devonald M.A., Ftouh S., Laing C., Latchem S., Lewington A., Milford D.V., Ostermann M. (2015) The definition of acute kidney injury and its use in practice. Kidney Int. 87, 62–73.

Thongprayoon C., Cheungpasitporn W., Harrison A.M., Kittanamongkolchai W., Ungprasert P., Srivali N., Akhoundi A. Kashani K.B. (2016) The comparison of the commonly used surrogates for baseline renal function in acute kidney injury diagnosis and staging. BMC Nephrol.17, 6.

Thongprayoon C., Cheungpasitporn W., Kittanamongkolchai W., Srivali N., Ungprasert P., Kashani K. (2015) Optimum methodology for estimating baseline serum creatinine for the acute kidney injury classification. Nephrology (Carlton) 20, 881–886.

Torban E., Dziarmaga A., Iglesias D. (2006) PAX2 activates WNT4 ex-pression during mammalian kidney development. J Biol Chem 281: 12705–12712.

Torban E., Eccles M.R., Favor J., Goodyer P.R. (2000) Pax2 suppresses apoptosis in renal collecting duct cells. Am J Pathol. 157: 833–842.

Torres M., Gomez-Pardo E., Dressler G. (1995) Pax-2 controls multiples steps of urogenital development. Development. 121: 4057–4065.

Torres M., Gomez-Pardo E., Dressler G.R., Gruss P. (1995) Pax-2 controls multiple steps of urogenital development. Development. 121:4057–4065.

Tsang T.E., Shawlot W., Kinder S.J., Kobayashi A., Kwan K.M., Schughart K., Kania A., Jessell T.M., Behringer R.R., Tam P.P. (2000) Lim1 activity is required for intermediate mesoderm differentiation in the mouse embryo. Dev Biol. 223(1):77-90.

Tsung A., Sahai R., Tanaka H., Nakao A., Fink M.P., Lotze M.T., Yang H., Li J., Tracey K.J., Geller D.A., Billiar T.R. (2005) The nuclear factor HMGB1 mediates hepatic injury after murine liver ischemia-reperfusion. J Exp Med 201: 1135–1143.

Turner M.D., Nedjai B., Hurst T., Pennington D.J. (2014) Cytokines and chemokines: At the crossroads of cell signalling and inflammatory disease. Biochimica et Biophysica Acta 1843: 2563–2582.

Tutal Y. (2012) Pseudogenes. Comp Funct Genomics. ID 424526.

Uchino S., Bellomo R., Goldsmith D., Bates S., Ronco C. (2006) An assessment of the RIFLE criteria for acute renal failure in hospitalized patients. Crit. Care Med. 34, 1913–1917.

Ulloa L., Ochani M., Yang H., Tanovic M., Halperin D., Yang R., Czura C.J., Fink M.P., Tracey K.J. (2002) Ethyl pyruvate prevents lethality in mice with established lethal sepsis and systemic inflammation. Proc Natl Acad Sci USA 99: 12351–12356.

Van Houten B., Woshner V., Santos J.H. (2006) Role of mitochondrial DNA in toxic responses to oxidative stress. DNA Repair (Amst). 5(2):145–152.

Vanhaesebroeck B., Alessi D.R. (2000). The PI3K-PDK1 connection: more than just a road to PKB. Biochem J. 346 (3): 561–576.

Vanherweghem J.L., Depierreux M., Tielemans C., Abramowicz D., Dratwa M., Jadoul M., Richard C., Vandervelde D., Verbeelen D., Vanhaelen-Fastre R.（1993） Rapidly progressive interstitial renal fibrosis in young women:

association with slimming regimen including Chinese herbs. Lancet 341: 387-391.

Vanherweghem, J.L. (1998) Misuse of Herbal Remedies: The case of an outbreak of terminal renal failure in Belgium (Chinese Herbs Nephropathy). J Altern Complement Med. 4: 9-13.

Vanmassenhove J., Vanholder R., Nagler E., Van Biesen W. (2013) Urinary and serum biomarkers for the diagnosis of acute kidney injury: an in-depth review of the literature. Nephrol Dial Transplant 28:254–273.

VanPatten S., Al-Abed Y. (2018) High Mobility Group Box-1 (HMGb1): Current Wisdom and Villa-Morales M., Fernandez-Piqueras J. (2012) Targeting the Fas/FasL signaling pathway in cancer therapy. Expert Opin. Ther. Targets 16: 85–101.

Vousden K. (1990). Human papillomavirus oncoproteins. *Semin Cancer Biol* (1), 415-424.

Waikar S.S., Curhan G.C., Wald R., McCarthy E.P. (2006) Chertow G.M. Declining mortality in patients with acute renal failure, 1988 to 2002. J Am Soc Nephrol 17: 1143–50.

Wasung M.E., Chawla L.S., Madero M. (2015) Biomarkers of renal function, which and when? Clin Chim Acta 1:350–438.

Watanabe M., de Moura Neiva L.B., da Costa Santos C.X., Martins Laurindo FR, de Fátima Fernandes Vattimo M (2007) Isoflavone and the heme

oxygenase system in ischemic acute kidney injury in rats. Food Chem Toxicol. 45(12):2366–2371

Wei Y.H., Lu C.Y., Wei C.Y., (2001) Oxidative stress in human aging and mitochondrial disease?

Weiner I.D., Mitch W.E., Sands J.M. (2015) Urea and ammonia metabolism and the control of renal nitrogen excretion. Clinical Journal of the American Society of Nephrology, 10(8), 1444-1458.

Wellik D.M. (2007) Hox patterning of the vertebrate axial skeleton. Dev Dyn. 236(9):2454-63.

Whiteman M., Spencer J.P., Szeto H.H., Armstrong J.S. (2008) Do mitochondriotropic antioxidants prevent chlorinative stress-induced mitochondrial and cellular injury? Antioxid Redox Signal 10:641–650.

Wolf G. (2002) Angiotensin II and tubular development. Nephrol Dial Transplant 17: 48–51.

Woolf A.S., Kolatsi-Joannou M., Hardman P., Andermarcher E., Moorby C., Fine L.G., Jat P.S., Noble M.D., Gherardi E. (1995) Roles of hepatocyte growth factor/scatter factor and the met receptor in the early development of the metanephros. J Cell Biol. 128(1-2):171-84.

Wright A.J., Dainty J.R., Finglas P.M. (2007) Folic acid metabolism in human subjects revisited: potential implications for proposed mandatory folic acid fortification in the UK. Br. J. Nutr. 98(4):667-675.

Wu H., Ma J., Wang P., Corpuz T.M., Panchapakesan U., Wyburn K.R., Chadban S.J. (2010) HMGB1 contributes to kidney ischemia reperfusion injury. J Am Soc Nephrol. 21(11):1878-1890.

Wu H., Ma J., Wang P., Corpuz T.M., Panchapakesan U., Wyburn K.R., Chadban S.J. (2010) HMGB1 contributes to kidney ischemia reperfusion injury. J Am Soc Nephrol. 21: 1878–1890.

Wu H.L., Ma J., Wang P., Corpuz T.M., Panchapakesan U., Wyburn K.R. (2010) HMGB1 contributes to kidney ischemia reperfusion injury. J Am Soc Nephrol 21:1878–90.

Wu H.L., Ma J., Wang P., Corpuz T.M., Panchapakesan U., Wyburn K.R. (2010) HMGB1 contributes to kidney ischemia reperfusion injury. J Am Soc Nephrol. 21:1878–90.

Wu J., Liu X., Fan J., Chen W., Wang J., Zeng Y., Feng X., Yu X., Yang X. (2014) Bardoxolone methyl (BARD) ameliorates aristolochic acid (AA)-induced acute kidney injury through Nrf2 pathway. Toxicology. 318:22-31.

Wu T.K., Wei C.W., Pan Y.R., Cheng S.H., Chang W.J., Wang H.F., Yu Y.L. (2015) Vitamin C attenuates the toxic effect of aristolochic acid on renal tubular cells via decreasing oxidative stress mediated cell death pathways. Mol Med Rep. 12: 6086-6092.

Xiang K., Cheng L., Luo Z., Ren J., Tian F., Tang L., Chen T., Dai R. (2014) Glycyrrhizin suppresses the expressions of HMGB1 and relieves the severity of traumatic pancreatitis in rats. PLoS One. 26, 9(12): e115982.

Xiao Y., Ge M., Xue X., Wang C., Wang H., Wu X., Li L., Liu L., Qi X., Zhang Y., Li Y., Luo H., Xie T., Gu J., Ren J. (2008) Hepatic cytochrome P450s metabolize aristolochic acid and reduce its kidney toxicity. Kidney Int. 73(11):1231-1239.

Xiao Y., Xue X., Wu Y.F., Xin G.Z., Qian Y., Xie T.P., Gong L.K., Ren J. (2009) β-Naphthoflavone protects mice from aristolochic acid-I-induced acute kidney injury in a CYP1A dependent mechanism. Acta Pharmacologica Sinica. 30: 1559–1565.

Xu F., Mack C.P., Quandt K.S., Shlafer M., Massey V., Hultquist D.E. (1993) Pyrrolo- quinoline quinone acts with flavin reductase to reduce ferrylmyoglobin in vitro and protects isolated heart from re-oxygenation injury. Biochem Biophys Res Commun. 193: 434–439.

Yamamoto A., Tagawa Y., Yosgimori T., Moriyama Y., Masaka R., Tashiro Y. (1998) Bafilomycin A1 prevents maturation of autophagic vacuoles by inhibiting fusion between autophagosomes and lysosomes in rat hepatoma cell line, H-4-II-E cells. Cell Struct Funct. 23(1):33-42.

Yang C., Kaushal V., Shah S.V. (2008) Autophagy is associated with apoptosis in cisplatin injury to renal tubular epithelial cells. Am J Physiol Renal Physiol. 294: 777–787.

Yang D., Chen Q., Yang H., Tracey K.J., Bustin M., Oppenheim J.J. (2007) High mobility group box-1 protein induces the migration and activation of human dendritic cells and acts as an alarmin. J Leukoc Biol. 81:59-66.

Yang L., Besschetnova T.Y., Brooks C.R. (2010) Epithelial cell cycle arrest in G2/M mediates kidney fibrosis after injury. Nat Med. 16: 535–543.

Yang L., Su T., Li X.M., Wang X., Cai, S.Q., Meng L.Q., Zou W.Z., Wang H.Y. (2012) Aristolochic acid nephropathy: Variation in presentation and prognosis. Nephrol Dial Transplant. 27: 292-298.

Yang X., Chen C., Teng S. (2017) Urinary matrix metalloproteinase-7 predicts severe AKI and poor outcomes after cardiac surgery. J Am Soc Nephrol. 28:3373–3382.

Yoon H.Y., Kang N.I., Lee H.K., Jang K.Y., Park J.W., Park B.H. (2008) Sulforaphane protects kidneys against ischemia-reperfusion injury through induction of the Nrf2-dependent phase 2 enzyme. Biochem Pharmacol. 75(11):2214–2223.

Yu F.Y., Wu T.S., Chen T.W., Liu B.H. (2011) Aristolochic acid I induced oxidative DNA damage associated with glutathione depletion and ERK1/2 activation in human cells. Toxicol In Vitro 25: 810-816.

Yu F.Y., Wu T.S., Chen T.W., Liu B.H. (2011) Aristolochic acid I induced oxidative DNA damage associated with glutathione depletion and ERK1/2 activation in human cells. Toxicol In Vitro. 25(4):810-816.

Yu J., Carroll T.J., Rajagopal J., Kobayashi A., Ren Q., McMahon A.P. (2009). A Wnt7b-dependent pathway regulates the orientation of epithelial cell division and establishes the cortico-medullary axis of the mammalian kidney. Development. 136 (1): 161–171.

Yuan F., Gu L., Guo S., Wang C., Li G.M. (2004) Evidence for involvement of HMGB1 protein in human DNA mismatch repair. J Biol Chem. 279(20):20935-20940.

Yun B.H., Rosenquist T.A., Sidorenko V., Iden C.R., Chen C.H., Pu Y.S., Bonala R., Johnson F., Dickman K.G., Grollman A.P. (2012) Biomonitoring of aristolactam-DNA adducts in human tissues using ultra-performance liquid chromatography/ion-trap mass spectrometry. Chem Res Toxicol. 25: 1119-1131.

Zager R.A., Schimpf B.A. and Gmur D.J. (1993) Physiological pH. Effects on posthypoxic proximal tubular injury. Circulation Research, 72, 837-846.

Zakiyanov O., Kriha V., Vachek J., Zima T., Tesar V., Kalousova M. (2013) Placental growth factor, pregnancy-associated plasma protein-a, soluble receptor for advanced glycation end products, extracellular newly identified receptor for receptor for advanced glycation end products binding protein and high mobility group box 1 levels in patients with acute kidney injury: a cross sectional study. BMC Nephrol. 14:245.

Zeeshan H.M.A., Lee G.H., Kim H.R., Chae H.J. (2016) Endoplasmic Reticulum Stress and Associated ROS *Int. J. Mol.* Sci. 17, 327.

Zeng X., McMahon G.M., Brunelli S.M., Bates D.W., Waikar S.S. (2014) Incidence, outcomes, and comparisons across definitions of AKI in hospitalized individuals. Clin. J. Am. Soc. Nephrol. 9, 12–20.

Zeng Y., Li S., Wu J., Chen W., Sun H., Peng W., Yu X., Yang X. (2014) Autophagy inhibitors promoted aristolochic acid I induced renal tubular epithelial cell apoptosis via mitochondrial pathway but alleviated nonapoptotic cell death in mouse acute aritolochic acid nephropathy model. Apoptosis. 19(8):1215-1224.

Zhan J., Wang K., Zhang C., Zhang C., Li Y., Zhang Y., Chang X., Zhou Q., Yao Y., Liu Y., Xu G. (2016) GSPE inhibits HMGB1 release, attenuating renal IRinduced acute renal injury and chronic renal fibrosis. Int J Mol Sci. 17.

Zhang H., Zhang R., Chen J., Shi M., Li W., Zhang X. (2017) High Mobility Group Box1 Inhibitor Glycyrrhizic Acid Attenuates Kidney Injury in Streptozotocin-Induced Diabetic Rats. Kidney Blood Press Res. 42: 894–904.

Zhang J., Ney P.A. (2009). Role of BNIP3 and NIX in cell death, autophagy, and mitophagy. Cell Death and Differentiation. 16 (7): 939–46.

Zhang L., Deng M., Parthasarathy R. (2005) MEKK1 transduces activins signals in keratinocytes to induce actin stress fiber formation and migration. Mol Cell Biol. 25: 60–65.

Zhang S.L., Guo J., Moini B. (2004) Angiotensin II stimulates Pax-2 in rat kidney proximal tubular cells: impact on proliferation and apoptosis. Kidney Int 66: 2181–2192.

Zhang S.L., Guo J., Moini B., Ingelfinger J.R. (2004) Angiotensin II stimulates Pax-2 in rat kidney proximal tubular cells: impact on proliferation and apoptosis. Kidney Int. 66: 2181–2192.

Zhang S.L., Moini B., Ingelfinger J.R. (2004) Angiotensin II increases Pax-2 expression in fetal kidney cells via the AT2 receptor. J Am Soc Nephrol. 15, 1452–1465.

Zhao F., Fang Y., Deng S.X., Li X.T., Zhou Y., Gong Y., Zhu H.C., Wang W. (2017) Glycyrrhizin Protects Rats from Sepsis by Blocking HMGB1 Signaling. Biomed Res Int. 2017: 9719647.

Zhao L., Saitsu H., Sun X., Shiota K., Ishibashi M. (2010) Sonic hedgehog is involved in formation of the ventral optic cup by limiting Bmp4 expression to the dorsal domain. Mech Dev. 127(1-2):62-72.

Zhao W.Y., Han S., Zhang L., Zhu Y.H., Wang L.M., Zeng L. (2013) Mitochondria-Targeted Antioxidant Peptide SS31 Prevents Hypoxia/ Reoxygenation-Induced Apoptosis by Down-Regulating p66Shc in Renal Tubular Epithelial Cells. Cell Physiol Biochem 32:591-600.

Zhao X., Guan J.L. (2011) Focal adhesion kinase and its signaling pathways in cell migration and angiogenesis. Adv Drug Deliv Rev. 18;63(8): 610-615.

Zhou D., Tan R.J. Zhou L.L., Li Y.J., Liu Y.H. (2013) Kidney tubular β-catenin signaling controls interstitial fibroblast fate via epithelial-mesenchymal communication. Scientific Reports. 3: 1878.

Zhou D., Tian Y., Sun L., (2017) Matrix metalloproteinase-7 is a urinary biomarker and pathogenic mediator of kidney fibrosis. J Am Soc Nephrol. 28:598–611.

Zhou L., Fu P., Huang X.R., Liu F., Chung A.C., Lai K.N., Lan H.Y. (2010) Mechanism of chronic aristolochic acid nephropathy: role of Smad3. Am J Physiol Renal Physiol. 298(4):1006-1017.

Zhu F., Chong Lee Shin O.L., Xu H., Zhao Z., Pei G., Hu Z., Yang J., Guo Y., Mou J., Sun J., Zhu H., Wang Y., Wang M., Yang Q., Liao W., Xu G., Zeng R., Yao Y. (2017) Melatonin promoted renal regeneration in folic acid-induced acute kidney injury via inhibiting nucleocytoplasmic translocation of HMGB1 in tubular epithelial cells. Am J Transl Res. 9(4): 1694-1707.

Zhu Y.B., Zhang Y.P., Zhang J. Zhang Y.B. (2016) Evaluation of vitamin C supplementation on kidney function and vascular reactivity following renal ischemic injury in mice. Kidney Blood Press. Res. 41, 460–470.

Zuk A., Bonventre J.V. (2016) Acute kidney injury. Annu Rev Med. 67: 293–307.